LBL-11208

Lawrence Berkeley Laboratory
UNIVERSITY OF CALIFORNIA

Materials & Molecular
Research Division

ION-MOLECULE INTERACTIONS IN CROSSED-BEAMS

Steven George Hansen
(Ph.D. thesis)

September 1980

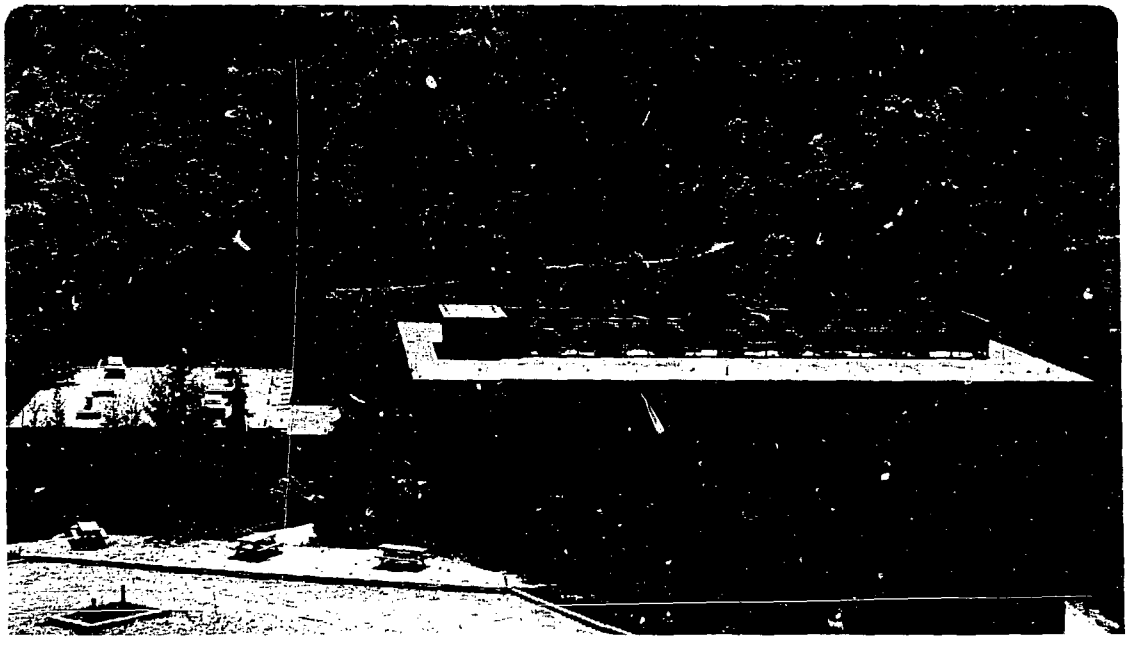

Prepared for the U.S. Department of Energy under Contract W-7405-ENG-48

ION-MOLECULE INTERACTIONS IN CROSSED-BEAMS

Steven George Hansen

Materials and Molecular Research Division
Lawrence Berkeley Laboratory
and Department of Chemistry
University of California
Berkeley, CA 94720

ABSTRACT

Interactions of the ions N^+, F^+, and CO_2^+ with H_2 and/or its isotopes were examined using the crossed-beam technique in the low (<4 eV) initial relative energy. Emphasis was placed on studying the reaction dynamics of the various electronic states of the reactant ions.

We demonstrated that for the reaction $N^+(^3P) + H_2 \rightarrow NH^+ + H$, complex formation dominates up to 1.9 eV and a substantial interaction occurs between all collision partners at energies as high as 3.6 eV. The distribution of N^+ scattered non-reactively from H_2 also showed a contribution from a long-lived complex channel at energies below 1.9 eV. The dynamics were adequately explained by a mechanism which involves accessing the deep $^3B_1$, potential well through an avoided crossing with the $^3A_2$ surface when the symmetry is relaxed from C_{2v} to C_s.

The reaction of a metastable electronic excited state, probably $N^+(^1D)$, was seen as a forward peak in the reactive distributions.

The reaction $F^+(^3P) + H_2 \rightarrow FH^+ + H$ was observed to proceed by a direct reaction mechanism in the 0.20-1.07 eV initial relative energy range. The reaction mechanism involves a nonadiabatic transition which can occur if the H_2 internuclear separation is decreased; collinear

approaches are probably preferred. No evidence for the reaction of $F^+(^1D)$ with H_2 was observed.

The reaction $CO_2^+ + D_2 \rightarrow DCO_2^+ + D$ was seen to give asymmetric product distributions at collision energies of 0.27 eV and above indicating a direct reaction mechanism. Symmetric low intensity contours suggested that many reactive events may involve snarled trajectories. CO_2^+-D_2 collisions can also produce DCO^+ exothermically, but there is a barrier to its formation; we measured the threshold for DCO^+ production to be 1.0 ± 0.3 eV. We found that the dynamics of CO_2^+-D_2 collisions was not explainable by statistical (RRKM) theory if the existence of barriers on the potential energy surface was neglected. Our results indicated that there are probably barriers in the exit channels for DCO_2^+, DCO^+, and D_2O^+ products.

The electronic state distributions of our N^+,F^+, and CO_2^+ beams was investigated using beam attenuation and total luminescence techniques. Microwave discharge and DC discharge ion sources, using N_2 as a source gas, yielded 92% $N^+(^3P)$ and 8% $N^+(^1D)$. 160 eV electron bombardment of N_2 gave an almost indecipherable mixture of states; however, we estimated 40% $N^+(^3P)$, 40% $N^+(^5S)$, 10% $N^+(^1D)$, and 10% N_2^{++}. A study of the electronic states of F^+ produced by 160 eV electron impact on CF_4 and NF_3 was inconclusive. Beam attenuation results were suggestive of multiple states, but total luminescence experiments showed the state distribution to be identical with that of F^+ produced by a microwave discharge through a CF_4:NO mixture. The latter beam should contain

almost exclusively $F^+(^3P)$. We detected no difference in the state distribution of microwave discharge produced CO_2^+ with that of electron impact produced CO_2^+. It is likely that both beams are almost exclusively ground state $CO_2^+(^2\Pi_g)$.

ACKNOWLEDGMENTS

I feel very lucky to have spent 5 years working and playing with the fine people I have met here in Berkeley. The resources of this place, both material and intellectual, are enormous, and I am sure that a student can develop more quickly and still have fun doing it, here, than he could elsewhere.

My research was performed under the direction of Professor Bruce Mahan. Although he is world-renowned as an educator, Bruce does not really "teach" his graduate students but rather inspires them by example. His commitment to excellence and his scientific integrity are unsurpassed and it is likely that the success of his previous students is attributable to the passing-on of these traits. It has been a privilege to work with Bruce.

I was very fortunate to have been inducted (abducted?) into the world of experimental physical chemistry by Jim Farrar. It is fair to say that I knew nothing about this subject when I first met Jim, but when he left nine months later I knew at least as much as I know today. Jim is a nice guy and never hit me even though I often deserved it (I believe my name was synonomous with "vacuum accident" for a while).

John Winn has been very important in the latter years of my graduate career. Since the onset of Bruce's illness he has filled an important role as the daily overseer of our research group. He is always eager to discuss matters scientific or otherwise; I thank him for the insights he shared.

I also profited greatly from discussions with Yuan T. Lee. Although he is a terribly busy man, he was never too busy to talk, and those talks helped me immeasurably. The design of the neutral source and much of the analysis in Chapter 3 hinged on discussions with Yuan.

I have always thought that the best way to learn something was to discuss it with your peers. When this is done weaknesses in arguments can be sought out and invariably a better understanding is attained. For this reason, I feel very grateful to those who engaged in such discussions with me. In particular I must thank Fred Grieman who would listen to (and often correct) me all day, and Mike Berman who would do the same thing when I went home. Tony O'Keefe, Bob Stachnik, and Henry Luftman were also willing and vocal participants in many of these interludes. Fred and Tony should also be thanked for their interest in my project and for helping me setup the total luminescence experiments.

I thank Tom Turner for his auto repair expertise and the many ideas he contributed to the beam apparatus; I thank Jim Kleckner for sharing some of his vast knowledge of electronics and computer systems and also for showing me how to perform attenuation experiments; and I thank Richard Davis for keeping things organized.

None of the work reported in this thesis would have been possible without the aid of the excellent support staff of the University of California and Lawrence Berkeley Laboratory. Almost everyone in the Chemistry Department machine shop helped me at various times and I consider them all good friends. Among them though, I must single out

Frank Lopez who machined virtually the entire apparatus and contributed many design suggestions along the way. Andy Anderson and Carl Baugh were able to fix everything I broke and Howard Wood taught me enough that I could fix some of them myself. People in the LBL electronics repair and ceramic shops saved me a number of times when things looked bad. Phil Eggers and Jack Wodei kept all of my power supplies working and helped me track down many elusive problems. Our group secretary Cordelle Yoder made our daily administrative tasks bearable and generally looked out for us. Nancy Monroe beautifully drew all of the difficult figures in this thesis and Marnie McElhiney typed the whole thing with speed and accuracy. I thank you all for your cheerfulness and your craftsmanship.

On a more personal level I must thank Susan who has been more than a molecular beam electric resonance spectroscopist to me, and my long-time housemate Shanta for being a good cook.

At this point I still have about 200 more people to thank. These are the people not already mentioned who helped make my stay in Berkeley so enjoyable. Whether we were drinking beer, playing ball, or merely sitting around imagining how good we were at both, we almost always had a good time. I would like to thank you all individually but I think I have carried on long enough. If you want to see your name look at Steve Winkle's or Jim Weisshaar's thesis acknowledgements. My sincere thanks goes to all of you.

This work was supported by the U. S. Department of Energy under contract No. W-7405-ENG-48.

ION-MOLECULE INTERACTIONS IN CROSSED-BEAMS

CONTENTS

CHAPTER 1. INTRODUCTION

Although modern chemistry encompasses a broad range of more specific fields, at the very heart of the subject lies the chemical reaction. Ancient man, using his wits and primitive tools, found ways to manufacture metals, dyes, perfumes, and drugs from the materials around him. The reasoning behind the alchemical procedures he used invariably depended on magic; it took thousands of years before any substantial progress was made in understanding microscopic processes. The first real attempt was by a German, George Ernst Stahl, who lived in the 17^{th} century. It had been thought for sometime that the mass lost when a substance was burned, was a volatile material, present in all objects, called "phlogiston." Stahl proposed that an analogy existed between combustion and rusting. That is, when a metal rusts, phlogiston has left, and calx (an oxide) remains. Therefore, calx is a pure substance or element, and metals are compounds composed of calx plus phlogiston. Stahl was on the right track, but ended up with exactly the wrong result. One hundred years later, Lavoisier gave the correct explanation for this process and other chemical reactions, along with the first table of the elements.

Lavoisier may have realized that the oxidation of iron involved the addition of a certain amount of gas to the metal, but he had no clue as to the details of the reaction. Work on elucidating such details did not begin until the $20^{\underline{th}}$ century, when scientists started addressing questions such as how could the reaction $H + D_2 \rightarrow HD + H$ break a bond

of over 100 kcal/mole at a collision energy of ~10 kcal/mole? The answer came in the form of the first theoretical potential energy surface; this semi-empirical London-Eyring-Polanyi surface was the object of considerable attention at the 1937 Faraday Discussion. The surface clearly showed the presence of the low barrier, and one could discern that the primary driving force in the reaction was the formation of the new bond.

The kind of reactions that will be considered in this thesis are reactions between ions and molecules. In 1916, Dempster[1] observed a signal in his mass spectrometer at m/e = 3 and attributed it to H_3^+. By 1925 it was well-established that this ion resulted from the reaction $H_2^+ + H_2 \rightarrow H_3^+ + H$, at elevated pressures in the mass spectrometer source.[2,3] The first measurement of a rate constant for an ion-molecule (IM) reaction came in 1952.[4]

Throughout the 1950's, work on IM reactions was conducted independently in the United States and Russia; by varying the pressure and/or electric field strength in a mass spectrometer ion source quantitative rates could be determined. The initial experiments demonstrated convincingly that exothermic ion molecule reactions generally have no activation barrier and that they are very rapid, often proceeding faster than the gas kinetic collision rate. It was further observed that the reaction rates were independent of temperature but decreased noticeably with increasing repeller voltage (ion energy).[5,6] These last two characteristics as well as the abnormally high (when compared to neutral-neutral reactions) rate constants were explained by Gioumousis and Stevensen who

took into account the long range ($\frac{1}{r^4}$) ion-induced dipole potential.[7] Their treatment resulted in a collision rate constant of $k = 2\pi e\{\alpha/\mu\}$, where α is the molecule's polarizability, e is the charge, and μ is the reduced mass; this rate constant is much greater than that calculated for neutral-neutral systems on the basis of London dispersion forces, and accurately gives the reaction rate for many exothermic IM reactions. The theory has been extended to include polar molecules by Su and Bowers (ADO theory).[8]

The early discovery that IM reactions proceed at essentially their collision rate led many kineticists to conclude that these processes were uninteresting. It should be pointed out, though, that a number of exothermic reactions such as

$$O^+ + N_2 \rightarrow NO^+ + N \quad k = 10^{-12} cm^3/sec \ @ \ 300^\circ K \tag{1}$$

and

$$He^+ + H_2 \rightarrow HeH^+ + H \quad k \leq 10^{-13} cm^3/sec \ @ \ 300^\circ K \tag{2}$$

are quite slow, proceeding once every 1000 and 10,000 collisions respectively.[9,10] The reasons for the unfavorability of these reactions is discussed later.

A point which has been glossed over by many authors, but was dealt with in a recent review article by Talrose, et al.,[11] is the reason IM reactions have no activation barrier. Their qualitative assertion, which is depicted in Fig. 1, is that the long range attraction of the

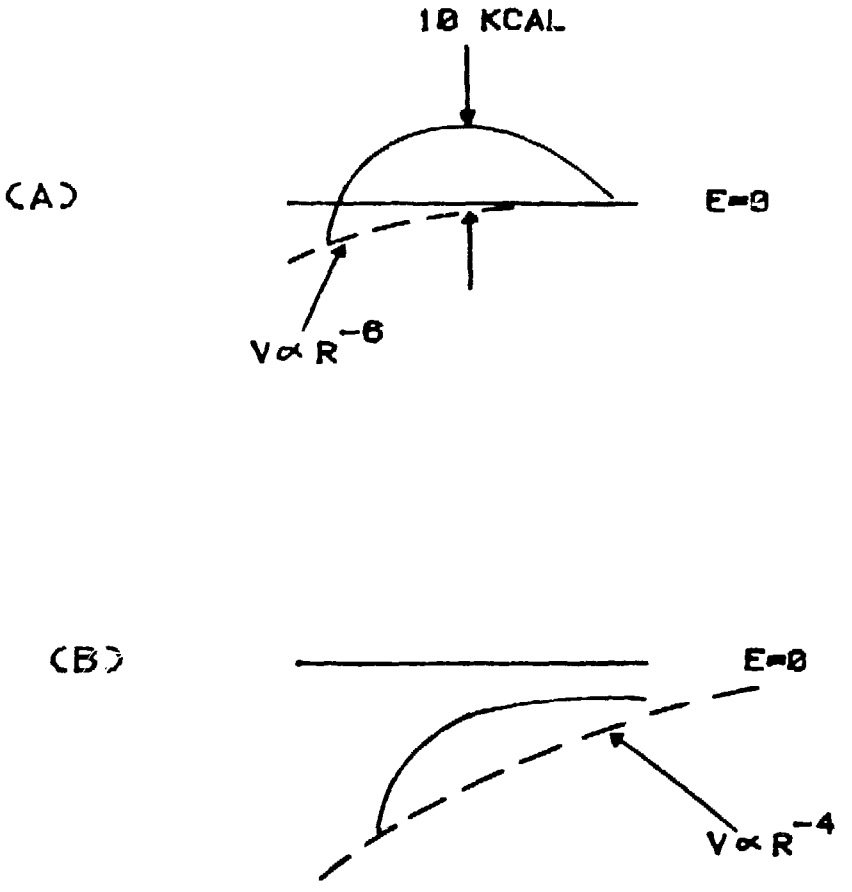

Fig. 1 The effect of the ion-induced dipole interaction on a potential energy curve. In (a) the attractive potential between two neutral turns on too slowly to counteract the activation barrier. In (b), by the time the distance for the activation barrier is encountered, the ion-induced dipole potential already dominates.

$\frac{1}{r^4}$ potential is greater than the repulsion at intermediate distances caused by chemical forces; hence no barrier is present. In neutral-neutral systems, the asymptotic $\frac{1}{r^6}$ dipole-induced dipole potential is swamped by this repulsion. A further point brought up in Ref. 11 is that because of the long range potential, the interaction time will often be greater for IM collision partners than neutral-neutral reactants. The longer an intermediate complex lives, the more phase space it can sample and the greater the probability that it will find the lowest energy exit channel. This concept would seem to be crucial in explaining the fact that many IM reactions proceed at the collision rate.

Ion-molecule reactions are important in combustion, atmospheric, and astrophysical processes, and since the mid 1960's a myriad of techniques for their study have been developed. Probably the most successful and prolific method up to this time is the flowing afterglow approach of Ferguson, Fehsenfeld and Schmeltekopf.[12] This technique involves transporting ions down a tube at ~1 torr and adding the neutral reactant downstream. Product ions are detected with an on-line mass spectrometer. By varying flow rates or the point at which the neutral is added, it is possible to measure accurate thermal rate constants. A problem with this method is that secondary reactions often make data interpretation difficult. This has been largely circumvented in a more recently developed apparatus called a selected ion flow tube (SIFT).[13] The SIFT technique gives information (rate constants and branching ratios) similar to that of the flowing afterglow, but mass

selects and injects the ions into the flow tube rather than forming them in situ. This is a clear advantage when working with fragment ions, and impressive results have been obtained. Another variation of the flowing afterglow technique is the drift tube.[14] Here ions are pulled by a weak electric field rather than simply flowing in a buffer gas (although this can be done simultaneously), and react with other gases placed in the tube. An obvious advantage of this technique is that the collision energy is more easiy varied than in a flow tube.

Ion cyclotron resonance[15] (ICR) is another important thermal energy technique, but operates in a lower pressure range than the previously mentioned experiments. In ICR, ions are confined to circular orbits by a strong magnetic field and may react with neutrals they encounter. Product ions are also confined to circular orbits. Detection is accomplished by scanning the frequency of an applied RF electric field and measuring the power absorbed; the frequency at which an ion absorbs depends on its mass. Rate constants measured using these different techniques generally agree to within ~20%.

Although the techniques described in the previous paragraphs have been of inestimable value in our understanding of IM reactions, they really do not go very far toward answering the basic question: what happens at a microscopic level? To answer this, one must consider the dynamics of the reaction. The reaction dynamicist wants to know with what probability a collision between particles in known quantum states, moving at known velocities, yields products at a certain angle and velocity, and in a certain quantum state. Given this information one

would know everything about the system. The macroscopic reaction rate constant could be calculated from the expression[16]

$$k(T) = \sum_i \sum_j a_i(T) a_j(T) \sum_m \sum_n \int_0^\infty v f_T(v) \int_0^{2\pi} \int_0^\pi d\sigma_{ij,mn}(v,\theta,\phi) \sin\theta d\theta d\phi dv. \quad (3)$$

Here the quantum state-to-state differential reaction cross section $d\sigma_{ij,mn}$ is integrated over polar and azimuthal scattering angles to produce the state-to-state reaction cross section, which is then averaged over the distribution f(v) of relative collision speeds to give the state-to-state reaction rate constant. This is summed over the product quantum states m and n and averaged over initial reactant quantum states i and j (with fractional populations a_i and a_j) to yield the macroscopic rate constant k(T). We see then, that if the state-to-state differential cross sections are known, we can obtain the macroscopic rate; but clearly the process cannot be inverted.

No one has yet performed the ideal experiment, primarily because of intensity problems, but any attempt would require the use of crossed beams of reactants. It is obvious that even without detailed knowledge of reactant and product quantum states, one benefits significantly from single collision conditions and precise information about product angular and velocity distributions. The first successful crossed beam experiments were performed in the early 1960's and used alkali metal containing compounds as one of the reactants. The thermal energy beams were prepared by physically collimating molecules which effused through small holes in ovens. The reactions studied had very large (> 100Å^2)

cross sections and products containing alkali metal atoms were easily detected by surface ionization. The first study of an IM reaction using a beam of ions was reported in 1965 by Henglein and coworkers.[17]

It is interesting to compare the relative experimental problems and information gained from neutral-neutral beam experiments, and IM beam experiments. Initially, ion beam workers had an advantage because of advances made through the years in mass spectrometry and electron optics. A further source of convenience was that charged products could be efficiently energy analyzed, mass analyzed, and detected. The disadvantages were (and still are) that beam intensities are always limited by space-charge effects, and these effects become more severe as the beam energy is lowered. For this reason, the very important thermal energy range is not readily accessible to ion beam experimenters. On the plus side though, ion energies are easily varied by turning a knob on a power supply and hence IM reactions can be studied over a wide energy range while neutral beams are confined to near thermal energies. The low intensity of an ion beam becomes glaring when one realizes that typical fluxes for low energy (~5 eV) ion beams are $\sim 10^{11}$ particles/cm^2sec as opposed to $\sim 10^{17}$ particles/cm^2 sec for modern supersonic neutral beams.[18]

In spite of the larger reactant flux associated with neutral-neutral beam reactions, products are much harder to detect. Workers were confined to alkali systems until 1969, when, by combining an ionizer and mass spectrometer, with several stages of differential pumping to minimize high background levels, the first "universal" detector was

developed.[19] The efficiency of a well designed ionizer is .01-.1%, which reduces the six order of magnitude advantage in beam flux to an effective two order of magnitude advantage in product flux.

The problems of low product flux and inefficient detection of very slow (< 1 eV) ions has generally restricted IM experiments to systems with heavy ions and light neutrals. A favorable mass ratio such as this confines products to a small region in velocity space and counting rates are higher. Recently though, improvements in experimental technique have allowed the routine study of systems where the masses are comparable,[20] and even systems where the ion is much lighter than the neutral.[21]

There have been a number of other important advances in the past few years in the use of ion beams. The merged beam technique of Gentry and co-workers[22] allows the study of IM reactions at relative energies as low as 0.002 eV, and the reactant mass ratio is unimportant. This method uses a fast (several keV) neutral beam which is produced by charge transfer from an ion beam, and merges it at a steep angle with a fast ion beam. By adjusting the laboratory energies of these beams, very low relative collision energies can be obtained; the uncertainty in initial conditions is small because of a phenomenon called "velocity compression" at high energies.[16] This technique gives accurate cross sections and centerline velocity distributions, but not angular distributions. Another recently developed approach to IM reactions that has great potential is the guided beam technique.[23] Ions are channeled and confined by an rf octopole field and the ion energy may be precisely

adjusted. The products are also confined by the rf field and the apparatus has essentially unit detection efficiency.[24] It is even possible, by operating the instrument in a pulsed mode, to detect products scattered backwards in the laboratory frame. Very accurate cross sections and branching ratios can be obtained but no information is gained about product velocity or angular distributions. A final important advancement in the study of IM reactions using ion beams is the dispersion of chemiluminescence resulting from beam-gas collisons.[25] This is a difficult experiment because of low light levels, but direct information on the internal state distribution of products formed in emitting electronic states is obtained. For further discussion of the results and techniques of modern ion beam studies, the reader is directed to the reviews by Gentry[26] and Koski.[27]

Kinematics

The most convenient method for displaying the results of a crossed-beam experiment is to plot product intensity in center-of-mass coordinates in velocity space. The transformation from laboratory to center-of-mass coordinates is best discussed with the aid of a Newton diagram. As shown in Fig. 2, a Newton diagram is constructed by placing the reactant's laboratory velocity vectors at a common origin, which corresponds to zero laboratory velocity, and connecting the tips to form the relative velocity vector ($\underset{\sim}{v}_{rel}$). The vector which describes the motion of the center-of-mass, $\underset{\sim}{v}_{cm}$, terminates on $\underset{\sim}{v}_{rel}$ at a point which divides $\underset{\sim}{v}_{rel}$ into the reactant center-of-mass velocity vectors;

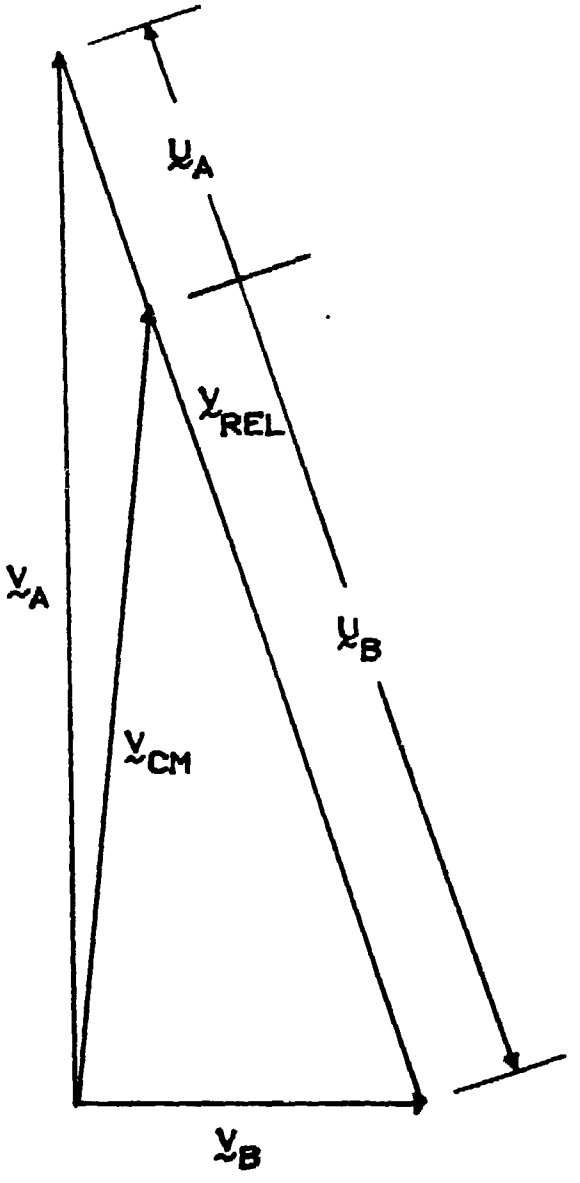

$$\underset{\sim}{u}_A = \underset{\sim}{v}_A - \underset{\sim}{v}_{CM}$$

$$\underset{\sim}{u}_B = \underset{\sim}{v}_B - \underset{\sim}{v}_{CM}$$

$$\underset{\sim}{v}_{REL} = \underset{\sim}{v}_A - \underset{\sim}{v}_B$$

Fig. 2. Newton diagram for an experiment with two beams colliding at 90°. $\underset{\sim}{v}_A$ and $\underset{\sim}{v}_B$ denote the most probably laboratory velocity vectors for reactants A and B. $\underset{\sim}{v}_{rel}$ and $\underset{\sim}{v}_{cm}$ are the relative and center-of-mass velocity vectors respectively. $\underset{\sim}{u}_A$ and $\underset{\sim}{u}_B$ are the center-of-mass velocity vectors for the reactants.

these vectors when mass-weighted, give center-of-mass momentum vectors of equal magnitude. By subtracting $\underset{\sim}{v}_{cm}$, which amounts to shifting the origin and rotating the coordinate system, the problem is transformed to one which is conceptually easier to deal with. We can now picture ourselves as moving with the center-of-mass, and in this frame, the reactants approach each other at 180° rather than 90°. The orientation of the line on which they travel is given by $\underset{\sim}{v}_{rel}$. Products also depart along a straight line and the angle this line makes with $\underset{\sim}{v}_{rel}$ is called the center-of-mass scattering angle, θ. If the velocity vector of one of the products is measured, that of the other is uniquely determined by invoking the constraint that linear momentum is conserved. The energy of the collision in center-of-mass coordinates, also called the relative energy, is given by

$$E_{rel} = \frac{1}{2} \mu v_{rel}^2 \qquad (4)$$

where $\mu = m_A m_B/(m_A + m_B)$. The relative energy represents the <u>available</u> translational energy in the collision and is therefore the quantity of interest. The energy associated with the motion of the center-of-mass remains constant throughout the process and cannot be used by the reactants. A further feature of the transformation is that it becomes easier to see, given a random assortment of impact parameters, that the product distribution should be symmetric about $\underset{\sim}{v}_{rel}$.

Conservation of energy limits the products to a certain region of velocity space. This is shown in Fig. 3 which considers the dynamics of the reaction

$$A + B \rightarrow C + D. \tag{5}$$

In this figure, the result of a single reactive event is indicated with the C product scattered through an angle of Θ in the lab frame and θ in the center-of-mass frame. As mentioned earlier, the location of the D velocity vector can be deduced from conservation of linear momentum:

$$m_C \underline{u}'_C + m_D \underline{u}'_D = 0 \tag{6}$$

The circles labeled Q_{min} and Q_{max} in Fig. 3 given information as to where product intensity is allowed. Q is defined as the translational exoergicity of a process, or

$$Q = E'_{rel} - E_{rel} \tag{7}$$

where the prime denotes a quantity associated with the products. For a non-reactive process, with no energy transfer during the collision, $Q = 0$. This circle, also called the elastic circle, is centered at the center-of-mass origin (as are all Q circles) and has radius u_A for A products and u_B for B products. Elastic events will give products only on these circles. If ground state reactants are used it is

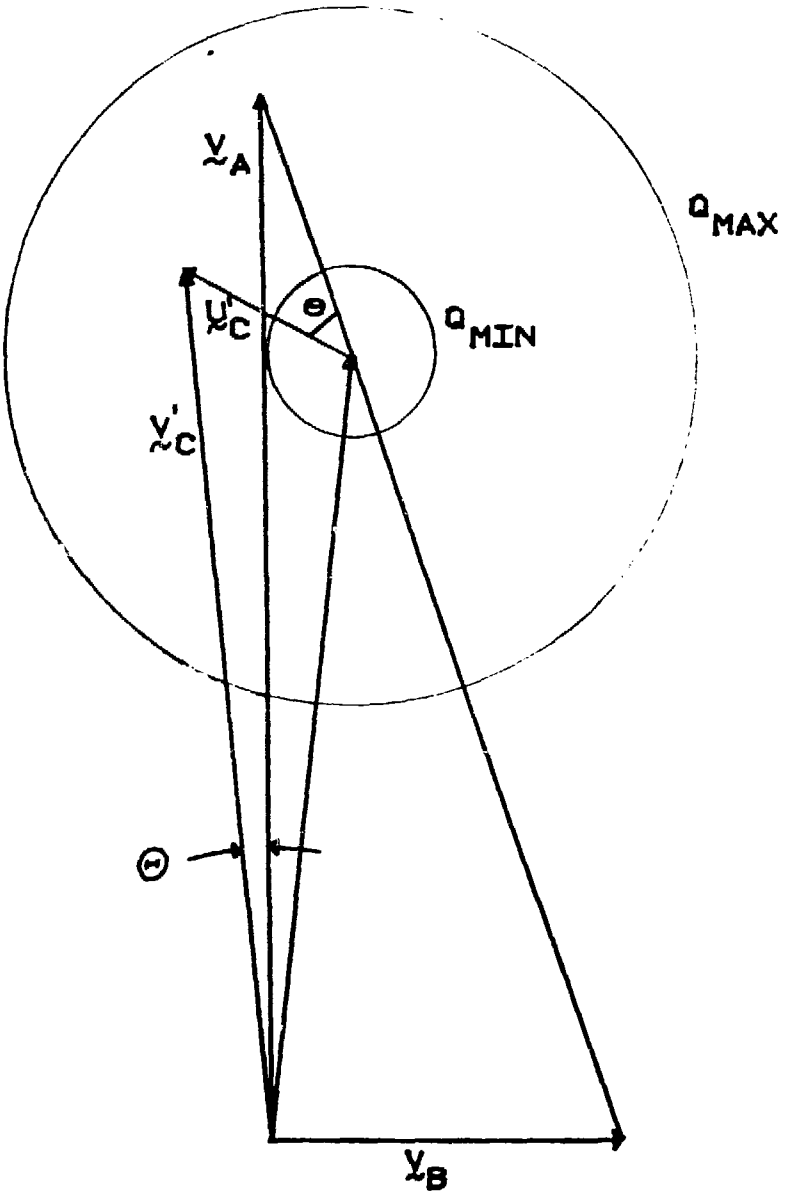

Fig. 3. Newton diagram for A + B → C + D with product C being detected. v_A and v_B are the laboratory velocity vectors for the reactants and v'_C and u'_C are the final lab and center-of-mass velocity vectors of C. Product intensity is confined between Q_{min} and Q_{max} for energetic reasons.

impossible in a non-reactive collision for products to appear outside the Q = 0 circle (superelastic scattering), but upon collision, energy may be taken up by internal modes of one or both of the collision partners. If this happens, products appear at negative values of Q (inelastic scattering). The minimum possible value of Q is $-E_{rel}$; this corresponds to converting all initial translational energy into internal energy, and products will be constrained to have zero center-of-mass velocity.

In the case of reactive scattering, the reaction's energetics and product's stability must also be considered. The total energy available before the collision is given by

$$E = E_{rel} + U \tag{8}$$

where U is the internal energy of the reactants. This must equal the total post-collision energy of

$$E' = E'_{rel} + U' + \Delta H \tag{9}$$

where ΔH is the heat of the reaction. Equating (8) and (9) and then using (7), we obtain

$$Q = U - U' - \Delta H \tag{10}$$

If we make the assumption that $U = 0$ we find that since $U_{min} = 0$, $Q_{max} = -\Delta H$. This result states the rather obvious fact that the products of endoergic reactions will be confined to a region closer to the center-of-mass velocity than will those of exoergic reactions. An effective minimum Q comes about because there is only a limited amount of energy which can be internally assimilated by some products. This maximum internal energy corresponds to the dissociation energy (D_o) of that species. If the collision partners are an atom and a diatom, then one of the products will be an atom and the only place to store small amounts of energy will be in the internal modes of the molecular product. Therefore $U_{max}' = D_o$ and

$$Q_{min} = - D_o - \Delta H \quad . \tag{11}$$

Since most of the experiments described in this thesis were performed at low energy, $|Q_{min}|$ was generally greater than E_{rel} and was not a factor in the dynamics. However, even in low energy experiments, if the reaction has a large exoergicity, as might be expected for electronically excited reactants, then Q_{min} could be large enough to place a restriction on the product distribution.

A point which is important to discuss, primarily because it was the source of much confusion in the early literature, is the coordinate system and Jacobian used to display the results. Farrar[28] gives a good discussion of this potential trouble spot and the present account will be briefer and more qualitative. Basically, the problem is this:

it is desired by most experimenters to present their data in the form of intensity contour maps in velocity space, but the coordinate system used can effect the appearance of the results. To a certain extent this is analagous to the electron distribution in the 1s orbital of the H atom. A plot of $\psi^*\psi$ vs r yields a distribution peaked at r = 0 while the radial distribution, which is weighted by r^2, peaks at the Bohr radius. As long as it is clear which function is being plotted, there should be no ambiguity.

The apparatus used in this thesis has a detector which energy analyzes product ions. By pre-accelerating or decelerating the ions prior to energy analysis, we are able to pass ions at a fixed energy, and hence, data are obtained in energy space volume elements of constant size.[29] To convert the product intensity I(E)dE to an intensity in velocity space, it is necessary to bear in mind that $E \alpha v^2$ and $dE \alpha vdv$. By merely plotting the raw data in laboratory velocity space we would have the quantity I(v)vdv. Such a plot would not be very useful because it does not correspond to any commonly used coordinate system in 3-dimensional space. If the data are everywhere multiplied by v, then the quantity being plotted is $I(v)v^2dv$, which, within the angular factor, corresponds to laboratory spherical polar coordinates. This coodinate system is also not very useful because it is symmetric about the laboratory origin rather than the center-of-mass origin. If instead we divide the raw data by v (or $E^{1/2}$), we obtain a Cartesian plot in laboratory velocity space, I(v)dv, and all the volume elements are of equal size. The location of the origin in Cartesian coordinates is

unimportant so we may just as easily call these center-of-mass Cartesian coordinates, and we are done. Virtually all of the ion-molecule literature uses these coordinates; the suggestion for unanimity came formally from Wolfgang and Cross.[30] If one is careful enough to accurately include beam intensities and detector efficiency so that the measured specific intensities ($\bar{I}$) for the products have absolute quantitative value, then they can be integrated to get center-of-mass differential cross sections[31]:

$$I(\theta) = \int_0^{\pi} \bar{I}(\theta,\phi,u)u^2 du. \tag{12}$$

where θ, ϕ, and u are the center-of-mass scattering angles and speed. This can be further integrated to give the total cross section:

$$\sigma = 2\pi \int_0^{\pi} I(\theta)\sin\theta d\theta. \tag{13}$$

Many workers in neutral-neutral beam reactions prefer to express their results in terms of center-of-mass polar coordinates. In order to affect conversion to these coordinates, it is necessary to have good resolution in the center-of-mass frame; this requirement is often not met in ion-molecule experiments. The transformation is accomplished by everywhere multiplying the Cartesian intensity by u^2. The fact that the volume element disappears as one gets nearer to the center-of-mass implies that a crater will always exist there. The decision as to which

coordinate system is used is merely a matter of taste, and as long as it is clearly indicated by the author which system he is using, there should be no trouble. Hierl et al.[32] give an example of how changing coordinate system affects the appearance of a contour map.

Reaction Models

It was thought by many early workers in ion-molecule reactions, that many, if not all low energy collisions involved the formation of a long-lived collision complex. Their reasoning was based on the belief that the Langevin cross section represents a capture cross section and the fact that collisions between reactants such as Ar^+ + HD formed ArD^+ slightly more rapidly than ArH^+.[33] This latter point was taken as evidence for complex formation because the deuteride, with its lower zero point energy, would be favored in the decomposition of an $ArHD^+$ complex. The myth of the pervasiveness of these complexes was dispelled by the first beam experiments which clearly showed that the product distribution was asymmetric down to a relative energy of 0.06 eV.[34] If a long-lived intermediate had been formed, then the product distribution would have had forward-backward symmetry, i.e. symmetry with respect to the plane that passes through the center-of-mass velocity and lies perpendicular to the relative velocity vector. Subsequent work has shown that most simple IM reactions proceed by direct mechanisms down to collision energies of a few tenths of an eV. A dynamical model for explaining observed isotope effects has been developed,[35] and the old

idea that, due to the Langevin formulation, persistent intermediates should dominate, has been dismissed by Henchman[36] in an excellent review article.

As briefly mentioned above, reaction mechanisms can be divided into two categories: direct and indirect. An indirect reaction mechanism involves the formation of a long-lived intermediate lasting at least several rotational periods ($\sim 10^{-12}$ seconds) prior to decomposition. During the lifetime of such a complex, the orientation of the initial relative velocity vector is forgotten and hence the product velocity vector distribution is isotropic (about the center-of-mass) in the plane of the collision. The shape of the distribution that is measured experimentally is not necessarily isotropic, but should have forward-backward symmetry. Angular momentum disposal is crucial to the exact shape of the map when a long-lived complex is involved; this is discussed in Chap. 3. A long-lived complex will only be formed with high probability if there is a deep potential energy well associated with the intermediate.

Among the direct reaction mechanisms, there are several different models which have been proposed. The simplest, and also the one which correctly describes the gross features of the product velocity distribution for most IM reactions, is the "spectator stripping" model. It was found[17] in the first IM beam experiments that reactions such as

$$X^+ + Y_2 \rightarrow XY^+ + Y \qquad (14)$$

(where Y_2 was usually H_2) produced XY^+ velocity distributions peaked at what is now generally called the spectator stripping velocity:

$$\underline{v}_{ss} = \frac{m_X}{m_X + m_{Y_2}} \underline{v}_{X^+} \quad . \tag{15}$$

It is implicit in expression (15) that the velocity of Y_2 is negligible compared to that of the ion. If this is not a good approximation, as in the case of a low energy crossed beam experiment, then we have

$$\underline{v}_{ss} = \underline{v}_{cm} + \frac{m_X m_{Y_2}}{(m_X + m_Y)(m_X + m_{Y_2})} \underline{v}_{rel} \quad . \tag{16}$$

The model, as it applies to reaction (14), states that the collision takes place between X^+ and only one of the Y atoms; the other Y atom, which is merely a spectator during the process, does not have its initial velocity vector altered. Since in center-of-mass coordinates X^+ and Y_2 have, prior to collision, equal but opposite momenta, a single Y atom has half the momentum of X^+, and thus the XY^+ will be forward scattered (in the initial X^+ direction) with half the momentum of the X^+ reactant. This conservation of linear momentum approach leads to equation (16). The spectator stripping model was first proposed by nuclear physicists to explain some of their observed product distributions

The fact that this simplest of all reaction models is successful in describing many experimental product distributions is no doubt fortuitous. Few people believe that it accurately portrays microscopic dynamics, and there has been some effort put toward modifying the model to make it more physically reasonable. The first attempt[37] at modification included an estimate of the incoming and outgoing potentials. The ion-induced dipole potential, $V = -\frac{\alpha e^2}{2r^4}$, was used, with e the charge on the ion and α the polariability of the neutral. The fact that a Y atom is generally not as polarizable as Y_2 implies that products will not be decelerated in the exit channel as much as reactants were accelerated in the entrance channel, and hence velocities greater than the stripping velocity should be seen. Though the effect predicted by this "modified stripping" approach only become noticeable at very low collision energies, it gave an excellent fit to data for $Ar^+(D_2,D)ArD^+$.[37,38]

Another variation of the spectator stripping model is the "elastic spectator" model. Like spectator stripping and unlike modified stripping, this is a billiard ball model in that no long-range forces are included between collision partners. An elastic spectator event involves a completely inelastic collision between X^+ and one Y atom and then an elastic collision with the other Y atom. Hence this model constrains products to appear at the spectator stripping center-of-mass velocity, but center-of-mass angles other than 0° are allowed. The model does a reasonably good job of predicting the product distributions for the reactions $N_2^+(H_2,H)N_2H^+$[31] and $O^+(H_2,H)OH^+$[39] at moderate energies. In the special instance where a collinear approach is pre-

ferred, the elastic spectator model states that the product is backscattered; this particular case is generally called the "ideal rebound" model. Another impulsive model which has been proposed to explain a product backscattered peak is the "ideal knockout" model.[40,41] Here, it is assumed that the initial collision between the ion and one of the H atoms is completely elastic and then reaction occurs with the other atom.

An interesting characteristic of all of the hard-sphere-type models is that conservation of linear momentum defines the product velocity and thus the internal energy of the products is fixed. In a spectator stripping event, all of the relative energy of collision X^+ and the single Y atom in their own center-of-mass frame, plus any heat released in the reaction, is converted to internal energy. Mathematically this corresponds to

$$E_{int} = \frac{m_Y}{m_{Y_2}} \frac{m_X + m_{Y_2}}{(m_X + m_Y)} E_{rel} + \Delta H. \qquad (17)$$

Because of this constraint, one can see that as the relative collision energy is raised, a point will be reached where the product attempts to store more energy than its dissociation energy. A way of stating this in the language of the previous section is that the Q_{min} circle has moved out to the spectator stripping velocity. At this collision energy, stable products cannot be formed by a simple stripping process. Experiments in the high energy regime, where this effect "turns on," have led to some interesting results. In the reaction $X^+(H_2,H)XH^+$,

where X^+ is N_2^+, CO^+, or Ar^+, the spectator stripping peak moves forward with higher collision energies, staying in the zone of the stability,[42-44] while for O^+ and N^+ the forward peak at 0° disappears,[39,45] and is replaced by side peaks. The first three reactions are significantly exoergic ($\Delta H \approx -1.4$ eV) and the reaction mechanism apparently allows for the channeling of this energy into forward product recoil. The reactions with O^+ and N^+ are decidely less exoergic ($\Delta H = -0.4$ and 0 eV respectively), so the availability of energy released by the reaction seems important. A hard-sphere reaction mechanism for describing dynamics in the trans-stripping energy range, has been proposed by Bates et al.[46] and refined by Mahan and collaborators.[47] The model assumes that X^+ strikes one Y atom elastically which in turn elastically strikes the other Y atom; this approach is appropriately called the sequential impulse model (SIM). Reaction is accomplished if the final relative kinetic energy of two of the collision partners is less than the bond energy of the molecule they form. Agreement between the predictions of this model, and experiments, has been encouraging.[39,45]

The fact that for many IM reactions the peak in the product distribution will move ahead of the spectator stipping velocity if energetically necessary indicates the shortcomings of the spectator stripping model. A slightly more complicated reaction mechanism, which better explains the experimental results but is still physically understandable, has been given. This mechanism states that X^+ strikes first one Y atom and then reacts with the other and hence is called the

"migration" mechanism. This is really a variation of the SIM and has been suggested through the consideration of classical trajectory calculations.[48,50] In a classical trajectory calculation one actually solves the equations of motion for a system moving in a potential energy field. By running a number of trajectories using properly averaged initial conditions one can attempt to see how the reaction actually takes place. It was found[50] that the aforementioned migration mechanism was important at high collision energies while stripping events, which result from grazing collisions, are less so. At lower energies stripping is dominant. It should be added that the agreement between these calculated product distributions and experiment is quite good.[48,50]

A feature of IM reactive systems which should be mentioned when discussing reaction mechanisms is the following. Because reactive ions generally have holes in their electronic shells, there will often be several low-lying potential energy surfaces, and the interplay of these surfaces can greatly affect the reaction dynamics. The surface on which a trajectory moves is crucial in explaining whether a reaction will be direct or indirect, whether the preferred approach is collinear, C_{2v}, or in between, and, most importantly, whether the reaction will take place at all. Most classical trajectory calculations confine motion to one surface, but an important improvement, which allows trajectores to "hop" onto another surface, has been made.[51] This extension, which is called the trajectory surface hopping (TSH) method, has great potential for completely explaining ion-molecule reaction dynamics. Coupled with

the ability of modern ab initio techniques to accurately calculate the surfaces, the TSH method can be counted on to give results which duplicate experiments, but at the same time directly describe the microscopic processes.

Another theoretical approach used in elucidating reaction dynamics involves application of the correlation diagrams. A correlation diagram shows the pertinent potential energy surfaces and indicates which are easily accessible, which should lead to reaction, and sometimes sheds light on the reaction mechanism. The diagram is constructed by placing electronic states of the reactants, products, and intermediates on a graph of energy vs reaction coordinate and connecting states using spin and symmetry rules. The lines connecting the states qualitatively represent potential energy surfaces; further details are given in Chapter 3. The application of correlation diagrams to low energy IM reactions has been very successful in explaining some previously puzzling results. As mentioned earlier in this chapter, the reaction $O^+(N_2,N)NO^+$ which is exothermic, is quite slow. A molecular state correlation diagram shows,[52] that ground state reactants are connected with ground state products through a linear $^4\Sigma^-$ state of the N_2O^+ intermediate. The ground state of N_2O^+ is $^2\Pi$ and the $^4\Sigma^-$ state is presumably of significantly higher energy. Assuming the reaction involves a collinear approach, then there is probably a barrier along the reaction coordinate and the reaction should be, as observed, slow. A similar argument, only using orbital correlation diagrams, was given by

Mahan[53] to explain the difference between the reactions $X^+(H_2,H)XH^+$ and $X(H_2^+,H)XH^+$ where X = He and Ne. It seems that the reactions involving He^+ and Ne^+, though very exothermic, are also very slow, while the charge transfer analogues, which are endothermic, proceed rapidly if supplied sufficient energy. A consideration of the orbital correlation diagrams clearly showed that while $X + H_2^+$ could easily give XH^+ products, $X^+ + H_2$ could not. For further demonstrations of the utility of correlation diagrams, the reader is directed to the reviews by Donovan and Husain[54] and Mahan[55].

References

1. A. J. Dempster, Phil. Mag. 31, 438 (1916).
2. H. D. Smyth, Phys. REv. 25, 452 (1925).
3. T. R. Hogness and E. G. Lunn, Phys. Rev. 26, 44 (1925).
4. V. L. Talrose, A. K. Lyubimova, Dokl. Akad. Nauk. SSSR 86, 209 (1952).
5. F. H. Field, J. L. Franklin, and F. W. Lampe, J. Am. Chem. Soc. 79, 2419, 2665 (1957).
6. D. P. Stevenson and D. O. Schissler, J. Chem. Phys. 29, 282 (1958).
7. G. Gioumousis and D. P. Stevenson, J. Chem. Phys. 29, 294 (1958).
8. T. Su and M. T. Bowers, Int. J. Mass Spectrom. Ion Phys. 12, 347 (1973).
9. E. E. Ferguson, F. C. Fehsenfeld, P. D. Golden, and A. L. Schmeltekopf, J. Geophys. Res. 70, 4323 (1965).
10. C. F. Giese and W. B. Maier, J. Chem. Phys. 35, 1913 (1961).
11. V. L. Talrose, P. S. Vinogradov, and I. K. Larin, in Gas Phase Ion Chemistry, Vol. 1, Ed. M. T. Bowers (Academic Press, NY) 1979, pp. 305-347.
12. E. E. Ferguson, in Ion-Molecules Reactions, Vol. 2, Ed. J. L. Franklin (Plenum Press, NY) 1972, pp. 363-393.
13. D. Smith and N. G. Adams, in Gas Phase Ion Chemistry, Vol. 1, Ed. M. T. Bowers (Adacemic Press, NY) 1979, pp. 1-42.
14. D. L. Albritton, in Interactions Between Ions and Molecules, Ed. P. Ausloos (Plenum Press, NY) 1979, pp. 119-142.

15. J. M. S. Henis, in Ion-Molecule Reactions, Vol. 2, Ed. J. L. Franklin (Plenum Press, NY) 1972, pp. 395-455.

16. W. R. Gentry, in Interactions Between Ions and Molecules, Ed. P. Ausloos (Plenum Press, NY) 1979, pp. 81-102.

17. A. Henglein, K. Lacmann, and G. Jacobs, Ber. Bunsenges Phys. Chem. 69, 279 (1965).

18. C.-Y. Ng. Ph.D. thesis, Univ. of California, LBL Report LBL-5439 (1976).

19. Y. T. Lee, J. D. McDonald, P. R. LeBreton, and D. R. Herschbach, Rev. Sci. Instrum. 40, 1402 (1969).

20. See for example: P. W. Ryan, C. R. Blakely, M. L. Vestal, and J. H. Futrell, J. Phys. Chem. 84, 561 (1980); M. F. Jarrold, K. Birkinshaw, and D. M. Hirst, Mol. Phys. 39, 787 (1980).

21. R. M. Bilotta, F. N. Preuninger, and J. M. Farrar, J. Chem. Phys. 72, 1583 (1980).

22. W. R. Gentry, D. J. McClure, C. H. Douglas, Rev. Sci. Instrum. 46, 367 (1975).

23. E. Teloy and D. Gerlich, Chem. Phys. 4, 417 (1974).

24. W. Frobin, Ch. Schlier, K. Strein, and E. Teloy, J. Chem. Phys. 67, 5505 (1977).

25. See for example, D. Brandt, Ch. Ottinger, and J. Simonis, Ber. Bunsenges. Phys. Chem. 77, 648 (1973).
H. H. Harris and J. J. Leventhal, J. Chem. Phys. 64, 3185 (1976).
I. Kusunoki and Ch. Ottinger, J. Chem. Phys. 71, 4227 (1979).

26. W. R. Gentry, in Gas Phase Ion Chemistry, Vol. 2, Ed. M. T. Bowers (Academic Press, NY) 1979, pp. 221-297.

27. W. S. Koski, in Advances in Chemical Physics, Vol. 30, Ed. K. P. Lawley (Wiley-Interscience, NY) 1975, pp. 185-246.

28. J. M. Farrar, LBL Report, LBL-5478 (1976).

29. This is in distinct contract to the older apparatus in our laboratory which does not energy analyze at a constant potential. Since the resolution of the energy analyzer is proportional to the energy being passed, the volume element goes as E. It is necessary to divide raw data obtained with this appparatus by an additional factor of E to remove this bias.

30. R. Wolfgang and R. J. Cross, J. Chem. Phys. 73, 743 (1969).

31. W. R. Gentry, E. A. Gislason, B. H. Mahan, C.-W. Tsao, J. Chem. Phys. 49, 3058 (1968).

32. P. M. Hierl, Z. Herman, and R. Wolfgang, J. Chem. Phys. 53, 660 (1970).

33. F. S. Klein and L. Friedman, J. Chem. Phys. 41, 1789 (1964).

34. See discussion by Z. Herman and R. Wolfgang, in Ion-Molecule Reactions, Vol. 2, Ed. J. L. Franklin (Plenum Press, NY) 1972, pp. 553-599.

35. P. M. Heirl, J. Chem. Phys. 67, 4665 (1977).

36. M. Henchman, in Ion-Molecule Reactions, Vol. 1, Ed. J. L. Franklin (Plenum Press, NY) 1972, pp. 101-259.

37. Z. Herman, J. Kerstetter, T. Rose, and R. Wolfgang, Disc. Faraday Soc. 44, 12123 (1967).

38. This notation for a chemical reaction is borrowed from nuclear physics and simply implies the reaction $Ar^+ + D_2 \rightarrow ArD^+ + D$, with ArD^+ the product detected.

39. K. T. Gillen, B. H. Mahan, and J. S. Winn, J. Chem. Phys. 59, 6380 (1973).

40. E. A. Gislason, B. H. Mahan, C.-W. Tsao, and A. J. Werner, J. Chem. Phys. 50, 142 (1969).

41. R. J. Cross and R. Wolfgang, J. Chem. Phys. 35, 2002 (1961).

42. K. Lacmann and A. Henglein, Ber. Bunsenges. Phys. Chem. 69, 292 (1965).

43. M. Chiang, E. A. Gislason, B. H. Mahan, C.-W. Tsao, and A. S. Werner, J. Chem. Phys. 52, 2698 (1970).

44. L. Doverspike, R. Champion, and T. Bailey, J. Chem. Phys. 45, 4385 (1966).

45. B. H. Mahan and W. E. W. Ruska, J. Chem. Phys. 65, 5044 (1976).

46. D. R. Bates, C. J. Cook, and F. J. Smith, Proc. Phys. Soc. London 83, 49 (1964).

47. B. H. Mahan, W. E. W. Ruska, and J. S. Winn, J. Chem. Phys. 65, 3888 (1976).

48. T. F. Geoerge and R. J. Suplinskas, J. Chem. Phys. 54, 1037 (1971).

49. P. J. Kuntz, M. H. Mok, and J. C. Polanyi, J. Chem. Phys. 50, 4623 (1969).

50. P. J. Kuntz and A. C. Roach, J. Chem. Phys. 59, 6299 (1973).

51. J. C. Tully and R. K. Preston, J. Chem. Phys. 55, 562 (1971).

52. J. J. Kaufman and W. S. Koski, J. Chem. Phys. 50, 1942 (1969).

53. B. H. Mahan, J. Chem. Phys. 55, 1436 (1971).

54. R. J. Donovan and D. Husain, Chem. Rev. 70, 489 (1970).

55. B. H. Mahan, Acc. Chem. Res. 8, 55 (1975).

CHAPTER 2. EXPERIMENTAL

The apparatus used for most of the experiments described in this thesis is a crossed ion-molecular beam instrument which was designed and assembled by James M. Farrar in 1974-75. It has been previously described in some detail,[1] so the present account will be briefer and emphasize later additions and alterations.

The apparatus is quite similar to an older one which has been in use in our laboratory since the late 1960's but this one is designed to operate specifically in the low (1-20 eV) laboratory energy range. Low energy ion beams are notoriously difficult to work with as they are easily deflected by stray electric and magnetic fields and their intensity is limited because of ion-ion repulsion. Further complicating matters is the fact that the velocity of a 1 eV ion of moderate mass is about the same as the thermal velocity of an H_2 molecule. Thus, in order to limit the uncertainty in initial conditions, a crossed beam approach is necessary. By using a beam of neutrals rather than neutrals confined to a scattering cell, one loses at least an order of magnitude in product intensity.

Fig. 1 shows a schematic block diagram of the apparatus. Ions are formed, mass analyzed, and focused before colliding with a beam of neutral molecules, approaching at a 90° angle. Products are then measured for mass and energy by rotatable detector. The individual components will be described more completely in the following sections.

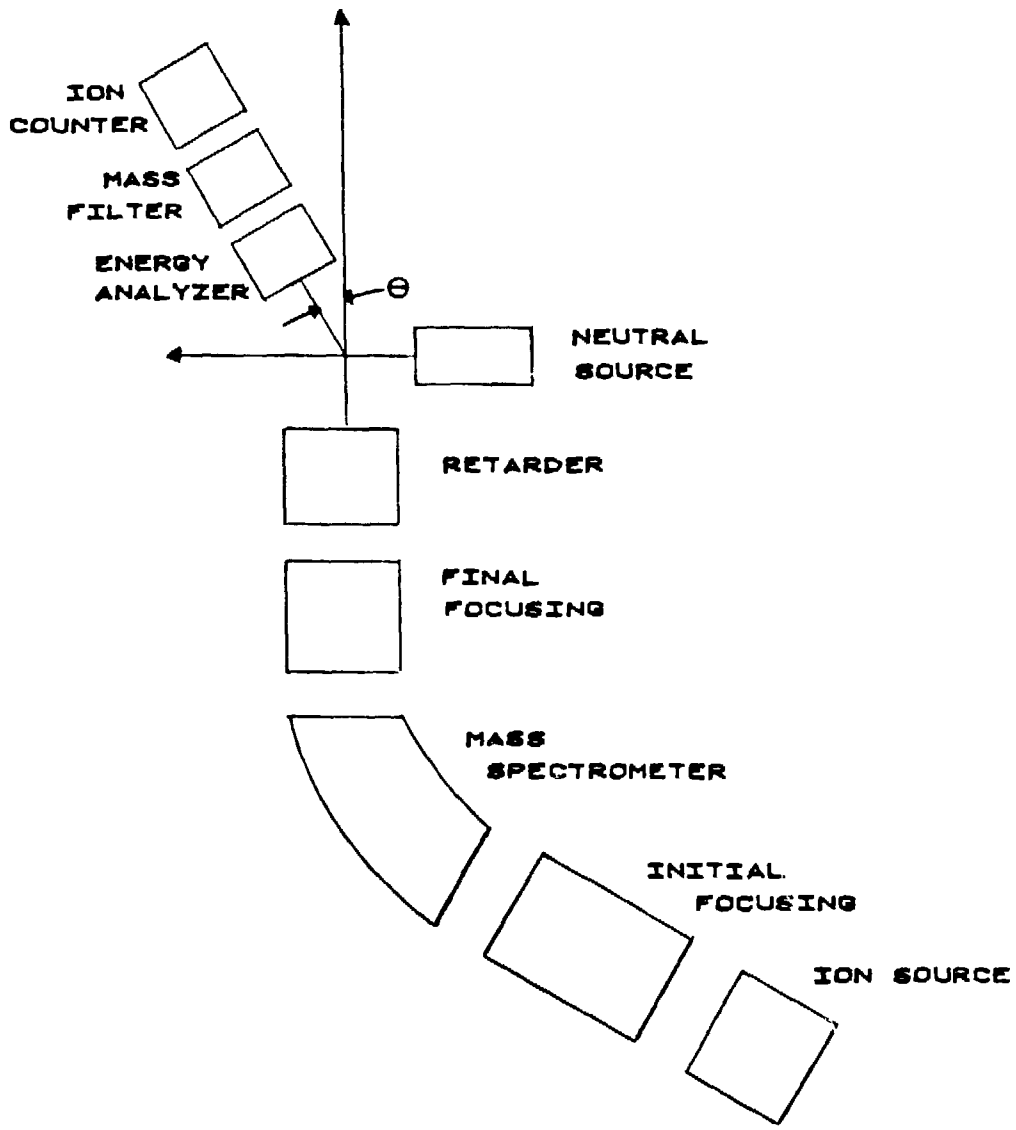

Fig. 1. Schematic diagram of the apparatus.

Ion Sources

The apparatus employs three interchangeable ion sources. The oldest of these sources creates ions in a microwave discharge and has been described previously.[2,3] This source uses a Broida cavity[4] to maintain a discharge in a 1.2 cm I.D. quartz tube at a pressure of 10^{-2}-10^{-1} torr. The discharge is initiated with a Tesla coil, and is powered by a 3 GHz commercial diathermy power supply. The cavity can be externally tuned. The plasma is confined to a 3.8 cm length of the quartz tube by a stainless steel mesh electrode and a flange which contains the 1.1 mm diameter exit aperture through which the ions are extracted. It is characteristic of microwave discharges that they have a low (~ 5 eV) electron temperature.[5] If we consider a nitrogen discharge, relatively few electrons will have enough energy (19.4 eV) to produce N^+ from N_2, and it is likely that a two step mechanism involving first N_2 dissociation and then ionization of N atoms (14.54 eV) is operative.[6] This process occurs far out on the Boltzmann tail of electron energy, but even fewer should have the extra 1.9 eV needed to produce the lowest metastable state of N^+. For this reason the microwave source can be considered a gentle ion source and it produces predominately ground state ions.

Fig. 2 shows a portion of the emission spectrum of a microwave discharge in pure N_2 as measured by an optical multichannel analyzer. $N_2^+(B \rightarrow X)$ emission can be seen in the center but lines from the second positive system ($C \rightarrow B$) of N_2 are also very prominent. Because of differences in Franck-Condon factors the N_2^+ emission is

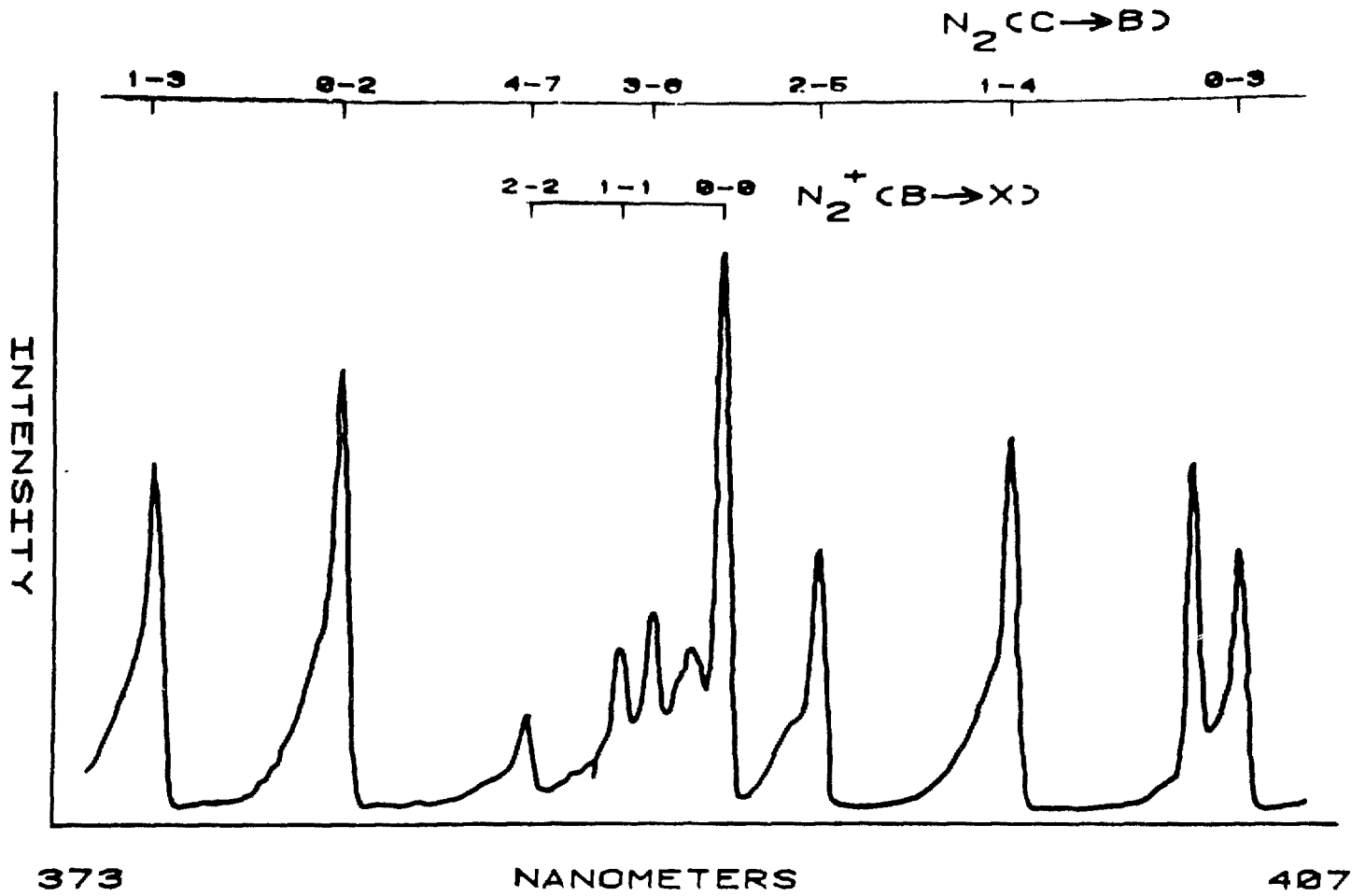

Fig. 2. Emission spectrum of N_2 in a microwave discharge.

localized while the ($C \rightarrow B$) system of the neutral molecule has a long progression of lines. Despite this, and the fact that the N_2^+ transition has a large oscillator strength, it is somewhat amazing to find the ion's emission nearly as strong as that of the neutral. It is this high ion density which makes the microwave source so attractive. Parent ion intensities, measured at the collision center, (e.g. N_2^+) range up to 2×10^{-8}A for 10 eV beams while fragment (e.g. N^+) intensities are a factor of 5 to 10 lower.

The major disadvantages of this ion source are a fairly large energy spread in the ions, an unavoidable plasma potential, and the inability to form ions from atoms with large ionization potentials. Since the apparatus does not allow for energy selection of the primary ion beam, the spread in ion energies is determined completely in the ion source. Ions formed in regions of different potential will have different energies. Fragment ions will have an additonal energy spread coming from the fragmentation process, though this effect is reduced by thermalizing collisions in the microwave source. Typical energy spreads for this source are 2 eV between beam 20% points, i.e. where the intensity is down to 20% of its maximum value, although 4 eV spreads were occasionally seen. This uncertainty in initial conditions precluded using this source in experiments at energies below 5 eV laboratory. A less serious disadvantage associated with this ion source was the constant presence of a plasma potential. Because the electrons move to the wall faster than the positive ions, there is a net charge separation,[7] and the main body of the plasma is at a positive potential relative to its

surroundings. Depending on source conditions this effect can add 10-60 eV of energy to the ions, making it necessary to float the source at negative potentials to produce low energy ions. The final disadvantage is that due to the lower electron temperature, species with high ionization potentials are difficult to ionize. Discharges in He and Ne are possible, but difficult to maintain. Gases containing F atoms such as CF_4 or NF_3 also inhibit the discharge and produce very little F^+. It was further observed that discharges containing these difficult-to-ionize atoms rapidly eroded the quartz discharge tube.

A low pressure electron impact source similar to that described by Udseth et al.[8] is also available. In this source electrons emitted from a heated strip of tungsten mesh are accelerated toward a 1.5 mm I.D. metal tube which has gas flowing from it. The mesh has 30 lines/inch with a .003" linewidth and .001" thickness. A piece 1" long and 4 lines wide will produce ~5 mA of emission current when heated with 3A D.C. The tip of the tube is kept at the nominal ion energy and the filament is biased negatively with respect to this potential. To a good approximation, ions are formed in the tube because they emerge with a small energy spread centered about the tube potential. Ions are accelerated out of the tube and through the filament mesh by the same potential difference which attracts the electrons to the tube. This potential is variable, but most experiments used 160 V. After five years of use, this source produces ion beams which are about 1.5 eV between 20% points

for fragment ions (< 1 eV for parents) with about 50% the intensity of the microwave discharge source. Its performance was somewhat better when it was new.

Because the gas is leaving a fairly large aperture and entering a chamber pumped to ~1 x 10^{-5} torr, we consider this a low pressure ion source. This fact coupled with the high electron energy employed, makes our electron impact source an efficient producer of metastable ions.

The third ion source, which has been implemented more recently than the other two, closely follows the design of Menzinger and Wahlin.[9] It is a direct current discharge source which produces ions in a plasma at 0.1 to 1 torr between a "Christmas tree" shaped 0.25 mm tungsten filament and a molybdenum anode. The source is shown schematically in Fig. 3. The anode is a molybdenum cylinder (4 cm long by 2.4 cm inner diameter) which is threaded on one end and has a 0.34 mm hole in the other end through which the ions exit. The anode is kept at the nominal ion energy and the filament is usually kept 100 V higher. The alumina pieces which fit inside the anode spatially confine the discharge. The anode screws onto a boron nitride support which provides electrical isolation. The choice of materials in the source is critical as the discharge is very hot; and the anode can often be seen glowing a dull red. The boron nitride supports screws onto a stainless steel support flange, and gas flows through them into the discharge area. The filament electrical connections are made by spot welding each end of the filament on to a 0.127 cm dia. stainless steel wire which passes snugly through a hole in the boron nitride and connects via a sleeve to another

Fig. 3. 1. Gas inlet tube.

2. Glass-metal Stupikoff feedthru.

3. Stainless steel support flange.

4. Boron nitride anode support.

5. Molybdenum anode.

6. Alumina insulators.

7. Source can.

8. Nylon insulating flange.

9. Filament.

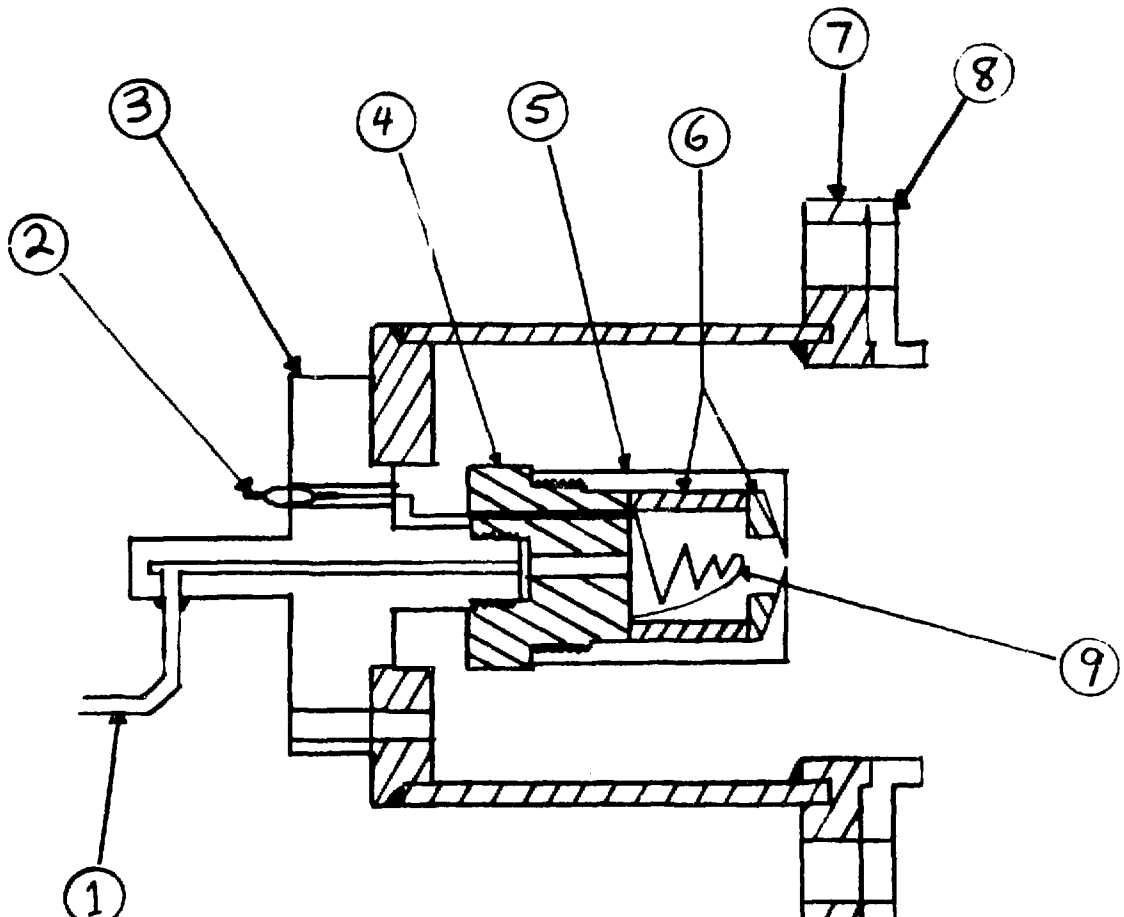

Fig. 3. Schematic diagram of the DC discharge ion source.

wire. This wire is soldered to a feedthrough in the stainless steel flange which supplies the external connection. It is usually desirable to cool the source can by blowing air on it with a fan.

Gas is leaked into the source, and current to the filament is increased until the discharge is initiated. The discharge (emission) current can be monitored by observing the current output of the filament bias power supply. With a new filament, approximately 7A of heater current is required to initiate the discharge. When the discharge begins, emission current climbs rapidly, and it is necessary to use an emission control circuit to prevent power supply destruction. The circuit used is similar to one described by Ollison et al.[10] and works by continuously adjusting the heater current to maintain the designated emission current. At high emission currents (>100 mA) filament lifetime is reduced to eight hours or less and thus lesser values are used. Ion intensity generally increases with increasing emission current except for a "resonance" which often appears near 15 mA; this is the preferred point of operation. At this low emission current, filament life can approach 100 hours. Filament failure is imminent when the heater current required to maintain the discharge has dropped to ~2A.

The design of this source makes use of the fact that a sharp potential drop occurs near the cathode while a near equipotential plasma exists near the anode. By extracting ions from this so-called "positive column" of the discharge one produces beams with an energy spread approximately equal to the thermal energy spread of the plasma. Our own experience with the source is that it produces beams with about a 1 eV spread

between 20 points, at intensities approaching those of the microwave discharge source. Because of the high pressure in the discharge, one might expect that this source produces mainly ground state ions. Our experiments tend to confirm this, but there may be some variation depending on source details.

Beam Transport System

Ions exiting the source encounter an extractor and focusing system which closely resembles the design of Gentry[11] for the older apparatus in our laboratory and is shown in Fig. 4. The beam is initially collimated by a double aperture lens and then focused by an einzel lens. The word "einzel" means single in German and is an appropriate name for this three-element lens as the first and last elements are at the same potential; focusing is accomplished by varying the potential on the middle lens, and hence the beam may be focused without changing its energy. After the einzel lens, ions are accelerated to the mass analysis potential by a grid, and the beam is then shaped for mass analysis. This is a crucial step because the magnetic mass spectrometer provides no focusing in the direction of the magnetic field, and ions with velocity components in this direction will be lost. We have employed a strong focusing electrostatic quadrupole doublet[12,13] to convert the axially symmetric beam into a ribbon-shaped beam. The first set of quadrupoles "stretches" the beam in the direction of the magnetic field, and the second set collimates the beam. After the mass spectrometer flight tube, the beam is reconverted to approximate cylindrical symmetry

Fig. 4. Block diagram showing ion lenses and attached power supplies. The ion source (which is on the left) is shown schematically. The lens system between the source and the mass spectrometer is referred to as the initial focusing state (IFS); the stage between the mass spectrometer and retarder is called the final focusing stage (FFS). This figure is adapted from Ref. 1.

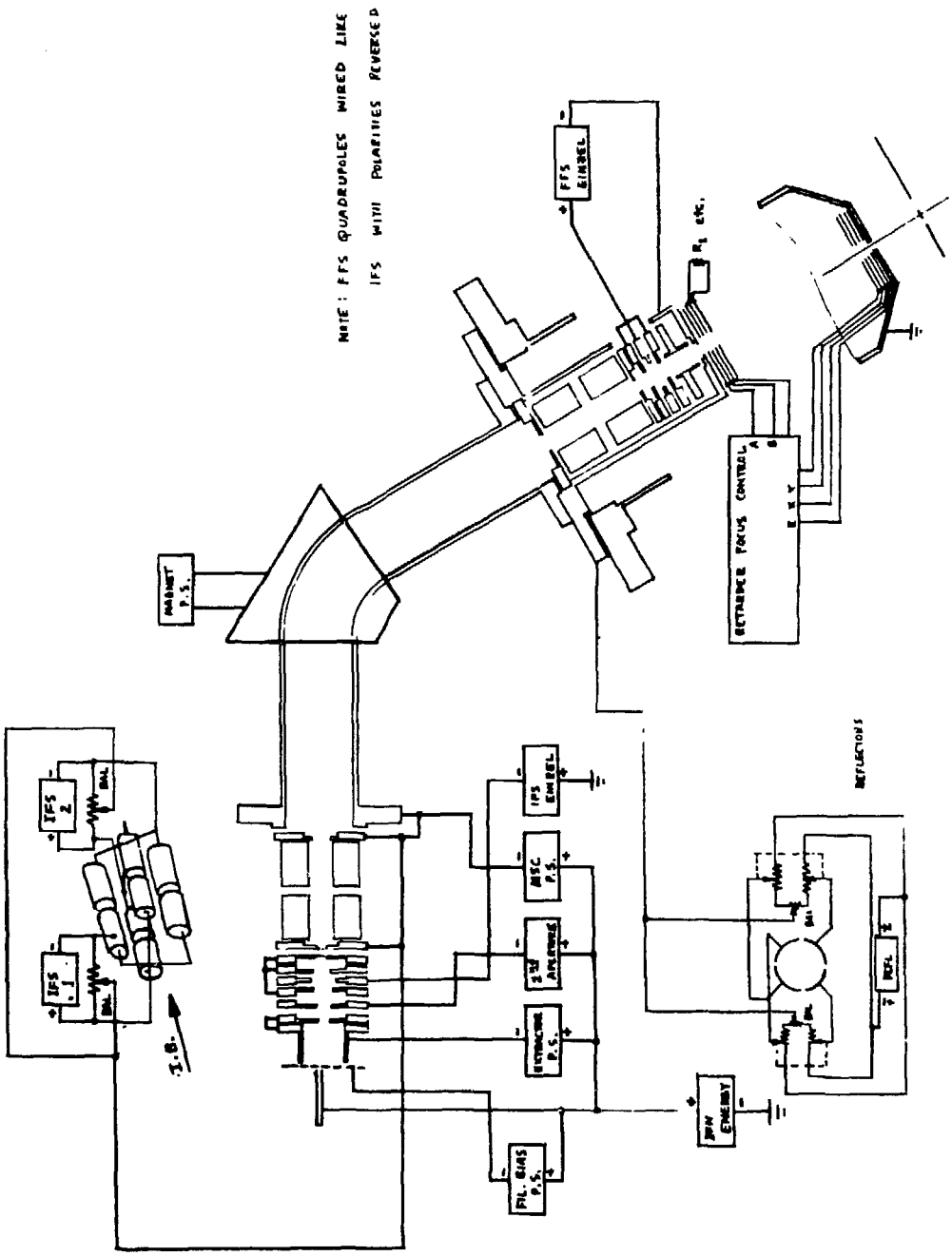
NOTE : FFS QUADRUPOLES WIRED LIKE
IFS WITH POLARITIES REVERSED
FFS EINZEL
MAGNET P.S.
EXTRACTOR FOCUS CONTROL
IFS 2
IFS 1
BAL
I.S.
IPS EINZEL
MSC P.S.
3RD APERTURE
EXTRACTOR P.S.
FIL. BIAS P.S.
ION ENERGY
REFLECTIONS
REFL

Fig. 4.

by a second quadrupole doublet. The lens elements between the ion source and the mass spectrometer flight tube are referred to as the initial focusing stage (IFS) and are located in the source chamber. This chamber is pumped by a 6" liquid nitrogen baffled oil diffusion pump which maintains a pressure of ~1 x 10^{-5} torr with the ion source on. The ion lenses themselves are made of aluminum except for the extractor and aperture lenses which, due to their proximity to the ion source, are stainless steel. All lenses are gold plated, and most surfaces which the ions view are covered with colloidal graphite (Aquadag).

The mass spectrometer consists of a 60° magnetic sector with a flight tube of radius 8 cm. The magnet itself consists of 1000 turns of 16 gauge copper wire wound in two pancake coils around mild steel cores and potted in epoxy resin. We have found to pass singly charged ions of mass M(amu) at an analysis energy E_A(eV), the required current is

$$i_m(\text{amps}) = \frac{\sqrt{ME_A}}{57} \quad . \qquad (1)$$

Typical entrance and exit slit widths are 2 mm and 1.2 mm respectively which give a resolution, $M/\Delta M$, of 48. Later versions have removed the exit slit and placed a 1 mm aperture at the entrance of the exponential retarder. With this charge, beam intensity is not significantly decreased, but mass resolution, and beam compactness is improved.

Ions exiting the mass spectrometer enter the final focusing stage (FFS) which contains aluminum lens elements similar to those in the IFS. As stated earlier the beam is reconverted to cylindrical symmetry

by a quadrupole doublet. Further focusing is supplied by another einzel lens and additional corrections are made by four deflection plates. Throughout the FFS, ions are at the mass analysis potential (~ 300 V). This relatively high energy is required to minimize intensity losses during mass selection but is much higher than the energy desired at the collision center. It is therefore necessary to decelerate the ions prior to their encounter with the neutral reactant. This could easily be done by merely placing a plate or grid at ground potential after the FFS. With the collision center at ground potential the ions would be at the energy set in the ion source. While this simple approach is used in the older apparatus in our laboratory, it was decided that the exponential retarder design of Vestal et al.[14] would be more desirable in the present apparatus.

The exponential retarder consists of 43 thin lens elements made of stainless steel, connected by an internal voltage divider. The first lens element is near the mass analysis potential and the last is at ground. The potential in between decreases exponentially allowing the ions to be slowed more gradually and preventing excessive beam divergence. The first two and last three[15] lens elements are connected to potentiometers outside of the vacuum system so that their voltages may be varied to compensate for edge effects.

As mentioned in the ion source discussion, beam intensities are high, and, furthermore, the beam is well-defined in the vicinity of collision center. The beam diameter is estimated to be 3 mm with a typical FWHM angular divergence of 2°.

The FFS and exponential retarder are located in a can which fits into the main chamber. This chamber is a ~3 ft^3 box which is pumped by a 6" liquid nitrogen baffled oil diffusion pump that maintains a pressure of ~2 x 10^{-7} torr with the neutral beam off.

Neutral Source

As alluded to earlier, it is necessary in low energy ion-molecule collisions to specify accurately the initial velocity vector of the neutral reactant as well the ion. This is best done by expanding the neutral gas through a small hole into a vacuum chamber. By doing this, one automatically has all of the neutral molecules moving in the same direction, rather than the isotropic distribution associated with a scattering cell.

The velocity distribution in the beam is determined by the details of the expansion. In the limit where the mean free path of the gas behind the hole is larger than the hole dimension, one obtains an effusive beam. Such beams possess a rather broad velocity distribution and are relatively low in intensity. This last point was actually an advantage to early experimenters who lacked the ability to pump large gas loads. Effusive beam sources have been in use since the early 1900's and in 1921 O. Stern and W. Gerlach first explicitly demonstrated space quantization using one.

If the pressure behind the nozzle is increased to the point that the mean free path is much smaller than the orifice diameter then we leave the regime of molecular flow, and hydrodynamic or viscous flow becomes

operative. The resultant beam is no longer effusive in character but is more accurately called a supersonic jet. The use of such a jet was initially suggested by Kantrowitz and Grey in 1951[16] but the first attempt to use one was unsuccessful,[17] and the technical problems associated with adequate pumping speed weren't overcome until the mid-1960's. With the present wide-spread use of high speed oil diffusion pumps, supersonic nozzle beams have become an important tool in chemical physics.

Supersonic beams possess several advantages over effusive beams. One obvious feature is that the intensity is higher; improvements of two or three orders of magnitude have been measured.[18] Another advantage is that the velocity distribution narrows, and the peak moves to higher velocities. This is a consequence of the fact that many collisions occur during the course of the expansion, and the expansion is isentropic. In an ideal case, all of the enthalpy of the gas is converted to forward translational energy.[19] The fact that energy is channeled preferentially into forward motion implies that the transverse temperature (and hence the velocity spread) will be significantly reduced. The degree to which the gas is cooled can be ascertained from the quoted Mach number (M) for the expansion. M is defined by

$$M = \frac{v}{c} \qquad (2)$$

where v is the flow velocity and c, the local speed of sound is given by the expression

$$c = \left(\frac{\gamma kT}{m}\right)^{1/2} \tag{3}$$

Here γ is the specific heat ratio C_p/C_v, k is Boltzmann's constant, T is the local temperature and m is the mass. Well designed experiments have achieved very narrow velocity distributions corresponding to M > 100 and local temperatures below 1°K.[20] While a Mach number greater than 1 implies supersonic conditions, it should be realized that large Mach numbers do not imply a tremendous increase in gas velocity. Assuming all of the enthalpy of the gas goes into forward motion we obtain

$$v_{max} = \frac{\gamma}{\gamma-1}\left(\frac{2kT}{m}\right)^{1/2} \tag{4}$$

For a diatomic gas at room temperature with a reasonably high vibrational frequency, vibration is not an active degree of freedom, and only the three translational and two rotational degrees can relax. This implies $\gamma = 7/5$ and $v_{max} = \sqrt{7kT/m}$. This value is only 87% higher than the most probably velocity in a bulk sample ($\sqrt{2kT/m}$) and 53% higher than the peak of the distribution from an effusive source ($\sqrt{3kT/m}$). Hence it is not so much an increase in flow velocity which leads to the term supersonic, but rather the drop in temperature and concomitant decrease in the local speed of sound.

The actual Mach number of the expansion is best determined by directly measuring the velocity distribution, but an empirical expression has been obtained:[20]

$$M = 1.17\ Kn_0^{-0.4} \tag{5}$$

Here Kn_0 is the Knudsen number which is defined as the ratio of the viscosity based mean free path to the nozzle diameter. Expression (5) was found to be accurate for monatomic gases and it was thought that the exponent should go as $(1-\gamma)/\gamma$ for more complex molecules. Later work with diatomic molecules demonstrated that substantial departures from both numerical parameters in (5) could be observed.[21]

In the original version of our experimental apparatus, a very rudimentary supersonic source was used. It consisted of a 0.025 mm orifice in a thin plate and a post collision center beam cather. The orifice was located 6-12 mm from the collision center and the conical beam cather was pumped by a 6" liquid nitrogen baffled oil diffusion pump. In principle such an arrangement should be sufficient for our purposes as most of the excess beam will be pumped away in the catcher chamber and the (small) angular divergence of the neutral beam is relatively unimportant. A problem existed though, in that the neutral beam was not easily chopped without greatly increasing the background pressure. The inability to modulate the beam efficiently precluded the use of phase sensitive detection and prompted us to build a more conventional source.

A drawing of this source is shown in Fig. 5. The design borrows heavily from Parson and Lee[22] for the nozzle-skimmer system but has one of its two stages of differential pumping after the collision center. The advantage of this arrangement is that the nozzle can be placed closer to the collision center thus giving higher beam intensities. The disadvantage is that the chopper sits in the main chamber and increases background pressure (and background signal) by scattering half the beam. The stainless steel nozzle consists of a 0.076 mm aperture in a thin plate. It is desirable for the wall thickness in the vicinity of the hole to be minimal so as to prevent cluster formation and numerous wall collisions during expansion. Hence the machining of the orifice plate is crucial; by grinding with a radiused wheel it is possible to make the plate thin (one or two nozzle diameters) near the orifice but still maintain structural integrity.

A 60°/70° skimmer with a 0.64 mm diameter entrance aperture allows molecules moving with small divergence angles to enter the main chamber. Molecules not moving along the center line strike the skimmer and bounce away. The fixture which maintains positive alignment between the nozzle and skimmer has large slots machined in it so that pressure will not build up in the skimmer region. This chamber is pumped by another 6" liquid nitrogen baffled oil diffusion pump, although a later modification removed the baffle thereby increasing pumping speed from ~750ℓ/sec to ~1500ℓ/sec. The alignment fixture itself keys into a precision groove in the face of the differential pumping chamber. The nozzle-skimmer distance is continuously variable from outside the vacuum

Fig. 5. 1. Beam catcher.

2. Turning-fork chopper.

3. Mu metal chopper support and shield.

4. Skimmer.

5. Nozzle.

6. Nozzle-skimmer alignment fixture.

7. Support rod for nozzle.

8. Differential pumping chamber.

9. Main chamber wall.

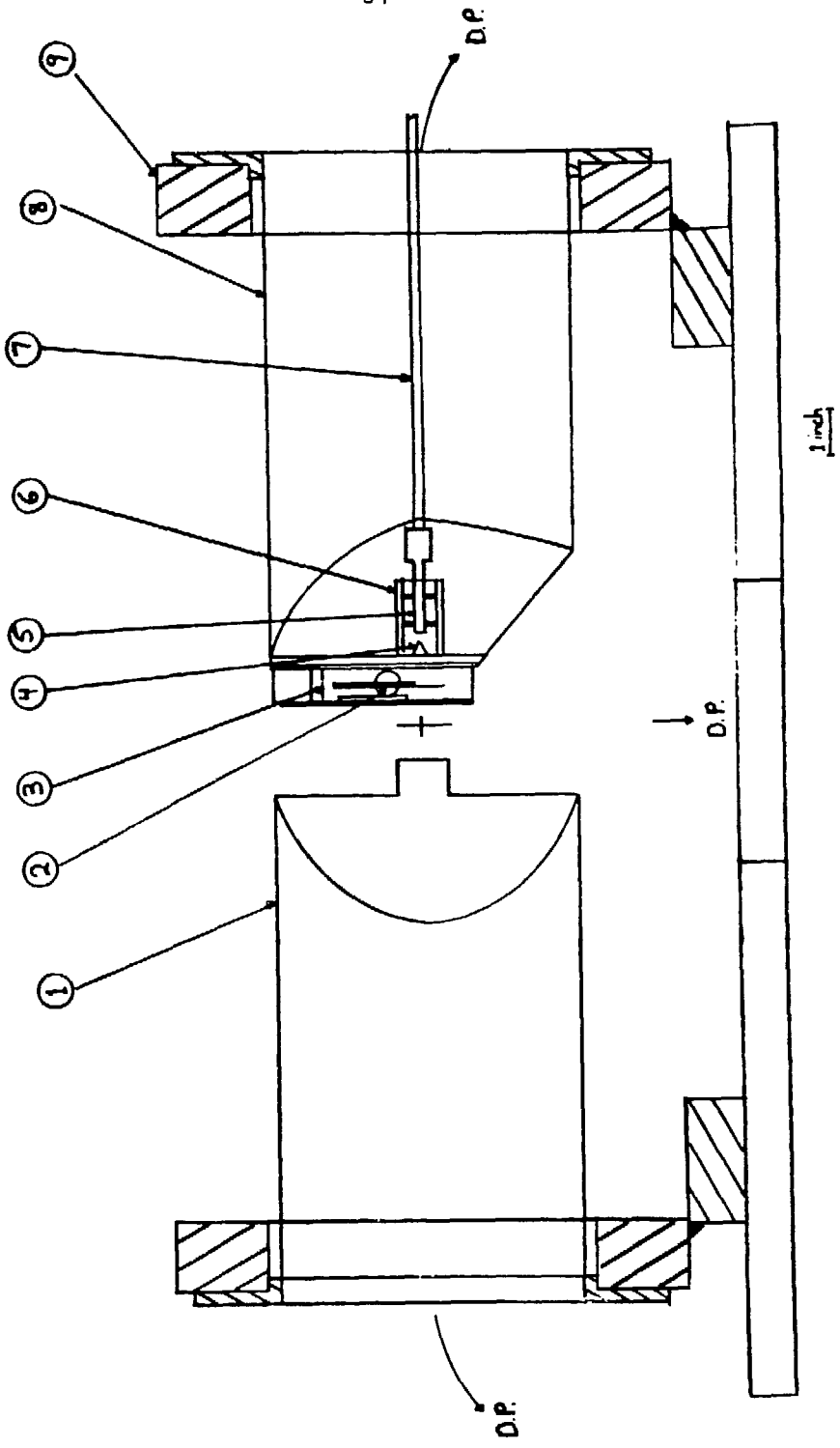

Fig. 5. The neutral beam source.

chamber by sliding the attached rod through a Wilson seal. This distance is usually kept at 4.2 mm which places the nozzle 5.1 cm from the collision center. The beam divergence angle is 4° and no further collimation is performed, resulting in a beam diameter at the collision center of 7.8mm. After the skimmer, the beam is modulated at 150 Hz by a tuning fork chopper which is housed in a mu metal box to prevent the ions from seeing stray fields. The top and bottom of the box are open to keep the pressure from building up in this area. Using dowel pins the box fits precisely into place on a block on the front face of the differential pumping chamber; the chopper position is manually adjusted until one blade obscures half the skimmer opening. After traversing the collision center, the beam enters the conical beam catcher and is pumped, as previously discussed.

The velocity distribution and flux produced by this source were not directly measured but we may estimate these properties. Parson and Lee,[22] using ethylene in a similar source, measured a Mach number of 9 at stagnation pressures of 400–700 torr. We found using H_2 in our source that backing pressures this high raised the pressure in the differential pumping chamber (DPC) to unacceptable levels. Our approximate maximum stagnation pressure was 200 torr which produced an ionization gauge-measured DPC pressure of 5×10^{-4} torr. If the efficiency of the ionization gauge for measuring H_z is taken into account,[23] the true pressure is closer to 1×10^{-3} torr. Normally, to prevent scattering of the beam between the nozzle and skimmer, and the accompanying intensity loses, one prefers to keep the DPC pressure around 1×10^{-4} torr;

however, it was decided that since hydrogen has a small hard-sphere cross section, a higher value would be acceptable. Pressures at typical operating conditions are given in Table 1.

Other beam parameters can be calculated theoretically. The mean free path (λ) for a molecule at 293°K is given by:[23]

$$\lambda\,(\text{cm}) = \frac{.06829}{P(\text{torr})d^2(\text{Å})} \tag{6}$$

where d is the molecular diameter. The viscosity determined diameter of H_2 is 2.40Å,[24] which implies at 200 torr, λ is 5.9×10^{-5}cm. As stated earlier, our nozzle diameter is 7.6×10^{-3}cm and hence the effective Knudsen number is

$$Kn_0 = \frac{\lambda}{d_{nozzle}} = 0.0078 \quad . \tag{7}$$

Using equation (5) to estimate the Mach number we obtain $M \approx 8$. The expression for the final local temperature in the beam is[25]

$$T = T_0\left[1 + \frac{\gamma-1}{2}M^2\right]^{-1} \tag{8}$$

which when calculated yields T = 22°K. The peak of the velocity distribution is given by[25]

$$v = Mv_e \frac{\gamma}{3 + \frac{3}{2}(\gamma-1)M^2}^{1/2} \tag{9}$$

Table 1

Stagnation pressure	200 torr
Differential pumping chamber (DPC) pressure	5×10^{-4} torr
DPC diffusion pump foreline pressure	0.2 torr
Main chamber pressure	5×10^{-6} torr

Typical uncorrected pressures measured with the H_2 beam on. The stagnation pressure is measured with a mechanical gauge, the chamber pressures are measured with ionization gauges and the foreline pressure is measured with thermocouple gauge.

where v_e is the most probable velocity from an effusive source at the same initial temperature. The result of this calculation is $v = 1.47\ v_e \approx 6.5kT/m$. For a completely isentropic expansion the number density on the beam axis can be taken as[26]

$$n(\frac{\text{molec.}}{\text{cc}}) = 5.22 \times 10^{15}\ P_0(\text{torr})(\frac{X}{D_0})^{-2} \quad , \qquad (10)$$

where P_0 is the stagnation pressure, X is the distance from the nozzle and D_0 is the hole diameter. The calculated number densities at the skimmer entrance and collision center are 3.4×10^{14} and 2.3×10^{12} molecules/cc, respectively. Dividing this last number by the number density at one torr (3.24×10^{16} molecules/cc) we obtain an effective "pressure" for the beam of 7.2×10^{-5} torr. Using this value we may calculate the expected signal to background ratio if we remember the beam width (0.78 cm), the main chamber pressure (5×10^{-6}torr) and estimate the reaction path length with background gas at 5 cm. The result is

$$\frac{\text{signal + background}}{\text{background}} = 3.2 \quad . \qquad (11)$$

In practice we find this ratio to be approximately 2, although both higher and lower values are expected and observed depending on the detector location in velocity space.[27]

The original design of this neutral source made allowance for an easy conversion to the more conventional double-differentially pumped configuration. This is done in the following manner. One replaces the beam catcher assembly by a blank flange, and rolls the catcher chamber and diffusion pump over to the other side of the machine. This pump now handles a new chamber which holds the skimmer and nozzle and fits inside the original DPC. The chopper and mu metal box are moved from the outside face the original DPC to the inside face. This chamber's main function now is to pump away gas scattered by the chopper. With this setup, the total gas load entering the main chamber should be quite low, thus reducing background substantially. However, the increased complexity of the source results in moving the nozzle another 3.8 cm away from the collision center. Because beam number density drops off as r^2, the total signal level would be significantly lowered. It has been our experience that even with the nozzle in the closer position, total signal levels are often marginal. For this reason, the alternate configuration has never been used.

Detector

The detector for the apparatus consists of a valvable, differentially pumped chamber, which can be rotated in laboratory angle, and contains devices for energy analyzing, mass analyzing, and counting ions. The chamber is pumped by a 75ℓ/sec ion pump (Veeco MI-75) which provides a very clean vacuum. This, coupled with the fact that the detector can be externally valved off from its surroundings, is

crucial in keeping detector components clean and in top working order. The extra pumping allows the detector to maintain a pressure one order of magnitude lower than the main chamber which reduces the probability of reactions with background gas in the detector. The normal detector background pressure is ~5 x 10^{-8} torr. The whole chamber is mounted on a rotatable lid and can be turned with relative easy by hand; the lid rotates in the plane of the crossed beams. The exact angular location of the detector can be read to 0.1° using a scribed scale; vacuum integrity in the main chamber is retained during lid motion by a differentially pumped Tec-ring.[28] A schematic drawing locating the detector relative to the other major components is given in Fig. 6. One can see that detector angular motion is limited by the neutral source and the beam catcher. The total laboratory angular range available is 27° to -12° which is sufficiently large for systems involving heavy ions and light neutrals. If necessary, the catcher chamber can be removed which leaves a 7" opening to the catcher pump; performance should not be significantly affected, but the accessible angular range greatly increases.

With the detector valved open, it is connected to the main chamber by a 3.1 mm aperture. Ions passing through this aperture immediately encounter the first lens element, which is grounded, and contains a 1 mm diameter hole. It is this small hole which defines the FWHM angular resolution to be 1.5°. Both this lens element, and the front face of the detector chamber, are heated to prevent the accretion of insulating layers which can charge up and deflect slow ions. It was observed, at

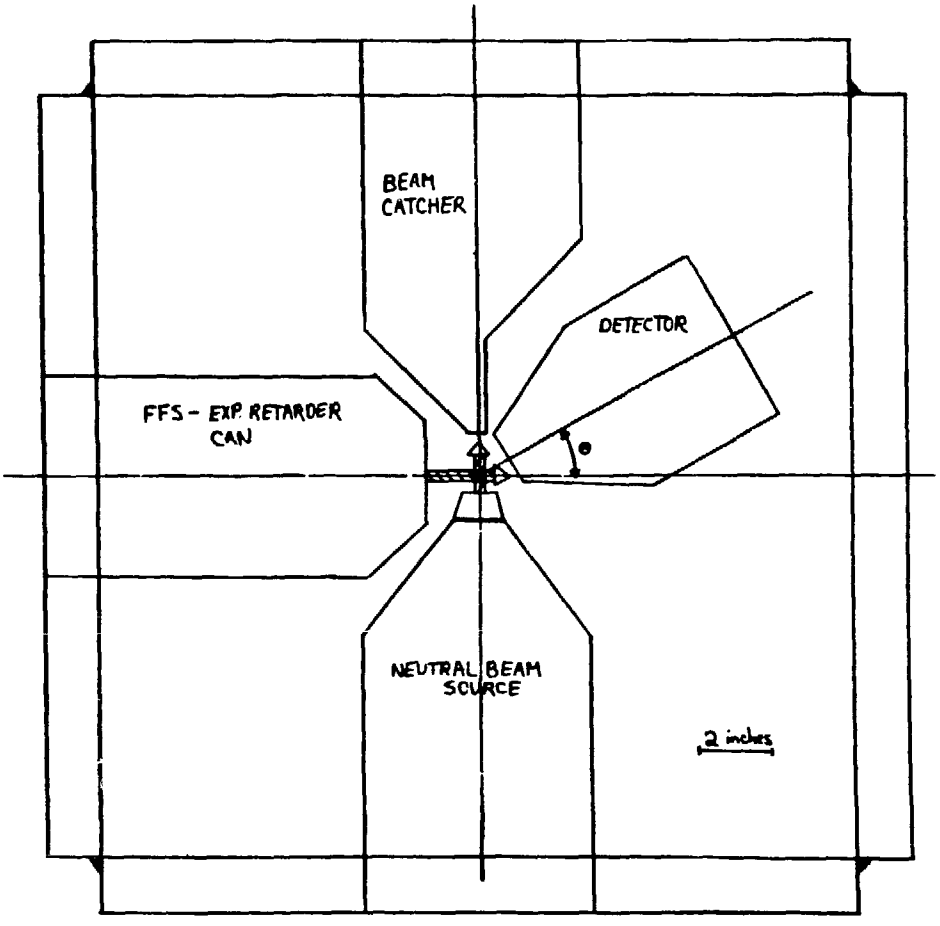

Fig. 6. Block diagram drawn to scale looking down on the collision center. The outside box represents the main chamber. The internal components are given schematically but the drawing accurately reflects the location of the walls of these components.

least in the case of the detector chamber heater, that heating to ~100°C increased the transmission of low energy (< 5 eV) ions by several orders of magnitude.

Once through the small aperture, ions are focused onto the entrance plane of the energy analyzer by the Read and field lenses. The Read lens[29,30] is a three element design with the first at ground, the second at the Read potential, and the third at the scan potential. The scan potential amounts to the centerline potential in the detector. We desire to energy analyze ions at a fixed value, say 10 eV, so that an 8 eV ion will have to be accelerated by 2 eV to pass through the energy analyzer. By setting the scan potential at -2 eV, this is accomplished. The Read voltage is varied to maximize throughtput. The field lens is effectively an einzel lens constructed from cylindrical lens elements. The first and third are kept at the scan potential and the second is varied to maximize signal.

The electrostatic spherical energy analyzer allows only ions of the desired energy to pass through. It consists of two precisely machined spherical sectors placed 1.125" apart. If different potentials are applied to the concave and convex electrodes, one finds that an ion trajectory negotiates the analyzer successfully only if it has the correct kinetic energy. For the surface radii and electrode separation used in our analyzer one calculates[1]

$$V_{EA} = 0.45E \qquad (12)$$

where V_{EA} is the electrode potential difference and E is the ion energy passed. We have found empirically though that the numerical parameter in (12) is actually 0.39.

Our spherical analyzer has an advantage over the more widely used 127° cylindrical analyzers[31] as it provides focusing in two directions while the cylindrical analyzer focuses in one; this improves ion transmission. There is also a large advantage over retarding energy analyzers where the signal has to be differentiated to obtain a velocity spectrum. With this type of analyzer one often cannot resolve weak backward scattering in the presence of strong forward scattering because the signal is lost in the noise. This problem is completely bypassed in our deflection analyzer because the higher energy ions would not successfully reach the ion counter. To further reduce background which might arise from these ions bouncing through the analyzer, the concave electrode has a slot machined in it that is covered with high transmission mesh. Undeflected ions can then exit through the back of the analyzer; a similar technique was used by Dimpfl and Mahan.[32] Although our energy analyzer deflects ions by only 90°, the resolution is very good; the magnification of the Read lens system coupled with the aperture size yields a FWHM resolution $\Delta E/E$ of 0.014. This value is generally much less than the uncertainty in initial conditions. The analyzer electrodes as well as the preanalyzer optics are made of molybdenum.

Ions exiting the energy analyzer are injected into the quadrupole mass filter (QPMF) by a Heddle lens.[33] This is a three element cylinder lens with the first element at the scan potential, the third at the QPMF potential and the second varied to maximize signal. The QPMF is usually floated at a low voltage (~-10 V) and allows only ions of the designated mass to pass through. The advantages of a QPMF over the more traditional magnetic mass spectrometer include compactness and high transmission. Our particular mass filter was built in the mid-1960's[34] and operates at lower frequencies than most modern commerical units. In spite of this drawback we have found its resolution sufficient to study weak signals one mass unit away from strong signals at masses less than 30. Above mass 30, however, adjacent channel crosstalk prohibits this practice.

Ions which have survived the trip through the energy analyzer and the QPMF deserve to be counted, and we do everything in our power to make sure that they are. Upon exiting the mass filter ions are sharply accelerated and focused by a three element cylindrical lens. The first and last lens elements are at -2 kV and the middle is at -600 V. These lens elements bring the ions into our Daly-type detector[35] which is a very efficient ion counter and works in the following manner. The ion trajectories are bent by a -25 kV potential applied to an aluminum coated stainless steel "doorknob." Upon impact, several electrons are ejected and accelerate toward an aluminum coated plastic scintillator. The thin (1000 Å) aluminum coating is grounded and the 25 kV electrons easily pass through it and into the scintillation material. Here, the

high energy electrons each produce a number of visible photons which are measured by the adjacent RCA 8575 photomultiplier tube. Even though the process started with a single ion, the resultant output from the photomultiplier tube is quite large, and can be handled by a LeCroy 321B discriminator without amplification. With the discriminator threshold set to the minimum value of 100 mV, the counting system noise is less than 0.5 cps. The output from the discriminator is sent to two identical Harshaw NE30 scalers which are gated at the chopper frequency. The chopper generates a reference sine wave which is squared by a tuned amplifier. The square wave is fed into a dual channel gate which puts out gating pulses for the Harshaw counters. Both the tuned amplifier and the dual channel gate were built by J. M. Farrar. The gating pulses are variable both in phase (relative to the chopper) and width, and in practice are varied to maximize net signal.

Wien Filter

A continuing problem in our low energy experiments is the energy spread of the primary ion beam. As often as not, it is this factor which establishes the effective lowest energy that we can perform experiments. Other workers, notably Koski's group at Johns Hopkins, use an electrostatic deflector similar to the one in our detector to energy select the primary ion beam.[36] Typical FWHM energy spreads in their apparatus are reportedly .07 eV but the resultant decrease in beam intensity precludes the use of a nozzle beam for the neutral reactant. Instead, one must use a scattering cell and much of the energy resolution

gained in the primary ion beam is lost. At the time of this writing, the lack of product intensity associated with an energy selected ion beam and crossed neutral beam is a problem which has yet to be solved.

Our first attempt to narrow the spread in our primary ion beam was to merely reduce the mass spectrometer analysis energy. A magnetic mass spectrometer is in reality a momentum analyzer. If the analysis voltage is high compared to the spread in ion energies, all ions in the analyzer will have approximately the same energy and the analyzer works as a mass selector. If, instead, the analysis energy is comparable to the energy spread, then ions of the same mass will have a range of momenta, and the analyzer works as a velocity selector. Starting with the mass spectrometer equation,

$$\frac{mv^2}{R} = qvB, \tag{13}$$

one can differentiate, rearrange, and obtain,

$$E = \frac{R\Delta E}{2\Delta R}, \tag{14}$$

where m is the mass, v is the ion's velocity, R is the radius of the mass spectrometer, q is the charge on the ion, B is the magnetic field intensity, E is the analysis energy, and ΔE is the energy spread passed by a final slit of half-width ΔR. Using the normal slit widths in our apparatus one calculates that to obtain $\Delta E = 0.5$ eV, E must be lowered

to 31 eV. Fig. 7 shows a diagram of the transmission of our mass spectrometer as a function of analysis energy. Clearly intensity falls off much too steeply for this technique to be used to velocity select the primary ions. Attempts using smaller mass spectrometer slits, which would allow the use of a higher analysis potential, were also unsuccessful.

With the failure of this method, it was decided to attempt to add a Wien filter to velocity select the primary ions. The major advantage of a Wien filter over a spherical deflector is that ions with the correct velocity emerge with their initial direction unchanged, and hence it is easier to adapt to the existing apparatus. A further advantage is that we were already in possession of a Wien filter. This filter had been used in the detector of an older apparatus in our laboratory and is described in detail by Fair.[37]

The basic idea behind the operation of a Wien filter is that the force an ion feels in a magnetic field is proportional to its velocity while the force in an electric field is not. By passing an ion between two parallel plates with an electric field pulling it one direction and a magnetic field pulling it the other, one obtains the result that a straight trajectory is velocity dependent, with

$$v = \frac{E}{B} . \tag{15}$$

Here E is the electric field and B is the magnetic field. These devices have been used successfully for years; ours incorporates a suggestion by Legler[38] and is properly called a stigmatic Wien filter. By using

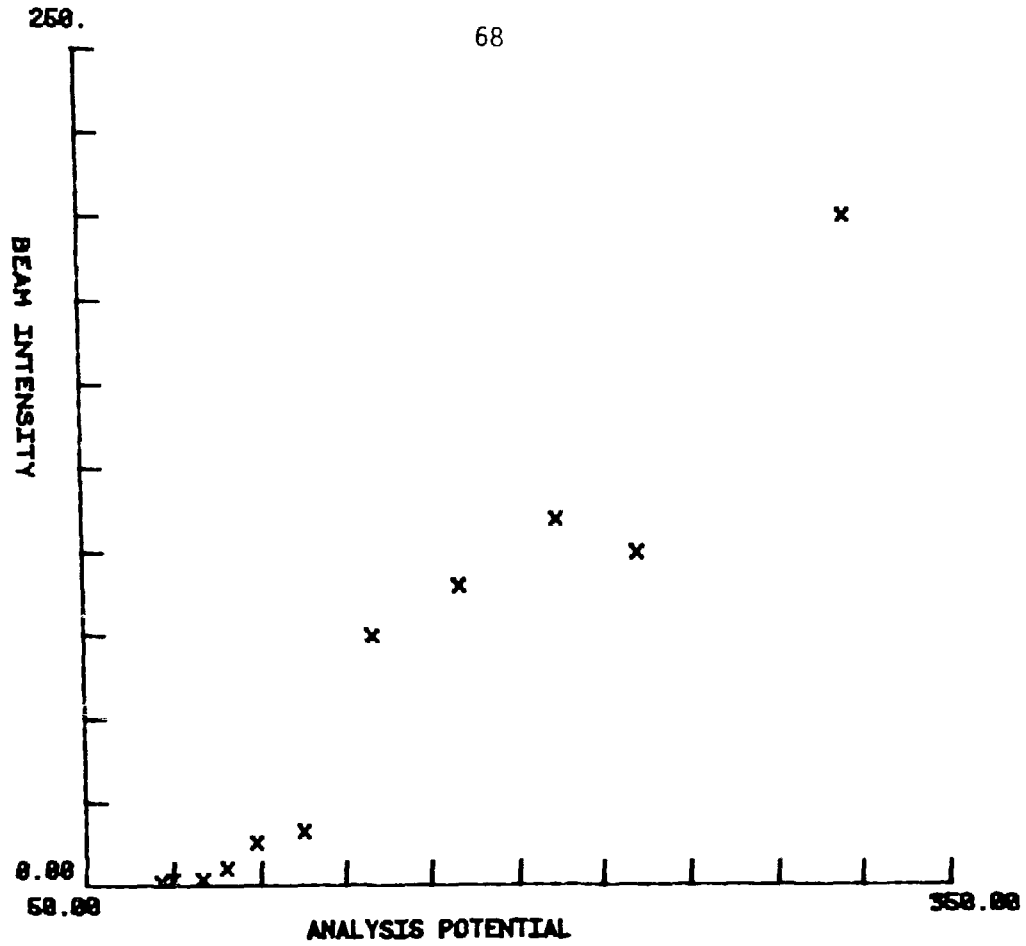

Fig. 7. Beam current measured at the collision center as a function of mass spectrometer voltage. No decrease in energy spread was observed.

curved electrodes it is possible to obtain focusing in both the x and y directions thus improving ion transmission. Unfortunately, the required conditions for optimal x and y focusing are rigorously determined mathematically.[38] One calculates that the specified ion energies while in our filter are only one or two eV, and we find at these low energies, ion transmission is very low. For this reason our normal operating point was 10–20 eV where the improvement in transmission far outstripped the losses in non-optimal y focusing.

The filter itself employs a pair of gold-plated electrodes separated by 5 mm and suspended between the poles of an electromagnet. The magnet consists of two 225 turn coils of enameled copper wire, wound around pole pieces. It was found that the maximum operating current was ~3A as higher currents generated excessive heat. This implied a maximum magnetic field of

$$B = 1.26 \frac{N(\text{turns})i(\text{amps})}{d(\text{cm})} = 567 \text{ gauss.} \qquad (16)$$

The magnet and electrode assembly reside in a mild steel box so as to prevent magnetic field leakage to other areas of the instrument. Inside the box, both before and after the electrodes, the slow ions are shielded from the magnetic field by steel tubes. The entrance slit to the filter is a 2.5mm round aperture and the exit slit is rectangular with a width of 1 mm.

The Wien filter was adapted for use in our instrument by hanging it from the far wall of the source chamber as shown in Fig. 8. The Wien assembly aligns precisely using dowel pins. It was necessary to construct an additional einzel lens assembly and a new shorter extractor to supply adequate focusing into the filter. Also a tube that fits between the source chamber and the mass spectrometer flight tube was added to extend the vacuum system. This was required to accommodate the extra length of the IFS.

An example of the performance of the filter is shown in Fig. 9. We see a substantial narrowing of the beam velocity distribution when the Wien magnetic and electric fields are turned up. It should be pointed out though, that on this particular day, the unfiltered beam was abnormally wide in energy and such a dramatic improvement was rarely observed. It was more common to start with a beam of width (distance between 20° point) 2.0 eV and use the filter to decrease it to 1.5 eV. This narrower beam was generally an order of magnitude weaker than a normal beam with the filter removed. Further narrowing of the energy spread to ~1.0 eV could be obtained, but only under more severe filtration conditions such as lower ion energy in the filter. It was always the case that these small improvements in energy spread were accompanied by large decreases in intensity; for this reason the filter was not used in any experiments described in this thesis.

As mentioned at the beginning of this discussion, the intensity problems associated with a velocity selected ion beam in a crossed beam apparatus are formidable. It is conceivable that the present apparatus

Fig. 8. 1. Ion source (electron impact source shown).

2. Extractor.

3. First aperture.

4. Second aperture.

5. Einzel lens element (side).

6. Einzel center.

7. Einzel lens element (side).

8. Support rod.

9. Wien filter assembly.

10. Insulating spacer.

11. Insulating spacer.

12. Ion source vacuum chamber.

13. Extender tube.

14. Grid #1.

15. Grid #2.

16. Quadrupole lens elements.

17. Final lens element.

18. Slit (initial).

19. Mass spectrometer flight tube.

20. Alumina rods.

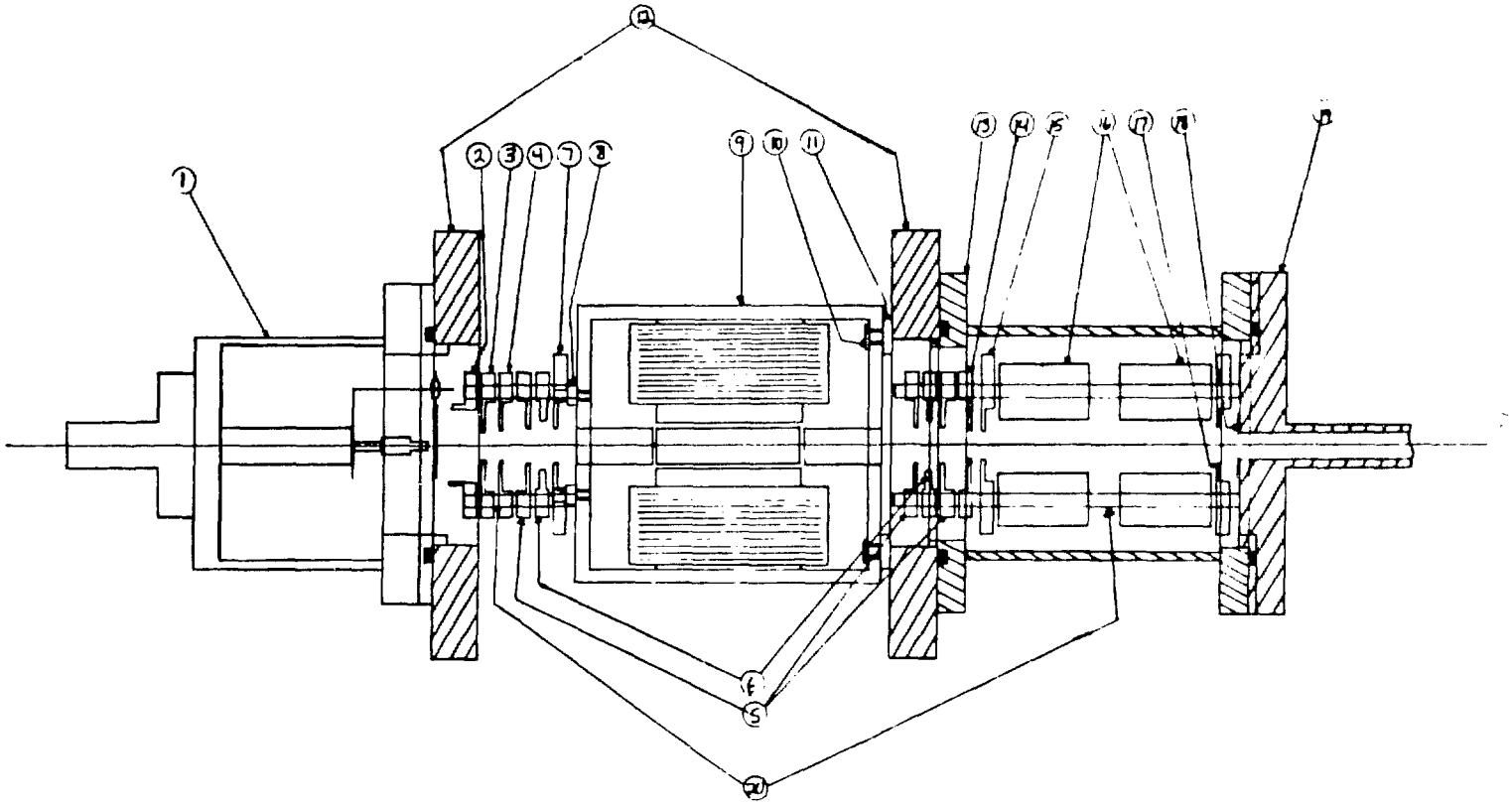

Fig. 8. Scale drawing of the initial focusing stage with the Wien filter installed.

Fig. 9. Demonstration of the potential effectiveness of the Wien filter. The plus signs indicate the beam energy distribution with the filter off, and the x's with the filter on (magnet current 3A). The FWHM energy spread of the unfiltered beam is 2.3 eV and the filtered beam is 0.8 eV wide. The distributions are normalized to the same intensity.

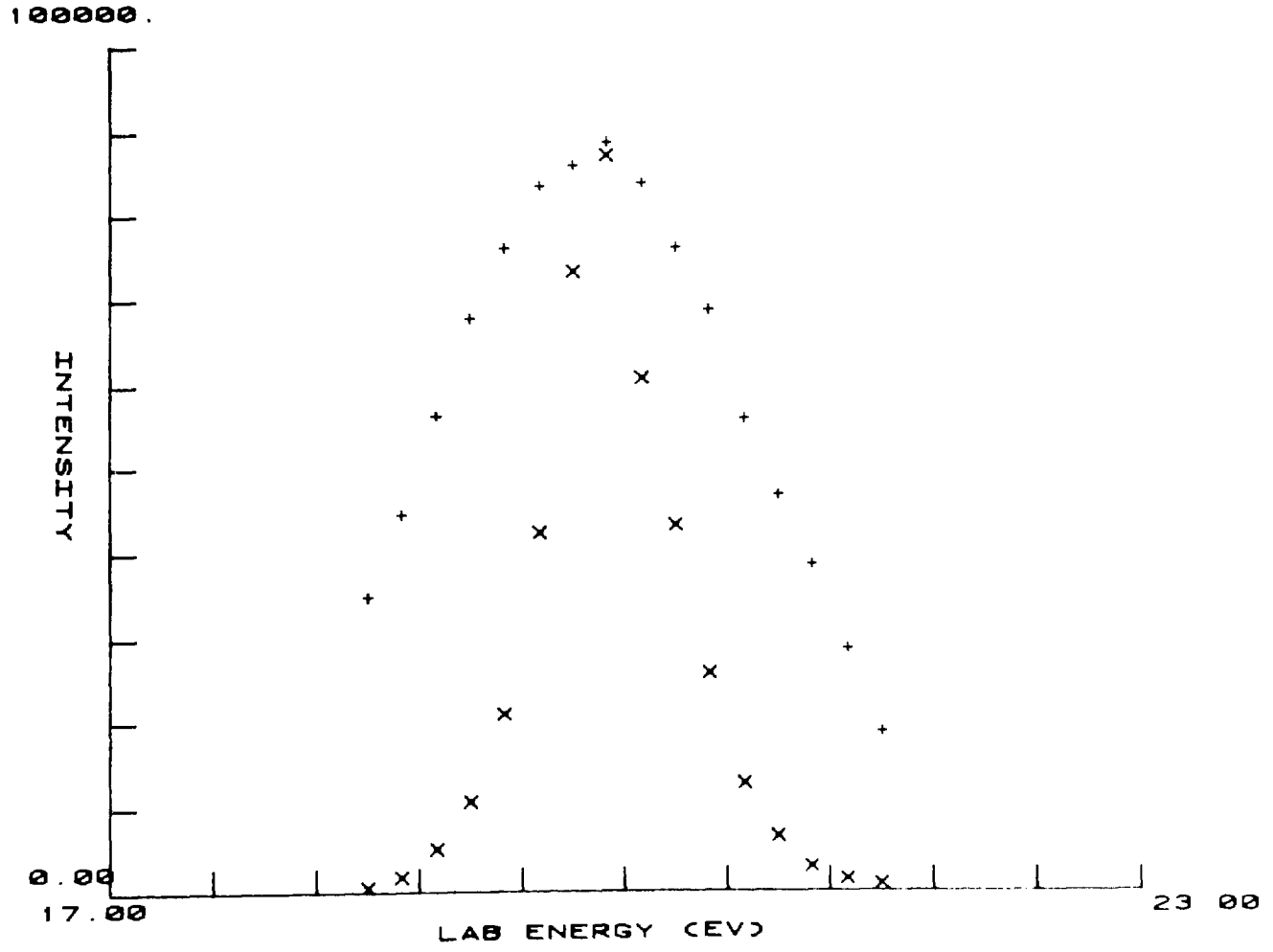

Fig. 9

with the Wien filter could be used to study large cross section processes or even less probable reactions if the neutral beam was replaced by a scattering cell. These actions are not justified at the present time, however, because the minimum observed energy spread is far from impressive and could probably only be reduced by redesigning the pre-filter ion optics, reducing slit sizes, and increasing the maximum available magnetic field.

Operation

To obtain the desired primary ion beam, the specified ion energy is set, the other lens element voltages are adjusted to their approximate optimum values, and the magnet current is varied until signal is measured on an ion collector located at the collision center. When the correct magnet setting is found, the other potentials are changed iteratively until the maximum ion current is obtained. After the beam is deemed stable, the detector valve is lifted open (this also removes the ion collector) and beam current is optimized on the detector by varying both beam transport and detector voltages. Although counting rates approaching 1 MHz can be obtained for the primary beam, it is usually kept a factor of ten lower by increasing the QPMF resolution. Typical operating conditions for the apparatus are given in Table 2.

Once the primary ion beam is stable, the neutral beam is turned on by putting gas at the desired stagnation pressure behind the nozzle. The chopper is then started and data taking can commence. A typical experiment is performed by adjusting the QPMF to pass the desired mass

Table 2

Ion Energy	10 V	
Extractor	-400	
2nd Aperture	-100	
IFS Einzel	0 or -500	
IFS Quadrupole 1	±30	
IFS Quadrupole 2	∓10	
Mass Analysis Potential	-300	Magnet 1.2A
FFS Quadrupole 1	∓20	
FFS Quadrupole 2	±30	
FFS Einzel	0 - -200 variable	
Horizontal Deflector	|variable| < 10	
Vertical Deflector	|variable| < 10	
Scan	0	
Read	0 - -70 variable	
Field	0 - -70 variable	
Energy Analyzer	3.90	
Heddle	+10	
QPMF float	-10	

The above values are typical focusing conditions for a 10 eV beam of N^+. Note that all of the voltages on the primary ion beam lenses with the exception of the two einzel potentials, are floated on the ion energy. The quadrupole and deflector voltages sit on the mass analysis potential. All of the detector lenses float on the scan potential.

and then data points are taken at various laboratory angles as viewed by the detector. Next, the energy passed by the detector is changed by altering the scan voltage, and another "cut" (angular scan) is performed. This process is repeated until a patchwork of 100-400 points, covering a suitable region of velocity space is obtained. Each point requires 5-30 seconds of counting time; signal (S) and background (B) are obtained simultaneously and displayed on two different scalers. The raw data are output to a teletype, manually punched onto cards and analyzed by a Fortran program on the LBL CDC 6600 computer. The program calculates a partially normalized Cartesian specific intensity (I) for each data point using

$$I = (S-B)\frac{\cos\theta}{(E)^{1/2}} \tag{17}$$

where θ and E are the laboratory scattering angle and energy of the data point. The $\cos\theta$ factor takes into account the detector viewing efficiency,[1] and $E^{-1/2}$ is the energy Jacobian discussed in the previous chapter. The quantity I determined by (17) is normalized in the sense that the numbers within a particular experiment are directly comparable; however, since beam intensities and the counting time are not input, there is no normalization between different experiments. A Calcomp plot locating the I values in velocity space is output, and a product contour map is obtained by drawing smooth curves through these points.

It is occasionally desirable to measure product intensity along the theoretical relative velocity vector rather than a full angular distribution. An experiment such as this requires only 20-40 points and hence longer counting times can be more conveniently used and better signal to noise ratios obtained. To perform these experiments it is necessary to know the location of the relative velocity vector. A geometrical treatment of the problem leads to

$$E = \frac{m}{2}\left(\frac{v_i}{\cos\theta + \frac{v_i}{v_n}\sin\theta}\right)^2 \qquad (18)$$

where E and m are the lab energy and mass of the product, v_i and v_n are the lab velocities of the reactant ion and neutral and θ is the lab angle with the ion beam defining 0°.

Although there are a myriad of problems, both real and imagined, which can prevent one from getting high quality data, we will mention only a few. One is an analogue to optical chromatic aberration. As discussed earlier, our mass spectrometer is really a momentum analyzer and thus ions of the same mass but with different velocities, will have different trajectories. In particular, faster ions will not be bent as much as slower ions. This velocity dependence of the laboratory angle can lead to a beam profile which is skewed in velocity space. The largest danger associaterd with this is that the skewness will not be noticed, and an experiment is performed with an unacceptable beam which wastes a lot of time. To fight the problem it is important to characterize the beam carefully and if the beam is excessively skewed,

focusing should be altered. We have found that sometimes it is helpful to change the magnet position.

Another, more pervasive problem, is one of cleanliness. Any insulating layer deposited on one of the lens surfaces can charge up to very high potentials and deflect low energy ions. The symptoms of dirty lens elements are beam instability, strong energy dependence on transmission or just plain low intensity. The location of the problem can often be pinpointed by measuring beam current on various lens elements, but the IFS is usually to blame. During constant machine use, the IFS normally has to be cleaned about every ten days. Cleaning is done by immersing the lens elements in an organic solvent and leaving them in an ultrasonic bath for ~ 1 hr. This procedure is usually sufficient to restore the apparatus to proper working order. It was originally thought that insulating layers were caused by diffusion pump oil getting around the cold baffles; however, the observation that it is the IFS that gets dirty rather than the FFS, retarder, or detector implies that the dirt comes from the ion source. In five years of operation, the exponential retarder has been cleaned only twice and neither time was their an improvement in beam performance. This indicates that contamination by pump oil is not a serious problem.

References

1. James M. Farrar, LBL Report LBL-5478 (1976).
2. M. H. Chiang, Ph.D. thesis, Univ. of California, LBL Report LBL-474 (1972).
3. M. H. Chiang, E. A. Gislason, B. H. Mahan, G. W. Tsao, and A. S. Werner, J. Phys. Chem. 75, 1426 (1971).
4. F. C. Fehsenfeld, K. M. Evenson, and H. P. Broida, Rev. Sci. Instrum. 36, 294 (1965). Our cavity is similar to their number 5 cavity.
5. D. K. Bohme and J. M. Goodings, J. Appl. Phys. 37, 4261 (1966).
6. K. T. Gillen, B. H. Mahan, and J. S. Winn, J. Chem. Phys. 58, 5373 (1973).
7. S. C. Brown, Introduction to Electrical Discharges in Gases (John Wiley and Sons, Inc., New York) 1966, Chapter 12.
8. H. Udseth, C. F. Giese, and W. R. Gentry, Phys. Rev. A 8, 2483 (1973).
9. M. Menzinger and L. Wahlin, Rev. Sci. Instrum. 40, 102 (1969).
10. W. M. Ollison, W. A. Peters, and R. J. Cross, Jr., Rev. Sci. Instrum. 47, 971 (1976).
11. W. R. Gentry, LRL Report, UCRL-17691 (1967).
12. C. F. Giese, Rev. Sci. Instrum. 30, 260 (1959).
13. C. Lu and H. E. Carr, Rev. Sci. Instrum. 33, 823 (1962).
14. M. L. Vestal, C. R. Blakely, P. W. Ryan, and J. H. Futrell, Rev. Sci. Instrum. 47, 15 (1976).

15. Actually this means the last three decelerator lens elements. After the last lens element, ions encounter an aperture in the can containing the FFS and exponential retarder which is electrically connected to ground.

16. A. Kantrowitz and J. Grey, Rev. Sci. Instrum. 22, 328 (1951).

17. G. B. Kistiakowsky and W. P. Slichter, Rev. Sci. Instrum. 22, 333 (1951).

18. N. Abuaf, Ph.D. Thesis, Princeton University (1966).

19. H. Ashkenas and F. S. Sherman, Adv. Appl. Mech. Suppl. 3, "Rarefied Gas Dynamics,", Vol. II, Ed. J. H. deLeeuw (Academic, New York) 1966, p. 84.

20. J. B. Anderson, R. P. Andres, and J. B. Fenn, in Advances in Chemical Physics, Vol. 10, Ed. J. Ross (John Wiley and Sons, New York) 1966, pp. 275-317.

21. R. J. Gordon, Y. T. Lee, and D. R. Herschbach, J. Chem. Phys. 54, 2393 (1971).

22. J. M. Parson and Y. T. Lee, J. Chem. Phys. 56, 4658 (1972).

23. S. Dushman, Scientific Foundations of Vacuum Technique, 2nd Ed., J. M. Lafferty Editor (John Wiley and Sons, N.Y.) 1962.

24. Handbook of Chemistry and Physics, 55th Ed., R. C. Weast Editor (CRC Press, Cleveland) 1974.

25. H. Pauly and J. P. Toennies in Methods of Experimental Physics, Vol. 7A, Ed. B. Bederson and W. L. Fite, (Academic Press, N.Y.) 1968.

26. C.-Y. Ng, Ph.D. Thesis, University of California, LBL Report LBL-5439 (1976).

27. Because signal associated with the beam is distributed symmetrically about the relative velocity vector and the background is symmetric with respect to the ion beam's velocity vector, S/N will be quite a bit better on the "neutral beam side" of the Newton diagram. Values of 20 or more have sometimes been measured.

28. D. E. Armstrong and N. Blais, Rev. Sci. Instrum. 34, 440 (1963).

29. R. E. Imhof and F. H. Read, J. Phys. E: Sci. Instrum. 1, 859 (1968).

30. F. H. Read, J. Phys. E: Sci Instrum. 2, 679 (1969).

31. P. Marmet and L. Kerwin, Can. J. Phys. 38, 787 (1960).

32. W. L. Dimpfl and B. H. Mahan, J. Chem. Phys. 60, 3238 (1974).

33. D. W. O. Heddle, J. Phys. E.: Sci. Instrum. 2, 1046 (1969).

34. K. R. Wilson, Lawrence Radiation Laboratory Report, UCRL-11605 (1964).

35. N. R. Daly, Rev. Sci. Instrum. 31, 264 (1960).

36. K. Wendell, C. A. Jones, J. J. Kaufman, and W. S. Koski, J. Chem. Phys. 63, 750 (1975).

37. J. A. Fair, Ph.D. thesis, Univ. of California, LBL Report LBL-3178 (1974).

38. W. Legler, Z. Physik 171, 424 (1963).

CHAPTER 3. $N^+ - H_2$ INTERACTIONS

Introduction

The reaction of a light atomic ion with H_2 gives the worker an excellent opportunity to compare experimental results with theoretical models for chemical reactions. While it is the inherent simplicity of these systems which makes them so attractive, the reaction of N^+ with H_2 has certain complicating factors which further boost one's interest. More specifically, there are a number of low-lying potential energy surfaces whose effects on a reactive trajectory are not readily predictable. The study of N^+-H_2 interactions should be helpful in understanding these effects.

Due to low abundances, N^+-H_2 interactions are not very important in flames or the atmosphere. It should be mentioned, however, that the reactions

$$N^+ + H_2 \rightarrow NH^+ + H \qquad (1)$$

$$N^+ + H_2 \rightarrow NH_2^+ + h\nu \qquad (2)$$

are potentially important to astrophysicists. H_2 is the most abundant interstellar molecule and NH^+ is thought to play an important role in the chemistry of outer space.[1] The radiative association reaction may be even more interesting than reaction (1) overall. Such processes are difficult to study because of their low cross sections, but the related radiative association reaction

$$C^+ + H_2 \rightarrow CH_2^+ + h\nu \qquad (3)$$

has been discussed by astrophysicists,[2] and has a calculated rate constant of $\sim 10^{-14}$ cm^3/sec.[3] There are a number of similarities between the potential surfaces involved in reactions (2) and (3) and there is some experimental evidence for the occurrence of both. In an experiment where a beam of N^+ was directed into a cell of H_2, visible luminescence, which was best assigned as a transition in NH_2^+, was observed.[4] The emission was very weak, with a cross section similar to that predicted for reaction (3). Our own unsuccessful search for reaction (2) is discussed later and we now direct our attention to reaction (1).

The transfer of an H atom from H_2 to N^+ was first studied in 1967 by the NOAA group using the flowing-afterglow technique.[5] They measured a thermal rate constant at 300° of 5.6×10^{-10} cm^3/sec. This value is only about 1/3 of the calculated collisional rate, and hence the reaction is slow compared to most ion-molecule reactions. The reluctance of reaction (1) to proceed has been confirmed via ion cyclotron resonance[6] (ICR) and the newly developed selected ion flow tube[7] (SIFT) technique which give values of 4.8×10^{-10} cm^3/sec and 6.2×10^{-10} cm^3/sec, respectively. The reason for the slowness of reaction (1) might be that the reaction is slightly ($0 < \Delta H < .05$eV) endothermic. Further discussion of the energetics is given later.

Reaction (1) has been studied at higher collision energies using the ion-beam technique. In 1972, Gislason et al.[8] measured product velocity vector distributions for NH^+ at initial N^+-H_2 relative collision

energies of 2.5–6.1 eV. They observed that NH^+ was predominately forward scattered[9] and that maximum product intensity occurred at a velocity slightly less than that predicted by the spectator stripping model. Since the NH^+ distribution was asymmetric in the barycentric frame, they concluded that in this energy range any NH_2^+ intermediate formed was very short-lived, and, therefore, the reaction mechanism was direct. It was further deduced by studying the peak of the product distribution as a function of collision energy, that NH^+ emerged predominantely in the $^4\Sigma^-$ state which lies ~.06 eV[10] above the $^2\Pi$ ground state.

The next ion-beam study appeared in 1974 and extended to slightly lower energies.[11] Here HD was used instead of H_2 and velocity distributions were measured in the direction of the primary ion beam for both NH^+ and ND^+ products. At energies about 2.36 eV the product distributions peaked near spectator stripping in agreement with Ref. 8, but at 1.15 eV the NH^+ distribution was almost bimodal in character. At this energy, the peak was still at the spectator stripping velocity, but there was a distinct broadening near the center-of-mass velocity. The authors also reported that an experiment at 0.5 eV relative energy yielded a product distribution peaked at the center-of-mass. Almost simultaneously the results of Fair and Mahan were published.[12] In this study, full angular product distributions were measured and increasing symmetry (with respect to the center-of-mass) of these distributions with decreasing initial energy was also observed. At 0.79 eV, which was the lowest energy studied, product intensity was

peaked at the center-of-mass and possessed sufficient forward-backward symmetry that the authors concluded the reaction was proceeding through a long-lived complex.

The fact that a long-lived NH_2^+ intermediate is involved was not surprising because NH_2^+ lies over 6 eV below the reaction's asymptotes; however, the energy dependence of the complex formation was unexpected. The analogous reaction

$$C^+ + H_2 \rightarrow CH^+ + H, \qquad (4)$$

shows considerable symmetry in its product distribution at collision energies as high as 3.5 eV though possessing a potential energy well only 4.4. eV deep.[13] The slightly more complex reaction,

$$O_2^+ + D_2 \rightarrow O_2D^+ + D, \qquad (5)$$

yields a symmetric distribution at energies below 5 eV although $D_2O_2^+$ is only 4.3 eV below the products.[14] In reaction (5) a truly long-lived complex lasting at least several rotational periods is thought to exist, while in (4) an "osculating" complex lasting about one rotational period was proposed. In light of the very deep well associated with NH_2^+, it came as some surprise that the initial collision energy had to drop below 2 eV before substantial complex formation was suggested by the product distributions. An explanation was proposed by Fair and Mahan.[12] By constructing an electronic state

correlation diagram for the low-lying potential energy surfaces of the $(N\text{-}H_2)^+$ system it was seen that the deep well might not be easily accessed. The only low energy, adiabatic pathway to ground state $NH_2^+(^3B_1)$ involved an avoided crossing between two surfaces in C_s symmetry. It was not possible to estimate how important diabatic behavior (surface hopping) might be, but it was certain to become more important as the collision energy was raised. The explanation then, was that as the energy increased above 2 eV, fewer trajectories sampled the deep well, and hence fewer reactive events involved a long-lived complex. A more detailed discussion of the reaction dynamics is given later.

As alluded to earlier, Ottinger and co-workers have put considerable effort into observing luminescence from $N^+\text{-}H_2$ collisions.[15-17] This is, of course, a very powerful technique because the results yield detailed information about the internal state distribution of any reaction products. A major disadvantage, however, is that no information is gained about states which do not readily emit in the visible or near uv. Since the expected reaction products are either $NH^+(^4\Sigma^-)$ or $NH^+(^2\Pi)$, neither of which fluoresce, little if any emission should be seen. Indeed, the observed chemiluminescence cross section is very low, about 10^4 times less than if propane is used as the target gas.[15] The dominant emission band seen can be assigned as

$$NH(A^3\Pi) \rightarrow NH(X^3\Sigma^-) + h\nu.$$

The reaction between $N^+(^3P)$ and H_2 to form NH(A), requires several surface hopping which would explain its low cross section. Furthermore, the fact that the cross section peaks at 17 eV relative energy, and emission is not even observable below ~7 eV[16] should be taken as support for the validity of adiabatic correlations at low energies. It was possible for Kusunoki and Ottinger to glean some dynamical information from their experiments. Since the emission cross section maximized at 17 eV, the reaction to form NH(A) does not occur via a spectator stripping mechanism.[17] A simple stripping event cannot yield bound NH(A) at initial energies above 10.4 eV. Hence, some mechanism which gives NH(A) the ability to assimilate excess energy into translation must be operative. This is in sharp contrast to the reaction to form NH^+. It was found in higher energy studies of reaction (1) that there was a significant decrease in the cross section when the energy was raised past the limit for NH^+ to be stable when formed by stripping.[18]

The related reaction

$$N + D_2^+ \rightarrow ND^+ + D \qquad (6)$$

has also been studied. Using the merged beam technique, Gentry and co-workers[19] examined this reaction in the 0.03-10.1 eV initial relative energy range. Asymmetry in the product velocity distribution indicated that throughout this energy range, the reaction is direct. By

using a correlation diagram argument similar to that of Fair and Mahan, it was concluded that the reaction proceeded via a collinear approach on the $^5\Sigma^-$ surface. Since there is not expected to be any large decrease in the potential energy as the $(N\text{-}H\text{-}H)^+$ intermediate is formed, the result that the reaction is direct is easily understood. Subsequent ab initio calculations of the quintet surfaces have confirmed this explanation.[20]

Reaction Energetics

The energetics of

$$N^+ + H_2 \rightarrow NH^+ + H \qquad (1)$$

can be the source of some confusion. One recent study[7] of this reaction states that it is exothermic by 0.7 eV, which is contrary to previous estimates that it is approximately thermoneutral. The source of these problems is the uncertainty in the ionization potential of NH and the dissociation energy of NH^+. The experimental value of I.P.(NH) is 13.1 eV as measured by two groups.[21,22] This quantity is not easily measured experimentally, as any method used to produce NH radicals may produce them with internal excitation. Subsequent ionization of these radicals can give a lower ionization potential than if they were internally cold. Although accurate values have been measured using the pulsed discharge technique of Foner and Hudsen,[22] it appears they have underestimated the value for NH.

Modern ab initio calculations are quite accurate and in a recently published reference book on diatomic molecules,[10] an ab initio value is quoted. This value, 13.63 eV, was obtained in 1970 by Liu and Verhaegen[23] but is probably not the best value available. 13.63 eV is greater than the ionization potential of the H atom (13.595 eV) and hence the reaction

$$N^+ + H_2 \rightarrow NH + H^+ \qquad (7)$$

would be more exothermic (or less endothermic) than (1). Not only would $NH + H^+$ be favored energetically, but the lowest $^3\Sigma^-$ potential surfaces in both $C_{\infty v}$ and $D_{\infty h}$ symmetries would then adiabatically correlate to these products. Since reaction (7) has, to our knowledge, never been observed at low energies, it seems likely that I.P.(NH) < I.P.(H). More recent calculations support this assertion. A 1971 SCF calculation which used an empirical correction for correlation energy gave I.P.(NH) = 13.47 eV.[24] Probably the best value available is that obtained by Rosmus and Meyer[25] using the pseudonatural orbital-configuration interaction technique (PNO-CI). Their answer, I.P.(NH) = 13.5 ±.1 eV, places the $NH^+ + H$ asymptote about 0.1 eV below $NH + H^+$.

Further problems arise when considering the bond energy of NH^+. As can be seen in Fig. 1, the $^2\Pi$ state which lies only about .06 eV below the $^4\Sigma^-$ state, does not adiabatically dissociate to the lowest asymptotic products. This fact, combined with possible interference

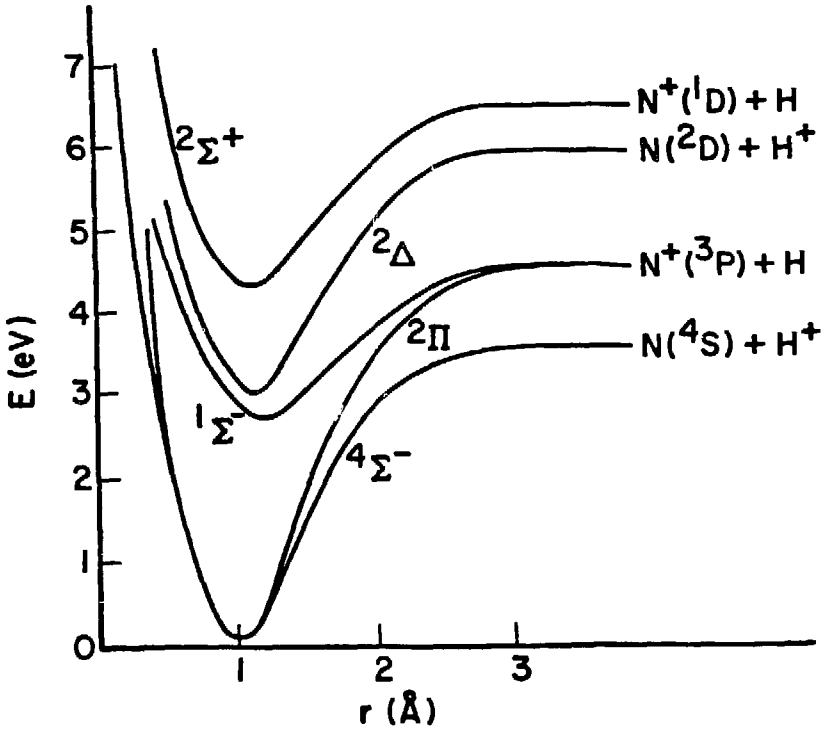

Fig. 1. Qualitative potential curves for the lowest states of NH^+. The figure is adapted from Ref. 8.

from the quartet state, might make direct experimental measurement of $D_0(NH^+)$ difficult. Indeed, the only experimental value available,[26] 3.7 ± .4 eV, is not of much help. The best theoretical work,[25] says that $NH^+(^2\Pi)$ is 3.50 ± .05 eV below $N(^4S) + H^+$ and seems much more dependable. The $N^+(^3P) + H$ asymptote is 0.95 eV (I.P.(N) - I.P.(H)) higher and we conclude that the bond energy of $NH^+(^2\Pi)$ is 4.45 eV. Since $D_0(H_2) = 4.478$ eV[10], one calculates for reaction (1) that

$$\Delta H = D_0(H_2) - D_0(NH^+) = .03 \text{ eV}.$$

This number is in good agreement with another ab initio study[27] which places $NH^+(^4\Sigma^-) + H$ .05 eV above $N^+(^3P) + H_2$, and hence $NH^+(^2\Pi) + H$ would be about .01 eV below. In light of these results, we conclude that the reaction is essentially thermoneutral.

Results

The cross section for the formation of NH^+ from $N^+ - H_2$ collisions is not particularly large. A typical maximum counting rate of net NH^+ signal was about 25 counts/sec. In contrast, it was quite easy to measure 5000 counts/sec N_2H^+ resulting from N_2^+–H_2 collisions. Part of this difference stems from the fact than N_2^+ beams were about 5 times more intense than N^+ beams, and the N_2H^+ was confined to a smaller laboratory angular region, but clearly NH^+ is formed with a lower cross section.

As mentioned in the introduction to this chapter, reaction (1) has been previously studied throughout a wide energy range. Our interest in the reaction was at low energies, where the chemical forces are most important. The work reported here has some overlap with earlier studies but improves on it or adds to it in several important ways.

All of the previous ion-beam work used a beam-scattering cell arrangement while in our experiments the crossed beam technique was used. This distinction can be important at low collision energies where the random orientation of the H_2 velocity vectors will smear the initial and hence final velocity distributions. Using a chart given by Chantry,[28] one obtains that this Doppler broadening induces a FWHM of ~0.5 eV in the initial center-of-mass energy distribution at 1 eV relative collision energy. By using a supersonic expansion to introduce the neutral reactant, the effective temperature of the neutral is decreased by at least a factor of 10 (see Chapter 2), which gives a concomitant increase in experimental resolution.

Another improvement over previous studies is the greater care we have taken to investigate the electronic state population of the N^+ beam. All of the previous studies used high energy electron impact on N_2 to produce N^+ beams. It is well-known that this form of ionization can produce an abundance of electronically excited metastable ions and that these ions may differ appreciably from the ground state in their chemical properties. By employing our three different ion sources, we could vary the fraction of metastable N^+ in our experiments. The relative populations of the states produced by these sources is discussed

in Chapter 6 and summarized in Table 1. The most important result in Table 1 is that the discharge sources produce beams which are nearly pure $N^+(^3P)$. Without a doubt, N^+ beams from these sources are more purely ground state than those of any previous study, and hence experiments with these ions will better reflect the chemistry of $N^+(^3P)$.

The final and perhaps most important addition we have made to the study of N^+-H_2 interactions is to map the velocity vector distribution of N^+ which has bounced off H_2 non-reactively. Our non-reactive results turn out to be quite helpful in understanding some of the features of the N^+-H_2 system.

$N^+(^3P)$: Reactive Scattering

More than 10 complete contour maps of the velocity vector distribution of NH^+ formed by $N^+(^3P)$-H_2 collisions were obtained. The microwave discharge source was preferred for these experiments because it could be counted on to produce > 90% $N^+(^3P)$ while the DC discharge source was less dependable in this regard.

Fig. 2 shows the NH^+ distribution obtained at 0.72 eV relative energy with the N^+ extracted from a microwave discharge in N_2. The distribution is, within experimental error, symmetric with respect to the $\pm 90^\circ$ axis. This forward-backward symmetry is consistent with a map published previously at 0.79 eV[12] and can be taken as support for the existence of a long-lived NH_2^+ intermediate.

Table 1

State	Appearance (eV) Potential	Microwave Discharge	DC Discharge	160 eV Electron Impact
N_2^{++}	42.7	0	0	~ .10
$N^+(^5S)$	30.1	0	0	~ .40
$N^+(^1S)$	28.4	0	0	~ 0
$N^+(^1D)$	26.2	.08	.09	~ .10
$N^+(^3P)$	24.3	.92	.91	~ .40

Estimated fraction of $\frac{m}{e} = 14$ species emanating from the three ion sources. For further discussion see Chapter 6. Note that for the electron impact source these are only crude estimates.

Fig. 2 Contour map of the intensity (Cartesian flux) of NH^+ resulting from N^+-H_2 collisions at an initial relative energy of 0.72 eV (5.30 eV lab). The large cross denotes the origin which is the laboratory center-of-mass velocity and 0° is the initial direction of the N^+ projectile in center-of-mass coordinates. The dot denotes the location of the primary beam and the 20% profile locates the contour where beam intensity is down to 20% of its maximum. N^+ was produced in a microwave discharge through N_2.

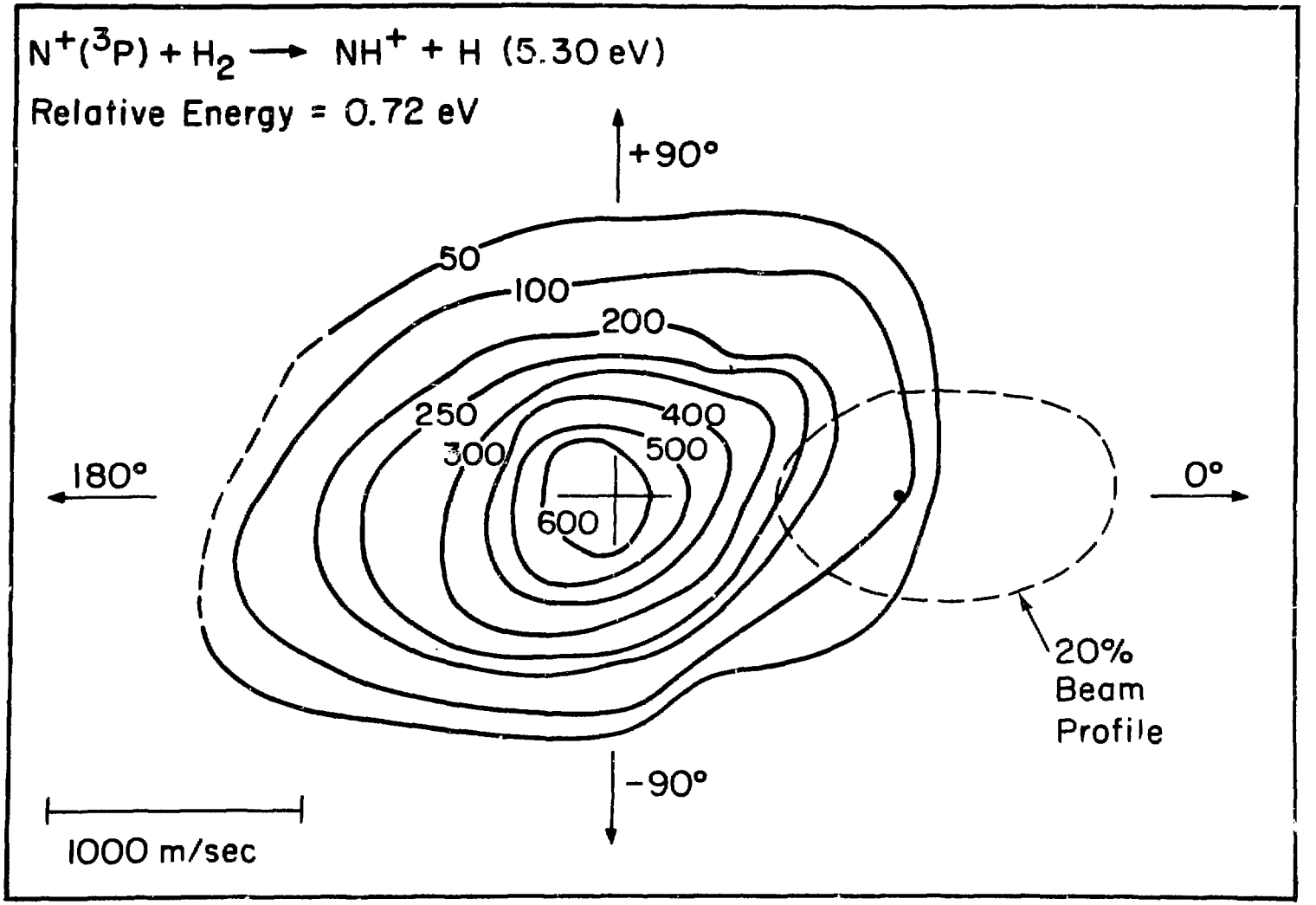
$N^+(^3P) + H_2 \longrightarrow NH^+ + H$ (5.30 eV)
Relative Energy = 0.72 eV
+90°
50
100
200
250
300
400
500
600
180°
0°
20%
Beam
Profile
-90°
1000 m/sec

Fig. 2

Fig. 3. The intensity distribution of NH^+ formed in N^+-H_2 collisions at an initial relative energy of 0.98 eV. N^+ was extracted from a DC discharge in N_2.

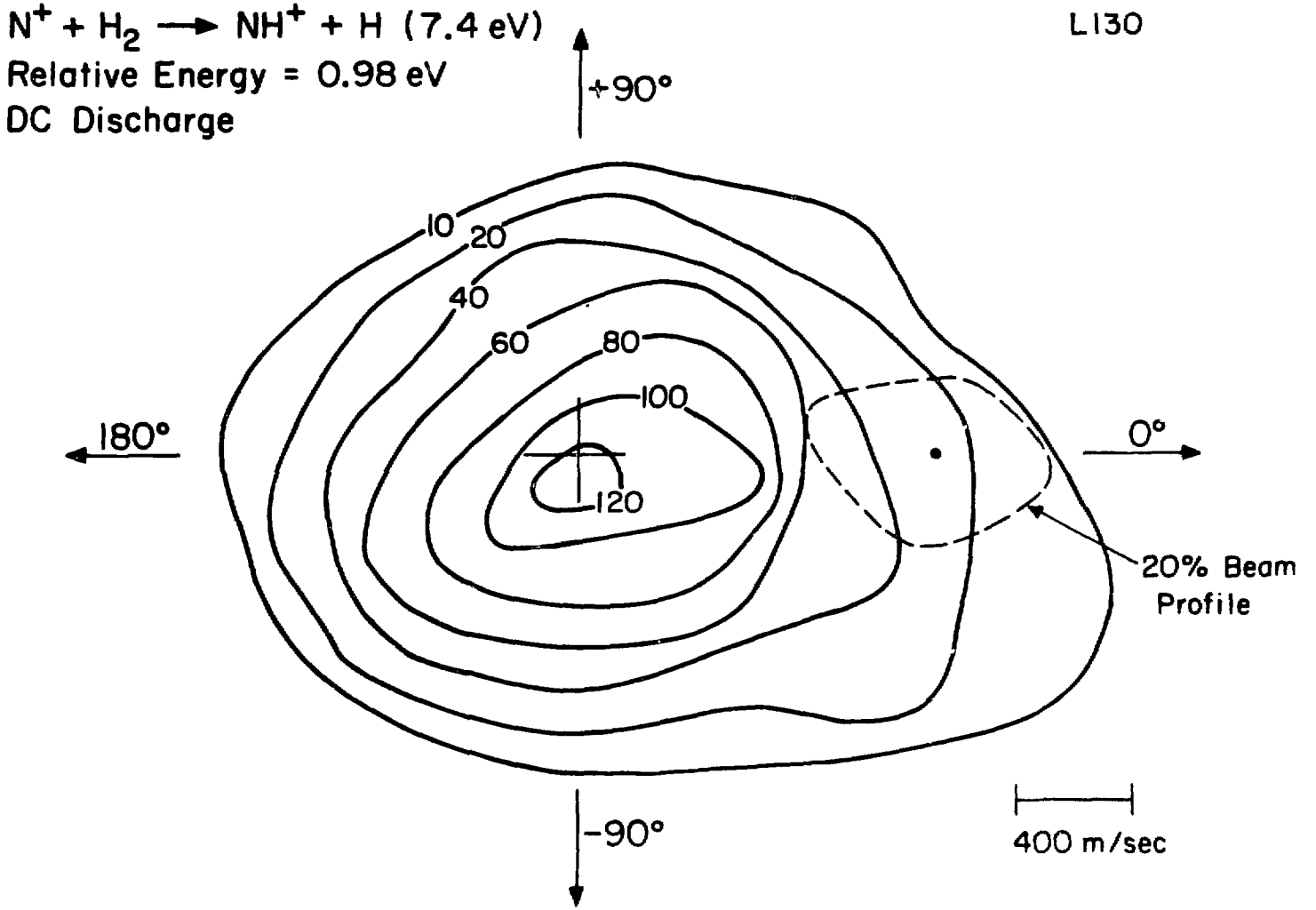
$N^+ + H_2 \longrightarrow NH^+ + H$ (7.4 eV)
Relative Energy = 0.98 eV
DC Discharge
L130
+90°
10
20
40
60
80
100
120
180°
0°
20% Beam Profile
-90°
400 m/sec

Fig. 3

Fig. 4. The intensity distribution of NH^+ formed in N^+-H_2 collisions at an initial relative energy of 1.36 eV. N^+ in Figs. 4-8 was extracted from a microwave discharge in N_2.

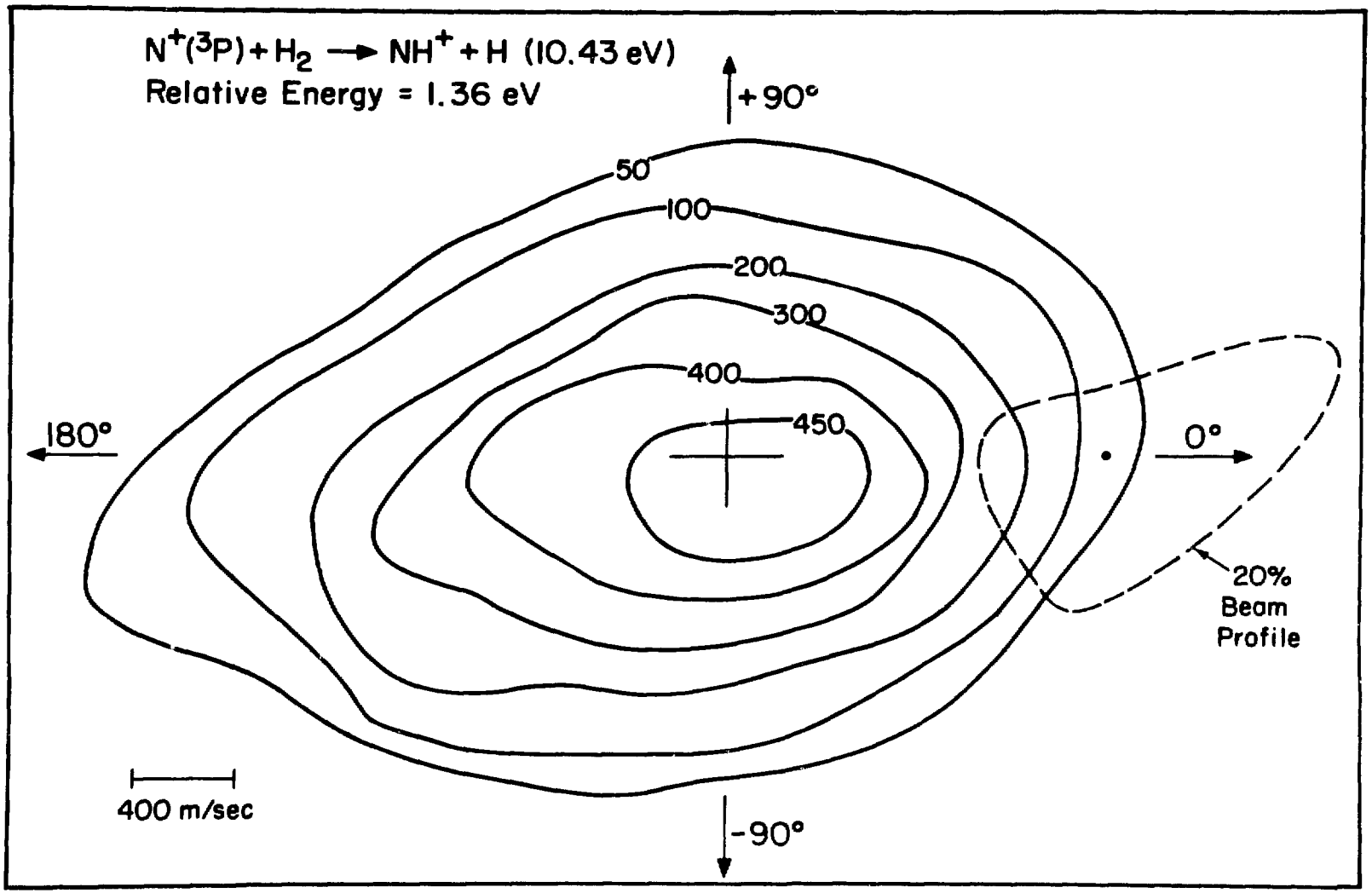
$N^+(^3P) + H_2 \rightarrow NH^+ + H$ (10.43 eV)
Relative Energy = 1.36 eV
+90°
50
100
200
300
400
450
180°
0°
20% Beam Profile
400 m/sec
-90°

Fig. 4

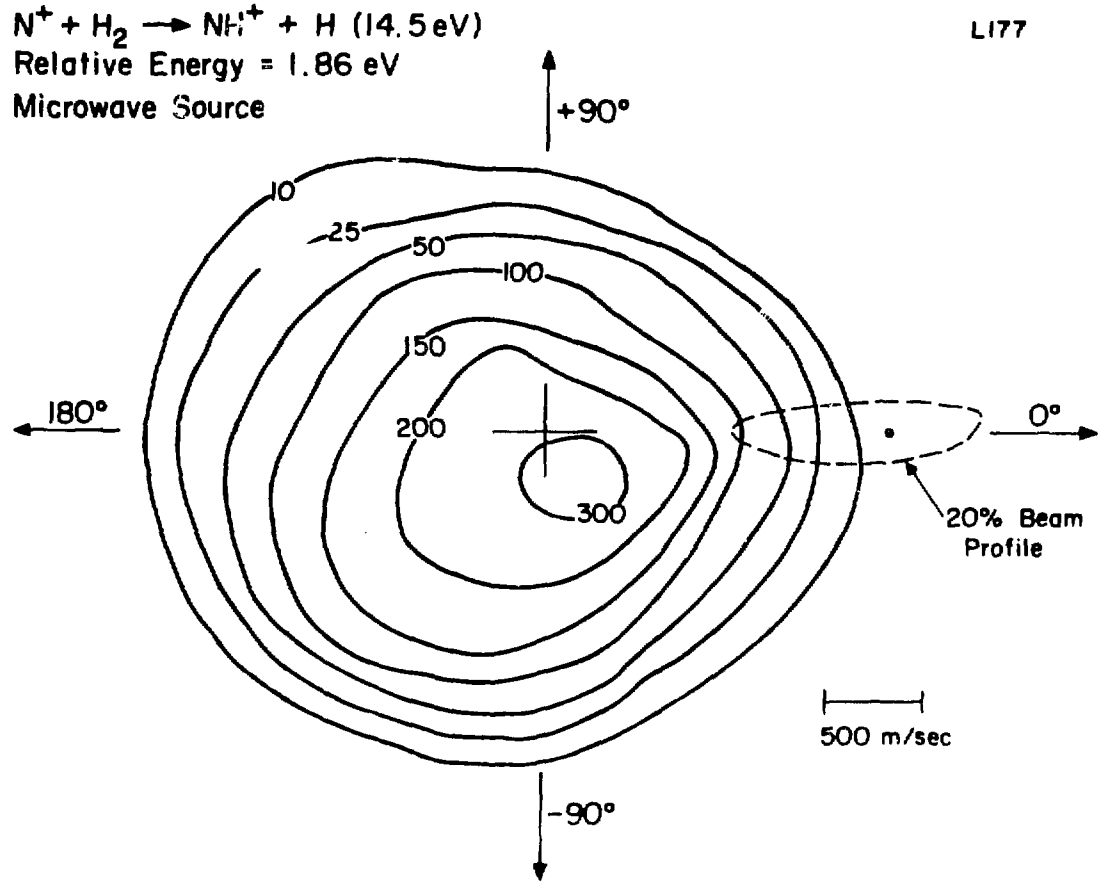

Fig. 5. The intensity distribution of NH^+ formed in N^+-H_2 collisions at an initial relative energy of 1.86 eV.

Fig. 6. The intensity distribution of NH^+ formed in N^+-H_2 collisions at an initial relative energy of 2.16 eV.

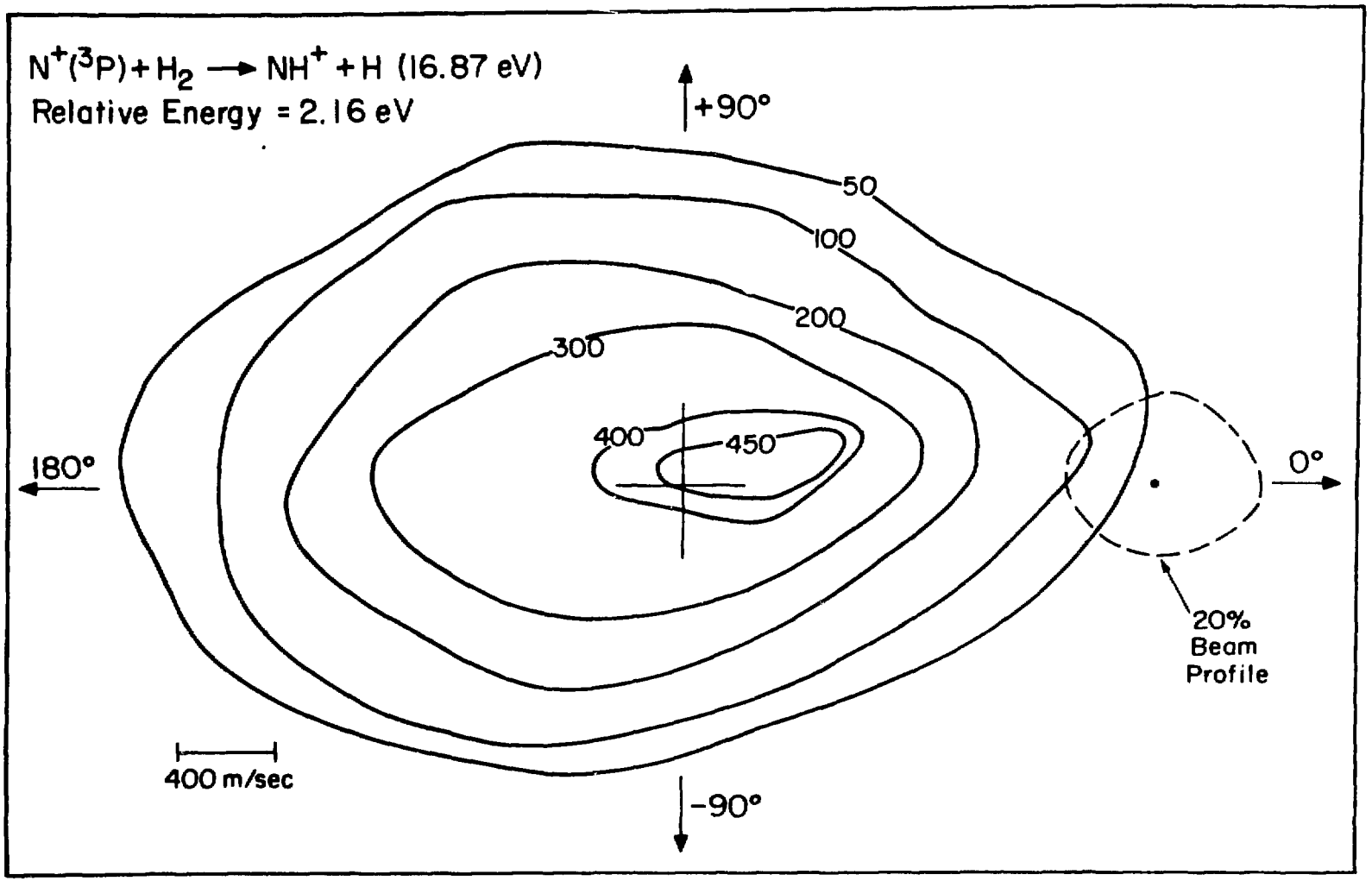
$N^+(^3P) + H_2 \rightarrow NH^+ + H$ (16.87 eV)
Relative Energy = 2.16 eV
+90°
50
100
200
300
400
450
180°
0°
20% Beam Profile
400 m/sec
-90°

Fig. 6

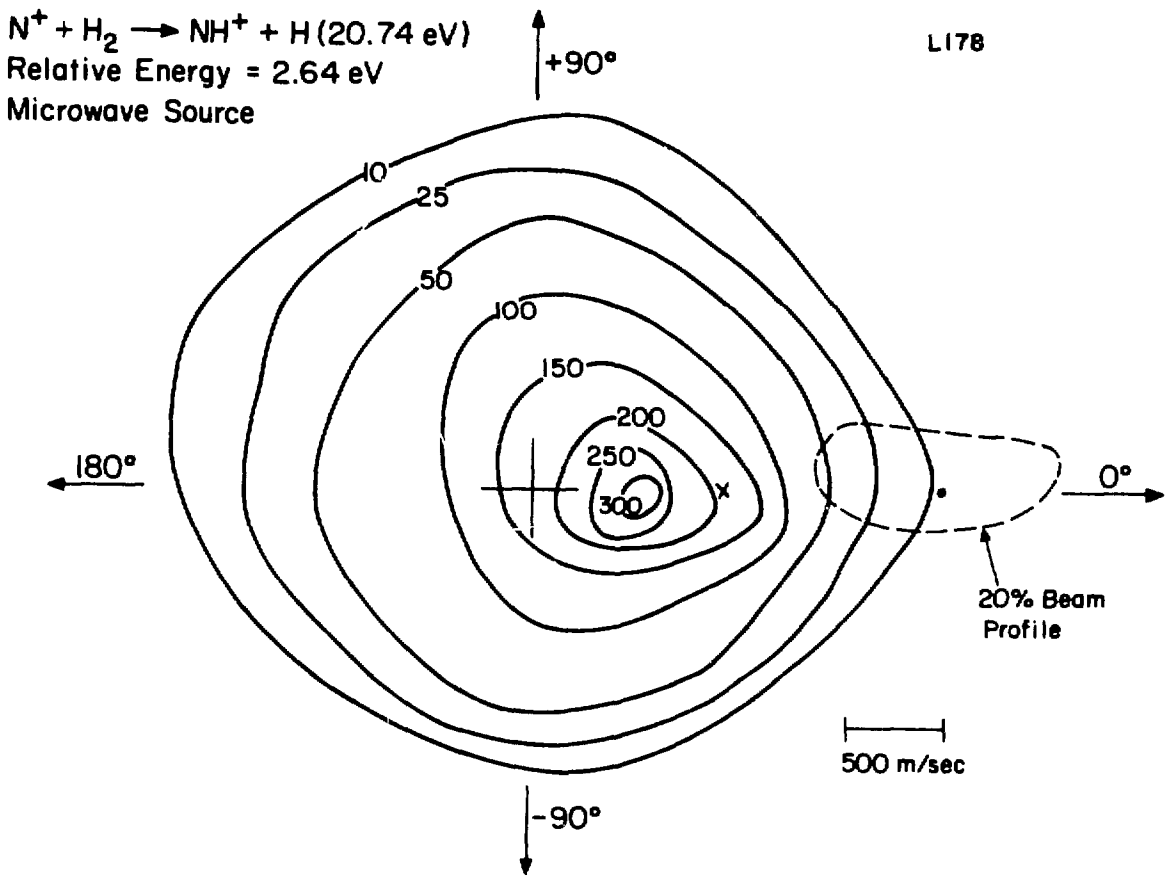

Fig. 7. The intensity distribution of NH^+ formed in N^+-H_2 collisions at an initial relative energy of 2.64 eV. The small cross locates the spectator stripping velocity.

Fig. 8. The intensity distribution of NH^+ formed in N^+-H_2 collisions at an initial relative energy of 3.60 eV.

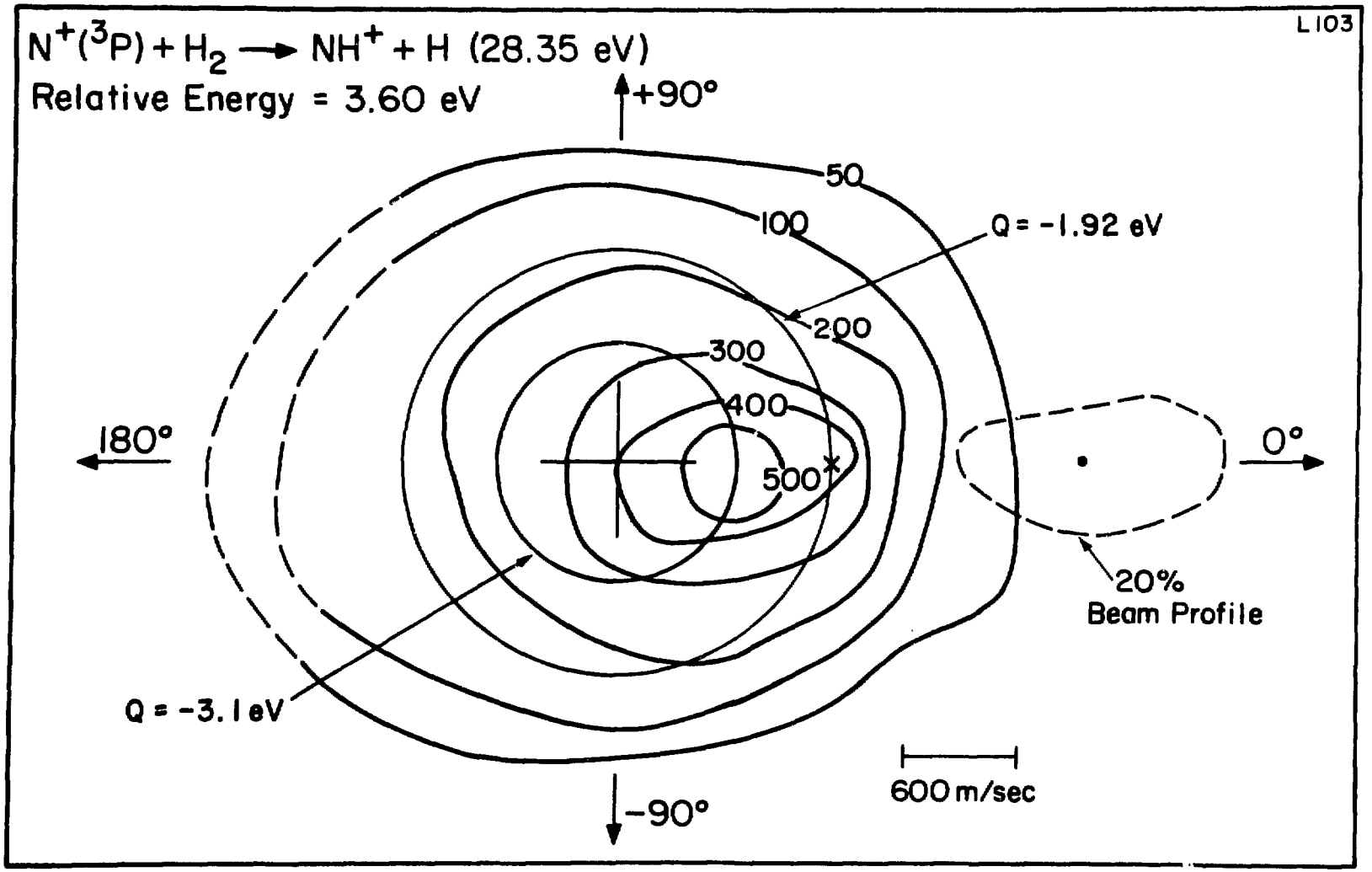
L103
$N^+(^3P) + H_2 \rightarrow NH^+ + H$ (28.35 eV)
Relative Energy = 3.60 eV
+90°
50
100
Q = -1.92 eV
200
300
400
500
180°
0°
20%
Beam Profile
Q = -3.1 eV
600 m/sec
-90°

Fig. 8

In Figs. 3-8 we see the evolution of the NH^+ scattering pattern as the energy is raised from 0.98 eV to 3.60 eV. The maps at 0.98 and 1.36 eV are peaked at the center-of-mass velocity and possess considerable forward-backward symmetry. At 1.86 eV, the distribution is no longer perfectly symmetric but has its peak displaced slightly forward and off the relative velocity vector. The lack of symmetry with respect to the relative velocity vector (0°-180° line) is due to experimental error. Scattering is necessarily axially symmetric and thus symmetry about this line should be guaranteed. The slight forward asymmetry, however, is probably real. The asymmetry is more pronounced at 2.16 eV and unmistakeable in the 2.64 and 3.60 eV maps. The cause of this shift is the onset of direct reaction processes.

If the NH_2^+ intermediate lives at least a few rotational periods, then the product distribution should have forward-backward symmetry.[29,30] In a more short-lived, or direct interaction, a preferred direction is remembered by the complex. This direction is that of the initial rela- relative velocity vector, and for most ion-molecule reactions studied, a peak scattered forward, near the spectator stripping velocity is seen. In the present reaction even at 3.60 eV, the distribution is peaked noticeably behind the spectator stripping velocity. This implies that throughout the energy range studied, $N^+(^3P)$ has substantial interaction with both H atoms during the course of the collision. One infers this from the fact that at 3.60 eV a spectator stripping event produces NH^+ at $Q = -1.92$ eV while the observed maximum is at $Q = -3.1$ eV. Q is defined as the translational exoergicity or the difference in product

and reactant relative translational energy. Assuming ground state reactants, and reaction thermoneutrality, Q is equal to the internal energy of the NH^+ product. The observed internal energy is greater than that predicted by the stripping model; so, we conclude that energy was transferred among all three atoms.

One should note that although the NH^+ distributions become more asymmetric as the energy is raised, the low intensity contours retain a high degree of forward-backward symmetry. The overall shape of the 2.64 and 3.60 eV maps is reminiscent of maps obtained at similar energies for $C^+(H_2,H)CH^+$.[13] The dynamics of this reaction were explained as possibly involving an "osculating" CH_2^+ complex which lasts for about one rotational period and hence does not completely forget the orientation of the initial relative velocity vector. A similar distribution (forward peaked with symmetric low intensity contours) could result if the reaction proceeded via two distinct mechanisms perhaps involving two different potential surfaces. One of these would obviously be a direct mechanism, to explain the asymmetry, while the other might well involve a long-lived complex. It is possible though for a direct hard-sphere-like interaction to produce an isotropic distribution. This is the reason given for symmetric low intensity contours seen in $Ar^+(D_2,D)ArD^+$.[32,32] The "hard-sphere contribution" to reactive scattering is most obvious in low cross section reactions, where its greater relative importance makes it more visible. For instance the reactions $Kr^+(D_2,D)KrD^+$ and $H_2^+(H_2,H)H_3^+$ show substantial symmetry in their product distributions though any potential energy well

associated with KrH_2^+ or H_4^+ is negligible.[33] Thus a long-lived intermediate is not likely, and it must be a direct interaction producing the symmetry in these low cross section reactions. For the above reasons it would be incorrect to assume that the symmetric low intensity contours of Figs. 7 and 8 indicate the continued presence of a long-lived intermediate.

The evolution of the dynamics shown in Figs. 2-8 is somewhat different from that reported in previous studies. As mentioned earlier, at 2.36 eV, Eisele et al.[11] found the product distribution peaked at the spectator stripping velocity. At higher energies, Gislason et al.[8] found peak product intensity at velocities slightly less than spectator stripping. The results of Fair and Mahan[12] which have extensive energetic overlap with the present results also move to higher velocities more rapidly with increasing energy than those observed here.

The explanation for this difference involves the state distribution of the reactant N^+ ions. It was previously alluded to that in the earlier work, N^+ was produced by electron impact. While the ionization conditions might have been less severe than in our electron impact source (lower electron energy, higher pressure), a quick glance at Table 1 establishes a potentially large departure from pure $N^+(^3P)$. Because of this, we assert that the present results more accurately reflect the dynamics associated with the ground state ion.

$N^+(^3P)$: Non-reactive Scattering

Thirteen experiments were performed in which complete contour maps were obtained for $N^+(^3P)$ scattered non-reactively from H_2. Because the DC discharge ion source produced the beams which were most compact in velocity space, it provided the best non-reactive distributions.

Fig. 9 shows a non-reactive contour map obtained at an initial relative energy of 0.66 eV. The distribution is quite diffuse, primarily due to the greater relative importance of beam energy and angular spread at low collision energies. The gross features which appear are elastic scattering in the forward hemisphere and a noticeable peak in the backward hemisphere. The ramifications of this backscattered peak will be discussed shortly.

The initial relative energy is raised in Figs. 10-12 but the basic features of the N^+ distributions stay the same. A large backscattered peak appears on the elastic circle and the small angle forward scattering is predominately elastic. (The forward elastic scattering indicates that little energy is transferred, in high impact parameter, impulsive collisions.)

The maps in Figs. 13-15 show that at ~1.9 eV, the back peak is significantly decreased in intensity and has moved inside the elastic circle. The small feature located at the center-of-mass in Fig. 15 may correspond to the spin unallowed transition, $N^+(^3P) \rightarrow N^+(^1D)$. The process requires 1.90 eV and hence all $N^+(^1D)$ formed would have insufficient translational energy to move very far from the center-of-

Fig. 9. The intensity distribution of N^+ scattered from H_2 at an initial relative energy of 0.66 eV. The Q = 0 (elastic) circle is the locus of all scattering events in which no energy is transferred between the collisions partners. The region labeled inaccessible indicates an area in which signal cannot be reliably measured due to high primary beam intensity. Notice the prominent backscattered peak which appears near the elastic circle in the 180° direction.

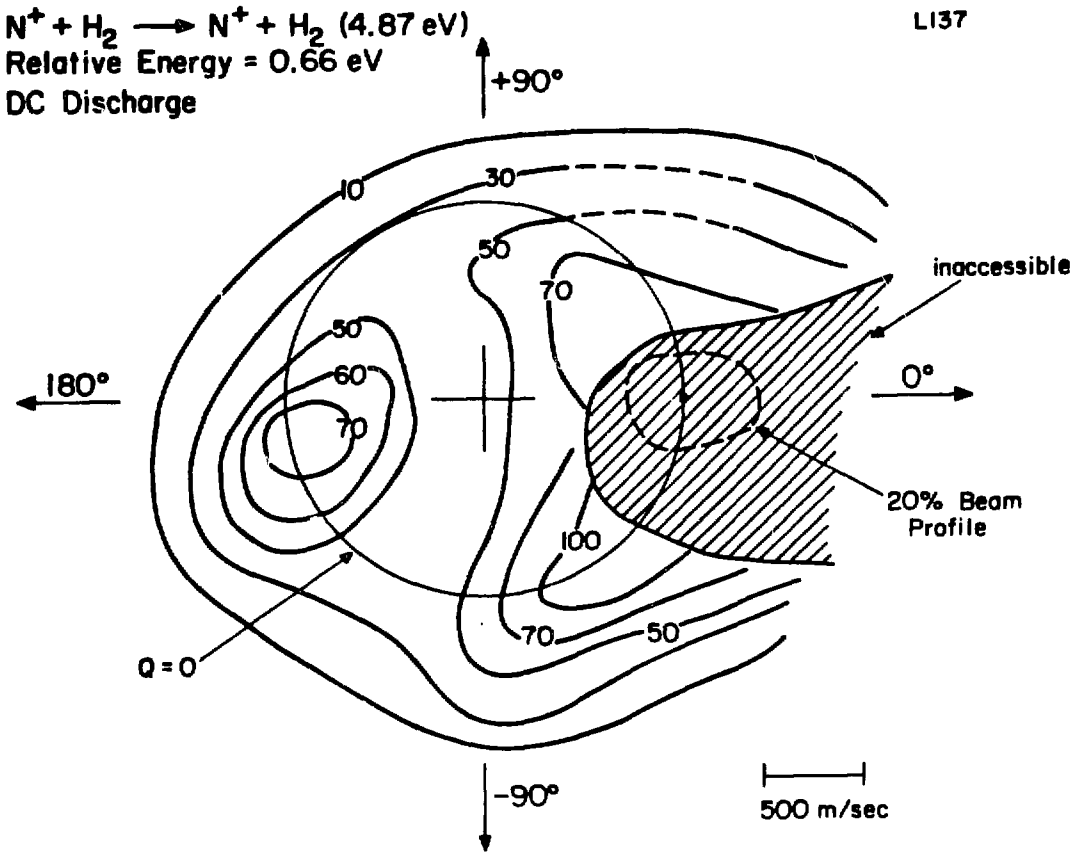
$N^+ + H_2 \longrightarrow N^+ + H_2$ (4.87 eV)
Relative Energy = 0.66 eV
DC Discharge
L137
+90°
-90°
180°
0°
10
30
50
70
50
60
70
100
70
50
inaccessible
20% Beam Profile
Q = 0
500 m/sec

Fig. 9

Fig. 10. The intensity distribution of N^+ scattered from H_2 at an initial relative energy of 0.96 eV.

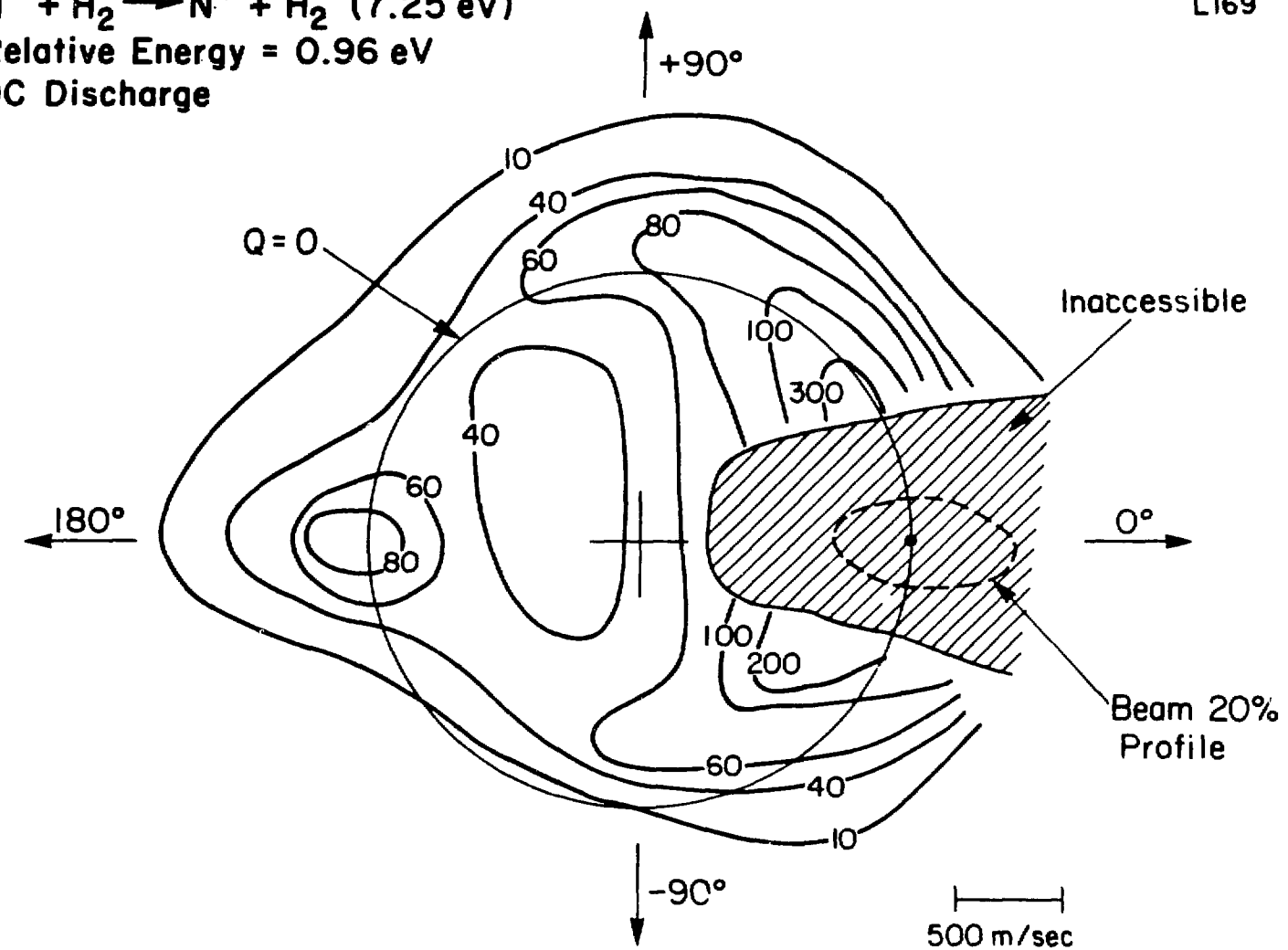
$N^+ + H_2 \rightarrow N^+ + H_2$ (7.25 eV)
Relative Energy = 0.96 eV
DC Discharge
L169
+90°
Q = 0
10
40
60
80
100
300
Inaccessible
40
60
80
180°
0°
100
200
Beam 20%
Profile
60
40
10
-90°
500 m/sec

Fig. 10

Fig. 11. The intensity distribution of N^+ scattered from H_2 at an initial relative energy of 1.40 eV.

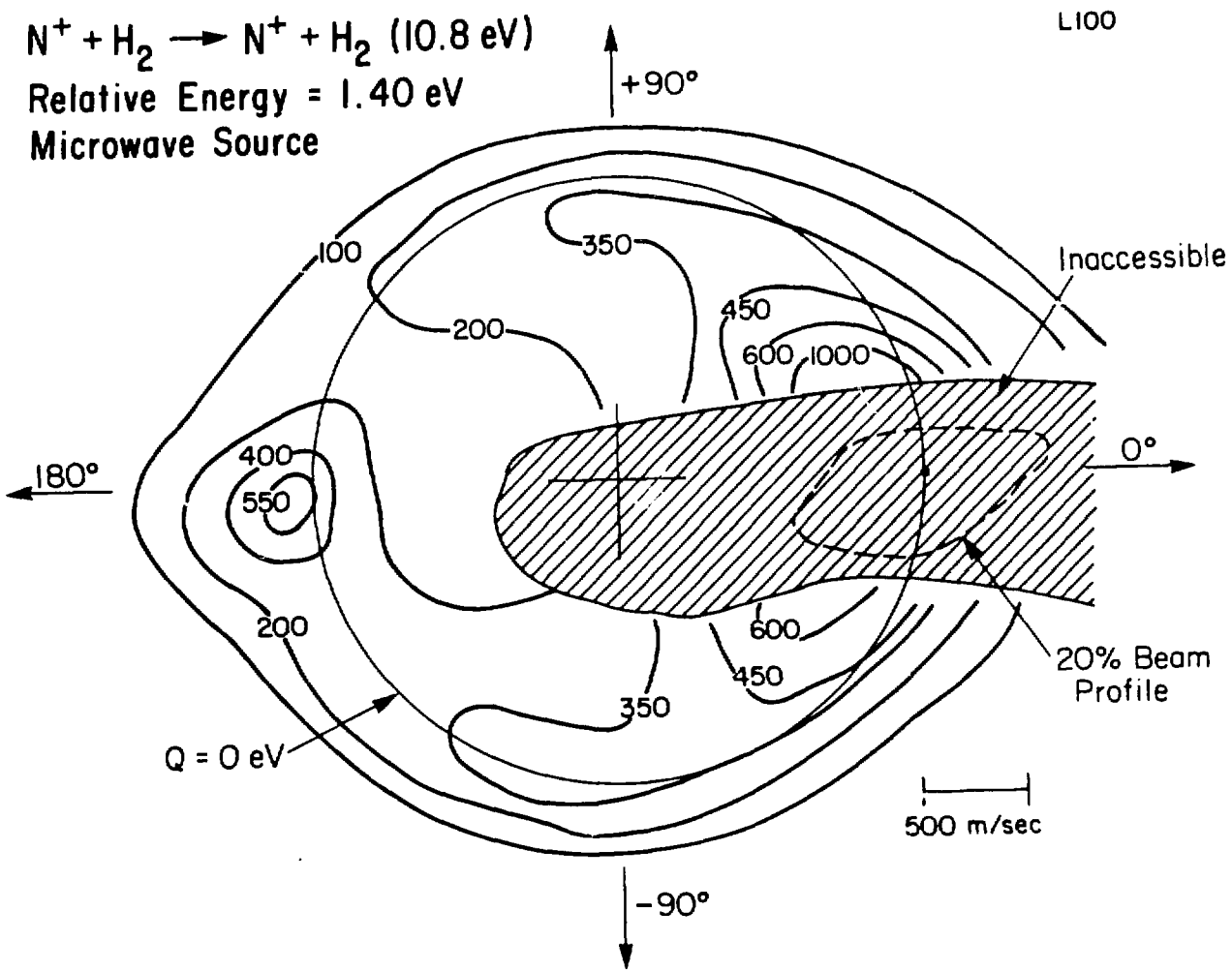
$N^+ + H_2 \rightarrow N^+ + H_2$ (10.8 eV)
Relative Energy = 1.40 eV
Microwave Source
L100
+90°
100
350
200
450
600
1000
Inaccessible
180°
400
550
0°
200
600
450
350
20% Beam Profile
Q = 0 eV
500 m/sec
-90°
XBL 807-10770

Fig. 11

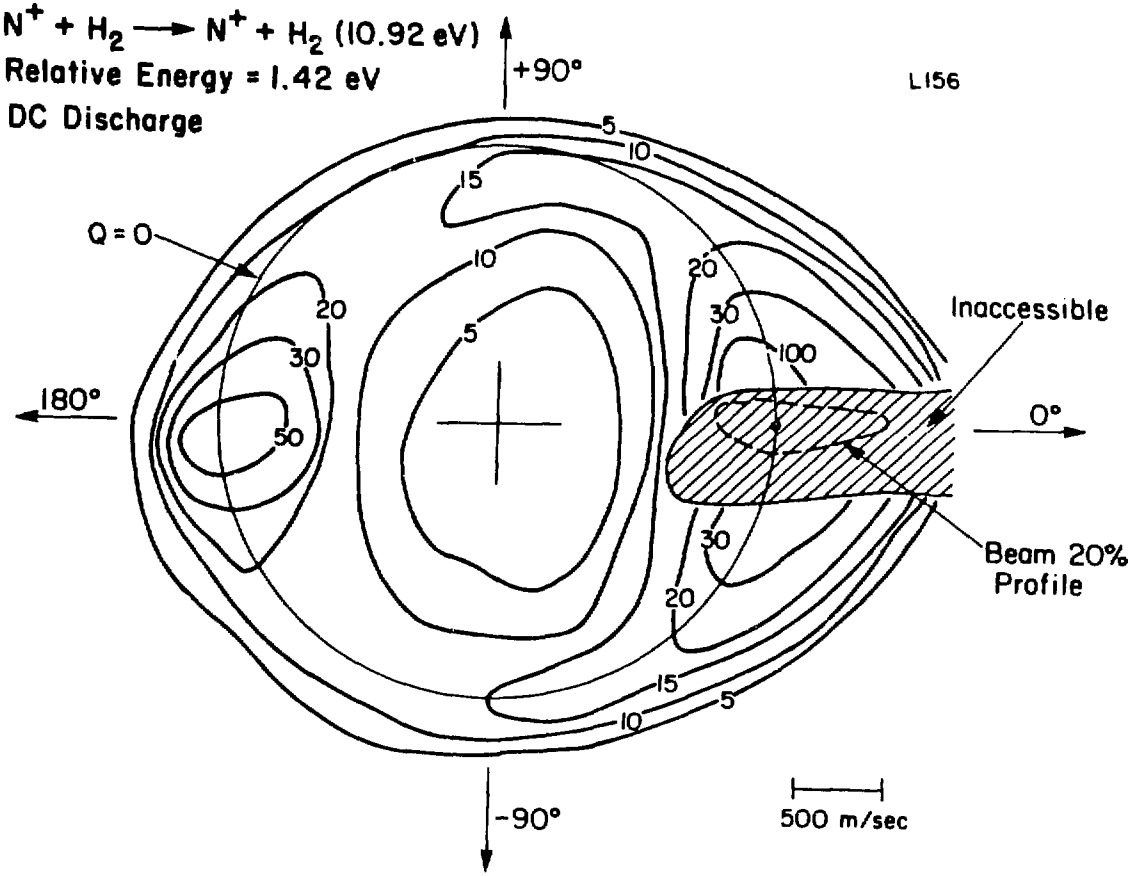

Fig. 12. The intensity distribution of N^+ scattered from H_2 at an initial relative energy of 1.42 eV.

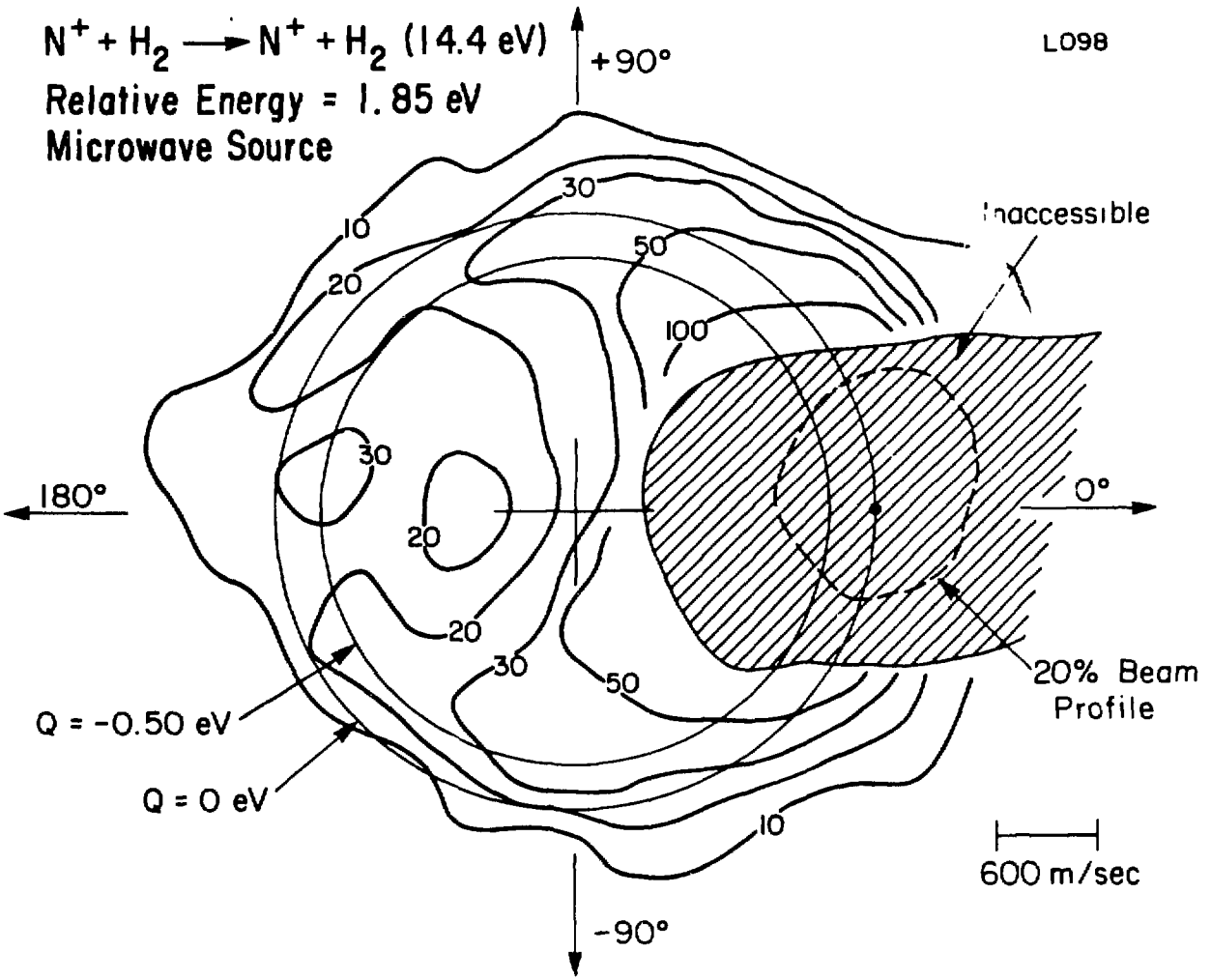

Fig. 13. The intensity distribution of N^+ scattered from H_2 at an initial relative energy of 1.85 eV.

XBL 807-10768

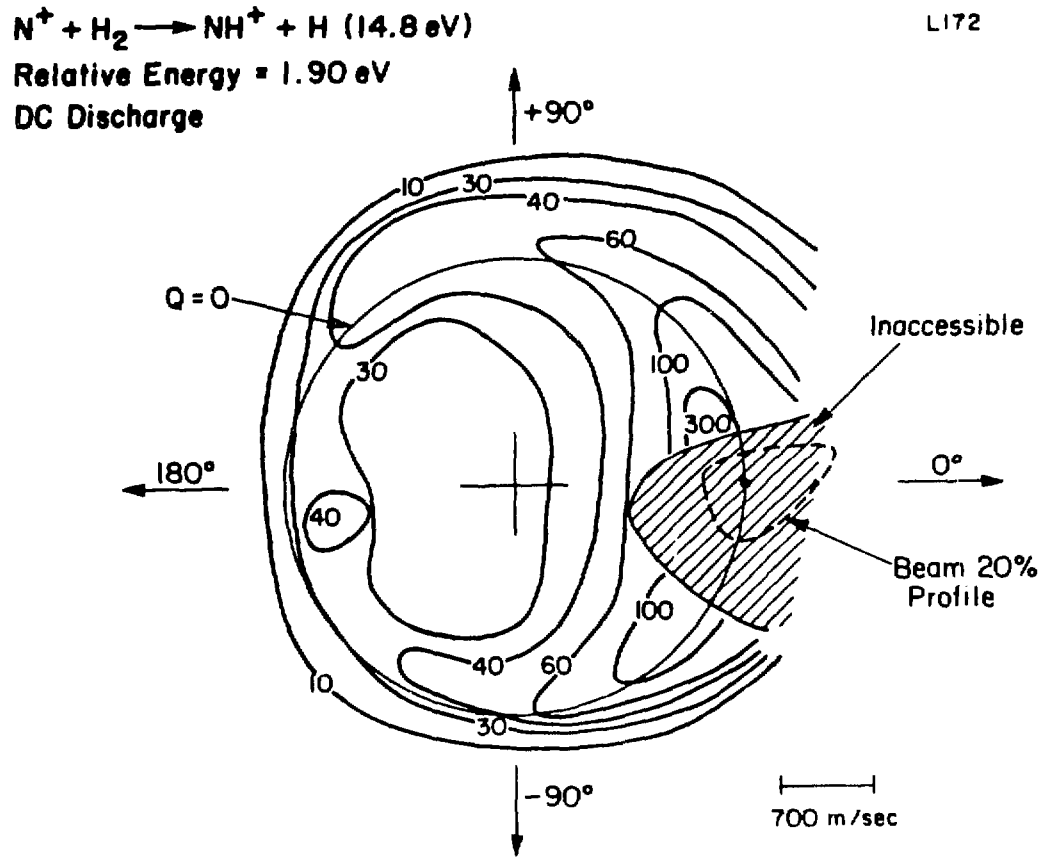

Fig. 14. The intensity distribution of N^+ scattered from H_2 at an initial relative energy of 1.90 eV.

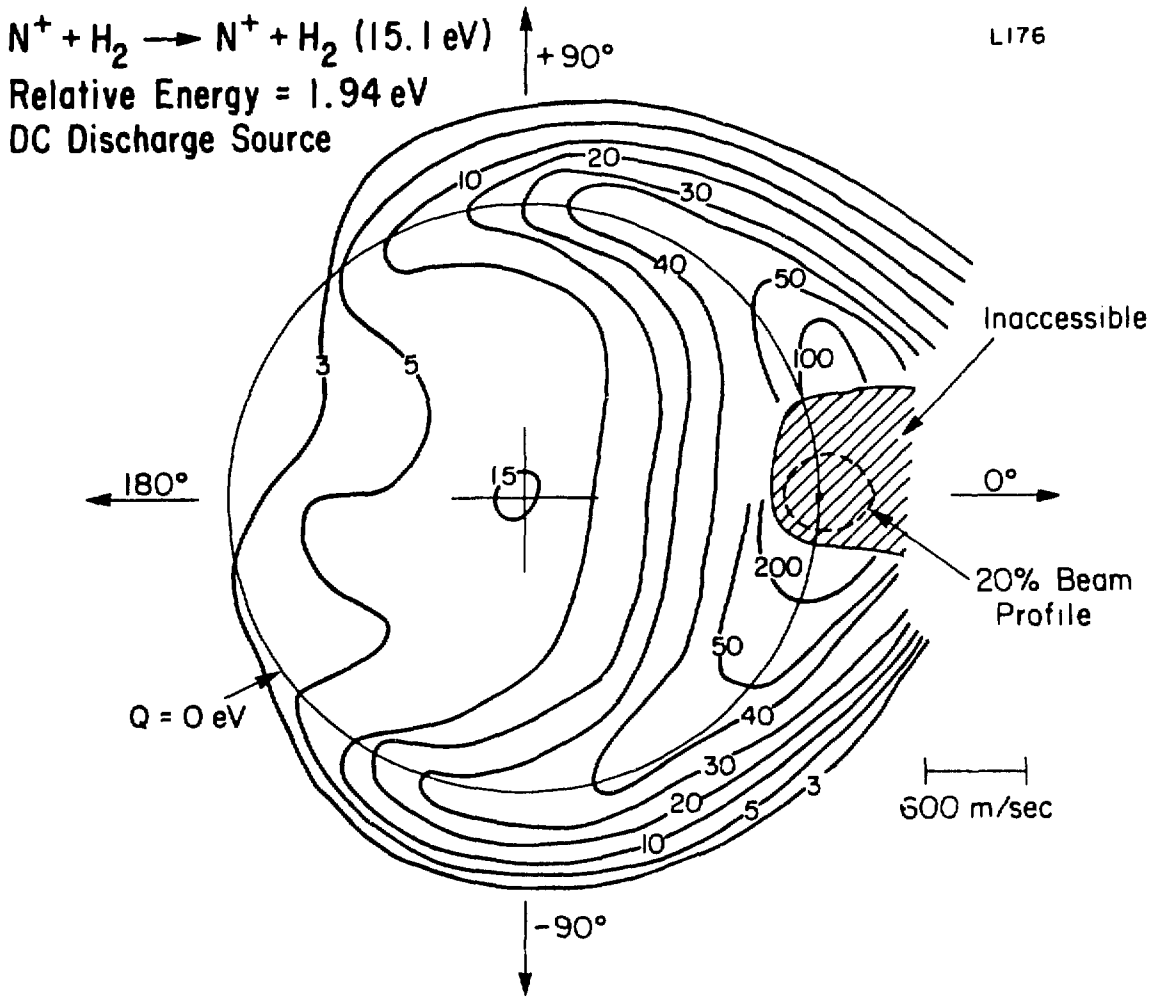

Fig. 15. The intensity distribution of N^+ scattered from H_2 at an initial relative energy of 1.94 eV.

XBL 807-10767

mass. This inelastic transition has been seen before in N^+-O_2 collisions,[34] but should be very weak when the collision partner has no unpaired electrons. If the small peak is due to this transition, we are able to see it only because the products are energetically confined to a small region in velocity space.

In Fig. 16, at 2.50 eV, we observe that the back peak and virtually all intensity has disappeared from behind the ±90° line. The same general scattering pattern was observed previously at the somewhat higher energy of 6.87 eV.[18] Assuming a direct, impulsive, non-reactive scattering mechanism, product scattered at large angles comes from low impact parameter collisions. The lack of large angle scattering implies that low impact parameter collisions lead to removal of N^+. The processes which could do this are H atom transfer to form NH^+, charge transfer to form H_2^+, hydride transfer to form NH, and radiative association to form NH_2^+. We may eliminate the last two possibilities, as the cross section for each is minute. Similarly the cross section for NH^+ formation is also small at these energies. Using graphs given by Eisele et al.[11] and Hyatt and Lacmann[35] we estimate for reaction (1), at 2.5 eV, $\sigma \leq 1$ Å^2. The charge transfer cross section, which is only a weak function of collision energy, has been measured to be 3.5 Å^2 at 12.5 eV relative energy.[36] The logical conclusion then is that charge transfer is depleting the non-reactive scattering at 2 eV and above, in agreement with Ruska.[37]

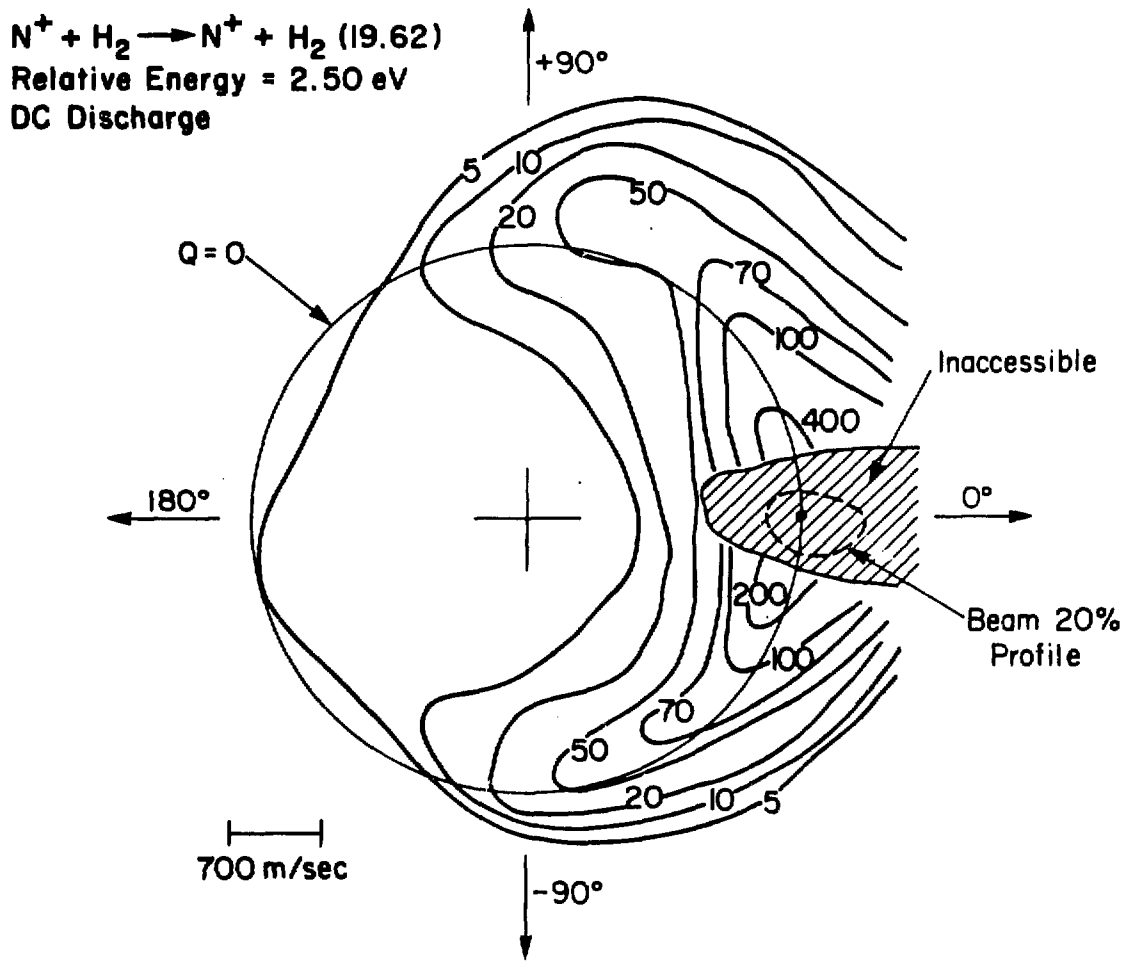

Fig. 16 The intensity distribution of N^+ scattered from H_2 at an initial relative energy of 2.50 eV.

The single most important feature in the non-reactive maps is the backscattered peak. Normal elastic scattering gives a product intensity distribution which is monotonically decreasing with center-of-mass angle except for rainbow oscillations.[38] It is unlikely that we would resolve these oscillations. We can also be certain that the back peak is not due to the primary rainbow. The center-of-mass angle of such a feature would be dependent on collision energy while the observed feature is not. Hence no direct process is responsible for this peak and it is likely, especially when one remembers the reactive results, that it comes from the decay of a long-lived complex.

Since products resulting from the decay of a long-lived complex are distributed symmetrically with respect to the $\pm 90^{\circ}$ line, a forward peak, mirroring the back one, should be present. Unfortunately, the presence of this feature cannot be checked as its location coincides with the main beam. (It would also be swamped by intense low-angle scattering.) Forward-backward peaking in non-reactive distributions is well-known in neutral-neutral collisions,[39] but the present results are apparently the first such observation in ion-neutral collisions.

The theory of angular distributions for products resulting from the decay of a long-lived complex was initially developed for understanding nuclear processes. It was adapted for the use of physical chemists by Herschbach and co-workers.[40] The points pertinent to our discussion are as follows. The total angular momentum vector for the complex $\mathcal{J}$ is equal to the sum of the initial orbital, $\underline{L}$, and rotational, $\underline{J}$, angular momentum vectors. If J is small, as one would expect for supersonically

expanded H_2, then $\mathcal{J} \approx \underline{L}$. Making the additional assumption that the products come off rotationally cold, i.e. $J' \approx 0$ (where the prime denotes quantities associated with the products), then $\underline{L}' \approx \mathcal{J}'$ which implies $\underline{L} \approx \underline{L}'$. This situation is depicted in Fig. 17a. Since $\underline{L} = \mu \underline{v} \times \underline{b}$, with μ = reduced mass, $\underline{v}$ = relative velocity vector, and $\underline{b}$ = impact parameter, $\mathcal{J}$ for the complex lies at a right angle to the relative velocity vector. If the complex lasts at least a few rotational periods, it will forget the initial direction of approach but, of course, remember $\mathcal{J}$ due to conservation of angular momentum. The complex can then decompose along any diameter of the circle in Fig. 17a. Since the initial orientation of $\underline{b}$ is random, the problem has axial symmetry and all azimuthal angles for $\mathcal{J}$ are equally likely. If one integrates the distribution of Fig. 17a over all azimuthal angles, the result is that intensity builds up on the initial relative velocity vector both forward and backward.[40] This is seen physically by realizing that the detector rotates in a plane containing the initial relative velocity vector, and intersects every azimuthally rotated circle of Fig. 17a at two points. These points are on the initial relative velocity vector, and distributed symmetrically about the center of mass. It is natural that product intensity will be highest at these two points.

If a significant fraction of the initial angular momentum is released as product rotation ($J' > L'$), the polarization of $\underline{L}'$ is largely lost and a more isotropic product distribution results. No longer does every circle intersect the initial relative velocity vector at the same two points. This is shown in Fig. 17b. A truly isotropic

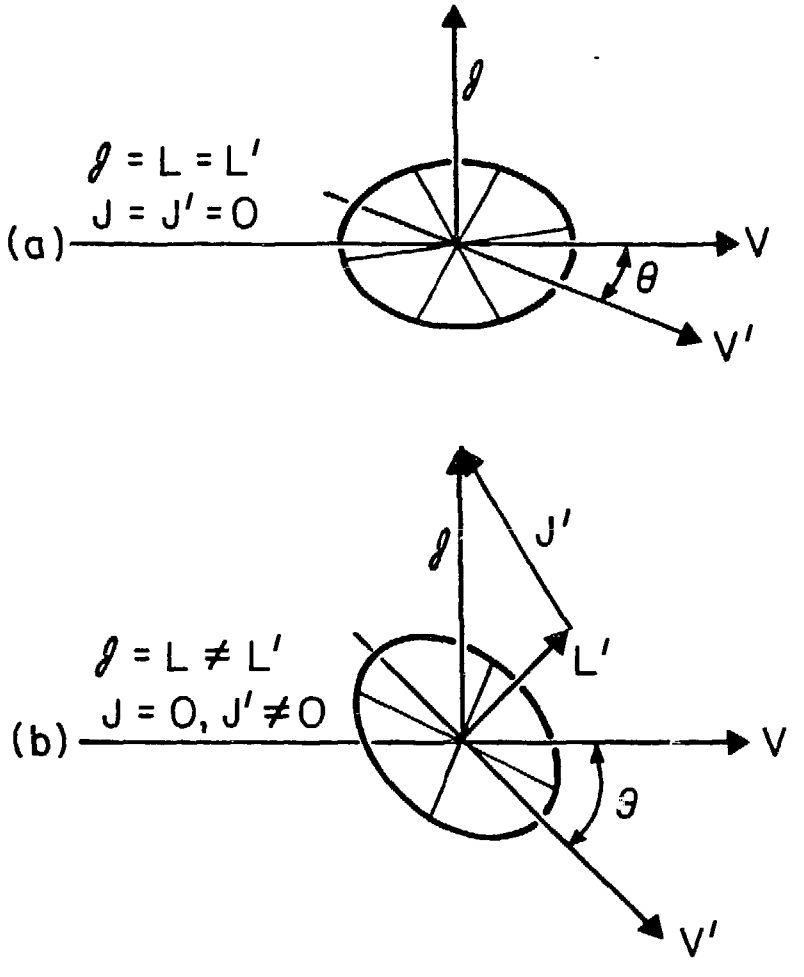

XBL 807-10763

Fig. 17. Relationship between initial and final velocity vectors as determined by angular momentum constraints. In (a) there is no reactant or product rotation and the entire event takes place in one plane. In (b) there is considerable product rotation and $\underset{\sim}{v}$ and $\underset{\sim}{v}'$ will not necessarily be in the same plane.

product distribution cannot really be expected unless the orientation of $\vec{J}$ is completely random. A situation like this is encountered if the reactants are rotationally hot ($J \gg L$). Examples of both isotropic and forward-backward reactive scattering are given by Birkinshaw et al.[41] but these arguments apply to non-reactive scattering as well.

In the preceding paragraphs we have explained how a backscattered peak in a non-reactive distribution can be interpreted as evidence for the existence of a long-lived complex. Reaction (1) is thermoneutral, so that once a complex is formed there should be little preference as to whether it decays to $NH^+ + H$ or $N^+ + H_2$. For this reason, it is not surprising that the complex channel does manifest itself in the non-reactive distributions.

There have been relatively few studies of non-reactive scattering from ion molecule collisions in which a long-lived complex is thought to exist. The processes $O_2^+(D_2,D_2)O_2^+$[14] and $C^+(H_2,H_2)C^+$[13] give distributions showing large amounts of inelastic scattering, demonstrating an intimate interaction, but in neither is a backscattered peak seen. The difference between these processes and $N^+(H_2,H_2)N^+$ probably lies in the details of the potential energy surfaces. Apparently NH_2^+ can decompose to $N^+ + H_2$ leaving the H_2 internally cold so that $J' \approx 0$ and forward-backward peaking results.

By watching the back peak as a function of collision energy we can follow the evolution of NH_2^+ long-lived complex formation. Figs. 9-12 show complex behavior in the energy range 0.66-1.42 eV. Figs. 13-15 give the consistent result that in the vicinity of 1.9 eV, complex formation

is reduced. The fact that the backscattered feature has moved inside the elastic circle shows that H_2 is carrying away some energy internally. The back peak appears at $Q \approx -0.6$ eV in this energy range indicating that H_2 comes off in $v = 1$, $J \approx 0$ or $v = 0$, $J \approx 9$. At 2.50 eV, in Fig. 16, the peak is gone and clearly complex formation plays no role in the non-reactive dynamics.

At this point a natural question arises: Why are the low energy reactive distributions roughly isotropic while the non-reactive are apparently forward-backward peaked? One obvious difference in the two decomposition channels is that the rotational constant for H_2 is roughly 4 times greater than that of NH^+. Thus for similar values of J', 4 times more energy resides in H_2 rotation than would in NH^+. Any statistical parceling of the energy would therefore favor lower rotational quantum numbers for H_2. Another related factor which could be important is the difference in reduced mass associated with the two channels. As discussed later, due to the long-range nature of the ion-induced dipole potential, the critical configuration geometries are very stretched out. Thus the complex can be treated as a diatom of mass 14 and 2 for non-reactive dissociation and 15 and 1 for reactive dissociation. The reduced mass will be nearly twice as large for $N^+ + H_2$ products as $NH^+ + H$ and since $L' = \mu' v' b'$, comparable exit impact parameters make L' (non-reactive) > L' (reactive). Both of these simple arguments yield the result that the non-reactive distributions should be more sharply forward-backward peaked than the reactive distributions. While this trend is dramatically born out by the experimental results,

the large change in dynamics associated with the two channels would be difficult to anticipate and is probably due to the details of the potential energy surfaces. Further discussion of this is given later.

If we consider the non-reactive and reactive results together we see general agreement as to the gross features of the dynamics. The non-reactive data show the existence of a long-lived complex at energies below ~1.9eV. The reactive experiment at 1.86 eV gives a nearly symmetric distribution, while the 2.16 eV map is more obviously asymmetric yielding the similar result that complex formation dominates only up to ~1.9 eV. If the asymmetry of the higher energy reactive experiments was due to the opening of a new direct reactive channel, perhaps involving another potential surface, then the continued presence of the complex channel should be seen in the non-reactive distributions. Since the channel appears to close in the non-reactive experiments also, the two-surface possibility is weakened. The data support a mechanism involving a single path in which complex formation becomes less favorable with increasing energy.

Interactions with Metastable N^+

Our first studies of reaction (1) were done under slightly different experimental conditions than the experiments discussed in the previous two sections. The differences are that the electron impact ion source, as well as a more rudimentary neutral source were used. This neutral source consisted of a nozzle with a .025mm orifice located 6-12mm from

quite different from what is seen when N^+ is produced in a microwave discharge. Fig. 22 nicely shows that at 1.45 eV, the forward peak occurs at spectator stripping.

The logical explanation for the difference in the distributions obtained with electron impact and microwave discharge produced N^+ lies in the electronic state populations. As was shown in Table 1, these populations are very source dependent. Apparently the metastable ions that are reacting, react in a direct fashion. The fact that the beams containing metastable ions give more forward peaked distributions is consistent with our earlier argument for explaining the difference between our $N^+(^3P)$ work and previous results.

A bimodal distribution attributable to two different reactant states has been reported before for $O_2^+(D_2,D)O_2D^+$.[42] The excited reactant, $O_2^+(^4{}_u)$, for which the reaction is 2.0 eV exothermic, produces O_2D^+ at

velocities greater than spectator stripping in the energy range 1.0-4.14 eV. The ground state reactant gives symmetric product distributions in this energy range.[14].

The complete domination of Figs. 19-22 by the forward peak would suggest that the reaction cross section of the metastable(s) is much larger than that of $N^+(^3P)$. This is not surprising since the cross section is small with the ground state ion, but recent thermal energy work indicates that charge transfer is preferred to H atom transfer in metastable N^+-H_2 collisions.[7] Also we observe similar signal levels with all ion sources implying that a large forward peak did not "grow" on a symmetric distribution but rather a modest peak was added

Fig. 18. The intensity distribution of NH^+ resulting from N^+-H_2 collisions at an initial relative energy of 0.23 eV. ^{2}In Figs. 18-21 N^+ was produced by the impact of 160 eV electrons on N_2. The 20% beam profile is displaced for clarity.

$N^+ + H_2 \longrightarrow NH^+ + H$ (1.41 eV)

Relative Energy = 0.23 eV

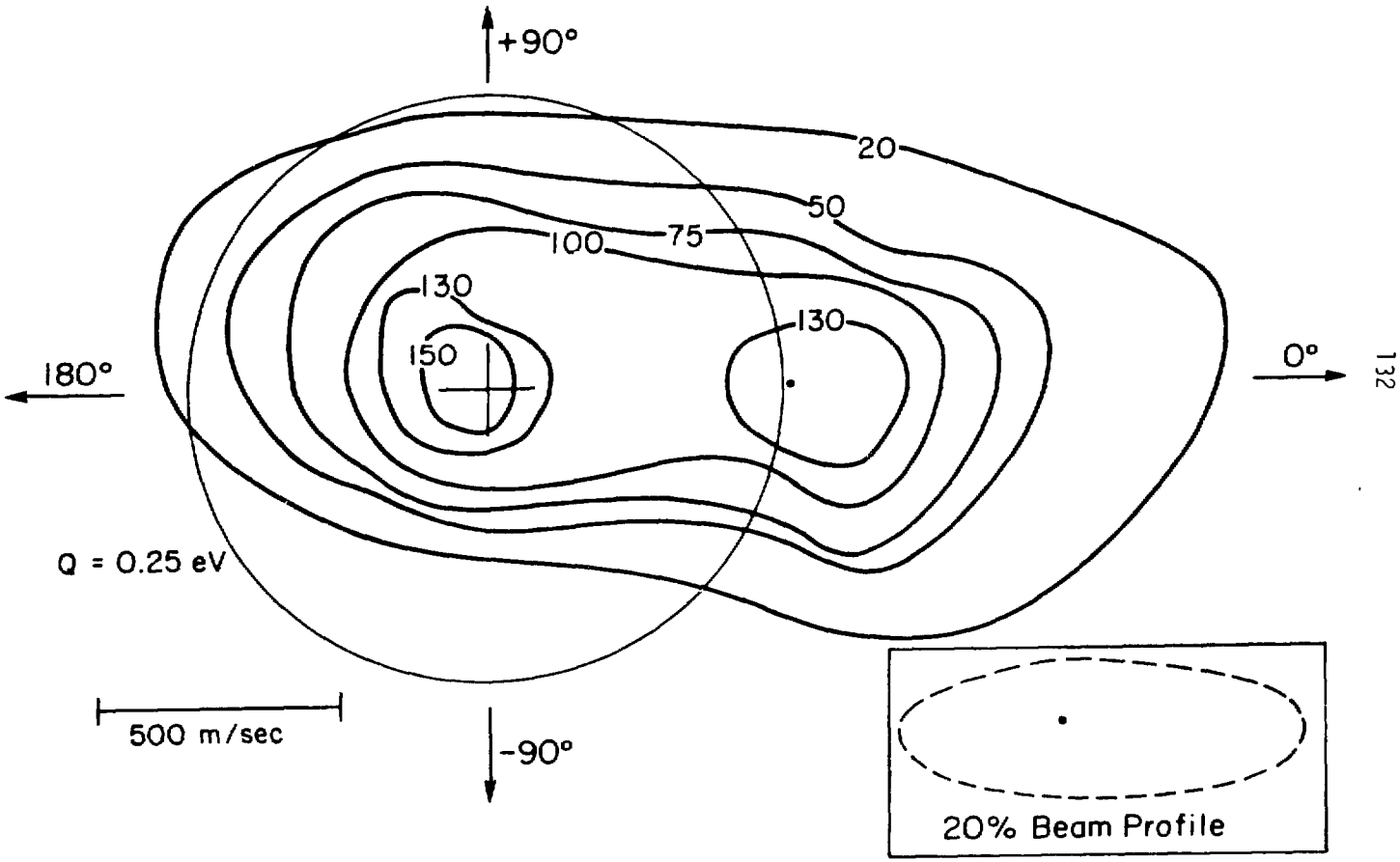

Fig. 18

Fig. 19 The intensity distribution of NH^+ from N^+-H_2 collisions at an initial relative energy of 0.69 eV.

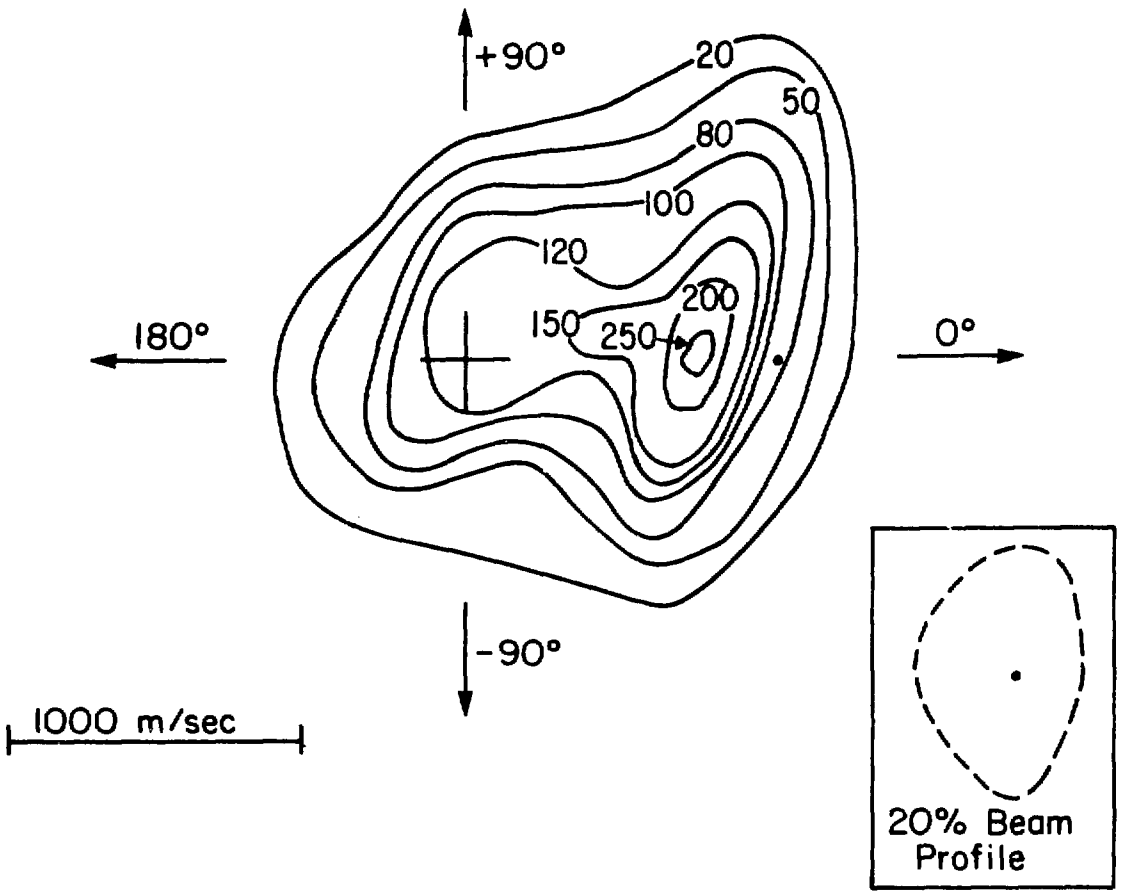
$N^+ + H_2 \longrightarrow NH^+ + H$ (5.05 eV)
Relative Energy = 0.69 eV
+90°
20
50
80
100
120
150
200
250
180°
0°
-90°
1000 m/sec
20% Beam Profile

Fig. 19

Fig. 20 The intensity distribution of NH^+ resulting from N^+-H_2 collisions at an initial relative energy of 0.95 eV.

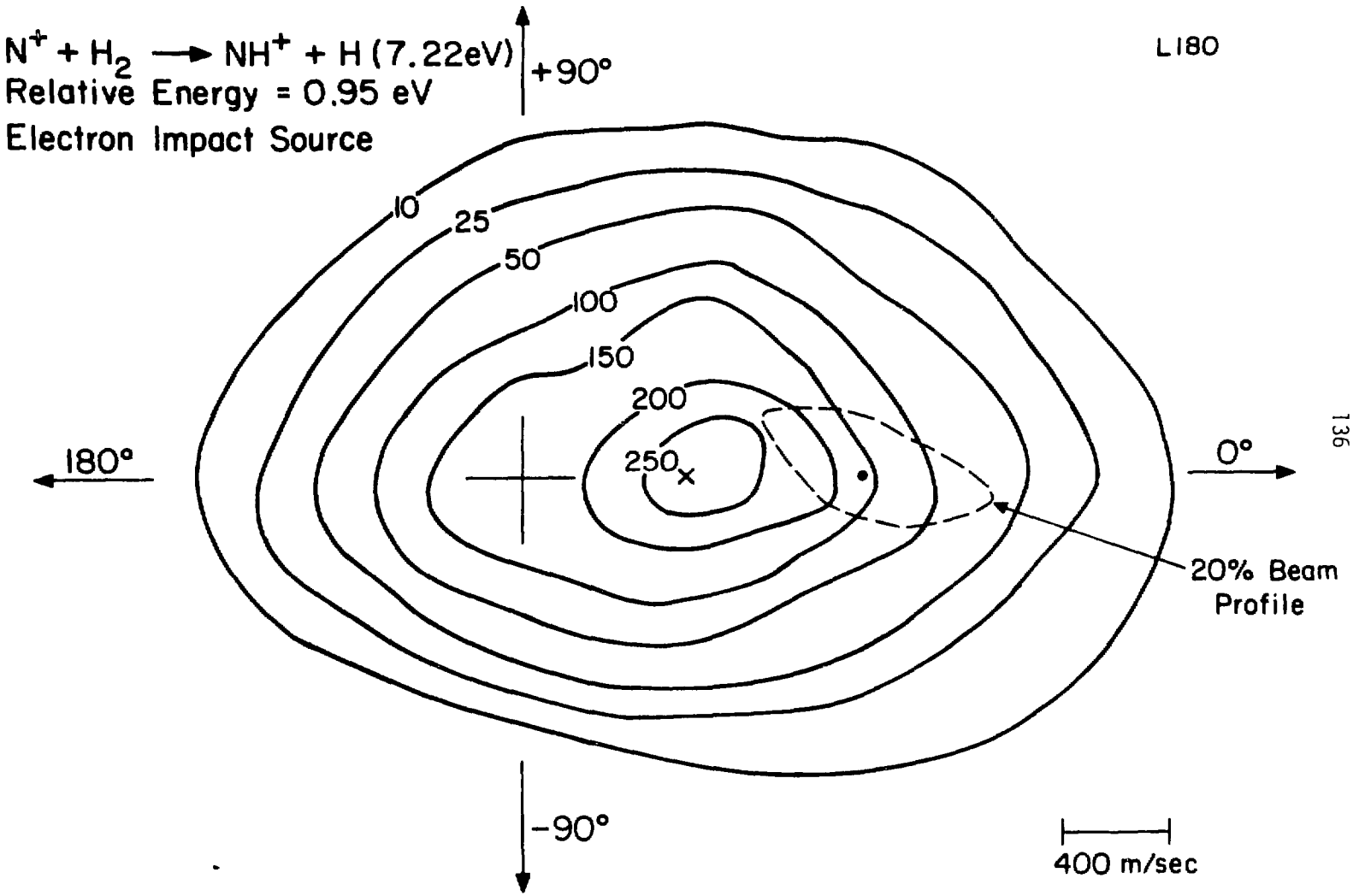
$N^+ + H_2 \longrightarrow NH^+ + H\,(7.22eV)$
Relative Energy = 0.95 eV
Electron Impact Source
L180
+90°
10
25
50
100
150
200
250
180°
0°
-90°
20% Beam Profile
400 m/sec

Fig. 20

Fig. 21 The intensity distribution of NH^+ resulting from N^+-H_2 collisions at an initial relative energy of 1.43 eV.

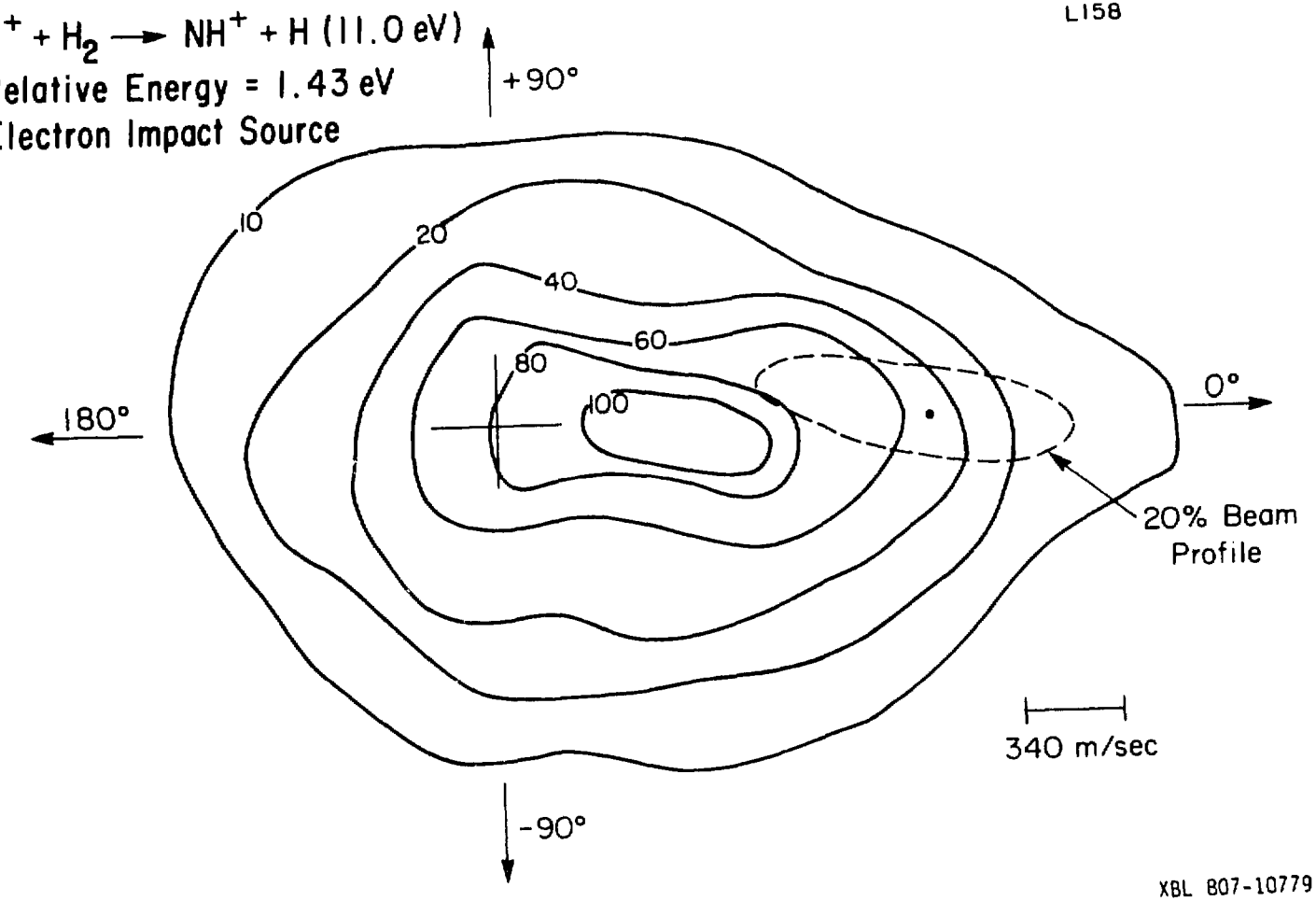

XBL 807-10779

Fig. 21

Fig. 22. Relative velocity vector scan of NH^+ produced by N^+-H_2 collisions at an initial relative energy of 1.45 eV. N^+ was produced by the impact of 160 eV electrons on N_2. Data was taken along the theoretical relative velocity vector. Error bars represent one standard deviation. v_{cm} and v_{ss} denote the center-of-mass and spectator stripping velocities respectively.

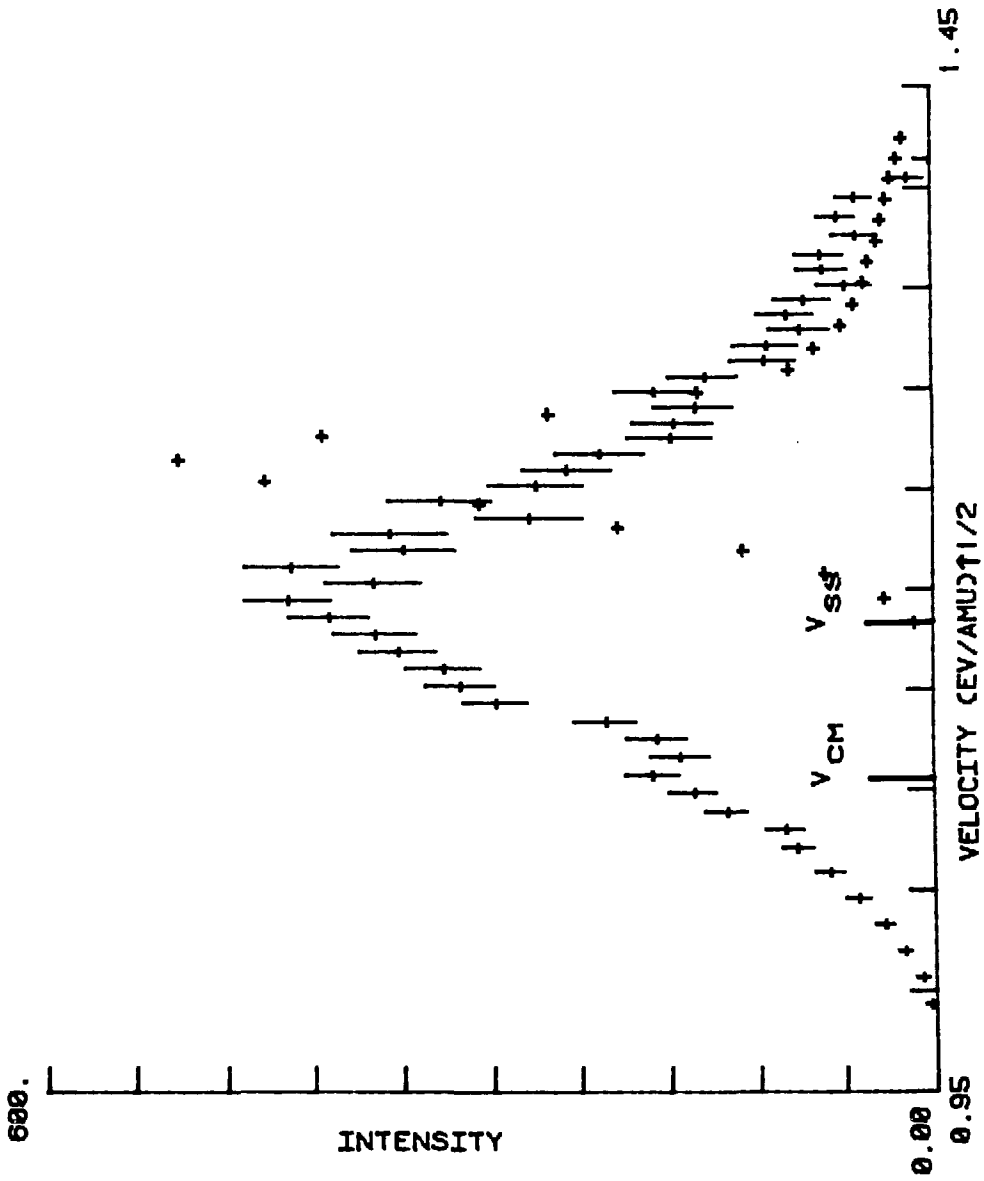

Fig. 22

quite different from what is seen when N^+ is produced in a microwave discharge. Fig. 22 nicely shows that at 1.45 eV, the forward peak occurs at spectator stripping.

The logical explanation for the difference in the distributions obtained with electron impact and microwave discharge produced N^+ lies in the electronic state populations. As was shown in Table 1, these populations are very source dependent. Apparently the metastable ions that are reacting, react in a direct fashion. The fact that the beams containing metastable ions give more forward peaked distributions is consistent with our earlier argument for explaining the difference between our $N^+(^3P)$ work and previous results.

A bimodal distribution attributable to two different reactant states has been reported before for $O_2^+(D_2,D)O_2D^+$.[42] The excited reactant, $O_2^+(^4\Pi_u)$, for which the reaction is 2.0 eV exothermic, produces O_2D^+ at velocities greater than spectator stripping in the energy range 1.0-4.14 eV. The ground state reactant gives symmetric product distributions in this energy range.[14].

The complete domination of Figs. 19-22 by the forward peak would suggest that the reaction cross section of the metastable(s) is much larger than that of $N^+(^3P)$. This is not surprising since the cross section is small with the ground state ion, but recent thermal energy work indicates that charge transfer is preferred to H atom transfer in metastable N^+-H_2 collisions.[7] Also we observe similar signal levels with all ion sources implying that a large forward peak did not "grow" on a symmetric distribution but rather a modest peak was added

and the symmetric part decreased in intensity. This conclusion is consistent with our belief that $N^+(^3P)$ comprises less than half of the electron impact produced beam. A discussion of the reactivity of the various metastables is included in a later section.

Fig. 23 shows a non-reactive distribution obtained with the electron impact source at an initial relative energy of 1.63 eV. The distribution is rather broad in the forward hemisphere and appears to be more inelastic than Figs. 12 and 14. Also, any backward peaking seems decreased with this source which is logical, considering the lower $N^+(^3P)$ fraction and thus reduced long-lived complex formation. Two other non-reactive experiments were performed using the electron impact source in this energy range, but in neither is a prominent backscattered peak seen.

Radiative Association

As mentioned previously, the reaction

$$N^+ + H_2 \rightarrow NH_2^+ + h\nu \qquad (2)$$

is an interesting process which has been tentatively reported by Ottinger.[4] His conclusions were based on otherwise unexplained emission observed in N^+–H_2 collisions. We attempted to measure directly the NH_2^+ formed in such collisions.

Fig. 23. The intensity distribution of N^+ scattered from H_2 at an initial relative energy of 1.63 eV. N^+ was produced by the impact of 160 eV electrons on H_2.

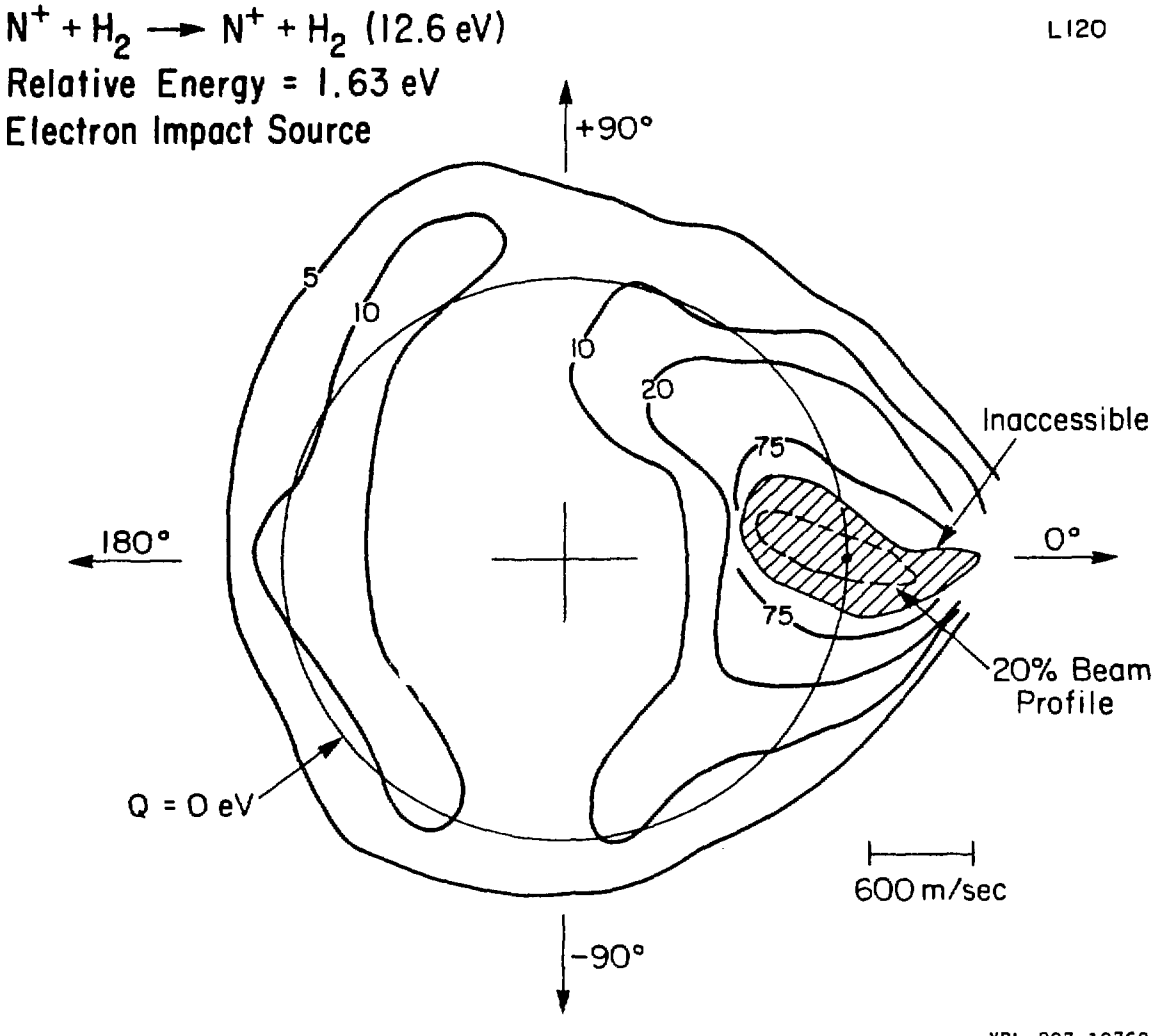
$N^+ + H_2 \longrightarrow N^+ + H_2$ (12.6 eV)
Relative Energy = 1.63 eV
Electron Impact Source
L120
+90°
5
10
10
20
75
75
Inaccessible
180°
0°
20% Beam Profile
Q = 0 eV
600 m/sec
-90°
XBL 807-10769

Fig. 23

Due to the low cross section of reaction (2) (Ottinger estimates $\sigma \approx 10^{-20} cm^2$), we did not attempt to observe it using a crossed H_2 beam, but instead leaked H_2 into the main chamber. This increased the probability of N^+-H_2 collisions and allowed the measurement of actual signal at mass 16. The problem with such an experiment though is that multiple collision events can produce NH_2^+ through the two step process:

$$\left.\begin{aligned} N^+ + N_2 &\rightarrow NH^+ + H \\ NH^+ + H_2 &\rightarrow NH_2^+ + H \end{aligned}\right\} \quad . \qquad (8)$$

Data were taken at H_2 pressures ranging from 3×10^{-5} to 2×10^{-4} torr as measured by an ion gauge. In principle, process (8) would have a quadratic dependence on H_2 pressure while reaction (2) would be linearly dependent. Our experiments were inconclusive as to this functionality, but the observation that 1×10^{-4} torr H_2 attenuated a 10 eV N^+ beam by ~60% confirms that multiple collisions may indeed be a factor. This was verified by an experiment in which HD was used as as collision partner. If process (2) was the primary reaction to form mass 17 (NHD^+) product then no mass 18 (ND_2^+) should be seen. If process (8) dominates, then the ratio NHD^+/ND_2^+ should equal two. Our experiment verified the latter possibility.

The cross section for $NH^+(H_2,H)NH_2^+$ has been investigated as a function of energy and is quite large.[11] At 2 eV relative energy we can estimate $\sigma(8b) \approx 10^{-15}cm^2$, $\sigma(8a) \approx 10^{-16}\ cm^2$, and using Ottinger's estimate, $\sigma(2) \approx 10^{-20}cm^2$. Even in an experiment which would "guarantee" single collision conditions by limiting the probability of N^+-H_2 collisions to 2% (as in a crossed beam experiment), there is substantial contamination from process (8). If we follow the trajectories of 10^7 N^+ ions, 2×10^5 have collisions with H_2. The cross section for H atom transfer is $\approx$1/10 of the (Langevin) collision cross section so 2×10^4 NH^+ ions are formed but only 2 NH_2^+ ions are formed via radiative association. The probability of NH^+ having another collision is roughly $(.02)^2 = .0004$ and hence ~80 NH^+-H_2 collisions occur. The reaction to form NH_2^+ proceeds at the Langevin rate so ~80 NH_2^+ ions are formed by the two step process. Hence even under "single collision conditions" the two step process dominates. It would take a very sensitive apparatus to go to low enough H_2 pressure to unambiguously verify reaction (2).

Analysis of Dynamics

NH_2^+ Orbitals

We begin our discussion of the dynamics of the N^+-H_2 system by discussing the structure of NH_2^+. Fig. 24 gives a qualitative picture of the orbitals of a general molecule XH_2. The schematic

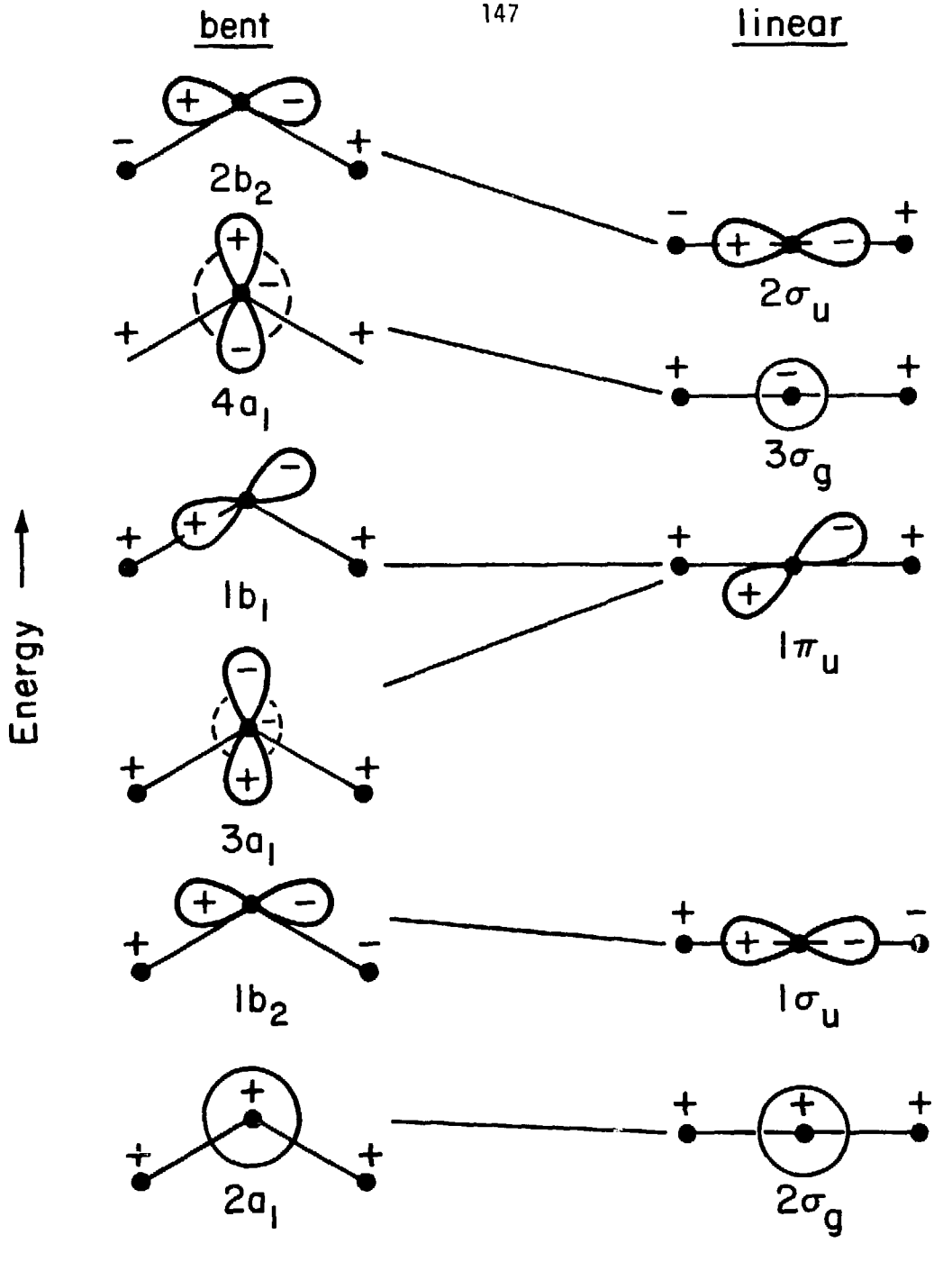

XBL 807-10762

Fig. 24. Molecular orbital pictures of an XH_2 molecule. The lines connecting bent and linear structures show qualitatively the evolution and energy change of the MO's as the geometry is changed.

orbitals rely heavily on an LCAO-MO approach as they are basically linear combinations of 2s and $2p_{x,y,z}$ orbitals of X and the 1s orbitals of H. The change in energy of the orbitals as a function of bond angle is adapted from a Walsh diagram given by Herzberg.[43] The energetic ordering of the orbitals is believed to be correct, but the energy scale is not meant to be quantitatively accurate. The $1a_1$-$1\sigma_g$ orbital, which is not shown, is essentially the 1s orbital of X, and lies much lower in energy.

It is interesting to consider just how accurate the LCAO-MO model is when applied to a real molecule. As discussed by Mulliken[44], a molecular orbital belongs to an irreducible representation of the point group of the molecule. By the variational principle, the best form for an MO is the linear combination of basis orbitals (belonging to the same irreducible representation) which minimizes the energy. For orbitals which are not the lowest roots of their symmetry class, the variational calculation is still done but is subject to the constraint that this orbital must be orthogonal to all lower roots. It is common to use symmetry-adapted atomic orbitals as the basis functions for such a calculation.

Levine,[45] quoting the results of Pitzer and Merrifield,[46] gives a good discussion of the MO's of H_2O; these should be quite similar to those of NH_2^+. Table 2 gives the coefficients obtained by the minimal-AO-basis-set calculation of Ref. 46. The computed coefficients largely confirm the validity of an LCAO-MO approach but the hard numbers add extra information when deciding the bonding properties of the MO's.

Table 2

	1s(O)	2s(O)	$2p_x$(O)	$2p_y$(O)	$2p_z$(O)	$1s(H_1)+1s(H_2)$	$1s(H_1)-1s(H_2)$
$1a_1$	1.00	.01	-	-	.003	-.0004	-
$2a_1$	-.03	.82	-	-	.13	.15	
$1b_2$	-	-	-	.62	-	-	.42
$3a_1$	-.03	-.50	-	-	.79	.26	-
$1b_1$	-	-	1.00	-	-	-	-
$4a_1$	.08	.84	-	-	.70	-.75	-
$2b_2$				.99	-	-	-.89

Coefficients obtained by Pitzer and Merrifield for the low-lying MO's of H_2O using a minimal-AO-basis set. The experimental geometry of H_2O was assumed in the calculation.

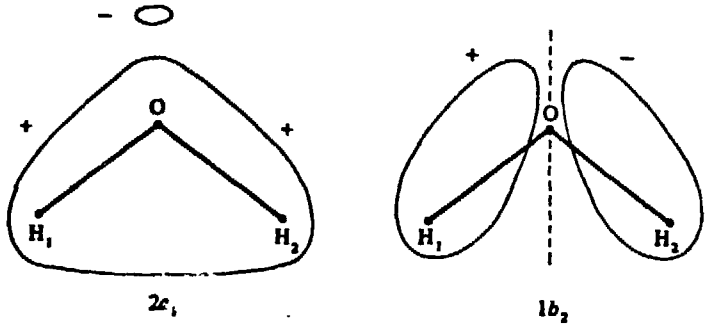

Fig. 25 Sketches of bonding MO's in H_2O adapted from Levine.

The $1a_1$ orbital, as mentioned already, is the 1s(O) orbital and hence is non-bonding. The $2a_1$ orbital, though mainly the 2s(O) orbital, has net overlap between the three atoms and is bonding. The $1b_2$ orbital is strongly O-H bonding. The $3a_1$ orbital is mainly non-bonding because any net gain from $2p_z$(O)-1s(H) overlap is largely offset by 2s(O)-1s(H) repulsion. $1b_1$ is a pure atomic orbital and so is non-bonding. The $4a_1$ and $2b_2$ orbitals are obviously (best seen in Fig. 24) antibonding. A further use of the variational calculation is that more accurate shapes of the MO's can be determined. The two strongly bonding orbitals are shown in Fig. 25. One should realize that the coefficients given in Table 2 are functions of the assumed molecular geometry. This is made obvious when one considers that the $4a_1$ orbital becomes $3\sigma_g$ in the linear molecule and that all $2p_z$(O) character must vanish due to its π symmetry.

Orbital Correlations

As N^+ approaches H_2, the orbitals of these separated species change smoothly into the MO's of NH_2^+ and then into those of the product molecules. By using symmetry rules, an orbital correlation diagram can be made and the evolution of the various orbitals can be traced. This was first done by Griffing[47] and an excellent discussion pertinent to ion-molecule reactions has been given by Mahan.[48]

An orbital correlation diagram pertinent to N^+–H_2 collisions is shown in Fig. 26. The reactant orbital energies are estimated by the amount of energy required to remove an electron from that orbital in the neutral species. There is some uncertainty associated with this procedure as vertical and adiabatic ionization potentials can be quite different. Some of the C_{2v} NH_2^+ orbitals are placed relative to each other with the aid of an extensive CI calculation on the states of NH_2^+.[49] These orbitals are located with respect to the reactant orbitals by assuming that the $1b_1$ orbital does not change energy as the complex is formed. This is also an uncertain proposition because the ionization energy of NH_2 is only 11.4 eV which would imply a 3 eV upward shift in the NH_2^+ orbitals. Further complicating matters is the fact that in NH_2 the $3a_1$ orbital is above the $1b_1$ orbital though there is an apparent reversal in the ion. Some of these problems can be traced back to the assumption that the energy of an orbital is equal to the amount of energy required to remove an electron from it. This is essentially Koopman's Theorem which is only approximately true for closed shell systems and can give large errors for open shells such as these. Therefore, the energy levels given in Fig. 26 are of only qualitative accuracy.

The actual correlation of the orbitals (the lines connecting the energy levels) is done virtually by inspection in this simple case but in general can be done with the aid of tables[43] for propagating symmetry species in different point groups. The non-crossing rule, which

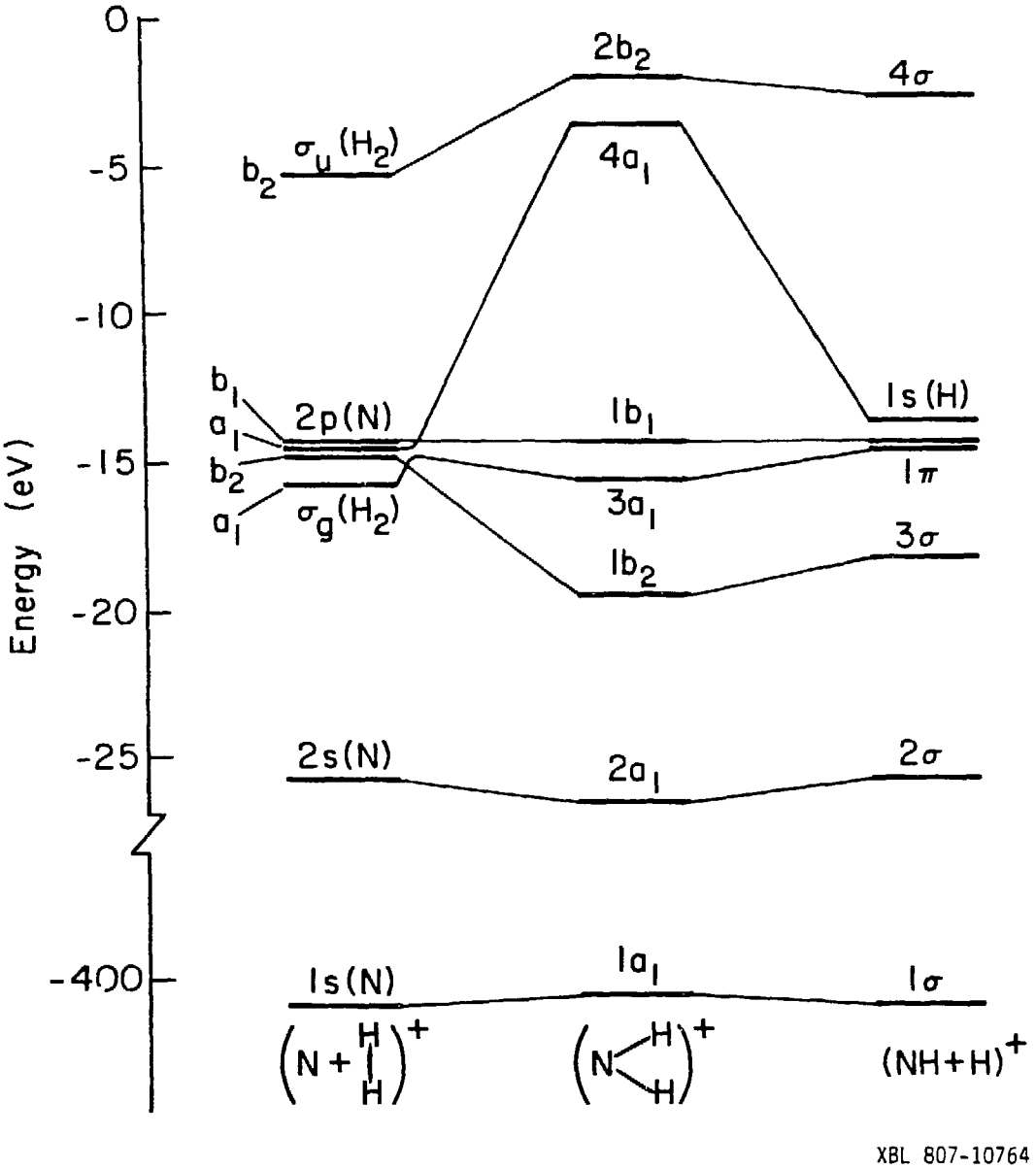

Fig. 26. An orbital correlation diagram for N^+-H_2 collisions. A C_{2v} approach is assumed for the reactants. Note the break in the energy scale.

says that potential energy curves of the same symmetry will not intersect,[50] has also been assumed.

By filling the orbitals on the reactant side and following the location of the electrons through the intermediate and products we can now begin to discuss the dynamics. The lowest three orbitals on the left side of Fig. 26 are all filled but there are only two electrons to be distributed among the three degenerate 2p orbitals of nitrogen. If $N^+(^3P)$ is the reactant ion, the electrons are in different orbitals (say $2p_x$ and $2p_y$) with parallel spins. Defining the z-axis as the direction of approach to the H_2 bond, then $2p_x$ and $2p_y$ evolve into the $1b_2$ and $1b_1$ orbitals respectively, which leads to the electron configuration $1a_1^2 2a_1^2 1b_2 3a_1^2 1b_1$ of NH_2^+. This is a $^3A_2$ state which should be much higher in energy than the lowest state of $NH_2^+(^3B_1\text{-}1a_1^2 2a_1^2 1b_2^2 3a_1 1b_1)$ due to the promotion of a strongly bonding $1b_2$ electron. Alternate placements of the two 2p electrons lead to even higher energy intermediates. The three possible approaches are shown schematically in Fig. 27. Because the deep well associated with $NH_2^+(^3B_1)$ is not accessible in the C_{2v} orbital correlation diagram, it was concluded by Mahan[48] that in the absence of a_1-b_2 orbital interaction, reaction (1) should be direct.

If N^+ does not approach along the perpendicular bisector of N_2 the C_s point group is appropriate. Transforming from C_{2v} to C_s symmetry can take both the a_1 and b_2 species to a". Thus in C_s symmetry the crossing between the $1b_2$-a" and $3a_1$-a" curves is avoided and the ground state orbital configuration can result. In

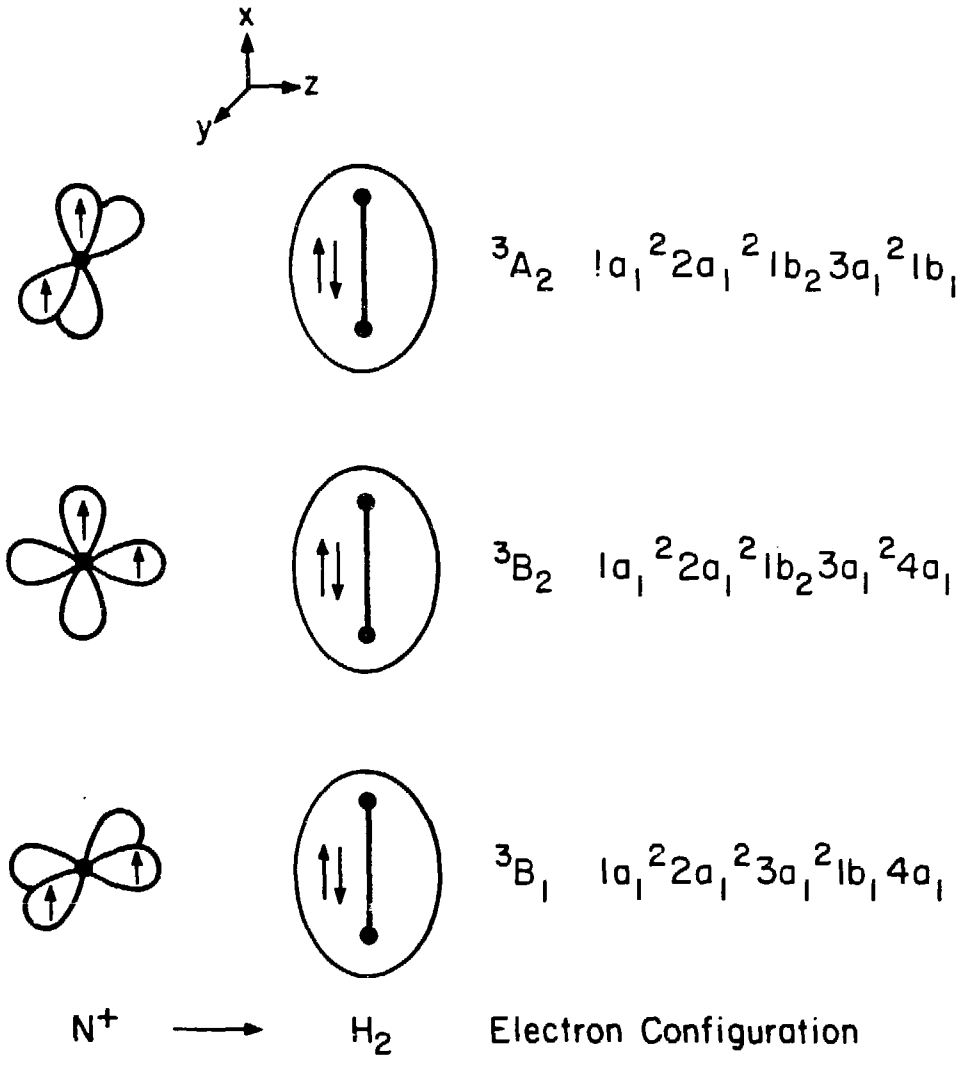

Fig. 27. Diagram of the three possible C_{2v} approaches of $N^+(^3P)$ to H_2.

tracing the electrons through the products we find that all end up in molecular rather than H atom orbitals and the predicted products are $NH + H^+$. The fact that the observed products are $NH^+ + H$ demonstrates a fallibility of the orbital correlation approach.

State Correlations

As was discussed in Chapter 1, the application of molecular state correlation diagrams has been crucial to the understanding of simple chemical reactions. These diagrams are especially well-suited to simple systems which maintain some elements of symmetry during the course of the reaction. In these systems, often more information is gained from the state diagram than the orbital diagram.

Fig. 28 shows a partial state correlation diagram for some of the lower electronic states of NH_2^+. It is very similar to one published previously;[12] however, there are several changes which reflect a refinement in the position of the energy levels thanks to modern ab initio techniques. Of particular help is the work of Peyerimhoff and Buenker[49] who calculated many states of NH_2^+.

As in the orbital correlation diagram, the energy levels for the various species are placed and then the correlations are done subject to symmetry and spin constraints. The energy of $N^+(^3P) + H_2$ is taken as zero and the other possible asymptotes are placed with the aid of tables given by Moore[51] and the known ionization potentials. The energies of the C_{2v} and $D_{\infty h}$ intermediates were determined theoreti-

Fig. 28. Electronic state correlation diagram for the important low-lying surfaces of the NH_2^+ system. The left-hand side considers the approach of N^+ (or N) along the perpendicular bisector of H_2 (or H_2^+). On the right, collinear approaches are considered. The dashed lines indicate pathways which are allowed in C_s symmetry.

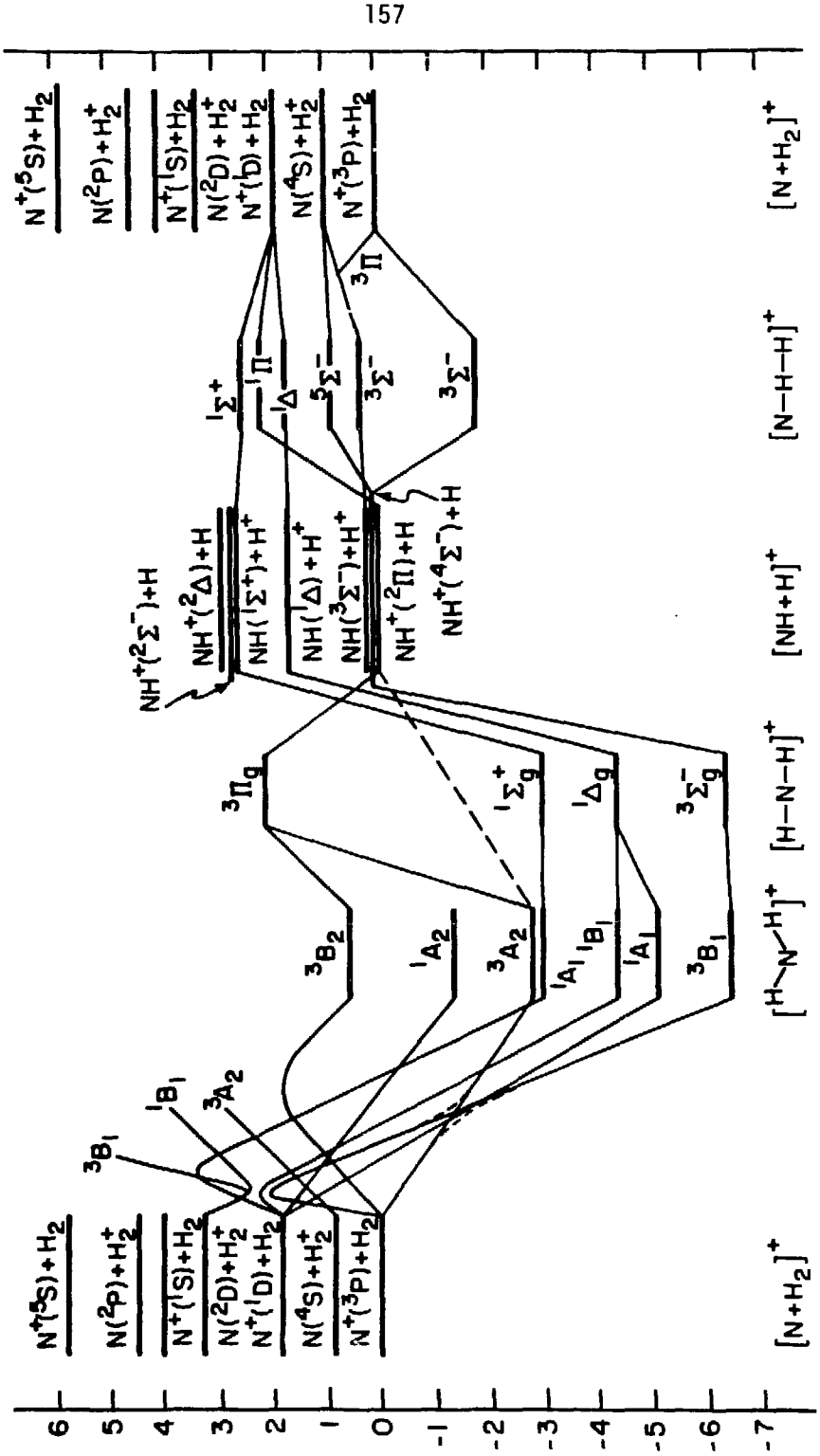
E (eV)
6
5
4
3
2
1
0
-1
-2
-3
-4
-5
-6
-7
N+(5S)+H2
N(2P)+H2+
N+(1S)+H2
N(2D)+H2+
N+(1D)+H2
N(4S)+H2+
N+(3P)+H2
3B1
1B1
3A2
3B2
1A2
3A2
1A1 1B1
1A1
3B1
3Πg
1Σg+
1Δg
3Σg−
NH+(2Σ−)+H
NH+(2Δ)+H
NH(1Σ+)+H+
NH(1Δ)+H+
NH(3Σ−)+H+
NH+(2Π)+H
NH+(4Σ−)+H
1Σ+
1Δ
1Π
5Σ−
3Σ−
3Σ−
3Π
3Σ−
N+(5S)+H2
N(2P)+H2+
N+(1S)+H2
N(2D)+H2+
N+(1D)+H2
N(4S)+H2+
N+(3P)+H2
[N+H2]+
[H—N—H]+
[NH+H]+
[N—H—H]+
[N+H2]+

Fig. 28

cally.[49] The $(NH + H)^+$ products are placed assuming the reaction is thermoneutral, I.P.(NH) = 13.5 eV, and then using the tables of Huber and Herzberg[10] for the excited states. The placement of the $C_{\infty v}$ NH_2^+ complex energy levels is more problematical. Ab initio calculations show the existence of a 1.7 eV well associated with the lowest $^3\Sigma^-$ surface.[52,53] These studies further showed that the $^3\Pi$ and second $^3\Sigma^-$ surfaces are both repulsive (not shown in the diagram for $2^3\Sigma^-$). The higher states are all estimated.

If we consider C_{2v} approaches, we see humps in some of the lines connecting reactants and intermediates. Since these lines can be thought of as qualitative potential energy curves, these humps are meant to represent potential energy barriers. The existence of a barrier can be predicted by taking into account orbital correlations. It was discussed earlier, and illustrated in Fig. 27, that as $N^+(^3P)$ approaches along the perpendicular bisector of H_2, the states $^3A_2$, $^3B_2$, and $^3B_1$ arise. A strict orbital correlation predicts $1b_2 3a_1^2 1b_1$, $1b_2 3a_1^2 4a_1$, and $3a_1^2 1b_1 4a_1$ respectively for the occupation of the outer orbitals of these states. Table 3, which uses information from Ref. 49, gives the orbital occupation and relative energies of the lowest states of NH_2^+. It can be seen that the $^3B_2$ and $^3B_1$ intermediates arising from ground state reactants are not the lowest states of these symmetries. Both the lowest $^3B_1$ and $^3B_2$ states orbitally correlate to $N(2p_n^2 2p_m) + H_2^+$ reactants which, in lowest energy, corresponds to $N(^2D) + H_2^+$. This means that as $N^+(^3P)$ and H_2 approach each other on one of these surfaces, the potential energy initially increases as the system begins to correlate to a high energy

Table 3

State	Configuration					Energy (eV)	Angle (deg)
	$2a_1$	$1b_2$	$3a_1$	$1b_1$	$4a_1$		
$^3B_1$	2	2	1	1	–	0.0	149.6
$^1A_1$	2	2	2	–	–	1.29	107.6
$^1B_1$	2	2	1	1	–	2.03	155.2
2^1A_1	2	2	–	2	–	3.45	180
$^3A_2$	2	1	2	1	–	4.12	60
$^1A_2$	2	1	2	1	–	5.64	63
$^3B_2$	2	1	1	2	–	7.42	89
4^1A_1	2	1	1	2	–	8.5	50
$^1B_2$	2	1	1	2	–	9.24	98
$^3A_1$	2	2	1	–	1	11.09	180
2^3B_1	2	2	–	1	1	11.09	180
3^1A_1						11.97	180
2^1B_1	2	2	–	1	1	11.97	180
$^5A_2$	2	1	1	1	1	14.2	180

Orbital occupations, relative energies, and optimized angles for NH_2^+. The energies were calculated at the (estimated) full CI limit assuming a fixed NH separation (1.027Å) but optimum bond angle.

state. The upward motion continues until we approach the surface descending from $N(^2D) + H_2$. This surface is heading toward the lowest state of that symmetry. The crossing between these surfaces will generally be avoided, and so the ascending surface reverses direction and moves down, with different orbital character, to the lowest energy state of that symmetry. Hence there does exist an adiabatic pathway for ground state reactants to the deep (6.45 eV) $^3B_1$ well of NH_2^+ in C_{2v} geometry, but the barrier blocks the way for low energy collisions.

In a similar way, we can see barriers arising for some $N^+(^1D) + H_2$, C_{2v} approaches. The lowest $^1B_1$ state is $2a_1^2 1b_2^2 3a_1 1b_1$ which is the equivalent of the ground state except for one spin flip. It also orbitally correlates the $N(^2D) + H_2^+$. The $^1B_1$ state arising from $N^+(^1D) + H_2$ is $2a_1^2 3a_1^2 1b_1 4a_1$ so that again an avoided crossing and barrier are indicated. The second $^1A_1$ state has the $3a_1$ orbital unoccupied and hence orbitally correlates with the high-lying $N^- + 2H^+$. Since the two lowest surfaces of $^1A_1$ symmetry both arise from $N^+(^1D) + H_2$, a barrier is expected for the upper one. It should be mentioned again that Herzberg[43] gives tables which tell how symmetry is propagated as the point group changes.

It can be seen that ground state reactants connect with $NH^+ + H$ products adiabatically for both C_{2v} and collinear approaches. The C_{2v} path is on the $^3A_2$ surface and collinearly it is the $^3\Sigma^-$

surface. The expected adiabatic product is $NH^+(^4\Sigma^-)$, not ground state $NH^+(^2\Pi)$, and there is experimental evidence that the quartet is the dominant product.[8] It is interesting to note that, as previously mentioned, the thermal rate constant for reaction (1) is 1/3 the Langevin rate. Of the three possible approaches in strict C_{2v} symmetry, two have barriers and thus would not lead to reaction. Similarly, two out of three collinear approaches will be on the repulsive $^3\Pi$ surface, and should also be non-reactive. Hence there is satisfying agreement between this argument and experiment. It is also interesting to consider how the states in $C_{\infty v}$ symmetry correlate with the C_{2v} states. This can be done by examining the behavior of the 2s and 2p orbitals[13] of nitrogen as linear NHH^+ is bent into symmetric HNH^+. The $2s\sigma$ orbital, which is essentially the 2s orbital of N, goes over the the $2a_1$ orbital in C_{2v} symmetry. The $2p\pi$ orbital in the plane perpendicular to the plane the molecule is bent goes over to the non-bonding $1b_1$ orbital. The $2p\sigma$ and in-plane $2p\pi$ both become a' orbitals in C_s symmetry and may become degenerate and mix before emerging as $1b_2$ and $3a_1$. Thus if the $^3\Sigma^-(2s\sigma^2 2p\sigma^2 \pi_x \pi_y)$ state is bent into C_{2v} symmetry, it can become $2a_1^2 1b_2^2 1b_1 3a_1$ which is the lowest $^3B_1$ state.

As discussed by Hirst[53] though, it appears that a correlation of $^3\Sigma^- - ^3A_2$ is more appropriate. This was concluded by performing <u>ab initio</u> calculations for various approach angles ranging from collinear to C_{2v}. The lowest potential curve for each geometry looked about the same (at fixed r(H-H)) and corresponded to $^3A_2$ in C_{2v}

and $^3\Sigma^-$ in $C_{\infty v}$. The logical explanation is that although $^3B_1$ can result, for large N–H_2 distances, the $^3A_2$ state is lower in energy (it goes to a lower asymptote) and hence is the state to which $^3\Sigma^-$, through an avoided crossing in C_s symmetry, correlates. For smaller N–H_2 distances, or larger H–H distances, we would expect that the $^3\Sigma^-$–$^3B_1$ correlation is possible. This argument strengthens our earlier argument for the rate of reaction (1) being 1/3 the Langevin rate. Regardless of the approach angle, only one of the three surfaces is not initially repulsive and can lead to reaction. If $^3\Sigma^-(C_{\infty v})$ and $^3B_1(C_{2v})$ correlated at large distances, then two out of three collisions might be expected to lead to reaction. This is because thermal encounters have sufficient time to align to the lowest energy path and both $^3\Sigma^-$–$^3A''$–$^3B_1$ and $^3\Pi$–$^3A''$–$^3A_2$ would have low energy approaches. That there is sufficient time for alignment can be inferred from the fact that $O^+(H_2,H)OH^+$ proceeds at the Langevin rate[6b] though the only low energy approach is a collinear one.[54]

As was discussed by Fair and Mahan,[12] an important change in the state correlations occurs if we allow the collision symmetry to distort from C_{2v}. The symmetry elements which distinguish the $^3A_2$ and $^3B_1$ surfaces are no longer possessed by the system and both surfaces become $^3A''$. Thus in C_s symmetry, the crossing between the $^3A_2$–$^3A''$ and $^3B_1$–$^3A''$ surfaces is avoided and it should be possible to attain the $^3B_1$ well without activation by moving initially on the $^3A_2$–$^3A''$ surface. This reaction path is indicated in Fig. 28 by a dotted line.

Once the system falls into the deep well it can be expected that the complex will exist for many vibrational periods as the trajectory rattles around, searching for an exit channel. The fact that an avoided crossing is encountered en route to the deep well immediately suggests a possible explanation for the observed dynamics. When two potential surfaces are near each other, the probability that a transition will occur non-adiabatically from one surface to the other is a function of the velocity of the trajectory. Perhaps then the anomalously short lifetime of the NH_2^+ complex at 2 eV reflects the difficulty in attaining the deep well rather than the lifetime of a trajectory in the deep well. This explanation is discussed in greater detail in the next section.

Conical Intersections and Surface Hopping

If we fix the distance between the two H atoms, the potential energy of the N^+–H_2 system becomes a function of r, the N^+–H_2 center-of-mass distance, and θ, the angle between $\underline{r}$ and the H_2 bond. C_{2v} symmetry is attained if $\theta = \pi/2$ and, at this angle, the $^3A_2$ and $^3B_1$ surfaces can intersect. For any other value of θ, both surfaces are $^3A''$ in C_s symmetry and the intersection is avoided. This special situation is known as a conical intersection.

Conical intersections were first discussed by Teller[55] but his work has been extended by others.[56,57] Fig. 29 shows a hypothetical conical intersection. It is a somewhat idealized representation because

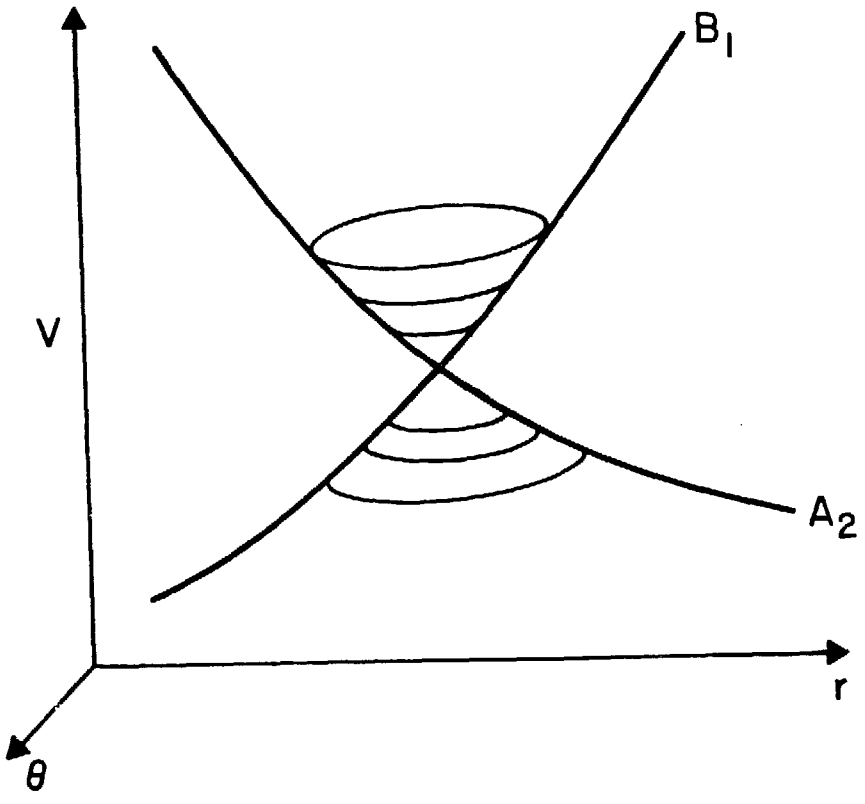

XBL 807-10765

Fig. 29. A conical intersection between B_1 and A_2 states in C_{2v} symmetry. The surfaces intersect at one point ($\theta = \pi/2$) and form a double cone for small excursions from this point.

in general one does not expect these cones to be circular as $(\frac{\partial V}{\partial r})_\theta$ and $(\frac{\partial V}{\partial \theta})_r$ can be quite different. Also, for the case at hand, it is not clear that the intersection occurs on a rising part of the $^3A_2$ surface and a falling part of the $^3B_1$ surface. This should not affect our discussion of the dynamics though.

At low initial relative energies, a C_{2v} trajectory, approaching from the right on the A_2 surface, will avoid the region near the apex of the cone.[55] It will move out of the plane of the paper (departure from $\theta = \frac{\pi}{2}$) and take a low energy path on the surface of the lower cone and emerge on the B_1 surface. A trajectory with higher initial relative energy can more easily visit the apex, hence increasing the probability of attaining the upper surface. In the N^+-H_2 system, adiabatic behavior (i.e. staying on the lower conical surface) would give access to the deep potential well and a long-lived intermediate would be expected. Higher energy collisions might cause considerable diabatic behavior, preventing a trajectory from sampling the deep well and hence giving NH^+ by a direct reaction mechanism. This explanation successfully explains the experimental results.

It should be noted that the above argument can be given completely qualitatively without any exact calculation of the surfaces involved. Because of subsequent theoretical work though, it appears now that the qualitative assertions are based in fact. A 1977 Faraday Discussion concerning potential energy surfaces received two papers on the lowest triplet surfaces of NH_2^+.[52,58] The predicted barriers in the $^3B_1$

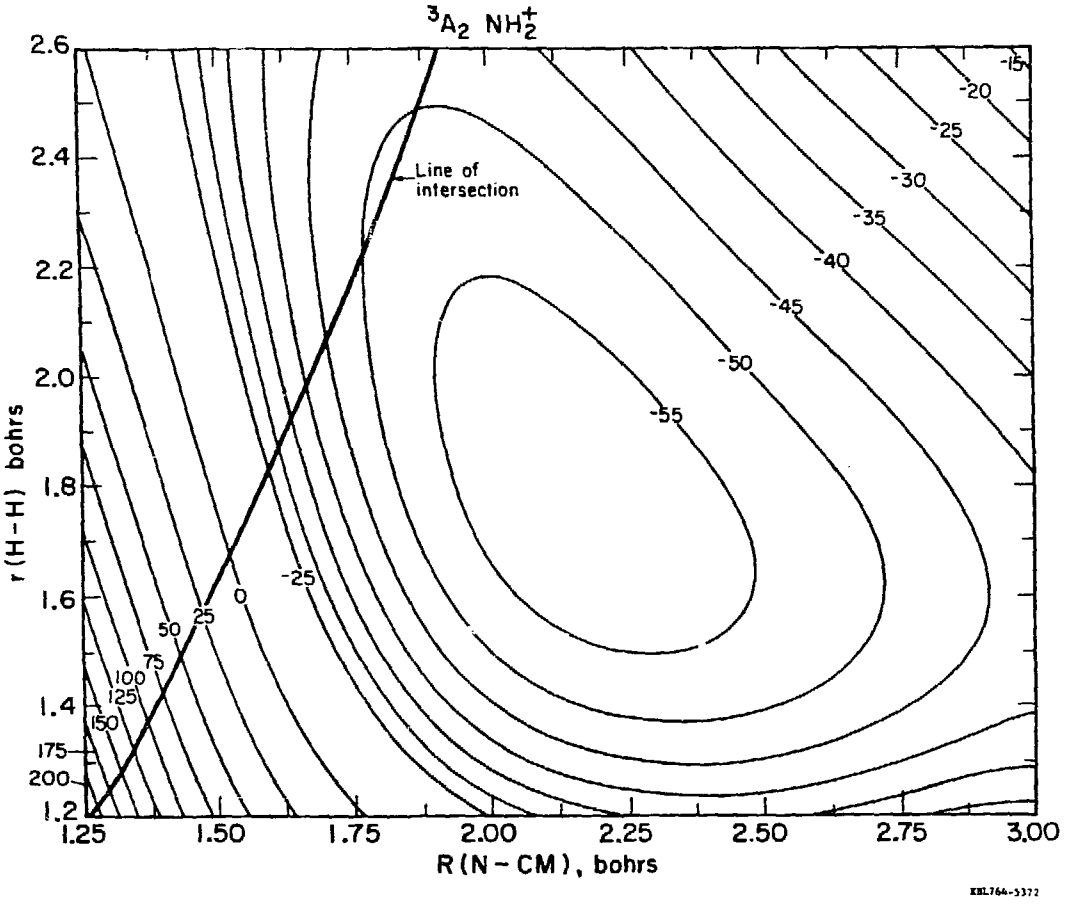

Fig. 30. A portion of the $^3A_2$ potential energy surface for NH_2^+. R(N-CM) is the distance from the nitrogen nucleus to the H_2 center-of-mass. Contours are labeled in kcal/mole relative to infinitely separated N^+ plus H_2.

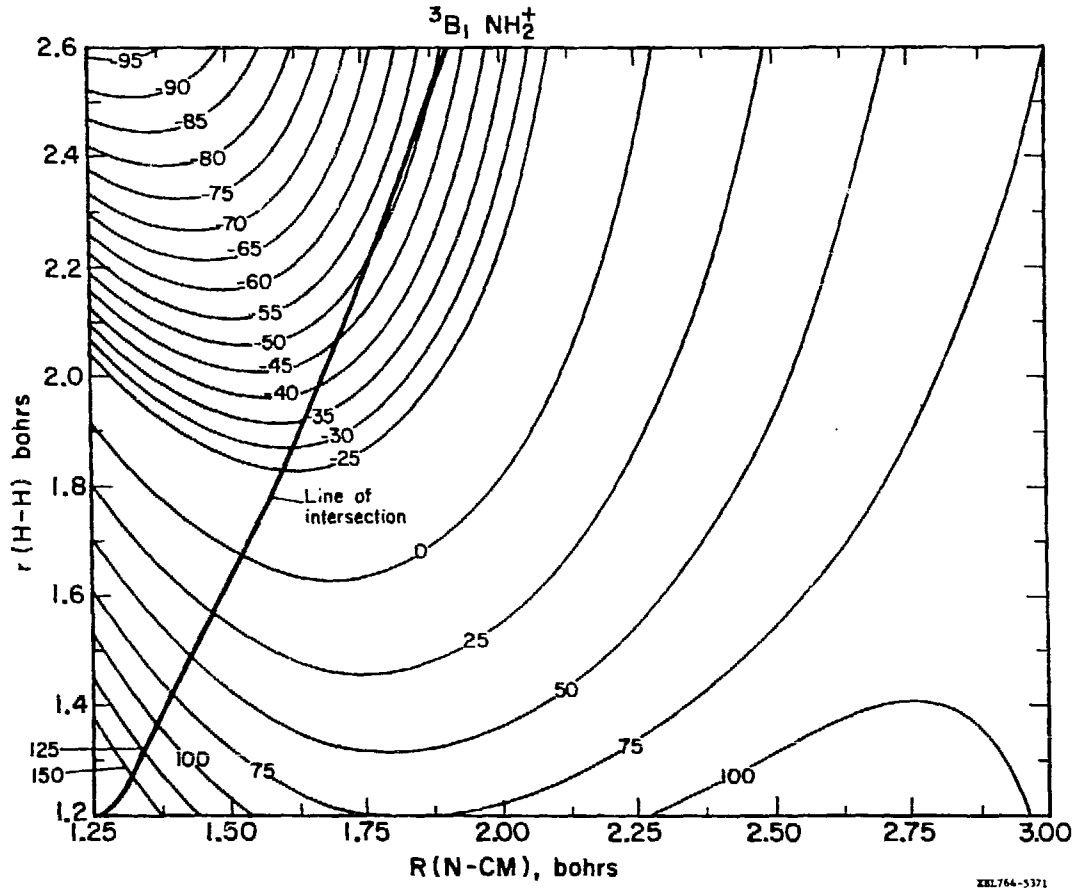

Fig. 31. A portion of the $^3B_1$ potential energy surface for NH_2^+. Note that this region is shown because of the presence of the $^3B_1$-$^3A_2$ seam. The minimum energy point of this surface (~140 kcal/mole) is not shown but occurs at R(N-CM) = 0.60 and R(H-H) = 3.65 bohrs.

and $^3B_2$ surfaces were verified, and it was further seen that the $^3A_2$ surface was attractive with a considerable well. This fact had not been anticipated in the early correlation diagram,[12] but does not significantly change any dynamical arguments. Of greatest interest though is the avoided crossing of the $^3A_2$-$^3A''$ and $^3B_1$-$^3A''$ surfaces, which was nicely demonstrated. Schaefer and collaborators[58] mapped out the intersection of the two surfaces in C_{2v} symmetry; their results are shown in Figs. 30 and 31. The first thing to notice is that the seam cannot be reached without activation on the $^3A_2$ surface until r(H–H) becomes ~1.7 bohr or 0.9 Å. The equilibrium bond distance of H_2 is 0.74 Å[10] so that an increase of ~.16 Å would be necessary to reach this point. One would expect that only in low energy collisions, where the atoms have sufficient time to rearrange themselves as directed by the weak chemical forces would the H_2 bond length increase enough to access the seam and then the deep well. Furthermore high energy collisions might not only miss the seam, but would most likely be non-reactive.[58] This is because with r(H–H) fixed at 1.4 bohr, the $^3A_2$ surface becomes repulsive very quickly. It can be seen in Fig. 31 that there is indeed a barrier in the $^3B_1$ surface for the least motion insertion of $N^+(^3P)$ to H_2. This is a strict consequence of the conservation of orbital occupation as discussed earlier and by Woodward and Hoffman.[59]

We can also use these surfaces to make more detailed dynamical arguments. The most likely place to encounter the seam and hence make the transition from $^3A_2$ to $^3B_1$ character is probably where r(H-H) increases the least, subject to the constraint that the seam is reached without activation. This corresponds to a roughly equilateral triangle geometry of r ≈ .85 Å. As a trajectory departs this region on the lower ($^3B_1$-$^3A''$) surface, the hydrogen atoms strongly repel each other and the nitrogen is drawn in; this can be readily inferred from Fig. 31. Such motion may be interpreted as a large excitation in the bending vibrational mode of NH_2^+. If the energy stays primarily in this mode, it is easy to see how decomposition to NH^+-H would leave the NH^+ rotationally hot which is consistent with the experimental results. Such a mechanism has been given previously by Carrington in a study of the photodissociation of H_2O.[60] In this experiment, Lyman α radiation dissociated H_2O and emission was measured from the $OH(^2\Sigma^+)$ fragment. The emission showed the fragment to be rotationally hot. This is a somewhat amazing result considering that H_2O^* itself should not be very rotationally excited, having absorbed only one photon. In order to conserve angular momentum in the process, the H atom would have to leave with an exit impact parameter of ~4 Å, spiraling out in the other direction. It is thought that the rapid bending in the linear H_2O intermediate was induced by a vertical transition from the bent ground state. This argument is applicable to the N^+-H_2 system due to the bent nature of NH_2^+ near the seam and the quasilinear $^3B_1$ ground state.[61]

The near-C_{2v} bending complex cannot dissociate non-reactively due to the presence of a barrier. In complexes formed by low energy collisions, non-reactive decomposition will occur only if the system reattains the $^3A_2$ surface or if the geometry significantly changes from C_{2v} symmetry. Regardless of which of these two paths is more likely, there is no a priori reason to expect considerable rotational excitation of H_2 and none is seen experimentally.

We have not yet considered just how likely it is that the $^3B_1$ surface is attained given that the seam is encountered. This problem has been addressed for the N^+-H_2 system by Gittins et al.[52] Their approach was to use the approximations of Bauschlicher et al.[62] to the Landau-Zener-Stuckelberg (LZS) formulation.[63-65] The LZS method is a one-dimensional approach formulated in terms of diabatic (intersecting) potential curves. In order to apply it to real systems, it was altered for use with adiabatic (non-intersecting) potential curves and several approximations were made.[62] The resulting equation is

$$P = \exp(-E_c/E)^{1/2}$$

where

$$E_c = \frac{\pi^2}{8}\left(\frac{\mu}{h^2}\right)\left(\frac{\Delta E_o^3}{\Delta E''_o}\right)$$

with P as the hopping probability, E the collision energy, E_c the "critical" energy at which the probability of hopping is $e^{-1} = 0.37$,

ΔE_0 the energy separation between the surfaces and $\Delta E''_0$ the second derivative of the separation at the avoided crossing. The results of this calculation for reaction (1) were that even at low collision energies (< 1 eV) there was a large probability of hopping from the lower surface to the upper one. (This is the same as staying on the $^3A_2$ surface in C_{2v} symmetry.) It should be mentioned though that this calculation concentrated on large r(H-H) distances, which may not be dynamically relevant, and the probability of adiabatic behavior seemed to increase with decreasing r(H-H) values. Also the basis set chosen lacked potentially important polarization functions.[66,58] For these reasons the surface hopping calculation must be considered suspect.

Complex Lifetime

In light of the possibility that diabatic behavior predominates even at low energies in this system, we decided to perform RRKM calculations to see if long-lived complex formation was probable on the $^3A_2$ surface. We normally would not expect that the well is deep enough (2.8 eV[49]) to allow complex formation in the 1-2 eV collision energy range, but the reaction $CH_2^+(H_2,H)CH_3^+$ gives a symmetric distribution at 1.5 eV although possessing a well only 2.65 eV deep.[67] Of course, the greater number of internal degrees of freedom should extend the lifetime of this complex over that of a triatomic complex.

The decay of a long-lived complex can be thought of as a unimolecular chemical reaction. To estimate the rate constant of this reaction, there have been several approaches, the most successful of which are

statistical in nature. The assumption that vibrational energy is rapidly redistributed throughout a highly excited molecule is generally accurate. When enough energy accumulates in the reaction coordinate, then the molecule can decompose; the rate of decomposition can be statistically determined by finding the probability that sufficient energy appear in the correct vibrational mode. This is the basic idea behind the theory of Rice, Ramsperger, and Kassel (RRK).[68,69] Using this approach one obtains

$$k(E) = A[(E-E_0)/E]^{s-1}$$

where k(E) is the dissociative rate constant, E is the energy in the complex, E_0 is the well depth, s is the number of effective oscillators, and A can be interpreted as the inverse of the energy redistribution time. In practice, A is taken to be the vibrational rate or $\sim 10^{13} sec^{-1}$. Also, the best value for s is generally considered to be 2/3 of the number of vibrational modes, as the other 1/3 may be inactive.[29] Performing this simple calculation for the $^3A_2$ well of NH_2^+ one obtains lifetimes (1/k(E)) of 3.6×10^{-13} and 2.3×10^{13} seconds for 1 and 2 eV collisions respectively. Lifetimes in the deeper $^3B_1$ well are about a factor of two longer. It should be stressed that this is a very crude calculation and can easily be wrong by an order of magnitude or more.

The theory was improved in later years, primarily through the work of Marcus and there now are several books mainly concerned with the so-called RRKM theory.[70,71] Marcus' additions (which include rotational degrees of freedom) have resulted in a theory which is quantitatively accurate for most real chemical systems. Unfortunately, NH_2^+ is not a promising candidate for an RRKM calculation because the implicit assumption that the energy is randomized on a time scale fast compared to decomposition is not a good one. Classical trajec · calculations which directly simulate complex decomposition show that for virtually all molecules, internal energy randomization is complete in 10^{-11} seconds except for triatomics with disparate masses.[72] The reason that vibrational equilibration is slow in these triatomics is related to the fact that the stretching modes are much higher frequency than the bend and therefore the vibrations are poorly coupled. Thus NH_2^+ would have to live longer than 10^{-11} seconds before an RRKM calculation could be considered accurate. The RRK calculation indicated that at the collision energies of interest, lifetimes of 10^{-13} seconds should be seen, so the RRKM calculation will be of questionable validity. We would expect though that our RRKM calculated lifetimes represent an upper limit to the true complex lifetime.

RRKM calculations were performed for motion on both the $^3A_2$ and $^3B_1$ surfaces using a computer program written by W. L. Hase and D. L. Bunker. The necessary input parameters are the collision energy, well depth, and vibrational frequencies and moments of inertia of both equilibrium NH_2^+ and NH_2^+ at the critical configuration. The

moments of inertia for NH_2^+ $^3B_1$ and $^3A_2$ were calculated from the theoretically determined geometries.[58] The vibrational frequencies using for the $^3B_1$ state were those calculated for isoelectronic CH_2.[73] The vibrational frequencies for the strangely shaped $^3A_2$ state had to be estimated. This is not a straightforward procedure because virtually no data exist on triatomics which are bent more than 90°. In $^3A_2$ NH_2^+, r(H-H) is only 0.92 Å, which is smaller than the distance in excited electronic states of H_2. For this reason it is useful to think of the $^3A_2$ state as being an H_2 molecule bound to an N^+ ion. The bend may be more accurately thought of as an H_2 stretch. Its frequency should lie between H_2 in the ground state (r = .74 Å, ω_e = 4401 cm^{-1}) and H_2 in the C state (r = 1.033 Å, ω_e = 2444 cm^{-1}) and we estimate it at 3000 cm^{-1}. Using a similar argument and approximating the symmetric stretch by an N-D stretch we estimate 1700 cm^{-1} for this mode. The asymmetric stretch can be thought of an an H_2 wag and its frequency is difficult to estimate. In $CH_2(^3B_1)$ it is quite stiff, 3453 cm^{-1}, but here with an increased bond length, and a barrier of only ~1 eV[58] to H_2 internal rotation, we estimate 1500 cm^{-1}.

The critical configuration is that molecular geometry which, if attained by the system, will immediately lead to products. It is usually assumed to be located at the top of the barrier in the effective potential. The effective potential is given by

$$V_{eff} = V + \frac{L^2}{2\mu r^2}$$

where V is the rotationless potential, L is the total angular momentum, μ is the reduced mass, and r is the distance of separation. At large r, V can be approximated by $-C/r^4$, which is the ion-induced dipole potential. We obtain the location of the barrier maximum by differentiating the effective potential and setting it equal to zero. This yields

$$r(\text{barrier}) = \left(\frac{4\mu C}{L^2}\right)^{1/2} \quad \text{and} \quad V_{max} = \frac{L^4}{16\mu^2 C} .$$

By applying a crude fit to one of Hirst's potentials for this system,[53] we obtain $C = 2.5 \times 10^{-11}$ ergs - $Å^4$. Using a reasonable estimate for the angular momentum of the complex, 15 , leads to the result that r (barrier) = 7.9 Å and 10.8 Å for reactive and non-reactive decomposition respectively. The barriers are at such great distances due to the long-range nature of the ion-induced dipole potential which also accounts for their insignificant (< .005 eV) heights. For reactive decomposition the critical configuration is well approximated by an NH^+ ion with an H atom 7.9 Å away. Similarly the non-reactive critical configuration is H_2 with a remote N^+. The moments of inertia are readily calculated from these geometries and one vibrational frequency (the diatomic stretch) is easily obtained. Only one other vibrational frequency is necessary because the third is associated with the reaction coordinate. Assuming the decomposition mode to be a stretch between the remote partners, the other will be a low frequency wag, which we estimate at 500 cm^{-1}. Fortunately the calculation is relatively insensitive to this parameter. The values input are summarized in Table 4.

Table 4

Species	Frequencies (cm^{-1})	Moments of Inertia (AMU-$Å^2$)
$NH_2^+(^3B_1)$	3566	2.05
	1131	1.87
	3453	0.18
$NH_2^+(^3A_2)$	1700	2.83
	3000	2.40
	1500	0.43
Critical configuration for $NH^+ + H$	3000	60.0
	500	59.0
		1.0
Critical configuration for $N^+ + H_2$	4000	204.0
	500	204.0
		0.3

The geometries, vibrational frequencies and moments inertia assumed for the RRKM calculation.

The computer program has three different options for estimating the density of internal states in the complex. These are, in order of increasing accuracy, classical, semi-classical, and direct count. The quantum state level density in NH_2^+ is very low due to the small moment of inertia, the small number of vibrational modes, and large vibrational frequencies. For this reason, a classical approach is not appropriate and attempts to use it seem to overestimate complex lifetime. There is also a problem with the direct count method as it is able to pick out fluctuations in level density and results in complex lifetimes not being monontonically decreasing with increasing collision energy. While this may indeed be true in the NH_2^+ system, the nature of the fluctuations is strongly dependent on the input parameters. Since these parameters are largely guessed at, it was decided that a semi-classical estimate, which damped out the fluctuations, was preferable.

In Table 5 are presented typical results for complex lifetimes as a function of collision energy. A semi-classical estimate of the level densities was made and well depths of 2.6 and 6.1 eV were assumed for the $^3A_2$ and $^3B_1$ surfaces, respectively. Also implicit in the calculation is a path degeneracy (2) which takes into account the fact that either N-H bond can break in the complex. This is not true for non-reactive decomposition although these calculations also were performed using this symmetry number. The resulting lifetimes for non-reactive decomposition agreed to within ~10 with the values in Table 5 demonstrating that the most important factor in the calculation is the

Table 5

Collision energy (eV)	lifetime (ps) $^3A_2$	$^3B_1$
.13	.34	.72
.43	.11	.21
.74	.06	.11
1.04	.04	.07
1.34	.03	.05
1.65	.02	.035
2.26	.02	.02
2.86	.01	.02

RRKM calculated lifetimes for NH_2^+ decaying to NH^++H.

energetics of the decomposition channel. Non-reactive decomposition should be treated using a symmetry number of 1 which will double the lifetimes in Table 5.

Recall that our initial reason for estimating complex lifetimes was to determine if the $^3A_2$ well is deep enough to explain the experimental results. The experiments show that at energies below ~1.9 eV an NH_2^+ intermediate is formed which apparently lasts at least several rotational periods and so we now need a value for the rotational period. This can be done by estimating the reaction cross section, from which a maximum inpact parameter and thus the total angular momentum of the complex can be obtained. The rotational period is then given by

$$\tau_r = 2\pi(I/L)$$

where I is the moment of inertia. Estimating the cross section from the curve published by Eisele et al.[11,35] we obtain 3 Å^2 and 1 Å^2 at 1 and 2 eV respectively. This leads to maximum complex angular momenta of 29 and 23 . We can approximate the complex as a symmetric top with a moment of inertia of 2.0 AMU Å^2 for the degenerate rotations, and a moment of inertia about the principle axis equal to about 1/10 of that. Assuming that the angular momentum is statistically distributed in the complex leads to the conclusion that rotation about the principle axis is not favored (K = 0) due to the high frequency of that motion. Thus with the rotation in the low frequency mode we obtain $\tau_r = 7.0 \times 10^{-14}$

and 8.8×10^{-14} seconds for complexes formed at 1 eV and 2 eV respectively. Comparing these values to those in Table 5 we see that the complex lifetime is only about 50% of the minimum rotational period even at 1 ev. The ratio decreases to 25% at 2 eV and our initial suspicion that the $^3A_2$ surface by itself cannot explain the experimental distributions seems correct.

Probably the most important effect of the $^3A_2$ well on the dynamics is that it may detain a trajectory long enough for it to encounter the $^3A_2$–$^3B_1$ seam several times. Even though the probability per pass may not be very high, several passes might take most trajectories to the lower surface. The line of intersection, as seen in Fig. 30, passes near the bottom of the rather broad flat $^3A_2$ well insuring that any snarled trajectory will traverse the seam often.

Comparison of the rotational period to complex lifetime in the $^3B_1$ well leads to some problems. At 1 eV collision energy, the complex lives the equivalent of one rotational period, and, as discussed previously, the lifetime estimate is an upper limit, and the rotational period a lower limit. Thus even with the uncertainties associated with this calculation, it seems likely that the complex does not live the several[74] rotational periods required to give a symmetric distribution.

In an attempt to come up with a model to explain the experimental results it is useful to consider the well-studied reaction

$$O(^1D) + H_2 \rightarrow OH + H. \qquad (9)$$

This reaction is similar to (1) for two reasons. First, the potential well associated with the H_2O intermediate is deep (4.7 eV below products, 6.7 eV below reactants); second, a C_{2v} approach for the reactants is favored. A classical trajectory calculation indicates that the average lifetime of H_2O complexes formed by thermal collisions is less than 10^{-13} seconds.[75] A later study, which combines experiments and classical trajectory calculations, shows that $O(^1D)$ insertion produces considerable bending excitation in the complex.[76] Much of the energy is retained in this mode and the resultant OH product is highly rotationally excited. Finally, a crossed beam study of this reaction yields a product distribution which has forward-backward symmetry.[77]

This information clearly demonstrates that reactions (1) and (9) have much in common. The short lifetime ($< 10^{-13}$ seconds) calculated for (9) lends some credence to our RRKM calculated lifetime for (1) (7×10^{-14} seconds). Neither value approaches several rotational periods in length. How then are the experimental distributions explained As pointed out by Buss et al.[77], a C_{2v} insertion into a homonuclear diatomic induces rapid bending in an intermediate with near equivalent bonds, and might be expected to yield a symmetric product distribution. The symmetry is generated by the fast bending which can completely destroy any memory of the direction of approach in less than a rotational period. Further contributing to this mechanism for rapid loss of memory in the complex is the fact that the H atoms in the C_{2v} complex are dynamically equivalent. Because either bond can break and still form products, the

scrambling time is decreased even more. A similar argument has been applied to explain symmetric product distributions seen at high energies for $O_2^+(D_2,OD)OD^+$.[14]

Even with this model, it would still be required that the complex last at least several vibrational periods. An estimate of the NH_2^+ vibrational period for the bend yields 3×10^{-14} seconds for $v = 1$. Hence the complex probably does live several vibrational periods for low energy collisions. Although this explanation for symmetric product distributions is unconventional, it successfully explains the experimental results for both reactions (1) and (9). A trajectory study of the related reaction $C^+(H_2,H)CH^+$ shows a nearly symmetric product distribution though the complex lifetimes are short.[78] This result could be taken as support for the above mechanism. If we contrast these reactions with those that favor collinear approaches such as $Ar^+(H_2,H)ArH^+$,[79] $F(H_2,H)FH$,[80] $O^+(H_2,H)OH^+$,[54,81] $N(H_2^+,H)NH^+$,[19] and $F^+(H_2,H)FH^+$,[82] we have further support as all these reactions give asymmetric distributions down to low energies.

As has been suggested by others,[58,53] the true nature of the dynamics of reaction (1) can probably only be discovered by a classical trajectory calculation including both the upper and lower potential energy surfaces and hopping between them. Such a calculation has been reported for the H^+-H_2 system, and agreement between theory and experiment is excellent.[83]

Before closing our discussion of the dynamics of $N^+(^3P)$-H_2 collisions a completely different argument which could explain the experimental results should be mentioned. Mayer,[84] in a paper which has escaped notoriety, explains that decreasing complex formation with increasing energy may be a rotational effect. That is, as the energy is increased at constant impact parameter, the total angular momentum of the complex increases and the well in the effective potential becomes less deep. A shallower well will, of course, decrease the lifetime of the complex. Mayer says that such an explanation is sufficient for explaining asymmetry in the product distributions of $CH^+(H_2,H)CH_2^+$, $NH_2^+(H_2,H)NH_3^+$ and $CH_2^+(H_2,H)CH_3^+$ at energies above 1.5 eV despite respective well depths of 6.03, 6.78, and 2.65 eV. Applying Mayer's argument to reaction (1) we obtain that at 1 eV collision energy (J_{max} = 29), the rotational contribution to the effective potential is only about 1 eV at r(N-H_2) of 1 Å. Since the $^3B_1$ well is over 6 eV deep we conclude that this rotational effect is negligible for reactive N^+-H_2 collisions.

Dynamics of the Metastable

As discussed earlier, when an appreciable amount of metastable N^+ is present in the beam, collisions with H_2 produce NH^+ peaked in the forward direction. The possible contaminants to ground state $N^+(^3P)$ are $N^+(^1D,^1S,^5S)$ and N_2^{++}. We may eliminate N_2^{++} as a possible reactant because any N_2H^{++} formed would appear at mass 14.5 and hence be largely suppressed by the mass filter. The $N^+(^5S)$ metastable is

also an unlikely reactant. It lies 5.8 eV above $N^+(^3P)$ and so the reaction to form $NH^+(^4\Sigma^-)$ product is about 5.8 eV exothermic. It can be seen in Fig. 1 that this state is bound by only 3.5 eV; at least 2.3 eV would have to be released into translation to yield stable NH^+ products. The peaks in the reactive distributions in Figs. 19-22 all appear at lesser Q values than this would predict. Bound products could conceivably result if a higher electronic state of NH^+ were formed, but this, too, seems unlikely. In a simple system such as this, with light atoms, the Wigner spin rule which allows no electrons to change spin, is a good approximation.[34] Therefore we would expect to form NH^+ adiabatically with a spin multiplicity of either 4 or 6. The only such known state of NH^+ is the low-lying $^4\Sigma^-$ state,[10] and hence we conclude that $N^+(^5S)$ is not the reacting metastable. We may also eliminate $N^+(^1S)$. This can be done because Table 1 states that little if any $N^+(^1S)$ is in the beam, and recent work on the isoelectronic reaction $C(H_2,H)CH$ showed that $C(^1S)$ reacts very slowly.[85] The reaction of $C(^1D)$ was much faster, and a glance at Fig. 28 indicates an adiabatically allowed reaction path exists for $N^+(^1D)$. A collinear approach or the $^1\Pi$ surface can take the reactants to $NH^+(^2\Pi)$ + H. There are not expected to be any deep wells associated with this surface and hence a direct reaction mechanism should be operative. A direct mechanism is observed experimentally and we conclude that the reacting species is $N^+(^1D)$.[86]

The correlation diagram also shows that approaches on other surfaces such as the $^1\Delta$ in $C_{\infty v}$ or the lowest $^1A_1$ in C_{2v} symmetry may lead to NH + H^+ products. It is possible that this other reaction channel may contribute to the experimental observation that the amount of NH^+ formed by the metastable is not particularly large.

The observation[7] that at thermal energies most metastable N^+–H_2 reactions give charge exchange is not easily explained by the correlation diagram. Assuming that these metastables are predominately $N^+(^1D)$, the only energetically allowed charge transfer product is $N(^4S)$. As stated earlier, the Wigner spin rule would predict a small cross section for this reaction.

Although at this point we have established self-consistent arguments for explaining the dynamics of the $N^+(^3P)$–H_2 and N^+ (metastable)–H_2 systems, we should point out an alternate mechanism which could also explain the experimental results. An $N^+(^3P)$ ion exists in one of three different fine structure states with a J quantum number of 0, 1, or 2. Of these states, $^3P_0$ is the lowest in energy with $^3P_1$ and $^3P_2$ at 49.1 and 131.3 cm^{-1} respectively.[51] At the present level of expertise, little can be predicted about the differences in reactivity of these ions. That there could be a difference is born out by the photoionization work of Chupka who showed that for $Ar^+(H_2,H)ArH^+$, the $^2P_{1/2}$ state of Ar^+ reacts 1.3 times faster the $^2P_{3/2}$ state[87] and for $Kr^+(H_2,H)KrH^+$ the $^2P_{3/2}$ state reacts 2.5 times faster than the higher-lying $^2P_{1/2}$.[88] If for a moment we imagine that reactions of the fine structure states of $N^+(^3P)$ differ, presumably because the ions have

unequal access to the various potential energy surfaces, then an interesting possibility arises. By constructing a suitable scenario, the experimental distributions could be explained by assuming different reaction dynamics associated with the individual sublevels of the ^3P state. Of course, any such scheme would, at this point, be highly speculative. The simple fact though, that we have no way to predict the reactivity of the sublevels, serves as an example that more work is necessary before the N^+-H_2 system is completely understood.

Summary

It seems worthwhile at this point to summarize the important points of this lengthy chapter. The reaction $N^+(^3P)$ $(H_2,H)NH^+$ goes predominately via a long-lived complex mechanism at energies below 1.9 eV. In the energy range 2.0-3.6 eV the reaction is direct but with considerable interaction between all three atoms. The formation of the long-lived intermediate below 1.9 eV was further verified by an elastic backscattered peak in non-reactive distributions. The general agreement between the reactive and non-reactive experiments as to the energy range that complex behavior dominates, is no doubt related to the thermoneutrality of the reaction. The dynamics of the reaction are adequately explained by a molecular state correlation diagram which shows that an avoided crossing between two potential energy surfaces in C_s symmetry can lead adiabatically to a deep well associated with NH_2^+. The decrease in complex formation with increasing collision energy may

indicate the importance of surface hopping. This argument has been qualitatively verified by accurate calculation of the surfaces involved. RRKM calculations show that the NH_2^+ intermediate may not live for the several rotational periods normally required to explain symmetric product distributions. An alternate explanation which says that directional scrambling can occur in a few (bending) vibrational periods has been proposed. N^+ produced by high energy electron impact gives more forward-peaked reactive product distributions. The shift is no doubt due to a different reaction mechanism associated with metastable N^+. The correlation diagram and energetic arguments lead to the conclusion that the reacting metastable state is $N^+(^1D)$.

References

1. R. Colins and A. E. Douglas, Can. J. Phys. 46, 61 (1968).
2. J. H. Black and A. Dalgarno, Astrophys. Letts. 15, 79 (1973).
3. E. Herbst, J. G. Schubart and P. R. Certain, Ap. J. 213, 696 (1977).
4. Ch. Ottinger, in Electronic and Atomic Collisions, Ed. G. Watel, (North-Holland, Amsterdam, 1978) 639-662.
5. F. C. Fehsenfeld, A. L. Schmeltekopf and E. E. Ferguson, J. Chem. Phys. 46, 2802 (1967).
6. J. K. Kim, L. P. Theard and W. T. Huntress, J. Chem. Phys. 62, 45 (1975). For a compilation of many ion-molecule rate constants as measured by ICR see W. T. Huntress, Astrophys. J. Suppl. Ser., 33, 495 (1977).
7. M. Tichy, A. B. Rakshit, D. G. Lister, N. D. Twiddy, N. G. Adams and D. Smith, Int. J. Mass Spectrom. Ion Phys. 29, 231 (1979).
8. E. A. Gislason, B. H. Mahan, C.-W. Tsao and A. S. Werner, J. Chem. Phys. 54, 3897 (1971).
9. "Forward scattered" means that in the center-of-mass frame of reference, the observed product (NH^+) was scattered in the same direction that the initial projectile (N^+) was traveling.
10. K. P. Huber and G. Herzberg, Constants of Diatomics Molecules (Van Nostrand Reinhold, N.Y., 1979).
11. G. Eisele, A. Henglein, P. Botschwina and M. Meyer, Ber. Bunsenges, Phys. Chem. 78, 1090 (1974).
12. J. A. Fair and B. H. Mahan, J. Chem. Phys. 62, 515 (1975).
13. B. H. Mahan and T. M. Sloane, J. Chem. Phys. 59, 5661 (1973).

14. M. H. Chiang, E. A. Gislason, B. H. Mahan, C.-W. Tsao and A. S. Werner, J. Phys. Chem. 75, 1426 (1971).

15. I. Kusunoki, Ch. Ottinger and J. Simonis, Chem. Phys. Lett. 41, 601 (1976).

16. I. Kusunoki and Ch. Ottinger, J. Chem. Phys. 70, 699 (1979).

17. I. Kusunoki and Ch. Ottinger, J. Chem. Phys. 70, 710 (1979).

18. B. H. Mahan and W. E. W. Ruska, J. Chem. Phys. 65, 5044 (1976).

19. D. J. McClure, C. H. Douglass and W. R. Gentry, J. Chem. Phys. 66, 2079 (1977).

20. D. M. Hirst, Chem. Phys. Lett. 53, 125 (1978).

21. R. J. Reed and W. Snedden, J. Chem. Soc. 4132 (1959).

22. S. N. Foner and R. L. Hudsen, J. Chem. Phys. 45, 40 (1966).

23. H. P. D. Liu and G. Verhaegen, J. Chem. Phys. 53, 735 (1970).

24. H. P. D. Liu and G. Verhaegen, Int. J. Quantum Chem. 55, 103 (1971).

25. P. Rosmus and W. Meyer, J. Chem. Phys. 66, 13 (1977).

26. A. G. Gaydon, Dissociation Energies and Spectra of Diatomic Molecules (Chapman and Hall, London, 1968).

27. D. M. Hirst, In General Discussion, Faraday Disc. Chem. Soc. 62, 138 (1977).

28. P. J. Chantry, J. Chem. Phys. 55, 2746 (1971).

29. For a good discussion of long-lived complexes in ion-molecule reactions see R. Wolfgang, Accounts Chem. Res. 3, 48 (1970).

30. This basic tenet of reaction dynamics has been recently questioned by G. M. McClelland and D. R. Herschbach, J. Phys. Chem. 83, 1445 (1979).

31. M. Chiang, E. A. Gislason, B. H. Mahan, C.-W. Tsao and A. S. Werner, J. Chem. Phys. 52, 2698 (1970).

32. A. Henglein, J. Phys. Chem. 76, 383 (1972).

33. W. S. Koski, in Advances in Chemical Physics, edited by K. P. Lawley (Wiley-Interscience, N.Y., 1975), Vol. 30.

34. J. H. Moore, Phys. Rev. A. 5, 2359 (1973).

35. D. Hyatt and K. Lacmann, Z. Naturforsch. 23a, 2080 (1968).

36. H. B. Gilbody and J. B. Hasted, Proc. R. Soc. London A, 238, 334 (1957).

37. W. E. W. Ruska, Ph.D. Thesis, University of California, LBL Report LBL-5120 (1976).

38. E. W. McDaniel, V. Cermak, A. Dalgarno, E. E. Ferguson and L. Friedman, Ion-Molecule Reactions (Wiley-Interscience, N.Y., 1970).

39. For a review see D. R. Herschbach, Faraday Disc. Chem. Soc. 55, 233 (1973).

40. W. B. Miller, S. A. Safron and D. R. Herschbach, Faraday Disc. Chem. Soc. 44, 108 (1967).

41. K. Birkinshaw, V. Pacak, and Z. Herman, in Interactions Between Ions and Molecules, Ed. P. Ausloos (Plenum Press, N.Y., 1975) pp. 95-121.

42. G. Bosse, A. Ding and A. Henglein, Ber. Bunsenges, Phys. Chem. 75, 413 (1971).

43. G. Herzberg, Electronic Spectra and Electronic Structure of Polyatomic Molecules (Van Nostrand, Princeton, N.J., 1966).

44. R. S. Mulliken, Phys. Rev. 43, 279 (1932).

45. I. N. Levine, Quantum Chemistry, 2nd Ed. (Allyn and Bacon, Boston, 1974) 390-397.

46. R. M. Pitzer and D. P. Merrified, J. Chem. Phys. 52, 4782 (1970).

47. V. Griffing, J. Chem. Phys. 23, 1015 (1955).
V. Griffing and J. T. Vanderslice, J. Chem. Phys. 23, 1039(1955).
V. Griffing and J. S. Dooling, J. Phys. Chem. 61, 11 (1957).

48. B. H. Mahan, J. Chem. Phys. 55, 1436 (1971).

49. S. D. Peyerimhoff and R. J. Buenker, Chem. Phys. 42, 167 (1979).

50. F. Hund, Z. Physik 40, 742 (1927).

51. C. E. Moore, NSRDS-NBS 35, Vol. 1.

52. M. A. Gittins, D. M. Hirst and M. F. Guest, Faraday Disc. Chem. Soc. 62, 59 (1977).

53. D. M. Hirst, Mol. Phys. 35, 1559 (1978).

54. K. T. Gillen, B. H. Mahan and J. S. Winn, J. Chem. Phys. 58, 5373 (1973).

55. E. Teller, J. Phys. Chem. 41, 109 (1937).

56. G. Herzberg and C. Longuett-Higgins, Disc. Faraday Soc. 35, 77 (1963).

57. T. Carrington, Acct. Chem. Res. 7, 20 (1974).

58. C. F. Bender, J. H. Meadows, and H. F. Schaefer III, Faraday Disc. Chem. Soc. 62, 59 (1977).

59. R. B. Woodward and R. Hoffman, The Conservation of Orbital Symmetry (Academic Press, N.Y., 1970).

60. T. Carrington, J. Chem. Phys. 41, 2012 (1964).

61. The minimum in the surface is at 143.3°,[58] but the barrier to linearity (~330 cm^{-1}) is comparable to the zero point energy of the bend (318 cm^{-1})[49].

62. C. W. Bauschlicher, S.V. O'Neill, R. K. Preston, H. F. Schaefer III and C. F. Bender, J. Chem. Phys. 59, 1286 (1973).

63. L. D. Landau, Phys. Z. Sowjetunion 2, 46 (1932).

64. C. Zener, Proc. Roy. Soc. A 137, 696 (1932).

65. E. C. G. Stuckelberg, Helv. Phys. Acta. 5, 369 (1932).

66. P. K. Pearson and E. Roueff, J. Chem. Phys. 64, 1240 (1976).

67. G. Eisele, A. Henglein and G. Bosse, Ber. Bunsenges. Phys. Chem. 78, 140 (1974).

68. O. K. Rice and H. C. Ramsperger, J. Amer. Chem. Soc. 49, 1617 (1927).

69. L. S. Kassel, J. Phys. Chem. 32, 225, 1065 (1928).

70. P. J. Robinson and K. A. Holbrook, Unimolecular Reactions (Wiley-Interscience, N.Y., 1972).

71. W. Forst, Theory of Unimolecular Reactions (Academic Press, N.Y., 1973).

72. Ref. 71, p. 25.

73. M. Y. Chu and J. S. Dahler, Mol. Phys. 27, 1045 (1974).

74. G. A. Fisk, J. D. McDonald and D. R. Herschbach, Discuss. Faraday Soc. 44, 228 (1967).

75. K. S. Sorbie and J. N. Murrell, Mol. Phys. 31, 905 (1976).

76. A. C. Luntz, R. Schinke, W. A. Lester, Jr., and Hs. H. Gunthard, J. Chem. Phys. 70, 5908 (1979).

77. R. J. Buss, P. Casavecchia, T. Hirooka, S. J. Sibener, and Y. T. Lee, to be published.

78. J. P. Sullivan and E. Herbst, Chem. Phys. Lett. 55, 226 (1978).

79. Z. Herman, J. Kersetter, T. L. Rose and R. Wolfgang, Disc. Faraday Soc. 44, 123 (1966).

80. T. P. Schafer, P. E. Siska, J. M. Parson, F. P. Tully, Y.C. Wong and Y. T. Lee, J. Chem. Phys. 53, 3385 (1970).

81. H. H. Harris and J. J. Leventhal, J. Chem. Phys. 58, 2333 (1973).

82. S. G. Hansen and B. H. Mahan, unpublished results.

83. J. R. Krenos, R. K. Preston, R. Wolfgang and J. C. Tully, J. Chem. Phys. 60, 1634 (1974).

84. T. M. Mayer, Ber. Bunsenges Phys. Chem. 79, 352 (1975).

85. D. Husain and P. E. Norris, Faraday Disc. Chem. Soc. 67, 273 (1979).

86. J. M. Farrar, S. G. Hansen and B. H. Mahan, J. Chem. Phys. 65, 2908 (1976).

87. W. A. Chupka and M. E. Russell, J. Chem. Phys. 49, 5426 (1968).

88. W. A. Chupka in Chemical Spectroscopy and Photochemistry in the Vacuum-Ultraviolet, Ed. C. Sandorfy, P. J. Ausloos and M. B. Robin (D. Reidel Publishing Co., Boston, 1974).

CHAPTER 4: $F^+ - H_2$ INTERACTIONS

The reaction of F^+ with H_2 is interesting for several reasons. For one thing, F^+ is closely related to N^+, which was discussed in the previous chapter, by the principle of particle-hole equivalence. Whereas N^+ has two electrons and four vacancies in its 2p shell, F^+ has four electrons and two vacancies; the ground state of each ion is ^3P and both have low-lying ^1D and ^1S metastable states. Also like the N^+-H_2 system, the collision intermediate, FH_2^+, is a stable species,[1] which presents the possibility that the reaction might involve a long-lived complex. A further reason for studying the FH_2^+ system is that it is isoelectronic with H_2O. The reactions $O(^3P)(H_2,H)OH$ and $O(^1D)(H_2,H)OH$ have been extensively studied both theoretically[2-4,6] and experimentally,[5,6] and one could hope to profit from this accumulated knowledge. A final point, which sets F^+-H_2 apart from either N^+-H_2 or $O-H_2$, is the fact that the $F^+(^3P) + H_2$ asymptote is not the lowest energy asymptote on the reactant side. Because F has a very high ionization potential (17.42 eV), the charge-exchanged reactants $F(^2P) + H_2^+$ actually lie 2 eV lower in energy. As we will see later, this situation greatly affects the dynamics.

There has been surprisingly little work reported previously on F^+-H_2 interactions. In 1971, Mahan,[7] in an article concerning orbital correlations, mentioned that in the absence of a_1-b_2 orbital interaction, the reaction

$$F^+(^3P) + H_2 \rightarrow HF^+ + H \qquad (1)$$

should be direct even at very low energies. A similar statement was made about $N^+(H_2,H)NH^+$, but as discussed in Chapter 3, a_1-b_2 interactions do occur and the reaction involves a long-lived complex at collision energies below 1.9 eV. The only experimental information on reaction (1) thus far published is the beam-gas work of Koski and coworkers.[8-10] Their results are summarized in the following paragraphs.

The first paper[8] was mainly concerned with the characterization of the electronic state distribution of F^+ in their beam and the cross section as a function of energy for reaction (1) with both $F^+(^3P)$ and $F^+(^1D)$ reactants. They concluded from beam attenuation experiments that > 40% of the F^+ produced by the impact of 100 eV electrons on CF_4 was in the metastable ^1D state; this state lies 2.59 eV above the ^3P state. It was also observed that by adding NO to their ion source, the metastable state was completely quenched. Further aspects of the F^+ state distribution is considered in Chapter 6.

The study of the cross section for reaction (1) yielded a smooth curve which paralleled the predictions of the Langevin polarization model and phase space theory, but gave consistently lower values. The measured cross section at 1 eV relative energy was 4Å^2 for $F^+(^3P)$ and 5Å^2 for $F^+(^1D)$; above 2.5 eV the two states have equal reactive cross sections. Lin et al.[8] also investigated the branching ratio for

ratio for the reaction of F^+ with HD and found $\sigma(FD^+)/\sigma(FH^+) > 1$ below 8 eV laboratory energy and < 1 above 8 eV. Such an isotope effect had been previously observed for Ar^+-HD. This coupled with the observation that reaction (1) has the same cross section with both H_2 and D_2 suggests a strong similarity between reaction (1) and $Ar^+(H_2,H)ArH^+$. The latter reaction is known to proceed via a direct reaction mechanism.[11]

In the second paper,[9] product centerline velocity distributions were measured and three full angular distributions were given. The angular distributions showed that at 0.91 and 0.39 eV the FD^+ distribution was peaked slightly behind the spectator stripping velocity, but at 0.21 eV the distribution was almost symmetric about the ±90° axis. Such a result implies that at this low energy, a strong interaction exists between all three collision partners.

By examining centerline velocity distributions, Wendell et al.[9] were able to plot the translational exoergicity, Q, as a function of relative collision energy. If a reaction proceeds through a long-lived complex and gives a product distribution peaked at the center-of-mass velocity, as many ion-molecule reactions do, then $Q = -E_{rel}$. If the product velocity distribution peaks at the spectator stripping velocity then, assuming the reaction is a simple H atom transfer from H_2,

$$Q = -\frac{m_i}{m_{H_2}} \frac{(m_i+m_{H_2})}{(m_i+m_H)} E_{rel} \quad . \qquad (2)$$

Here m_i is the mass of the projectile ion, and m_{H_2} and m_H denote the masses of the hydrogen molecule and atom. The Q values measured[9]

at 0.13 and 0.5 eV relative collision energies were consistent with complex formation and Q values more negative than predicted by the simple stripping model were obtained up to 0.5 eV. At higher energies, the peak positions leveled off at approximately Q = -0.8 eV. Wendell et al. concluded from these data that the FD^+ product was formed primarily in its first excited $^2\Sigma^+$ state. Their deduction was based on the fact that energy constraints prohibit FD^+ product ions from scattering into certain regions of velocity space. Using values for the heat of reaction (1) and dissociation energy of FD^+ obtained from thermochemical and photoelectron data, they calculated that the minimum Q for $FD^+(^2\pi)$ formation was -0.68 eV while for $FD^+(^2\Sigma^+)$ formation it was -0.81 eV. Since the data clustered around -0.8 eV, it was evident that the $^2\Sigma^+$ state was the favored product. However, a paper which was published approximately simultaneously clouded this interpretation. In this study,[12] the emission spectrum of $HF^+(A^2\Sigma^+ \rightarrow X^2\pi)$ was photographed under high resolution and more accurate molecular constants were obtained. It was possible to establish the heats of reaction for

$$F^+(^3P) + H_2 \rightarrow FH^+(^2\pi) + H \qquad \Delta H_0^0 = -2.77 \text{ eV}, \qquad (1A)$$

$$F^+(^3P) + H_2 \rightarrow FH^+(^2\Sigma^+) + H \qquad \Delta H_0^0 = 0.29 \text{ eV}, \qquad (1B)$$

$$F^+(^1D) + H_2 \rightarrow FH^+(^2\pi) + H \qquad \Delta H_0^0 = -5.36 \text{ eV}, \qquad (2)$$

$$F^+(^1D) + H_2 \rightarrow FH^+(^2\Sigma^+) + H \qquad \Delta H_0^0 = -2.30 \text{ eV}. \qquad (3)$$

The optical data also established that $D_0(HF^+{}^2\Pi) = 3.42$ eV and $D_0(HF^+{}^2\Sigma^+) = 0.40$ eV; it should be noted that $HF^+(^2\Pi)$ dissociates to $H^+ + F(^2P_{3/2})$ while $HF^+(^2\Sigma^+)$ correlates with $H^+ + F(^2P_{1/2})$. These energies imply that the products of reaction (1A) must appear between $-0.65 \leq Q \leq 2.77$ eV, and for (1B), $-0.69 \leq Q \leq -0.29$ eV. The upper limit is realized if all available energy goes into translation and the lower value denotes the point at which the product molecule is internally excited to its dissociation limit. Using these numbers, it can be seen that the data of Wendell et al.[9] indicate that product molecules are being formed with internal enegies above their dissociation energy. It should be realized that the $^2\Pi$ and $^2\Sigma^+$ states are the only bound electronic states known for HF^+.

In their third paper[10], Koski and coworkers re-examined reaction (1) under higher resolution, using energy selected F^+ beams with a 70 meV FWHM. A careful study of the cross section as a function of collision energy showed no break at the threshold energy for $FD^+(^2\Sigma^+)$ formation. Repeat measurements of Q as a function of collision energy again showed product formation in an energy region considered inaccessible to $FD^+(^2\Pi)$. Using D_2 as the reactant, FD^+ was found to have internal energies 60 meV above its $^2\Pi$ dissociation limit, and using H_2, FH^+ appeared at 25 meV above its corresponding $^2\Pi$ dissociation limit. From these observations it was concluded that the FH^+ (and FD^+) products were being formed in the ground $^2\Pi$ state with large amounts of rotational excitation. The resulting effective potential produces a barrier to decomposition which allows the existence

of metastable HF^+ containing internal energy higher than that permitted by the rotationless potential. Since H is lighter than D, it more readily tunnels through the barrier and hence highly exicted states of FD^+ live longer than the corresponding states of FH^+. The excited FD^+ is more likely to reach the detector than is FH^+ and its product velocity distribution will reflect this fact; the data are consistent with this model.

Although it was not discussed in the text, one could glean from the plots of Q vs. energy that Jones et al.[10] might be backing down a bit from the original contention[9] that at very low energies the product distribution was nearly symmetric. These plots showed the product peak to be only slightly behind the stripping velocity down to ~0.15 eV.

It was discussed by Wendell et al.[9] that spin and symmetry rules predict that HF^+ cannot be formed in $F^+(^3P)$-H_2 collisions and, therefore, a non-adiabatic process must be involved. Further work on this subject was published by Kendrick et al.[13] roughly simultaneously with Koski's third paper. Although basically a theoretical paper, Kendrick et al. reported some unpublished crossed beam results of A. Ding and collaborators. The Ding results[13,14] were quite a bit different from the Koski results in that at low energies, products retained a significant fraction of the total energy in translation. The interpretation of these experiments was hampered, however, by the belief that the F^+ beam, produced in a plasma source, contained a large fraction of mestatable ions.

Kendrick et al. constructed diatomics-in-molecules (DIM) potential energy surfaces for the six lowest $^3A'$ and six lowest $^3A''$ states of FH_2^+ and ran a small number of trajectories in an attempt to understand the dynamics. It was seen that a transition from an H_2-F^+-like surface to a lower H_2^+-F-like surface could occur when H_2 was compressed, and that the lower surface led directly to $HF^+(^2\Pi)$ + H. Upon transition to this surface there was a substantial amount of energy released, and it was not inconceivable that much of it channelled into product vibration. It was also shown that $F^+(^1D)$ could react with H_2 to yield FH^+ in both $^2\Pi$ and $^2\Sigma^+$ states. The large exothermicity of this reaction reaction made it quite likely that the products would come off translationally hot. Kendrick and coworkers' interpretation of the ^3P and ^1D dynamics made progress toward understanding the results of both Koski and Ding.

Results

A total of 29 reactive maps were obtained for F^+-H_2 collisions in the initial relative energy range of 0.20-1.07 eV. These experiments were, for the most part, performed prior to the implementation of the differentially pumped neutral source and hence did not have the advantage of phase-sensitive detection. Since results obtained using phase-sensitive detection are considered more reliable than those obtained using the original configuration, the former results are preferred.

Fig. 1 shows the results of a reactive experiment performed using phase-sensitive detection. One can see that at 0.40 eV the product distribution is peaked in the vicinity of the spectator stripping velocity. The asymmetry of the distribution with respect to the relative velocity vector (0°-180° line) probably can be attributed to the beam shape. The Q = 1.9 eV circle is noteworthy because reactions involving $F^+(^1D)$ cannot give FH^+ inside this region. As indicated previously, reaction (2) which gives $FH^+(^2\Pi)$, is 5.36 eV exothermic, and, coupling this with the knowledge that $D_0(^2\Pi) = 3.42$ eV, the products of reaction (2) are constrained to $1.94 \leq Q \leq 5.36$ eV. Applying similar arguments to reaction (3) leads to the result that $F^+(^1D)$ can give stable $FH^+(^2\Sigma^+)$ only in the region $1.90 \leq Q \leq 2.30$ eV. Jones et al.[10] showed that these lower limits may be only approximate because of the possibility that rotationally metastable HF^+ can be formed, but this effect amounts to only a few hundredths of an eV. Since virtually all of the product intensity lies within the Q = 1.9 eV circle, we can be quite sure that the distribution represents the reaction of $F^+(^3P)$. The question as to the actual electronic state composition of our F^+ beam was not unambiguously answered, although it is discussed in some detail in Chapter 6.

Figs. 2 and 3 show results obtained at lower energies. These experiments did not utilize phase-sensitive detection, but it is rather obvious that even at 0.20 eV, the product distribution is forward peaked, appearing near the spectator stripping velocity. The threshold for the formation of $FH^+(^2\Sigma^+)$ is 0.29 eV; so we can state with some

Fig. 1. Velocity vector distribution for FH^+ resulting from the collision of F^+ and H_2 at an initial relative collision energy of 0.40 eV. The F^+ was produced by the impact of 160 eV electrons on CF_4. The small cross denotes the location of the spectator stripping velocity.

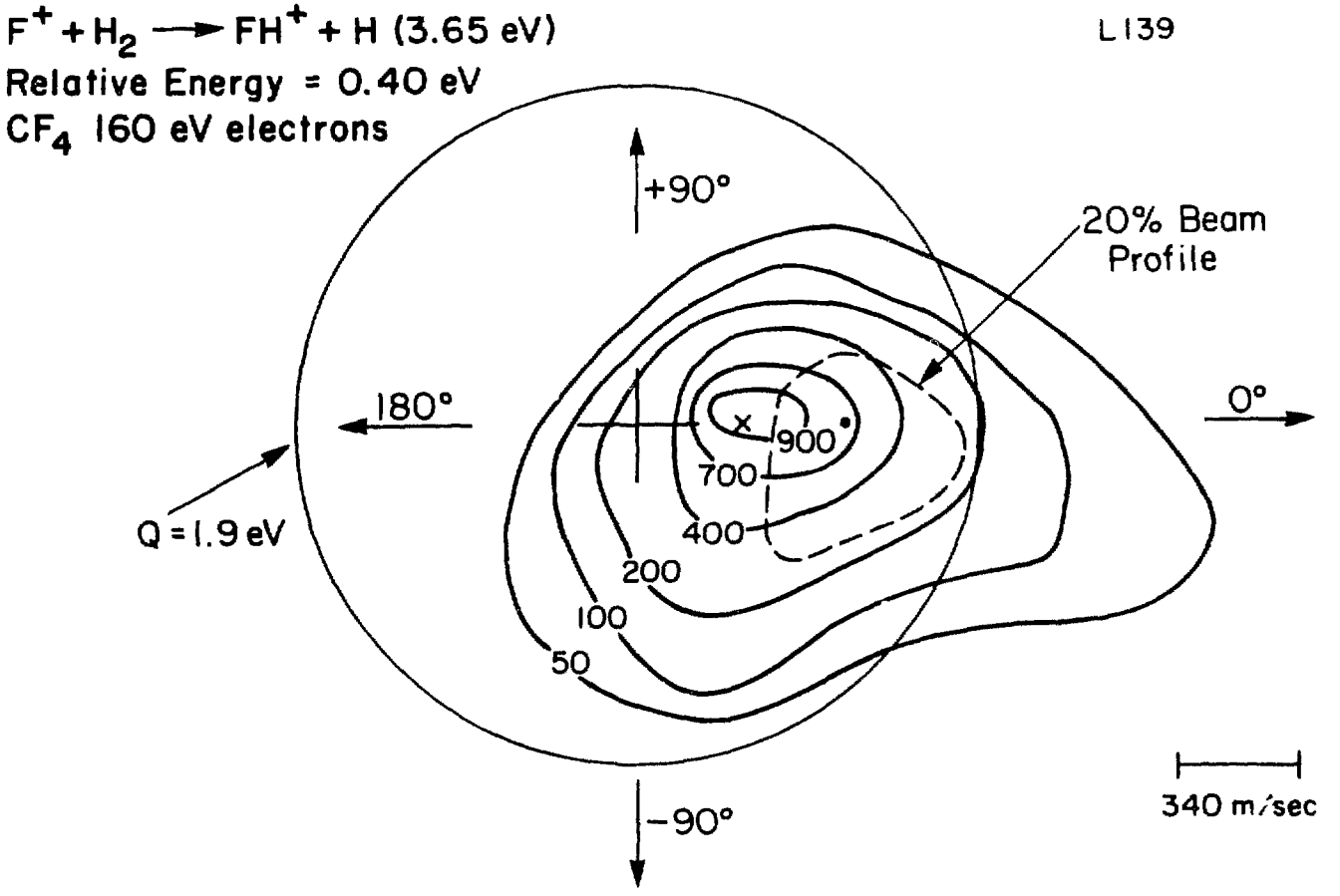
$F^+ + H_2 \longrightarrow FH^+ + H$ (3.65 eV)
Relative Energy = 0.40 eV
CF_4 160 eV electrons
L139
+90°
20% Beam Profile
180°
0°
900
700
400
200
100
50
Q = 1.9 eV
-90°
340 m/sec
XBL 808-11052

Fig. 1

Fig. 2. Contour map for FH^+ resulting from the collision of F^+ with H_2 at an initial relative energy of 0.27 eV. The F^+ was produced by the impact of 160 eV electrons on NF_3; the resulting F^+ state distribution is identical to that obtained using CF_4 (see Chapter 6). The beam is displaced for clarity.

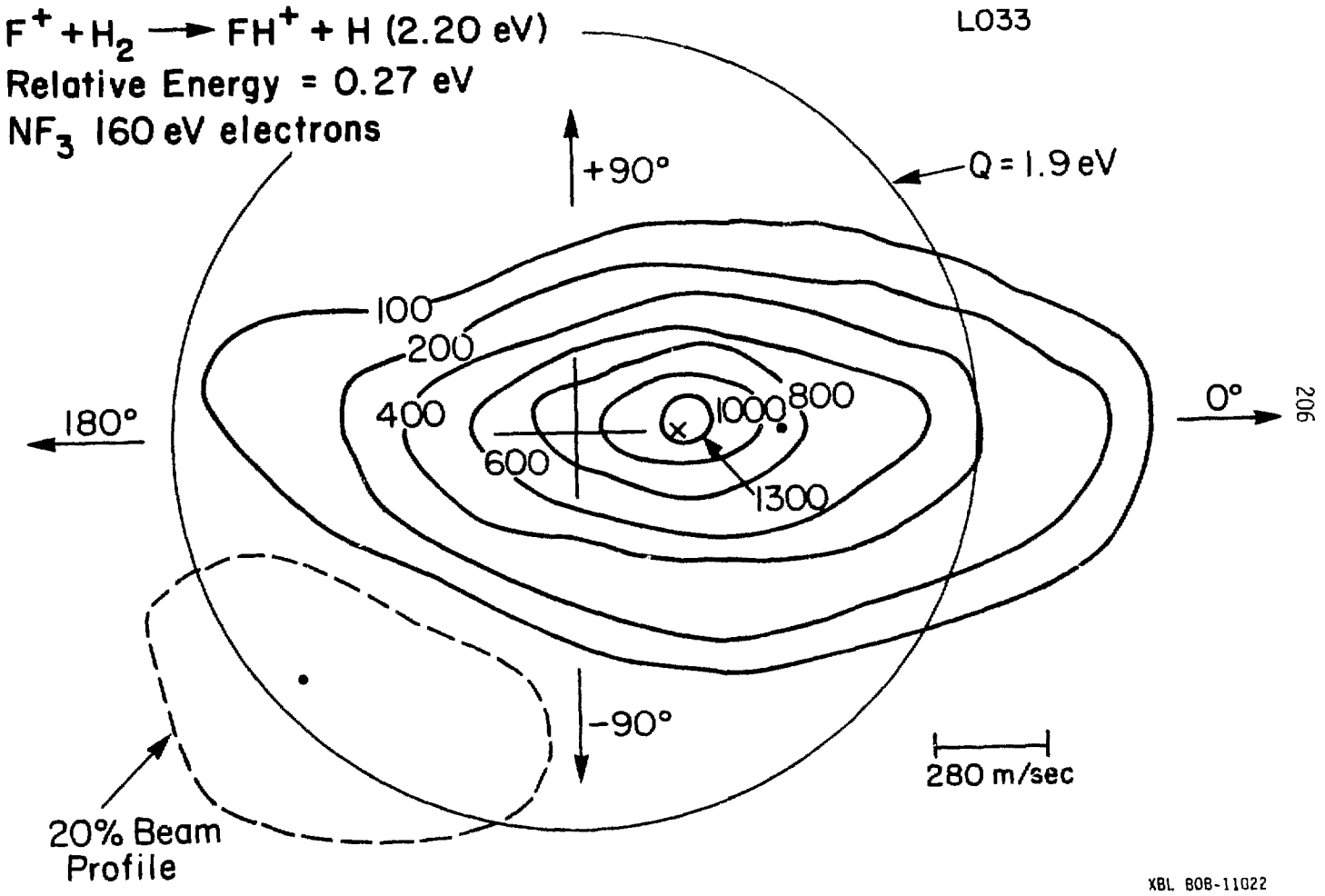
$F^+ + H_2 \rightarrow FH^+ + H$ (2.20 eV)
Relative Energy = 0.27 eV
NF_3 160 eV electrons
L033
+90°
Q = 1.9 eV
100
200
400
600
800
1000
1300
180°
0°
-90°
280 m/sec
20% Beam Profile
206
XBL 808-11022

Fig. 2

Fig. 3. Contour map for FH^+ resulting from the collision of F^+ with H_2 at an initial relative energy of 0.20 eV. F^+ was produced by the impact of 160 eV electrons on CF_4.

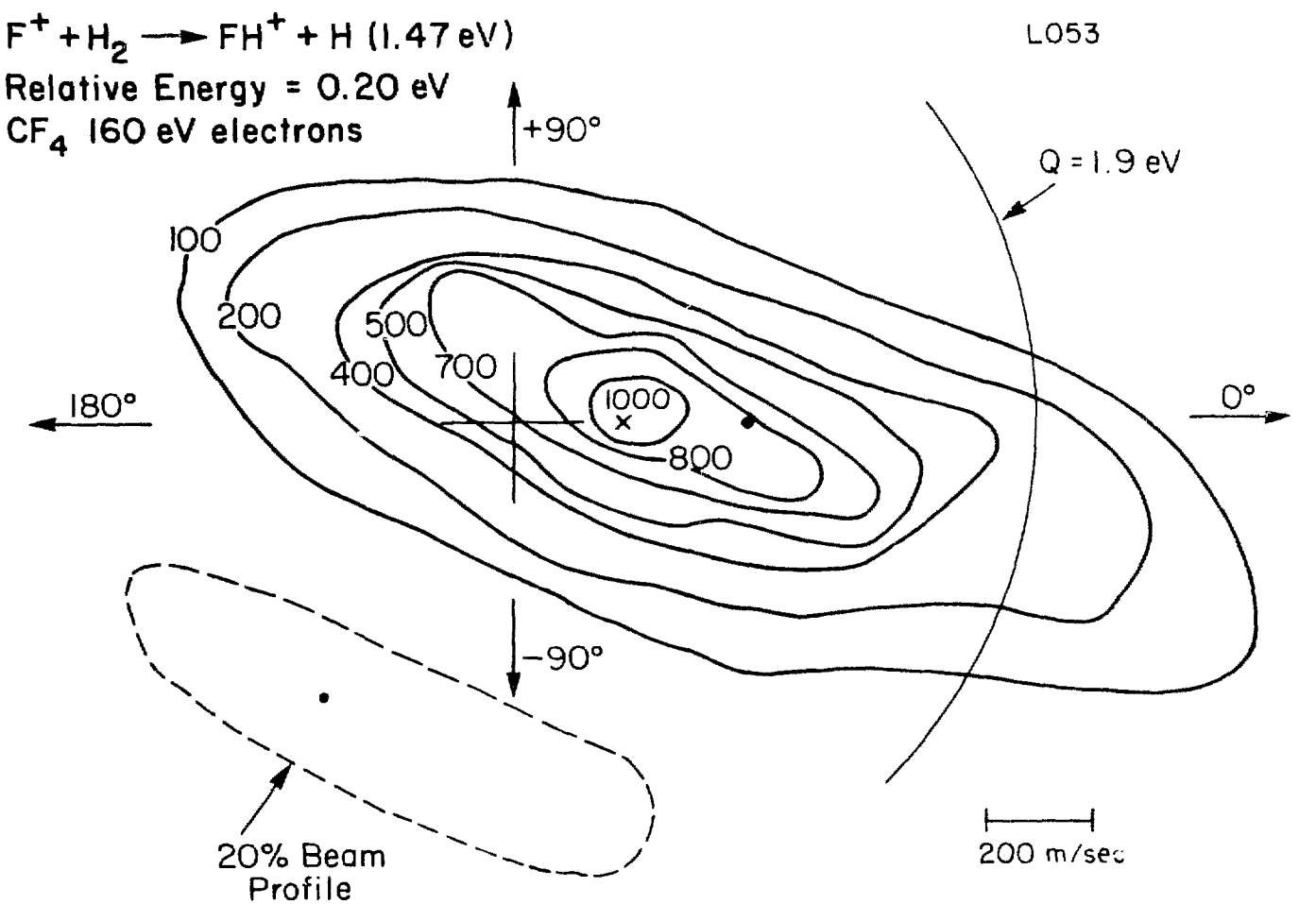

XBL 8611-11211

Fig. 3

certainty that these maps represent the reaction of $F^+(^3P)$ to give $FH^+(^2\Pi)$. Both of these experiments were performed at laboratory energies near the resolution limit of the apparatus. It can be seen in Figs. 1-3 that a product distribution 20% contour is not much broader than the beam 20% profile. This implies that the shape of the contour maps is largely determined by the beam shape; a deconvoluted product distribution would probably be quite narrow but still peaked near stripping. Attempts to improve our resolution at these low energies by velocity selecting the primary ion beam were unsuccessful.

These results cast doubt on the data of Wendell et al.[9] who found substantial symmetry in their product distributions at a relative collision energy of 0.21 eV. Our other maps (not shown) obtained at energies ranging up to 1.07 eV, generally showed a single peak which appeared at about the spectator stripping velocity.

We also performed experiments where product intensity was measured along the relative velocity vector using F^+ ions extracted from a CF_4: He microwave discharge. These F^+ beams were quite weak and had larger velocity spreads than electron impact produced beams, but we would expect them to contain nearly exclusively $F^+(^3P)$. Throughout the energy range 0.31-1.14 eV, the product velocity distribution peaked in the vicinity of the spectator stripping velocity. There may have been some tendency for the peaks to appear slightly behind stripping (in agreement with Koski) but this could not be unambiguously determined due to our reduced resolution using this ion source. A single experiment performed at 1.58 eV showed the product distribution shifted slightly

ahead of the stripping velocity as one would expect on energetic grounds. At this collision energy, the stripping velocity lies inside the Q = -0.65 eV circle, signifying $FH^+(^2\Pi)$ is not stable when formed by stripping, and, therefore, the peak is necessarily shifted forward.

Fig. 4 shows the results of an experiment in which F^+ scattered non-reactively from H_2 was measured. The map is dominated by elastic scattering although there appears to be some inelasticity in the back hemisphere; this implies that small impact parameter collisions transfer energy to the internal modes of H_2. Similar behavior was observed previously in collisions of Ar^+, Ne^+, and Na^+ with H_2 and its isotopes.[15-17] A modest back peak like the one in Fig. 4 was also seen in these systems. Since the interactions of Ar^+, Ne^+, and Na^+ with H_2 are known to be short-lived, the results of Fig. 4 can be taken as evidence that at 1.24 eV, the F^+-H_2 interaction is also short-lived. This is, of course, consistent with the reactive results. The presence of signal at 180° in the non-reactive map indicates that even head-on collisions do not always lead to reaction.

Discussion and Conclusions

Our results indicate that reaction (1) is direct down to 0.2 eV as was originally predicted by Mahan.[7] This is contrary to the observations of Wendell et al.,[9] and it is of some interest to compare our experiments with theirs. We use a crossed-beam approach while they employ a beam-gas arrangement. For this reason, we have defined the velocity of our neutral reactant more precisely than they. However, the

Fig. 4 Velocity vector distribution of F^+ scattered from H_2 at an initial relative energy of 1.24 eV. F^+ was produced by the impact of 160 eV electrons on CF_4.

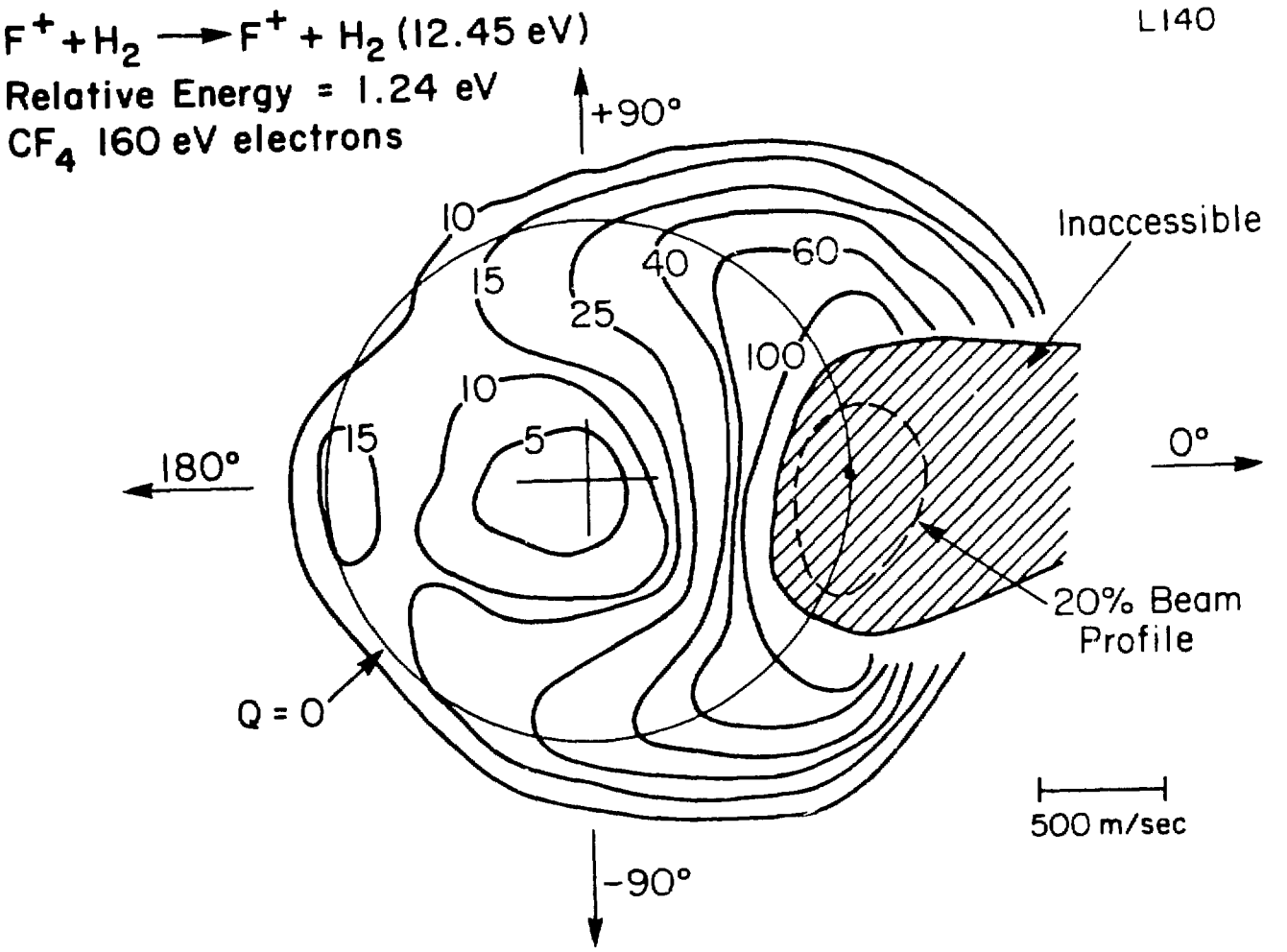
$F^+ + H_2 \longrightarrow F^+ + H_2$ (12.45 eV)
Relative Energy = 1.24 eV
CF_4 160 eV electrons
+90°
10
15
40
60
25
100
10
15
5
180°
0°
Inaccessible
20% Beam Profile
Q = 0
500 m/sec
-90°

Fig. 4

apparatus of Wendell et al. apparently is capable of performing experiments at lower laboratory energies than is ours. While our 0.2 eV experiment used H_2 as a reactant, their experiment used D_2, which, due to the difference in kinematics, gives better center-of-mass resolution. These facts by themselves make it difficult to choose between the two experiments, but if one considers the later, high resolution study by Jones et al.,[10] support for a direct mechanism even at low energies is obtained. Although not explicity discussed in Ref. 10, a diagram which plots Q vs. collision energy for reaction (1) appears to be more consistent with a stripping process than one involving a substantial interaction among all three collision partners. This information can be taken as confirmatory of our results that the reaction remains direct down to 0.2 eV.

As was discussed at some length in the previous chapter, probably the most successful approach to the understanding of the reaction dynamics of atomic ions with H_2 is the electronic state correlation diagram. Such a diagram appropriate to the $(F + H_2)^+$ system is shown in Fig. 5. After some perusal, two features stand out: 1) ground state $F^+ + H_2$ reactants do not constitute the lowest energy asymptote, and, 2) ground state $F^+ + H_2$ reactants are not connected to $FH^+ + H$, which are the observed products. These two points are intimately related, because if $F^+(^3P) + H_2$ was the lowest energy reactant asymptote then the $^3B_1$ surface in C_{2v} symmetry, and the $^3\Pi$ colinear surface would connect reactants and products, and the reaction could be easily understood. The fact that there is no

adiabatic pathway indicated by the correlation diagram implies that the reaction involves a non-adiabatic transition. Judging from the substantial cross section for reaction (1), the transition occurs quite readily.

The correlation diagram in Fig. 5 was constructed by Mahan prior to ab initio calculations performed by Schaefer and Ungemach, but the results were presented in a single paper.[18] It was the purpose of the calculations to test the accuracy of the correlation diagram and attempt to explain the reaction dynamics. The minimum energy point within the whole manifold of potential energy surfaces was found to lie ~10 eV below $F^+(^3P) + H_2$ reactants on the $^1A_1$ surface at r(F–H) = 0.963Å and $\theta = 112.1^\circ$. This singlet state closely resembles its isoelectronic analogue H_2O, but because of spin restrictions is not accessible to $F^+(^3P) + H_2$ reactants. Triplet states of H_2F^+ calculated at this geometry all lie quite high in energy ($\geq$ 13 eV above $^1A_1$). The ordering of these states as given in Fig. 5 is accurate except that the $^3A_2$ state actually lies below the lowest $^3B_2$ state. Potential curves were also calculated for the six lowest triplet states in C_{2v} symmetry as a function of r ($F–H_2$), keeping the H_2 (or H_2^+) bond distance fixed at its equilibrium value of 0.74Å (or 1.04 Å). The lowest $^3B_1$ and $^3B_2$ curves were found to have minima of 17.5 and 14.5 kcal/mole respectively, occurring rather early in the approach of F to H_2^+. Of the three triplet surfaces emanating from $F^+(^3P) + H_2$, only the $^3A_2$ has a slight well

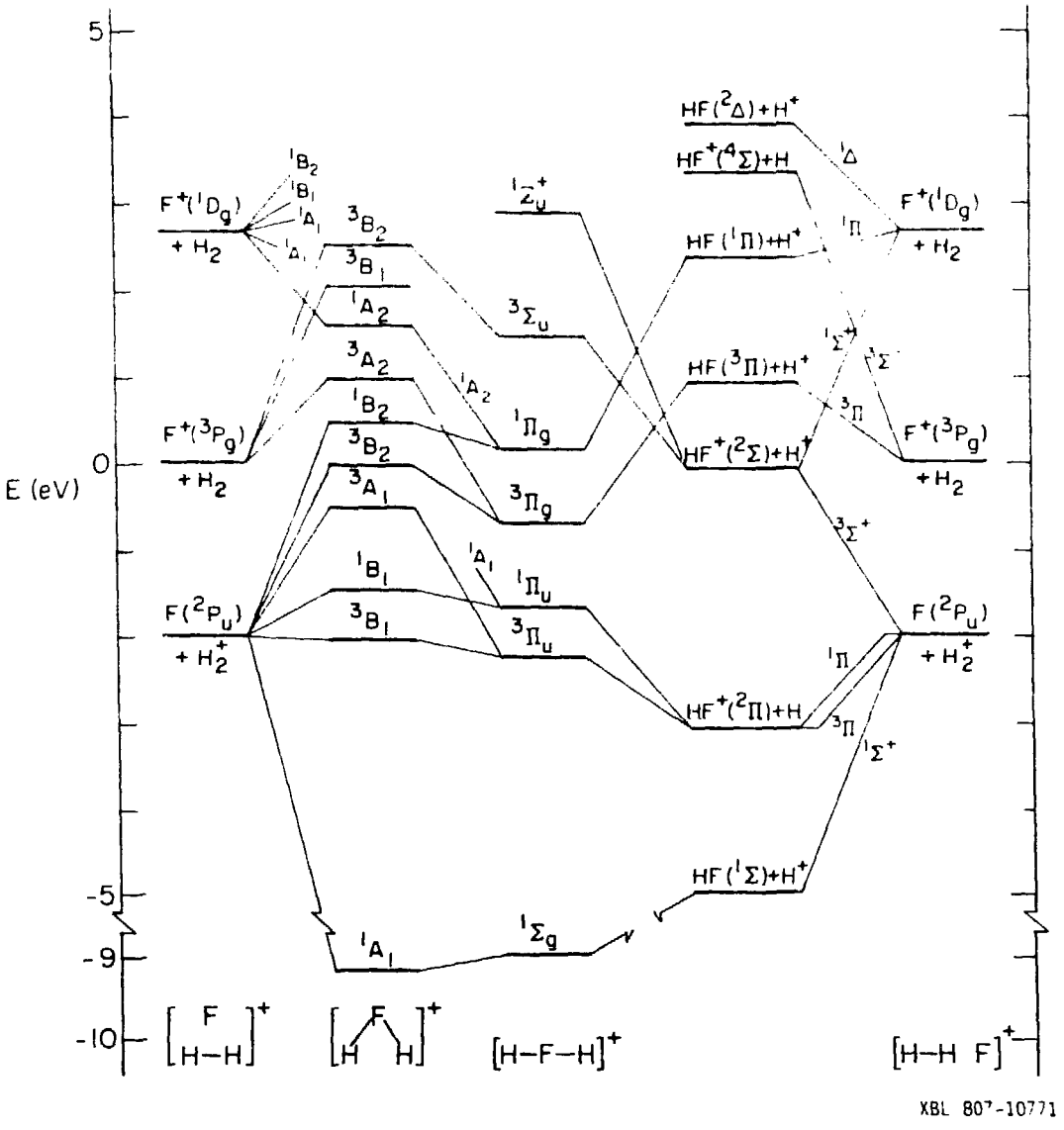

Fig. 5. Electronic state correlation diagram for the important low-lying surfaces of the FH_2^+ system. The left-hand side considers C_{2v} approaches of F^+ (or F) to H_2 (or H_2^+). On the right collinear approaches are considered.

(< 1 kcal/mole) and the $^3B_1$ and $^3B_2$ curves are rather strongly repulsive. It should be mentioned, though, that all of these surfaces could exhibit more substantial minima if r(H-H) was optimized as well.

As they stand, these calculations shed little light on the dynamics of reaction (1). It was concluded[18] that a suitable distortion of the lowest $^3B_1$ or $^3B_2$ surfaces in C_s symmetry might lead to surface hopping which could result in FH^+. It was thought perhaps more likely though, that an interaction of collinear surfaces, not considered in the calculations of Ref. 18, leads to HF^+ product.

The correlation diagram gives no clue as to how a collinear approach leads to products, but Fig. 6 can be used to see how the process might take place. The potential curves in Fig. 6 are those corresponding to H_2^+ and H_2, but the H_2 curve is shifted upward by 3.83 eV, which is equal to the difference in ionization potentials of F and H. Fig. 6 can be taken to represent a look down the entrance channel of the two lowest $^3\Pi$ surfaces in $C_{\infty v}$ geometry, for large $F-H_2$ distances. When $r(F-H_2) = \infty$, the crossing indicated in Fig. 6 is allowed; as r decreases, the crossing is avoided but the area near the avoided crossing remains a region of strong non-adiabatic coupling. Since the crossing in Fig. 6 occurs near the turning point of v = 0 for the H_2 curve, the region is traversed many times during approach, making it easy to see why the transition is favorable. When a transition is made from the $H_2 + F^+$ curve to the $H_2^+ + F$ curve, the trajectory is sharply accelerated away from the seam and $HF^+(^2\Pi)$ products can result.

Fig. 6. Potential curves for H_2 and H_2^+ traced from Ref. 19. The curves are offset by the difference in ionization potential of F and H. The zero of energy is taken as H_2 (v = 0) + F^+.

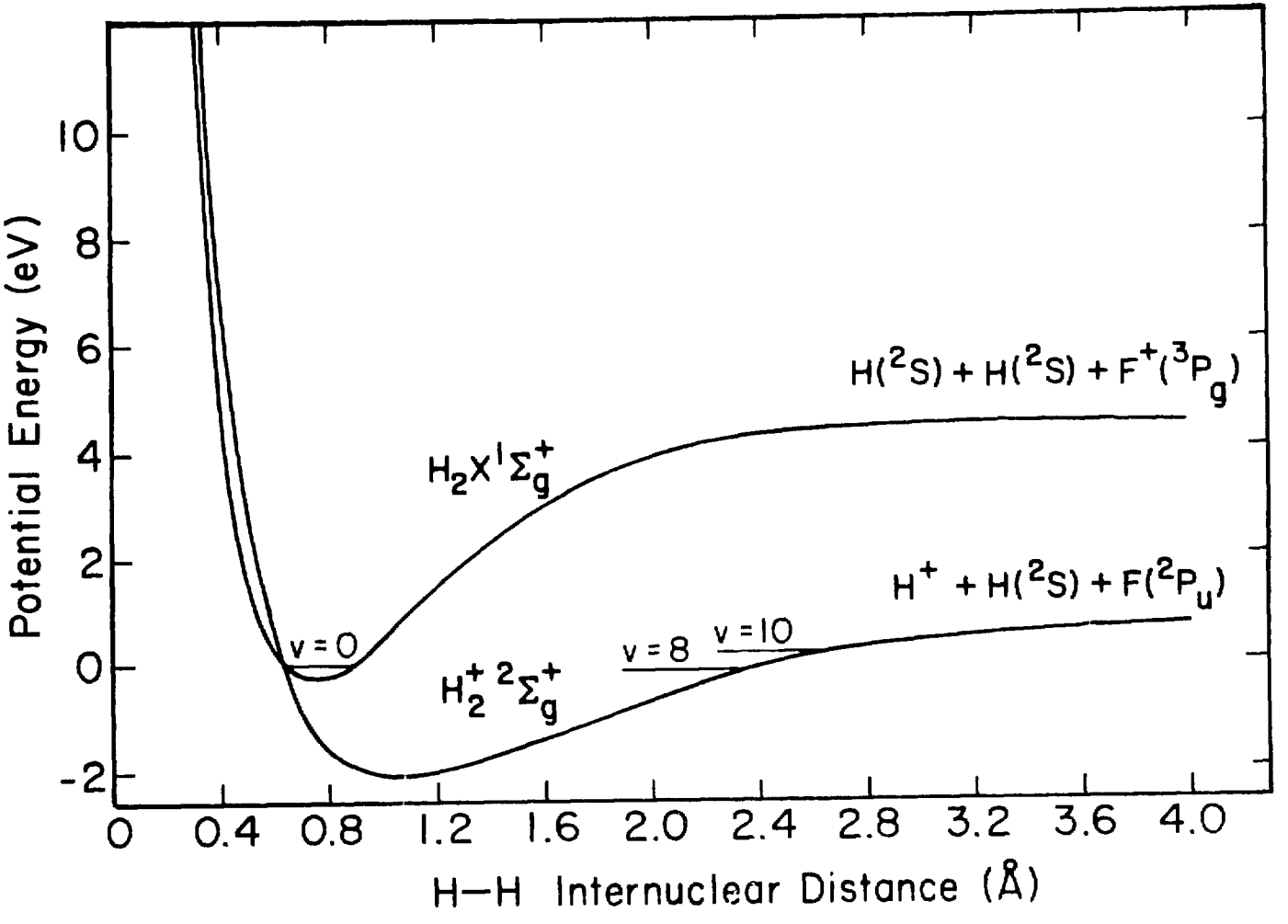
Potential Energy (eV)
10
8
6
4
2
0
-2
0
0.4
0.8
1.2
1.6
2.0
2.4
2.8
3.2
3.6
4.0
H—H Internuclear Distance (Å)
H(²S) + H(²S) + F⁺(³Pg)
H₂X¹Σg⁺
H⁺ + H(²S) + F(²Pu)
v = 0
v = 8
v = 10
H₂⁺ ²Σg⁺

Fig. 6

Although it is perhaps easiest to think of Fig. 6 in terms of a collinear approach of F^+ to H_2, the argument given above is valid for all geometries. This is because at $F^+ - H_2$ separations of 2Å or more, the interaction is essentially angle-independent,[20] and electron transfer should be easily accomplished at these distances. After the transition is made from the upper surface to the lower surface, collinear geometries are favored. This conclusion is drawn from the calculations of Kendrick et al.[13] who found that the minimum energy point regardless of geometry on the lowest triplet surface, corresponds to $(F\text{-}H\text{-}H)^+$ with r(FH) = 1.082Å and r(HH) = 1.352Å. In this configuration the system lies 0.14 eV below $HF^+(^2\Pi)$ + H. The lack of a deep potential well for the H_2F^+ intermediate is consistent with our observation that the reaction is direct at all energies.

We can also use the F^+–H_2 system as a mild check on a hypothesis put forth in Chapter 3. In that chapter it was pointed out that RRKM theory predicts complexes formed in simple triatomic reactions such as $N^+(H_2,H)NH^+$, $C^+(H_2,H)CH^+$, and $O(^1D)(H_2,H)OH$, should be relatively short-lived. Yet in all three of these reactions, the product distributions show considerable symmetry at low collision energies. One normally associates a symmetric product distribution with an intermediate complex lifetime of at least several rotational periods; since that is apparently not true for these reactions, an alternative explanation was offered. This explanation involved a C_{2v} approach of the reactants, and the formation of a short-lived, rapidly bending complex. The initial direction of approach is quickly forgotten in such a complex, and symmetric

product distributions can result in less than a rotational period. This argument leaves open the possibility that symmetric distributions might be seen even in systems possessing insignificant potential wells, if a C_{2v} approach was favored. The fact that $F^+(^3P) + H_2$ gives asymmetric product distributions while apparently preferring collinear approaches is consistent with the hypothesis given above.

The electronic state correlation diagram for the $(F + H_2)^+$ system is unable to show the reaction pathway due to the inherent limitations of a two-dimensional picture. The levels given in Fig. 5 correspond to the energy of an electronic state at its equilibrium geometry, and the lines connecting the states represent only a qualitative slice through the potential energy surfaces involved. For complicated systems, like the one at hand, it is necessary to consider somewhat arbitrary geometry changes in an attempt to find an intersection of diabatic potential surfaces. Fig. 6 depicts just such an intersection, and we see that it occurs when the H_2 bond is compressed; a two-dimensional state correlation diagram could not be expected to show this.

The reaction of $F^+(^1D)$ with H_2 is discussed by Kendrick et al.,[13] and their results show, as does the correlation diagram, that the reaction to give $FH^+(^2\Sigma^+)$ can proceed readily via the collinear $^1\Sigma^+$ surface. Ref. 13 also indicates that $FH^+(^2\Pi)$ can result via a non-adiabatic transition. The fact that these reactions are 2.30 and 5.36 eV exothermic, respectively, while the products are bound by only 0.40 and 3.42 eV might lead one to believe that there is a significant contribution from

$$F^+(^1D) + H_2 \rightarrow FH^{+*} + H \rightarrow F + H^+ + H \quad \Delta H = -1.9 \text{ eV}. \quad (4)$$

This is contrary to the results of Lin et al.[8] who found that $F^+(^1D)$ produced FH^+ with a cross section greater than or equal to that of $F^+(^3P)$. In any event the sum of the cross sections for reaction (2) and (3) will be larger than the cross section for (4) only if the potential energy surfaces allow for the efficient channelling of the exothermicity into translation. The fact that Ding[13,14] has found FH^+ resulting from low energy $F^+ - H_2$ collisions to have a substantial amount of translational energy could be taken as evidence for the $F^+(^1D)$ reaction. Whether this is actually the case cannot be decided for certain without greater knowledge of Ding's results. The energetic constraints of the $F^+(^1D)$ reaction are quite severe and it should be easy to tell which state of F^+ is responsible for the reaction.

Our own results show no evidence for the reaction of $F^+(^1D)$. FH^+ resulting from this reaction would appear near the Q = 1.9 eV circles in Figs. 1-3, and clearly there is no increase in product intensity there. As previously mentioned though, there is no guarantee that our beam contains $F^+(^1D)$ (see Chapter 6), and therefore our results are not a good test of its reactivity.

References

1. V. H. Dibeler, J. A. Walker, and K. E. McCulloh, J. Chem. Phys. 51, 4230 (1969).
2. R. A. Gangi and R. F. W. Bader, J. Chem. Phys. 55, 5369 (1971).
3. K. S. Sorbie and J. N. Murrell, Mol. Phys. 31, 905 (1976).
4. S. P. Walch, T. H. Dunning, R. C. Raffenetti, and F. W. Bobrowicz, 72, 406 (1980).
5. G. Dixon-Lewis and D. J. Williams, Comp. Chem. Kinet. 17, 1 (1977).
6. A. C. Luntz, R. Schinke, W. A. Lester, and Hs. H. Gunthard, J. Chem. Phys. 70, 5908 (1979).
7. B. H. Mahan, J. Chem. Phys. 55, 1436 (1971).
8. K. C. Lin, R. J. Cotter, and W. S. Koski, J. Chem. Phys. 61, 905 (1974).
9. K. Wendell, C. A. Jones, J. J. Kaufman, and W. S. Koski, J. Chem. Phys. 63, 750 (1975).
10. C. A. Jones, K. L. Wendell, and W. S. Koski, J. Chem. Phys. 67, 4917 (1977).
11. A. Henglein, Adv. Chem. Ser. 58, 63 (1966).
12. S. Gewurtz, H. Lew, and P. Flainek, Can. J. Phys. 53, 1097 (1975).
13. J. Kendrick, P. J. Kuntz, and I. H. Hillier, J. Chem. Phys. 68, 2373 (1978).
14. A. Ding, private communication.
15. M. Chiang, E. A. Gislason, B. H. Mahan, C. W. Tsao, and A. S. Werner, J. Chem. Phys. 52, 2698 (1970).

16. B. H. Mahan and J. S. Winn, J. Chem. Phys. 57, 4321 (1972).

17. W. L. Dimpfl and B. H. Mahan, J. Chem. Phys. 60, 3238 (1974).

18. B. H. Mahan, H. F. Schaefer, and S. R. Ungemach, J. Chem. Phys. 68, 781 (1978).

19. T. E. Sharp, Lockheed Missiles and Space Co. Report 5-10-69-9.

20. The approach is roughly angle-independent for motion involving the $^3A_2 - {}^3A'' - {}^3\Pi$ ($C_{2v} - C_s - C_{\infty v}$) surface.[18,13] Travel on the $^3B_1 - {}^3A'' - {}^3\Sigma^-$ or $^3B_2 - {}^3A' - {}^3\Pi$ surfaces probably prefers a collinear geometry due to the repulsive nature of the surfaces for C_{2v} approaches.[18]

CHAPTER 5. $CO_2^+ - D_2$ INTERACTIONS

In the two preceding chapters, reactions of atomic ions with H_2 have been discussed. Such systems are well-suited for theoretical modeling because of the small number of atoms involved and the concomitant ease with which symmetry rules can be applied. As soon as the complexity of the reactive system is increased, the models become much more difficult to use, and the interpretations are somewhat ambiguous. Nevertheless, it is the goal of the reaction dynamicist to understand all reactions from simple to complex, and hence our progression from a system involving a triatomic intermediate to the present pentatomic system, CO_2^+-D_2, is a natural one.

In an important paper, Mahan[1] discussed the application of orbital correlations to more complicated systems; in particular, he considered CO^+, N_2^+, O_2^+, and $C_2H_2^+$ with H_2. The four collision intermediates all lie 2.5-3 eV below the reactants, but experiments have demonstrated that the reaction dynamics differ appreciably. In particular CO^+ and N_2^+ abstract H atoms from H_2 by a direct reaction mechanism at all energies, while O_2^+ and $C_2H_2^+$ form long-lived collision complexes with H_2 at sufficiently low energies. Mahan[1] was able to rationalize this behavior using orbital correlation diagrams coupled with estimates of the importance of diabatic motion on the potential surfaces. Studying the CO_2^+-H_2 system will provide a further test of our ability to predict reaction mechanisms in more complex systems.

Two of the principle reaction products formed in CO_2^+-H_2 collisions are HCO_2^+ and HCO^+. This fact makes the CO_2^+-H_2 system all the more interesting because of the importance of these ions in interstellar space. The story concerning the discovery of HCO^+ in space is a colorful one, and it nicely illustrates the symbiotic relationship that exists between astro-physicists and physical chemists. Radio-astronomers[2] observed a line at 89.190 GHz which did not correspond to a transition of any known molecule, and hence the emitting species was dubbed "x-ogen." Klemperer,[3] acting on little more than intuition, suggested that it corresponded to a rotational transition in HCO^+. Ab initio calculations[4] confirmed that this assignment might be correct, and eventually the line was measured in the laboratory[5] and unambiguously attributed to $HCO^+(J = 1 \rightarrow 0)$. The reaction proposed for interstellar HCO^+ formation is[6]

$$H_3^+ + CO \rightarrow HCO^+ + H_2 \; ; \qquad (1)$$

this ion has been referred to as the cornerstone of ion-molecule chemistry in outer space.[7] It has also been suggested[8] that HCO_2^+ may be an abundant interstellar molecule; furthermore its direct observation could give information on the abundance of interstellar CO_2. The detection of symmetric molecules in space is hampered by the fact that molecules lacking permanent dipole moments do not possess pure rotational spectra; hence the observation of the protonated version is the next best thing. This technique has been used previously to suggest the

presence of interstellar N_2.[9] Ab initio calculations[8] have been performed on HCO_2^+ and frequencies corresponding to rotational transitions were determined; preliminary radio telescope searches were unsuccessful, however.

In addition to its astrophysical importance, HCO^+ also figures promimently in combustion processes. It has long been thought that through the reaction

$$CH + O \rightarrow HCO^+ + e^- \qquad (2)$$

ionization is initiated in a flame, and HCO^+ is considered to be the primary ion present in hydrocarbon flames.[10] The fact that HCO^+ and HCO_2^+ are important to a broad spectrum of scientists means that a significant amount of work has been done on them; we will draw on some of this knowledge as we proceed.

In addition to HCO_2^+ and HCO^+ there are a number of other products which can result from CO_2^+–H_2 collisions; some of the reaction channels are listed in Table 1. The heats of reaction given in Table 1 were calculated from the heats of formation of the various species. These values, except those for $H_2CO_2^+$, HCO_2^+, and HCO^+, were obtained from Refs. 11-13. The heat of formation of $H_2CO_2^+$, 7.40 eV, was calculated from $\Delta H_f(H_2CO_2)$[12] and the ionization potential of H_2CO_2[14]. The heats of formation for HCO_2^+ and HCO^+, 6.33 and 8.75 eV respectively, were deduced usign new ab initio estimates for the proton affinities of CO_2 and CO.[8,15]

TABLE 1

		ΔH(eV)
$CO_2^+ + H_2 \rightarrow$	$H_2CO_2^+$	-2.27
	$HCO_2^+ + H$	-1.08
	$H_2O^+ + CO$	-0.71
	$HCO^+ + OH$	-0.53
	$CO^+ + H_2O$	0.70
	$H_2^+ + CO_2$	1.69
	$H_2CO^+ + O$	2.58
	$OH^+ + HCO$	3.81
	$O^+ + H_2CO$	5.36
	$O_2^+ + CH_2$	6.51
	$HO_2^+ + CH$	8.24

Reaction products and heats of reaction for $CO_2^+ - H_2$ collisions.

Table 1 indicates that this system should be quite interesting as there is a 2.27 eV well associated with the intermediate, and there are no fewer than three sets of reaction products energetically accessible in low energy collisions.

It comes as some surprise then that the only reaction product seen in thermal energy collisions is HCO_2^+. This was first observed by Moran and Friedman[16] and confirmed by Fehsenfeld et al.[17] who noted that the rate of HCO_2^+ formation was the same as the CO_2^+ rate of depletion. The measured rate[17], 1.4×10^{-9} cm^3/sec, is equal to that predicted by the Langevin polarization model; this implies that the reaction proceeds upon every collision. Subsequent measurements using the low pressure ion cyclotron resonance (ICR) technique yield a somewhat slower rate[18,19] as do low pressure experiments in mass spectrometer sources.[20,21] However, data taken in a high pressure mass spectrometer source[22] agree with the flowing afterglow work of Fehsenfeld et al.[17] These results strongly suggest that excited states of CO_2^+ are produced by electron impact, and that these states react with a smaller rate constant. In a high pressure environment, numerous collisions thermalize the CO_2^+; the lowest vibrational states of $CO_2^+(^2\Pi_g)$ apparently react at the Langevin rate. This hypothesis was tested by Albritton[23] using a drift tube. It was found that the rate of HCO_2^+ formation was lower when Ar buffer gas was used than when He was used. At a fixed laboratory energy, collisions with Ar have a higher center-of-mass energy than those with He, and hence CO_2^+ in Ar should be vibrationally hotter.

The observation[23] that these ions react more slowly is consistent with the notion that CO_2^{+*} has a smaller reaction rate constant than $CO_2^+(v = 0,0,0)$.

Mahan and Schubart[24,25] measured angular distributions for DCO_2^+, DCO^+, CO^+, OD^+, and O^+ resulting from CO_2^+-D_2 beam-gas collisions. The last three products seen were seen only above 8 eV relative collision energy, but DCO_2^+ and DCO^+ appeared throughout the energy range studied (1-15 eV); no D_2O^+ was observed. At energies below 4 eV, DCO^+ distributions were symmetric, and it was suggested that DCO^+ resulted from the decay of a long-lived $D_2CO_2^+$ complex. At 10 eV DCO^+ distributions were forward peaked, and it apeared that this ion was formed from the decomposition of highly excited DCO_2^+.

The distributions for DCO_2^+ products were peaked at the spectator stripping velocity at 2 eV and above, although the low intensity contours on the 2 eV map were symmetric. Using H_2, it was observed[25] at 1.5 eV that HCO^+ was scattered fairly symmetrically; the reliability of this result is weakened, however, by the map's low center-of-mass resolution. It was therefore our intention to study CO_2^+-D_2 collisions at lower collision energies and find out if DCO_2^+ distributions indeed became symmetric. We also wished to measure the threshold for DCO^+ formation.

Results - DCO_2^+

We obtained approximately 10 complete product velocity vector distributions, and 15 relative velocity vector centerline distributions for the reaction

$$CO_2^+ + D_2 \rightarrow DCO_2^+ + D \quad . \tag{3}$$

The highest energy studied, 1.55 eV, is in the range of the lowest energy experiments of Schubart,[25] and our results extend down to 0.27 eV. Both the electron impact and microwave discharge sources were used to produce CO_2^+; as discussed in Chapter 6 we were unable to detect any differences in the state distributions or reactivity in the ions obtained from these sources. D_2 was preferred over H_2 as a reactant for two reasons: 1) the inability of our detector's quadrupole mass filter to separate masses 45 and 44, 2) at the same laboratory energy center-of-mass resolution is a factor of two better with D_2 than H_2. We found reaction (3) to have an appreciable cross section which is consistent with the thermal energy work and recent beam-gas measurements at higher energies.[26]

Fig. 1 shows a contour map in which the intensity of DCO_2^+ resulting from CO_2^+-D_2 collisions at a relative energy of 1.10 eV, is plotted. The distribution is asymmetric, peaking near the spectator stripping velocity, but the lower intensity contours have a high degree of forward-backward symmetry. Overall the map closely resembles the 2.03 eV map of Mahan and Schubart.[24] It is possible to interpret such

Fig. 1. Velocity vector distribution for DCO_2^+ resulting from 1.10 eV CO_2^+-D_2 collisions. The small cross denotes the location of the spectator stripping velocity.

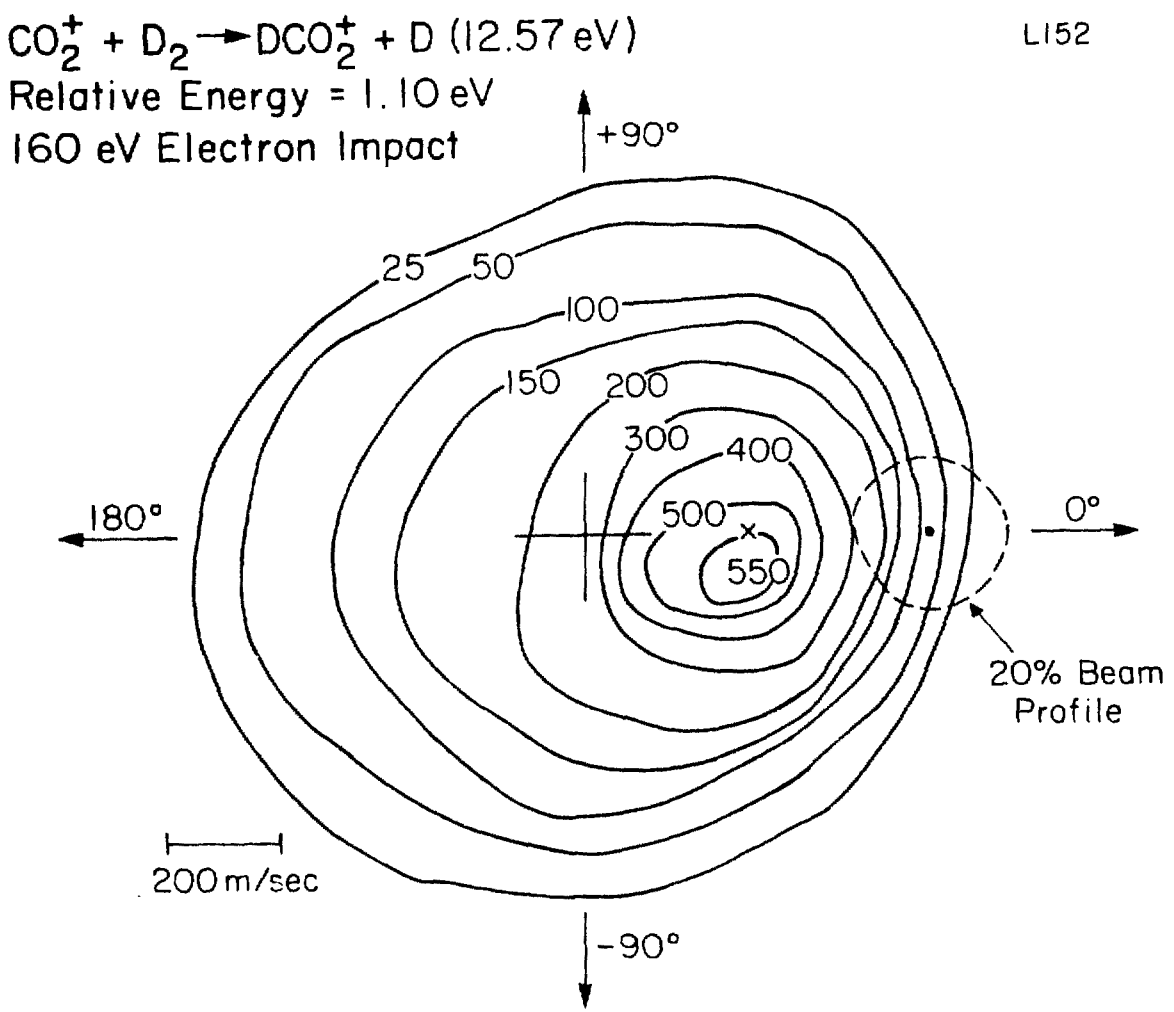
$CO_2^+ + D_2 \rightarrow DCO_2^+ + D$ (12.57 eV)
Relative Energy = 1.10 eV
160 eV Electron Impact
+90°
25
50
100
150
200
300
400
500
550
180°
0°
20% Beam Profile
200 m/sec
-90°

Fig. 1

a distribution as arising from two distinct reaction mechanisms occurring simultaneously: the peak near the stripping velocity results from grazing collisions in which a D atom is transferred at relatively large distances, and the symmetric contours reflect the participation of a long-lived collision complex. The complex would be formed from more intimate encounters. At this point, however, such an interpretation is somewhat speculative, as direct interactions can also lead to symmetric product distributions.[27]

Figs. 2 and 3 show DCO_2^+ product distributions resulting from 0.69 and 0.27 eV CO_2^+-D_2 collisions. The map at 0.69 eV is similar to Fig. 1 in that the distribution is peaked near stripping, but the lower intensity contours are reasonably symmetric. The resolution in the 0.27 eV map is not very good due to the increased importance of beam size at low collision energies. Nevertheless, the peak appears slightly ahead of the center-of-mass velocity indicating that even at this low energy much of the product is formed by a direct reaction mechanism.

Somewhat higher resolution results are obtained in experiments in which product intensity is measured along the theoretical relative velocity vector. Since fewer data points are taken, longer counting times can be used which yield better statistics. Also the experiment can be completed more quickly; this point is important because it minimizes the problem of beam drift. Fig. 4 shows the results of two such experiments at 1.55 and 1.03 eV, and there is good agreement between these velocity spectra and the previously given maps. Both

Fig. 2. Contour map for DCO_2^+ resulting from 0.69 eV CO_2^+-D_2 collisions. The CO_2^+ was produced by the impact of 160 eV electrons on CO_2.

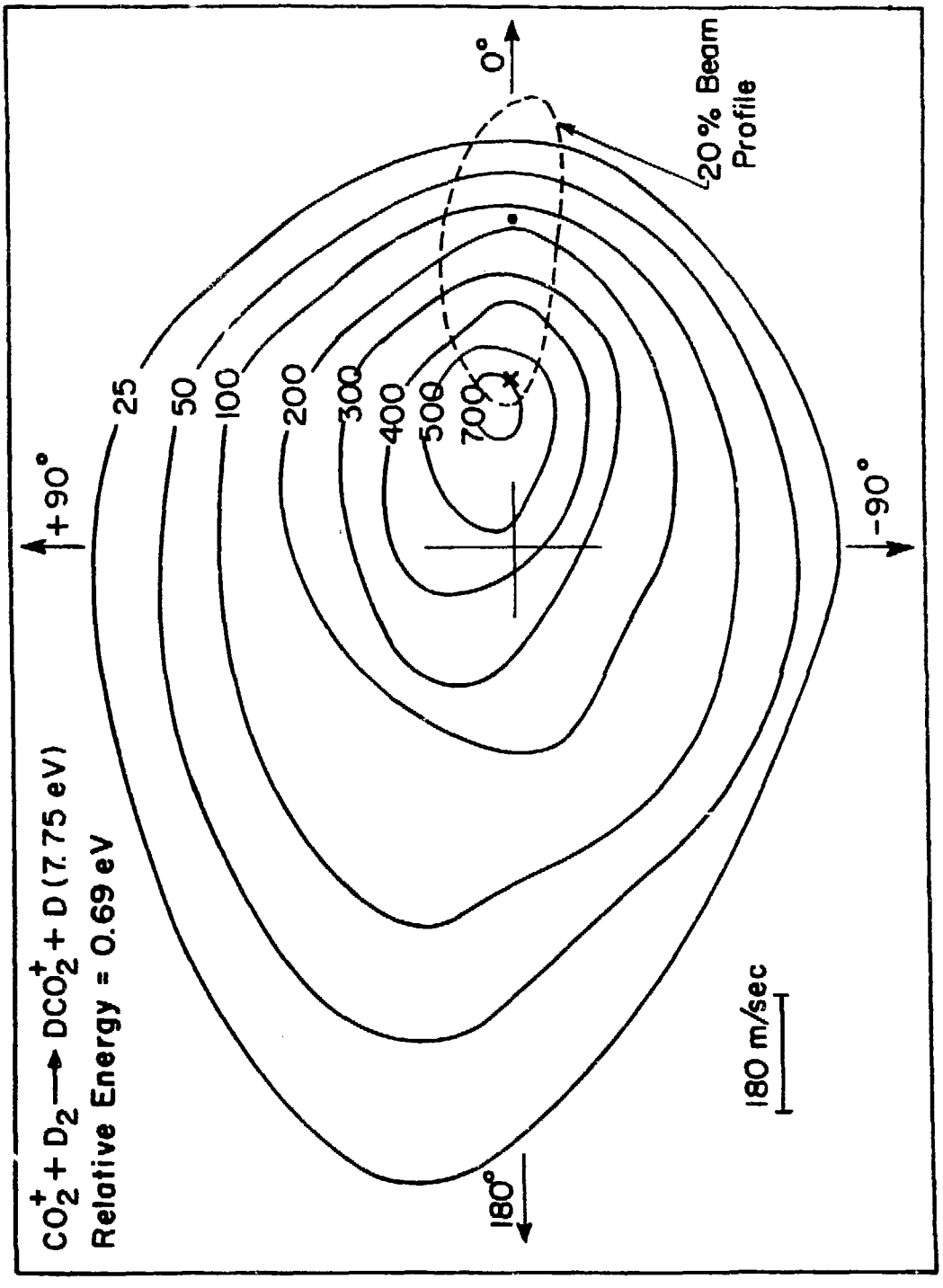
$CO_2^+ + D_2 \longrightarrow DCO_2^+ + D$ (7.75 eV)
Relative Energy = 0.69 eV
+90°
-90°
0°
180°
25
50
100
200
300
400
500
700
20% Beam Profile
180 m/sec

Fig. 2

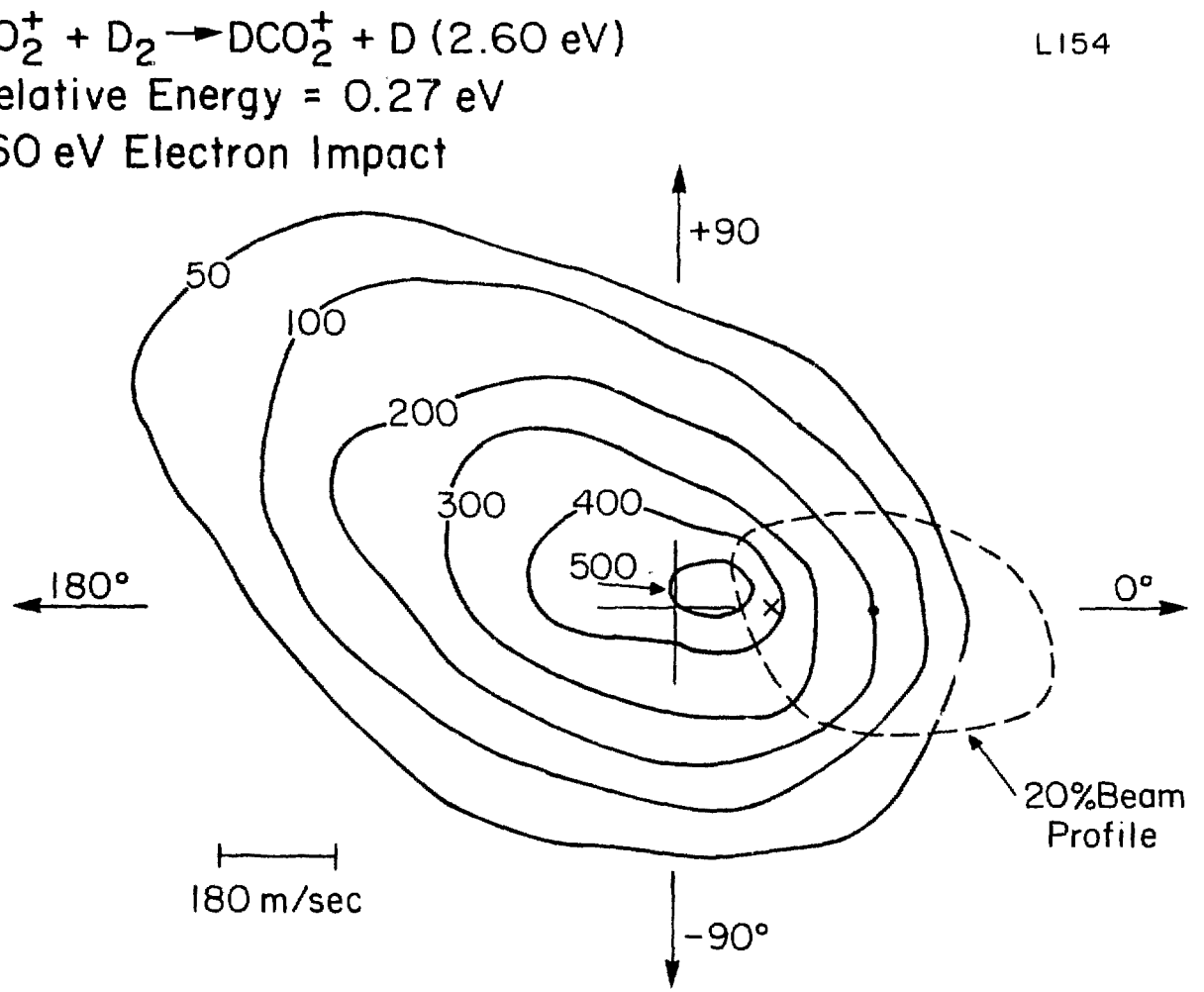

Fig. 3. Contour map for DCO_2^+ resulting from 0.27 eV CO_2^+-D_2 collisions.

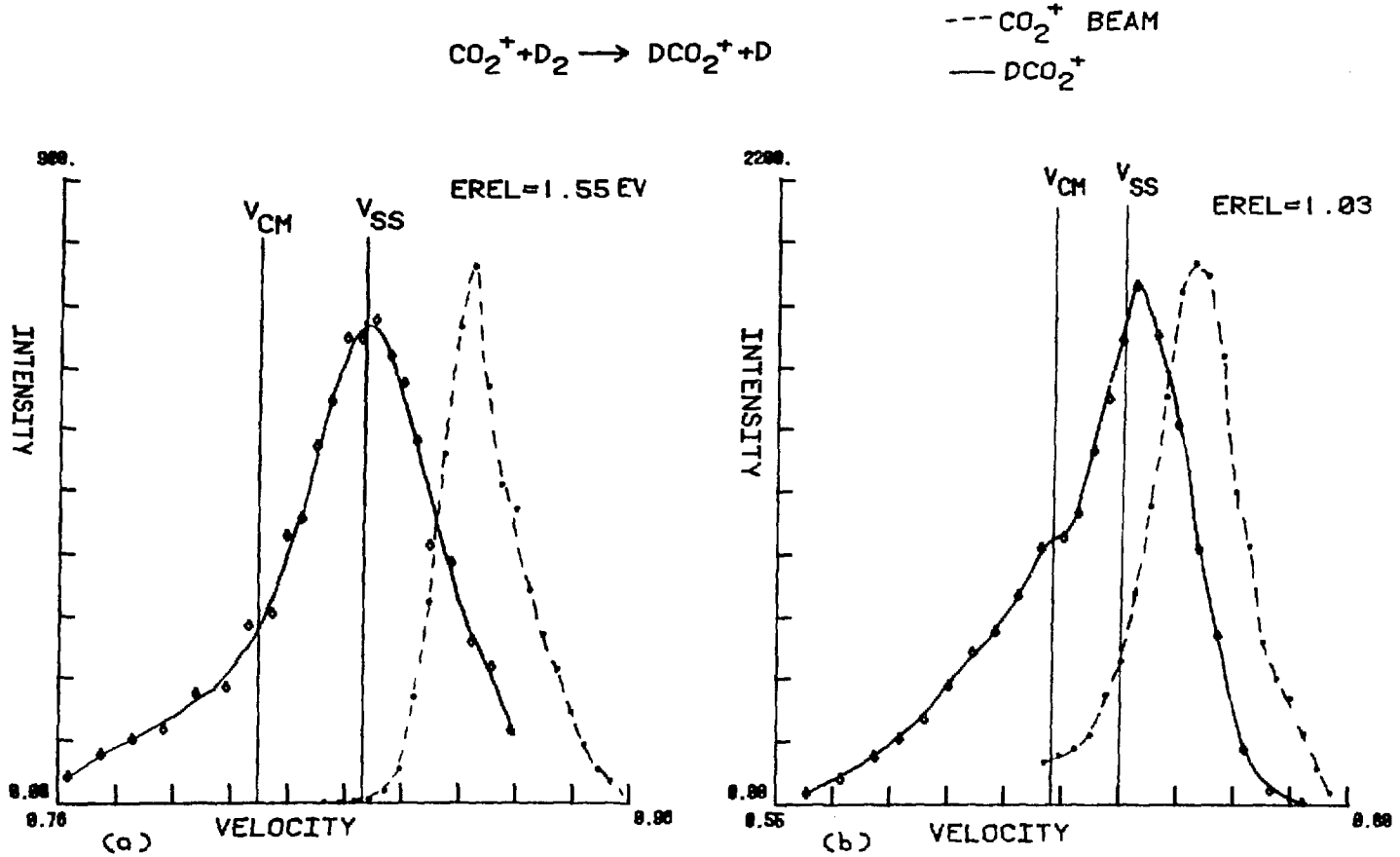

Fig. 4. Scans along the relative velocity vector for DCO_2^+ formed from 1.55 and 1.03 eV collisions of CO_2^+ and D_2. The units for the velocity scale are $(eV/amu)^{1/2}$. The dotted line represents the beam profile measured at the beam angle. In these experiments CO_2^+ was produced by a microwave discharge through CO_2.

distributions in Fig. 4 are peaked at the stripping velocity but tend to be symmetric about the center-of-mass velocity at lower intensities. The fact that these experiments were performed using the microwave discharge source, while the maps in Figs. 1-3 used electron impact produced ions, indicates that if the CO_2^+ internal state distributions are different, there is not a large difference in the reaction dynamics of the various states. It is also interesting to note the small hump at the center-of mass velocity in the product distribution in Fig. 4b. Our resolution was not always sufficient to resolve such a feature, but it did appear several times. This hump can be taken as evidence in favor of the two reaction mechanism argument. If a substantial fraction of DCO_2^+ resulted from the decay of a long-lived complex it is likely that a peak would appear at the center-of-mass velocity. The distribution in Fig. 4b is probably best explained as the sum of two Gaussian-like functions: a narrow one peaked at spectator stripping, and a broader one peaked at the center-of-mass.

Fig. 5 shows two more velocity spectra obtained at lower energies. At 0.65 eV, the distribution is rather similar to the higher energy results of Fig. 4 and the maps in Figs. 1 and 2. Again a slight hump appears at the center-of-mass velocity, but the distribution is rather sharply peaked at the stripping velocity. Fig. 5b shows the results of an experiment performed at 0.27 eV. As in the contour map obtained at this energy, resolution is low; however, it appears that the distribubution still peaks near the stripping. This result clearly demonstrates that the reaction remains direct down to 0.27 eV.

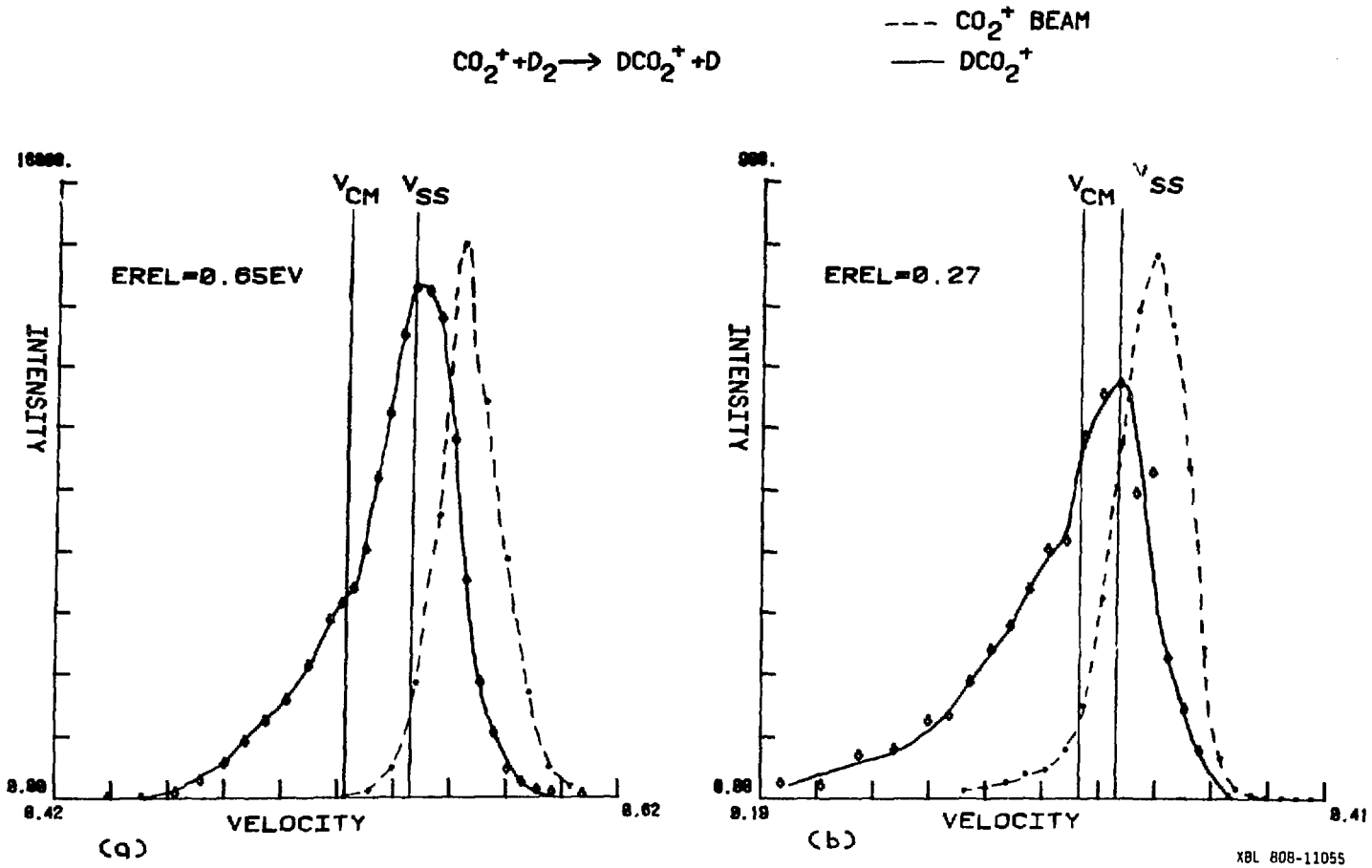

Fig. 5. Scans along the relative velocity vector for DCO_2^+ formed from 0.65 and 0.27 eV collisions of CO_2^+ and D_2. These experiments used CO_2 produced by 160 eV electron impact on CO_2.

Non-Reactive Scattering

We performed two experiments in which CO_2^+ scattered non-reactively was measured. The results are shown in Figs. 6 and 7.

These experiments were performed at roughly comparable energies (~1 eV); however, in Fig. 6 CO_2^+ is scattered from D_2, and in Fig. 7 it is scattered from He. The results using D_2 are noticeably more inelastic than the map obtained with He. There is some inelasticity in Fig. 7 which indicates a small amount of energy transfer from translation to internal modes of CO_2^+. No obvious superelastic scattering is present in either Fig. 6 or 7. Such events would give product signal outside the elastic circle and would result from energy transfer from internally excited CO_2^+ into translation. We made a careful search for superelastic scattering by examining CO_2^+ scattered non-reactively from Ne, a system with good center-of-mass resolution, but none was seen. This was true for both electron impact and microwave discharge produced ions. The small amount of signal which appears outside the elastic circle in Figs. 6 and 7 is attributable to finite beam widths and apparatus resolution.

Since the masses of D_2 and He are equal, the difference in the appearance of Figs. 6 and 7 is due to the different chemical forces operative in the two systems. Because He has a closed shell, and a low polarizability, the interaction potential between it and CO_2^+ is relatively flat until the hard-sphere distance is reached. Collisions will be impulsive, and one would predict that the scattering will be elastic except for the possibility that energy can be transferred into

Fig. 6. Contour map of CO_2^+ scattered from D_2 at a collision energy of 0.86 eV.

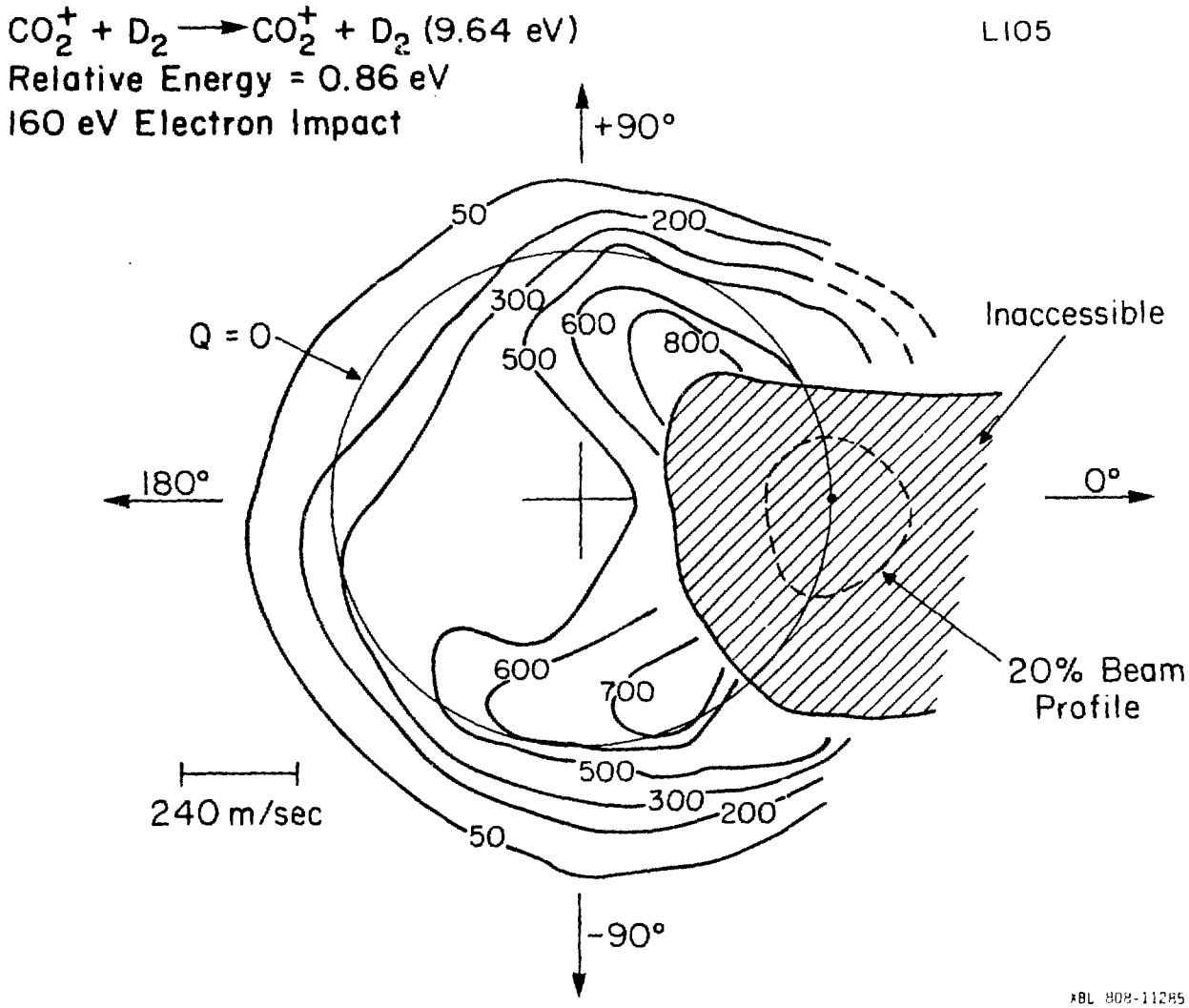
$CO_2^+ + D_2 \longrightarrow CO_2^+ + D_2$ (9.64 eV)
Relative Energy = 0.86 eV
160 eV Electron Impact
L105
+90°
50
200
300
600
800
500
Q = 0
Inaccessible
180°
0°
600
700
20% Beam Profile
500
300
200
240 m/sec
50
-90°
XBL 808-11285

Fig. 6.

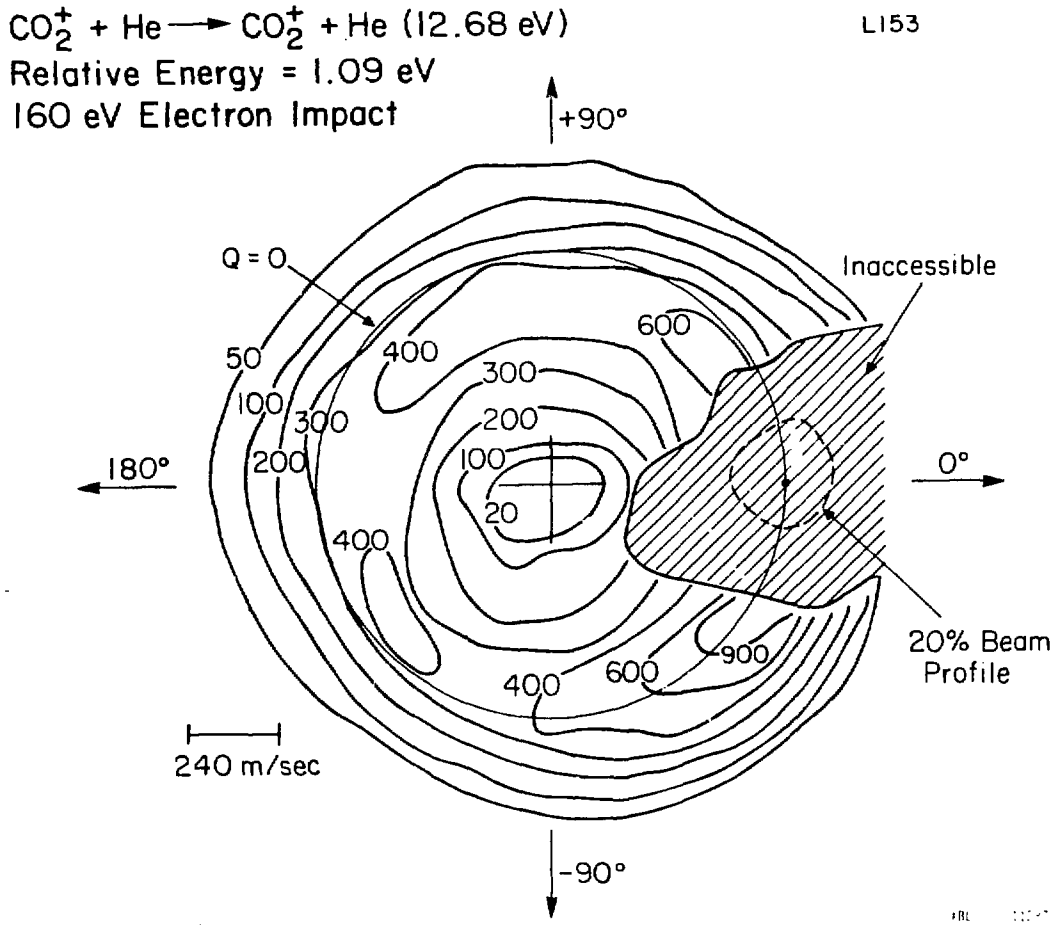

Fig. 7. Contour map of CO_2^+ scattered from He at a collision energy of 1.09 eV.

internal modes of CO_2^+. More energy should be transferred in low impact parameter collisions (back-scattered product) than in grazing collisions; Fig. 7 bears out this assertion.

As CO_2^+ approaches D_2 there is the possibility of accessing the 2.27 eV deep well associated with $D_2CO_2^+$. Hence a more intimate interaction would be expected, allowing for more energy transfer into internal modes. This is exactly what we observe in Fig. 6. It is impossible to decide from this map whether any of the non-reactive signal comes from the decay of a long-lived collision complex; however, if any does, it is probably a small fraction. One could predict this from the fact that the decay of such a complex to $CO_2^+ + D_2$ does not represent the most favorable energetic path.

A final point to note in comparing Figs. 6 and 7 is the intensity fall off as a function of center-of-mass scattering angle. In the He map the ratio of intensity at 90° to that at 180° is approximately one; in the D_2 map this ratio is closer to 1/2. The explanation for this difference is almost certainly that the non-reactive signal is depleted at large scattering angles by reactive processes when D_2 is used.

It should be pointed out that these results are almost identical to those obtained by Schubart[25] at 1.88 eV.

$\underline{DCO^+}$

As was mentioned in the introduction to this chapter, one of our goals in studying the CO_2^+-D_2 system was to find the threshold for the formation of DCO^+. Though the reaction

$$CO_2^+ + D_2 \rightarrow DCO^+ + OD \qquad (4)$$

is exoergic, it does not take place at thermal energies but was observed by Schubart[25] at energies above ~1.5 eV.

The study of this reaction is experimentally difficult for us. For one thing, the cross section for reaction (4) is quite low even well above its threshold,[25] and it decreases monotonically to zero as the energy is decreased. The product distributions are broad,[25] meaning that the amount of product scattered into a region of velocity space equal to the area viewed by the detector is also very small. Coupling these problems with the fact that DCO^+ appears at a substantially lower laboratory energy than does the main beam or DCO_2^+, hence requiring significant detector refocusing, makes the study of reaction (4) considerably more difficult than the other reactions discussed in this thesis.[28]

DCO^+ signal levels were low enough that it was impractical to study the reaction using crossed beams. However, data obtained using a neutral D_2 beam was consistent with Schubart's observation that at low energies (< 4 eV) DCO^+ was distributed symmetrically. In order to generate more realistic product counting rates it was necessary to employ a scattering cell to contain D_2 (or H_2). A scattering cell allows one to introduce the neutral reactant in greater concentrations

and with a longer interaction path than if a neutral beam is used, and hence more signal is produced. The scattering cell we used for these experiments was also used in the total luminescence experiments and is described in the next chapter.

Total DCO^+ and HCO^+ intensities were determined at various collision energies using the following technique. Beams of CO_2^+ were directed through the cell and D_2 (or H_2) was added until the beam was attenuated by ~20%. DCO^+ (or HCO^+) was then measured in the direction of the beam at various energies. From these data velocity spectra were plotted and contour maps were synthesized using Schubart's result that these distributions are isotropic about the center-of-mass. The total volume under the synthesized maps was determined and this quantity, divided by the beam current, was taken as the integrated intensity of DCO^+ (HCO^+) at that collision energy. Although this value is roughly analogous to the reaction cross section it is actually somewhat different. To obtain a number proportional to the true cross section it would be necessary to integrate the maps weighting the data points by the square of their center-of-mass velocity. This is a very questionable procedure for distributions peaked at the center-of-mass, especially if the center-of-mass resolution is poor. Since the DCO^+ distributions we measure are both low resolution and peaked at the center of mass, no attempt was made to obtain true cross sections.

Fig. 8 shows a plot of HCO^+ integrated intensity as a function of relative collision energy. The smooth line drawn through the data points indicates that the reaction threshold is about 1.0 eV.

Fig. 8. Plot of the integrated intensity of HCO^+ as a function of initial relative energy for reaction (4) using H_2 as a reactant. Different symbols denote data taken on different runs. A smooth line is drawn through the data points.

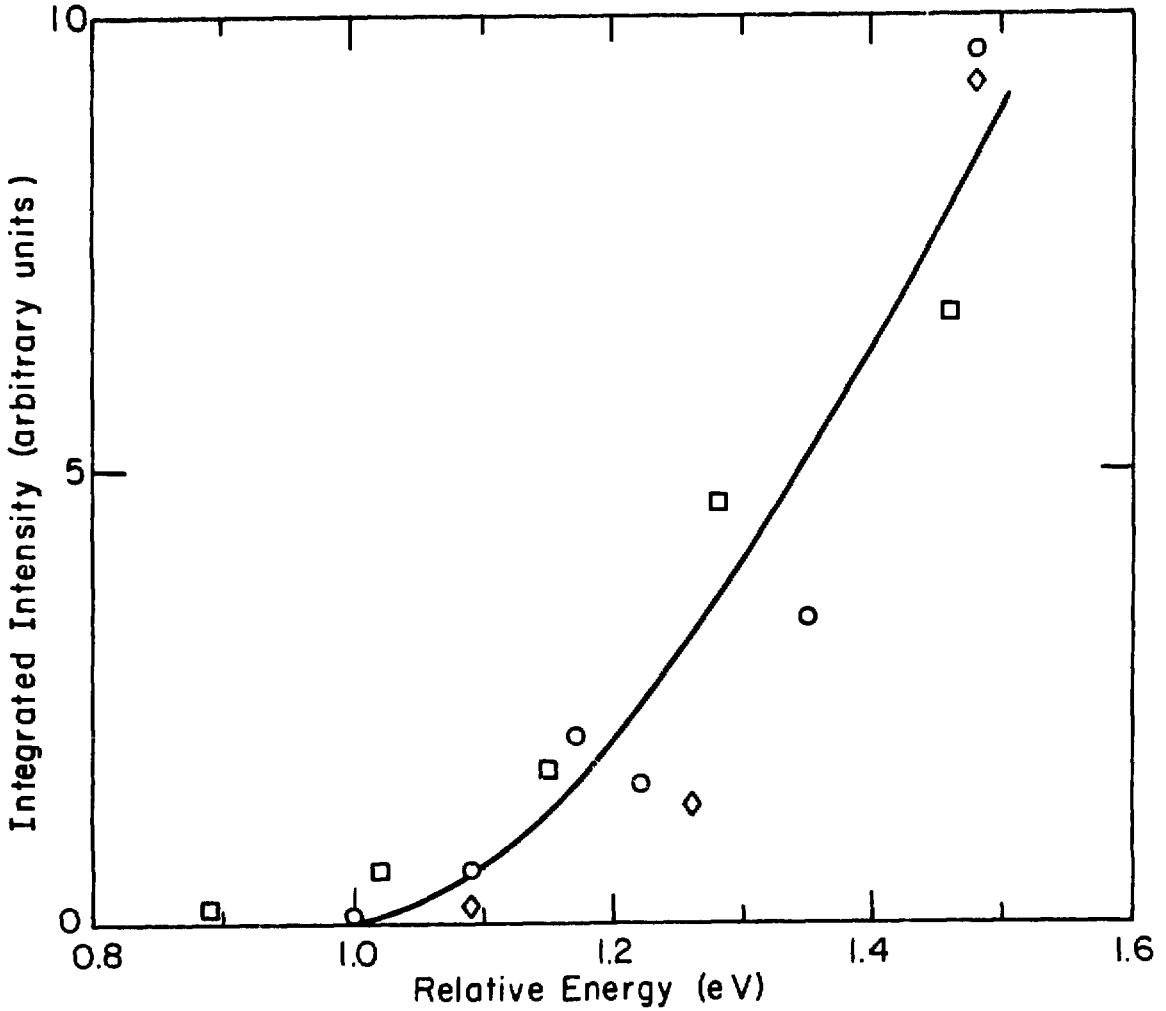
10
5
0
Integrated Intensity (arbitrary units)
0.8
1.0
1.2
1.4
1.6
Relative Energy (eV)

Fig. 8

Experiments performed with D_2, in which DCO^+ was measured, were somewhat less satisfactory in that the data contained more noise and appeared to rise less steeply in the vicinity of the threshold than the points in Fig. 8. Nevertheless, agreement was obtained in that DCO^+ was measurable at 14 eV lab (1.17 eV relative) but not at 11 eV (0.92 eV relative). One possible explanation for the slower rise from threshold for DCO^+ would be decreased detector transmission of lower energy ions. Since D_2 weighs twice as much as H_2, experiments performed at comparable relative energies are actually performed at approximately half the laboratory energy when D_2 is used rather than H_2. If our detector excessively discriminates against ions moving slowly in the laboratory frame then the apparent threshold with D_2 will be higher than with H_2. This possibility was checked by measuring DCO^+ produced in CO^+-D_2 collisions at a variety of energies. It was observed that detector transmission dropped as the energy decreased but not nearly enough to effect the present results. It is therefore likely that our measurement is approximately correct. It should be stressed though that the apparatus used in this experiment was not designed to measure total cross sections, and it is not inconceivable that some systematic errors were still made. Thus rather large error limits are appropriate and we wish to report the measured threshold for reaction (4) to be 1.0 ± 0.3 eV.

Discussion

The two major questions which we intended to answer as we embarked on the low energy study of CO_2^+-D_2 collisions were: do DCO_2^+ distributions remain asymmetric down to low energies, and, what is the energetic threshold for DCO^+ formation? These questions were answered in the previous section: the distribution does remain asymmetric and the threshold is ~1.0 eV. We can now attempt to rationalize these observations in terms of microscopic process. It is also natural to wonder why no D_2O^+ is formed though it is an energetically favorable product.

The discussion should begin by recounting some of Schubart's conclusions.[24,25] He constructed orbital correlation diagrams for C_s approaches of CO_2^+ and H_2 leading to the $H_2CO_2^+$ intermediate and then both HCO_2^+ and HCO^+ products. Also a C_{2v} orbital correlation diagram leading to H_2O^+ + CO products was made. It was seen in each case that the ground state electronic configuration of the products could be formed assuming that certain crossings were avoided. Schubart noted that the most important avoided crossing probably arose in the formation of the $H_2CO_2^+$ intermediate in C_s symmetry. The two interacting orbitals are the 7a' and 11a'; the 7a' orbital is a bonding CH σ orbital in the formic acid cation while the 11a' is an antibonding OH σ^* orbital. These orbitals diabatically correlate to the unoccupied $2\pi^*_u$ orbital of CO_2^+ and the $H_2 1\sigma_g$ orbital respectively. Since the H_2 orbital lies lower in energy than this CO_2^+ orbital, as the reactants approach, a crossing will be

attempted, but avoided. This situation might lead one to expect that a potential energy barrier exists in the entrance channel.

The problem is actually quite similar to the case of H_2 adding to ethylene. In this well-known reaction, symmetry restrictions are quite severe, and the addition is forbidden for ground state reactants. Using CO_2^+ rather than C_2H_4 lowers the symmetry so that the reaction is not strictly forbidden; however, the nodal properties of the orbitals are the same in both cases, and hence a potential energy barrier may be present.

Using their data Mahan and Schubart[24] were able to infer that the barrier is less than 1 eV high. This conclusion was based on the fact that they could observed DCO^+ down to ~1 eV and the symmetric distributions indicated that the DCO^+ was formed from the decay of the complex. It is implicit in this argument that the height of the barrier is equal to the threshold for DCO^+ formation. We indeed measured this value to be 1 eV; however, we have some evidence that suggests that the complex is formed below this energy. This evidence comes in the form of our low energy DCO_2^+ results. Mahan and Schubart had suggested that in the 2-3 eV energy range DCO_2^+ was formed both by a direct mechanism and by a complex mechanism; DCO^+ resulted only from complex decomposition. The fact that DCO^+ was not seen at thermal energies indicated a barrier to complex formation though DCO_2^+ could be produced at the same energy by a direct mechanism. If this model is accurate, then our DCO_2^+ distributions measured below the energetic threshold for DCO^+ formation should show no contribution from long-

lived complex decay. However, our maps at 0.69 and 0.27 eV (Figs. 2 and 3) do retain symmetry in the low intensity contours which is highly suggestive of the fact that the complex channel is still operative. This is seen even more dramatically by comparing Figs. 4a and 5b. In Fig. 4a, at 1.55 eV, direct processes are dominating, and the contribution from the complex-decay channel is quite small. In Fig. 5b though, the distribution, while still forward peaked, is really much more symmetric. Some of this increased symmetry is no doubt attributable to the greater importance of beam width in the latter experiment, but it appears, that if anything, complex formation is more important at 0.27 eV than 1.55 eV. This is, of course, what one expects for most reactive systems, since a complex containing less energy will live longer, but it indicates that any barrier to formic acid cation formation is lower than 0.27 eV. One is then left with the conclusion that the barrier to DCO^+ formation occurs in the exit channel. Such a barrier, if it does exist, is not predicted by the orbital correlation diagram.[25]

There are other reasons to believe that the barrier to DCO^+ formation is in the exit channel. It was pointed out by Mahan and Schubart[24] that the most logical explanation for the observed DCO_2^+ distributions was that direct interactions could occur by moving on the lowest potential energy surface but with intermediate geometries far removed from the equilibrium $D_2CO_2^+$ geometry. Trajectories such as these do not sample the deep well and hence an asymmetric distribution should result. This argument becomes less tenable at lower collision energies.

energies. When the reactants approach each other slowly they are more easily diverted by weak chemical forces, and if there exists a low-energy path to the deep well they should find it. It seems likely that a low-energy path would be present, as the system geometry has a large number of degrees of freedom, and a barrier, if it exists at all, would affect only certain approaches. This argument predicts that complex formation becomes more important at lower energies which is what we observe with DCO_2^+. The complex could also decompose to DCO^+ + OD, but since this channel is not seen below 1 eV, a barrier in the exit channel must be present

Another energetically favorable decomposition channel is the one which gives D_2O^+ + CO. As was indicated in Table 1, these products are 0.71 eV below the reactants; however, we were unable to observe this reaction throughout the energy range studied. Also, as previously mentioned, these products do not appear at thermal energy,[16,17] nor at energies ranging up to 15 eV.[25] The reasons for this were considered briefly by Schubart[25] who gave a simple C_{2v} orbital correlation diagram connecting reactants with products but ignoring the intermediate. He concluded that the reaction was unfavorable because it involved an avoided crossing between the $1\sigma_g(H_2)$ - $4a^*_1(H_2O)$ and $4\sigma^*_u(CO_2)$ - $3a_1(H_2O)$ orbitals. These orbitals are spatially quite far apart and hence likely to be poorly coupled. If diabatic behavior dominates, a highly excited form of H_2O^+ would result which might be subject to predissociation. This argument can be used to explain why, even if steric factors are neglected, the production of H_2O^+ by a direct interaction is unfavorable.

It is perhaps more pertinent for us to consider if it is also unlikely for a $D_2CO_2^+$ complex to decay into D_2O^+ and CO. Fig. 9 shows an orbital correlation diagram taking reactants through a C_s intermediate into products. Starting with ground state reactants, $CO_2^+(1\sigma_g^2 1\sigma_u^2 2\sigma_g^2 3\sigma_g^2 2\sigma_u^2 4\sigma_g^2 3\sigma_u^2 1\pi_u^4 1\pi_g^3)$ and $H_2(1\sigma_g^2)$ we see that the electronic ground state of $H_2CO_2^+(1a'^2 \ldots 8a'^2 1a''^2 9a'^2 2a''^2 10a')$ can be formed adiabatically. The avoided crossing between the 7a' and 11a' orbitals is the origin of the possible entrance channel barrier discussed by Schubart.

Tracing the electrons through to products we obtain excited H_2O^+ ($^2A_1, 1a_1^2 2a_1^2 1b_2^2 3a_1 1b_1^2$) and ground state CO. The $^2A_1$ state of H_2O is linear and lies 0.92 eV above the $^2B_1$ ground state.[29] The reaction of CO_2^+ with H_2 to form $H_2O^+(^2A_1)$ is 0.21 eV endothermic, and the avoided crossing between the 10a' and 11a' curves shown in Fig. 9 indicates that a barrier in excess of the endothermicity may exist. Perhaps more importantly though, there is a possibility that since the 10a' orbital is essentially the carbonyl O atom lone pair, it will go over to the $3a_1$, H_2O orbital with some difficulty. The large spatial separation implies that the orbitals will be poorly coupled, and hence the curves may pass very close to each other in the vicinity of their avoided crossing. In cases such as this, diabatic motion often dominates over adiabatic motion; here, diabatic motion does not lead to complex decomposition.

Also working against H_2O^+ formation are steric effects. Because the electron removed is a non-bonding one, the structure of $H_2CO_2^+$

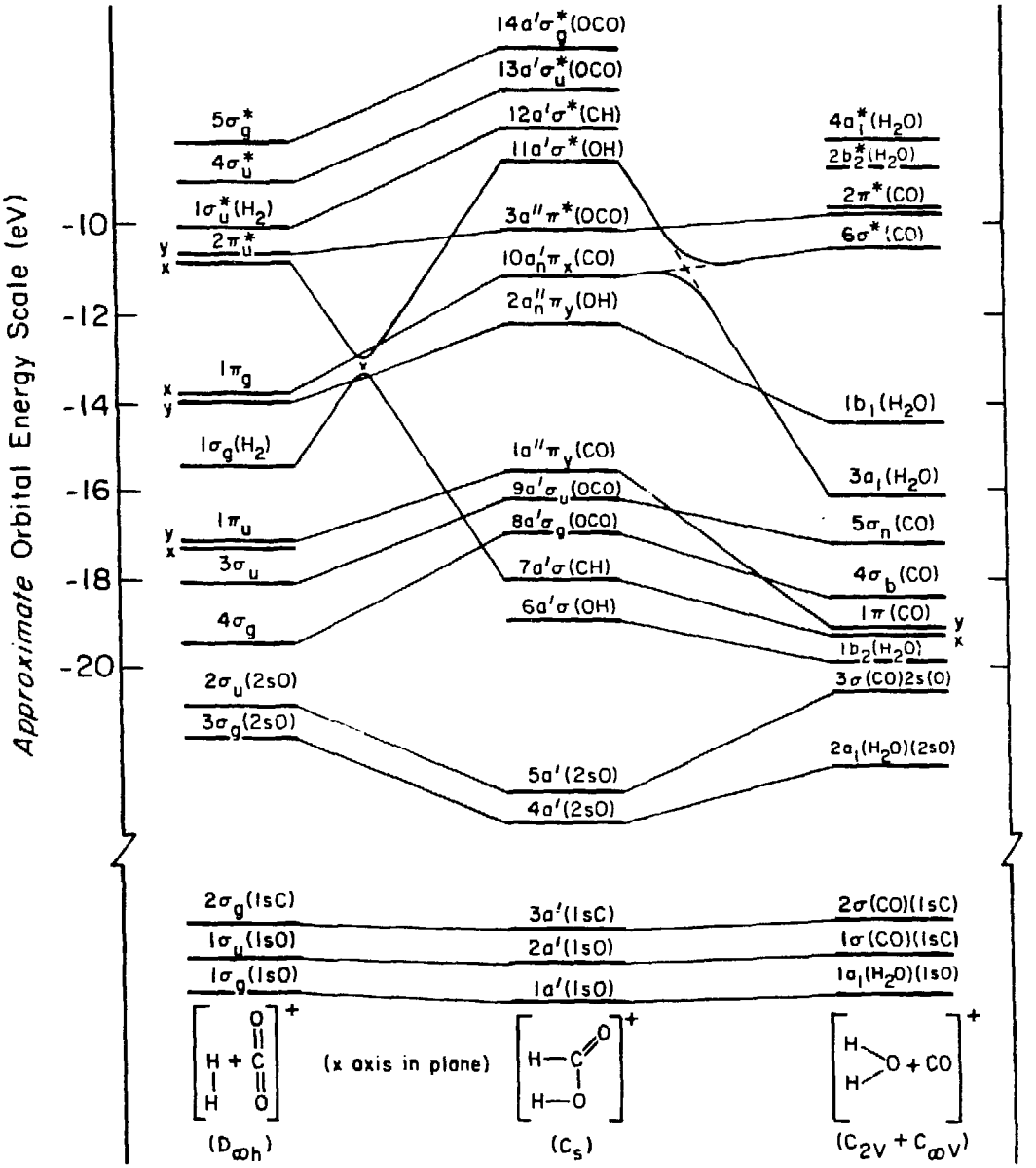

XBL 808-11288

Fig. 9. Molecular orbital correlation diagram for the formation of $[H_2O + CO]^+$ from $CO_2^+ + H_2$. This figure combines two figures from Ref. 25 and makes the correlations between intermediate and product orbitals.

at its equilibrium geometry can be taken as approximately the same as that of formic acid. This structure,[30] along with estimates of the critical configurations for dissociation to the indicated products is shown in Fig. 10. It should be stressed that the critical configurations are highly speculative although the equilibrium structures of HCO_2^+ and HCO^+ have been used.[9,15] Despite this disclaimer, it is obvious that any critical configuration leading to $H_2O^+ + CO$ necessarily involves a rather specific and perhaps unfavorable atomic arrangement. The phase space occupied by these geometries is probably rarely accessed, and hence decomposition to these products will be slow.

Complex Lifetime

In an attempt to characterize the CO_2^+-H_2 system further, we performed RRKM calculations to determine the complex lifetime with respect to the various decomposition channels. We can better visualize the problem with the aid of Fig. 11. This figure qualitatively represents a slice through the lowest potential energy surface; the surface, which is $^2A'$ in C_s symmetry, has two accessible exit channels, $HCO_2^+ + H$ and $HCO^+ + OH$. The product asymptotes are indicated on the far right and far left with the reactants in the middle and the low-lying intermediate on either side. The major point to glean from Fig. 11 other than that the lowest states are all adiabatically connected, is that once the complex is formed, there are three possible sets of products. $HCO_2^+ + H$ lies only 1.19 eV above the well, $CO_2^+ + H_2$ is 2.27 eV up

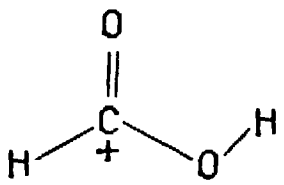

$H_2CO_2^+$

EQUILIBRIUM STRUCTURE

CRITICAL CONFIGURATION FOR BREAK-UP TO :

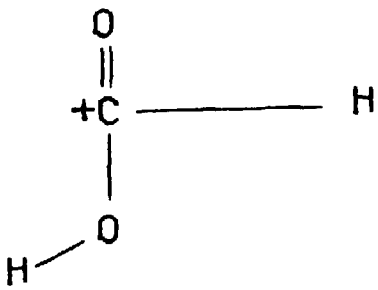

$HCO_2^+ + H$

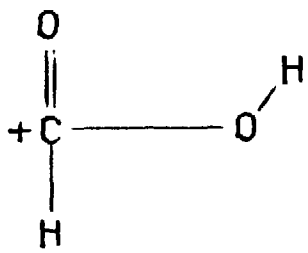

$HCO^+ + OH$

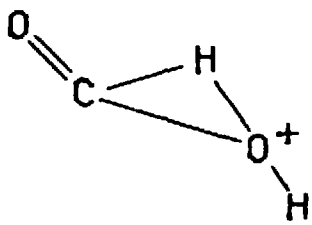

$H_2O^+ + CO$

XBL 808-11057

Fig. 10. Estimated structures for $H_2CO_2^+$ and the various critical configurations.

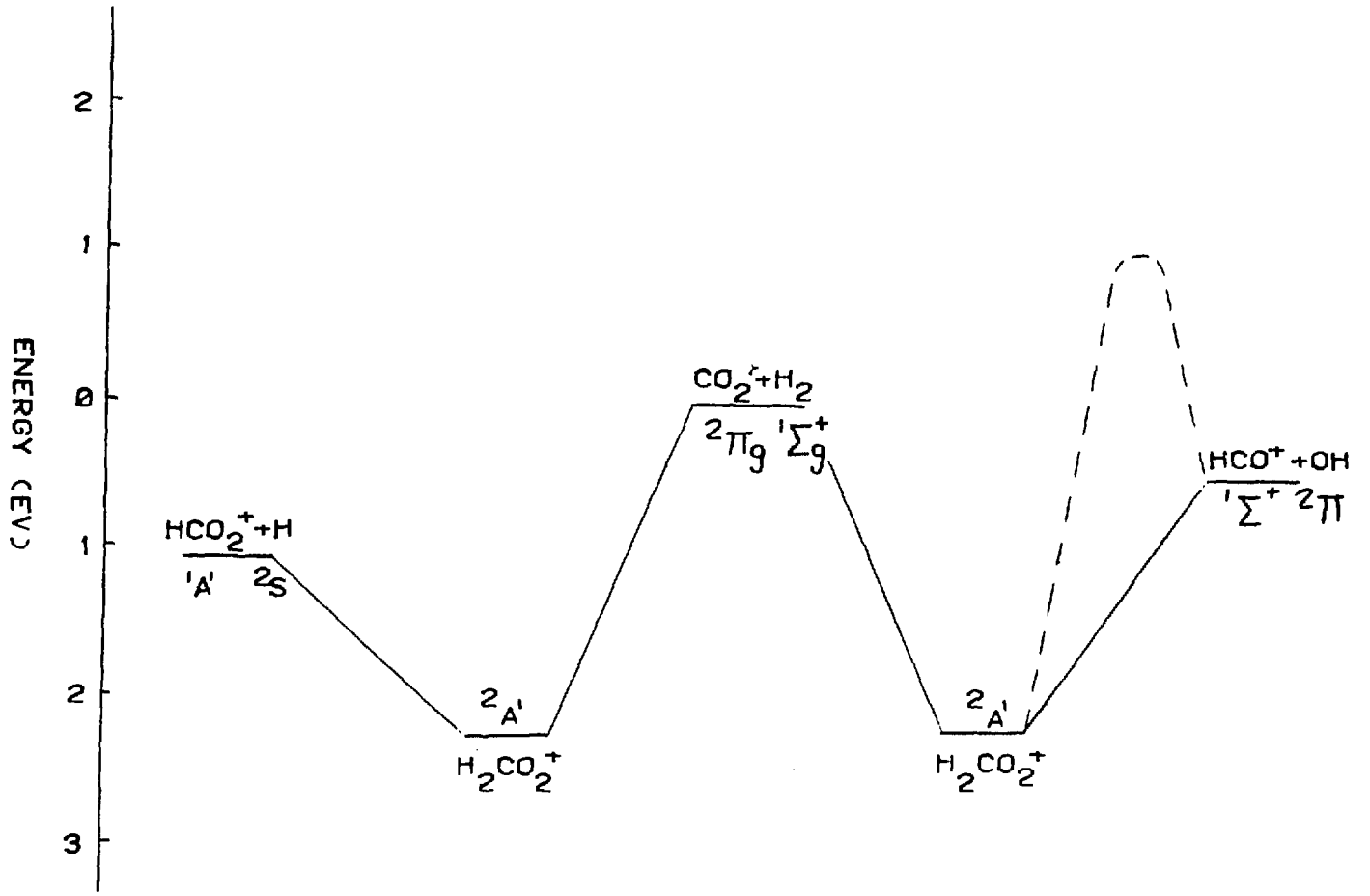

XBL 808-11056

Fig. 11. Correlation diagram in C_s symmetry for the lowest potential energy surface of the CO_2^+-H_2 system, showing two possible exit channels. The possible barrier in the HCO^+ exit channel is sketched in with a dotted line.

and HCO^+ + OH requires 1.74 or 3.3 eV depending on the existence of the proposed exit channel barrier. RRKM calculations were performed to determine the complex lifetime with respect to all of these decomposition channels. The program used is the same one discussed in Chapter 3.

The input parameters chosen for this calculation have a fairly large effect on the results; so we will describe briefly the values we used. The vibrational frequencies and moments of inertia for $H_2CO_2^+$ at its equilibrium geometry were taken to be equal to those of H_2CO_2.[31] As was mentioned previously, these species differ only by the presence of a single non-bonding electron. Two vibrational frequencies for $H_2CO_2^+$ have been determined,[14] and they are in reasonably good agreement with the corresponding frequencies in the neutral. For decomposition to HCO_2^+ + H we have assumed that the critical configuration vibrational frequencies are the same as those of $H_2CO_2^+$ except that a low frequency (100 cm^{-1}) mode has replaced a 1000 cm^{-1} vibration; this attempts to account for the weak coupling between H and HCO_2^+ at the critical configuration. For break-up to CO_2^+ + H_2 and HCO^+ + OH the frequencies used are those for the fragments[32] with the unaccounted modes arbitrarily assigned 700 cm^{-1} except for one 100 cm^{-1} mode. As in Chapter 3, we have decided to neglect rotation in our calculation, i.e. assume that the adiabatic rotational temperature is 0°. The major effect of this policy is that the calculated lifetimes reflect upper limits rather than actual lifetimes. Highly rotationally excited complexes decompose at a faster rate because the well in their effective potential is less deep than in the rotationless case.

The results of the RRKM calculation for the various decomposition channels are given in Table 2. Two calculations were performed for the HCO^+ + OH channel, one assuming no exit channel barrier and the other assuming a barrier of 1.5 eV. Both of these possibilities are indicated in Fig. 11.

Before discussing the significance of these lifetimes we should consider the uncertainty in them. Various other guesses as to the vibrational frequencies for the critical configurations gave numbers which differed from those in Table 2 by up to an order of magnitude. Of particular importance is the low frequency mode, as it strongly influences the density of states at the critical configuration. For instance, if 20 cm^{-1} rather than 100 cm^{-1} was used for the low frequency vibration, lifetimes decreased by a factor of five. Nevertheless, the values given in Table 2 represent the results obtained with our best estimates for the input parameters and as such are the preferred lifetimes.

The quantity to which we should compare these lifetimes is the rotational period of the $H_2CO_2^+$ intermediate. If the lifetime exceeds a few rotational periods, a symmetric product distribution should result. In order to determine the rotational period we need an estimate for the total angular momentum of the complex and its moments of inertia. The total angular momentum is assumed to arise entirely from the collision: $L = \mu v b$, where μ is the reduced mass, v is the

TABLE 2

Collision Energy (ev)	Complex lifetime (ps) with respect to decomposition to: HCO_2^+–H	$CO_2^+ + H_2$	$HCO^+ + OH$ with barrier	$HCO^+ + OH$ without barrier
0.09	0.33	980	∞	3.3
0.35	0.22	38	∞	1.2
0.61	0.16	7	∞	0.6
1.0	0.10	1.4	∞	0.25
1.39	–	0.5	300	0.14
1.91	–	0.2	20	–
2.95	–	0.05	1.3	–
3.86	–	0.02	0.36	–
5.16	–	0.01	0.12	–

relative velocity and b is the impact parameter. The maximum angular momentum results from the maximum impact parameter and this value can be estimated from experimental data. The cross section for DCO_2^+ production at 1 eV is 7Å^2,[26] but not all DCO_2^+ comes from long-lived complex decomposition. Using our data in this energy range we can estimate the cross section for complex formation to be about half this value. This implies a maximum impact parameter for complex formation of 1Å which for a 1 eV collision gives $L \approx 42\hbar$.

Using the approximation that the formic acid cation geometry is the same as that of the neutral, we have the result that it is a near-symmetric top with values of 6.5, 42.2, and 48.2 amu-Å^2 for it moments of inertia.[31] Obviously the rotational period of the complex will strongly depend on how the angular momentum is distributed. It was discussed by Chiang et al.[33] and mentioned in Chapter 3 that there is a tendency for the angular momentum to reside in low frequency rotational motion. This argument assumes that the three modes are in statistical equilibrium, or, to put it another way, that a rotational temperature exists. One concludes from this approach that approximately the same amount of energy resides in each mode; hence much more angular momentum resides in low frequency rotations. Placing $42\hbar$ into the low frequency rotation of $H_2CO_2^+$ and using the equation $\tau_r = 2\pi I/L$ from Chapter 3, we obtain $\tau_r = 1.4 \times 10^{-12}$ seconds. This number is roughly independent of collision energy because as the energy is raised, the cross section, and hence b_{max}, drops, but of course v increases.

Similarly, for lower collision energies b_{max} is higher but v is lower; the net effect is that the complex rotational period stays about the same.

Comparing this lifetime to the numbers in Table 2 we see that there are immediate problems. Even at the lowest collision energy considered, the complex falls apart to $HCO_2^+ + H$ in about 1/4 of a rotational period. This is not a completely unreasonable result given that this reaction is exothermic by 1.08 eV, and the well is only 1.19 eV deep with respect to these products. However, the experimental results suggest that the complex does live much longer than this. There are only two explanations for rationalizing this situation: 1) we have the reaction energetics wrong, or, 2) there is a barrier of sorts to HCO_2^+ formation. The former possibility cannot be completely dismissed as there is some uncertainty in the energetics, but it is unlikely that the error is large enough to explain the present dilemma. A problem also exists in rationalizing the experimental HCO^+ results. HCO^+ distributions are symmetric up to 4 eV, and it can be seen in Table 2 that even if the barrier is included in the exit channel it is difficult to explain a long-lived intermediate at this energy. Of course, it is much harder yet to understand this result in the absence of any barrier. If the barrier existed though, and there was no barrier to HCO_2^+ formation, virtually all the complexes would decay to $HCO_2^+ + H$ and no HCO^+ would be seen. Since experimentally HCO^+ is observed as a complex decay product, the best rationalization for the dynamics is that a barrier exists in the $HCO^+ + OH$ exit channel and

another barrier exists in the HCO_2^+ + H exit channel. The height of this latter barrier can only be guessed at but it would have to be appreciable (> 0.5 eV) to significantly effect the dynamics. However, it is certainly less than 1.35 eV; this conclusion can be drawn from our result that complex formation contributes at 0.27 eV combined with the fact that HCO_2^+ + H products lie 1.08 eV below reactants.

In any event, it is quite clear that a simple statistical approach to this problem is unable to explain the observed product distributions. This strongly suggests the presence of potential energy barriers and/or dynamical "bottlenecks" which affect complex decomposition.

Summary

We have extended the results of Mahan and Schubart on the CO_2^+-D_2 system down to lower relative collision energies. There are three exothermic reaction channels but only the most exothermic, DCO_2^+ + D, is seen below 1 eV, and this reaction proceeds by both a direct and indirect mechanism in the entire energy range studied (0.27-1.55 eV). The next most favorable product channel, H_2O^+ + CO, is not observed at all, presumably due to a potential energy barrier and possible steric hindrances. The product channel leading to HCO^+ + OH opens at 1 eV; this probably reflects another exit channel barrier. RRKM theory, app with no inclusion of barriers or bottlenecks, is unable to explain the observed product distributions. This is consistent with the notion that the potential energy surface for $H_2CO_2^+$ is rather complex and hence dynamics on it are not easily described by statistical models which neglect these complexities.

REFERENCES

1. B. H. Mahan, J. Chem. Phys. 55, 1436 (1971).

2. D. Buhl and L. E. Snyder, Nature 228, 267 (1970).

3. W. Klemperer, Nature 227, 1230 (1970).

4. V. Wahlgren, B. Liu, P. K. Pearson and H. F. Schaefer, Nature 246, 4 (1973).

5. R. C. Woods, T. A. Dixon, R. J. Saykally and P. G. Szanto, Phys. Rev. Lett. 35, 1269 (1975).

6. E. Herbst and W. Klemperer, Ap. J. 185, 505 (1973).

7. W. D. Watson, Astrophys. J. 188, 35 (1974).

8. S. Green, H. Schor, P. Siegbahn, and P. Thaddeus, Chem. Phys. 17, 479 (1976).

9. B. E. Turner, Astrophys. J. (Letters) 193, L83 (1974).
S. Green, J. A. Montgomery, and P. Thaddeus, Astrophys. J. (Letters) 193, L89 (1974).

10. A. N. Hayhurst and D. B. Kittelson, Combust. Flame 31, 37 (1978).

11. J. L. Franklin et al., NSRDS-NBS 26 (1969).

12. Lange's Handbook of Chemistry, 11th edition, ed. J. A. Dean (McGraw-Hill, N.Y.) 1973.

13. JANAF Interim Thermochemical Tables, Vol. 2 (1960).

14. D. W. Turner, C. Baker, A. D. Baker, and C. R. Brundle, Molecular Photoelectron Spectroscopy (Wiley-Interscience, N.Y.) 1970.

15. P. J. Bruna, S. D. Peyerimhoff, and R. J. Buenker, Chem. Phys. 10, 323 (1975).

16. T. F. Moran and L. Friedman, J. Chem. Phys. 42, 2391 (1965).

17. F. C. Fehsenfeld, A. L. Schmeltekopf, and E. E. Ferguson, J. Chem. Phys. 46, 2802 (1967).

18. D. L. Smith and J. H. Futrell, Int. J. Mass Spectrom. Ion Phys. 10, 405 (1972).

19. T. McAllister and P. Pitman, Int. J. Mass Spectrom. Ion Phys. 19, 423 (1976).

20. A. G. Harrison and J. H. Myher, J. Chem. Phys. 46, 3276 (1967).

21. K. R. Ryan, J. Chem. Phys. 61, 1559 (1974).

22. S. F. Kasper and J. L. Franklin, J. Chem. Phys. 56, 1156 (1972).

23. D. L. Albritton, in Interactions Between Ions and Molecules, Ed. P. Ausloos (Plenum Press, N.Y.) 1975, pp. 119-142.

24. B. H. Mahan and P. J. Schubart, J. Chem. Phys. 66, 3155 (1977).

25. P. J. Schubart, Ph.D. Thesis, LBL Report LBL-3154 (1974).

26. H. Tochihara and Y. Murata, Bull. Chem. Soc. Jap. 51, 1609 (1978).

27. This fact was discussed in Chap. 3.

28. DCO^+ appearing at the same laboratory velocity as DCO_2^+ will be seen at $m_{DCO^+}/m_{DCO^+} = 30/46$ of the DCO_2^+ laboratory energy. Detector focusing does not vary much over a few eV range, however, DCO^+ appears outside of the energy range in which focusing is optimized (beam energy). In practice, new focusing conditions were determined but of the several approaches used, none were very satisfactory.

29. W. Meyer, Int. J. Quantum Chem. 5, 341 (1971).

30. J. Bellet, A. Deldalle, C. Samson, G. Steenbeckeliers, and R. Wertheimer, J. Mol. Struct. 9, 65 (1971).

31. G. Herzberg, Electronic Spectra and Electronic Structure of Polyatomic Molecules (Van Nostrand, Princeton, N.J.) 1966.

32. Actually for CO_2^+ and HCO^+ the CO_2 and HCO frequencies are used.

33. M. H. Chiang, E. A. Gislason, B. H. Mahan, C. W. Tsao, and A. S. Werner, J. Phys. Chem. 75, 1426 (1971).

CHAPTER 6. ION BEAM STATE DISTRIBUTIONS

When the study of ion-molecule reactions was young, experimenters could not afford to worry about the internal state distribution of the reactants. The problems associated with determining gross properties of the collision partners, such as mass and velocity, were more important to solve. For this reason, the literature is full of results obtained using reactants with an unknown initial electronic state distribution. Such studies have been important to those engaged in modeling chemical reactions, but more detailed experimental information concerning the reactivity of each individual electronic state is necessary before experiment and theory can be meaningfully compared. This fact becomes clear when one realizes that, for example, the chemistry of $N^+(^1D)$ probably is closer to that of $F^+(^1D)$ than it is to $N^+(^3P)$. When the electronic structure of a species is altered, it becomes a completely different entity, and only the nucleus and to a lesser extent, core electrons, remain unchanged. Since it is the outer electrons which determine the chemistry of the species, it is not unreasonable that reactions of excited states may be very different from those of the ground state. An illustrative example is:

$$O^+ + N_2 \rightarrow N_2^+(B^2\,\Sigma_u^+) + O \qquad (1)$$

for which the cross section is 100 times greater when $O^+(^2P)$ is used rather than $O^+(^4S)$ (at a laboratory energy of 1000 eV)[1].

Methods for Metastable Detection

In recent years, attempts to at least characterize if not control the electronic state distribution of the reactant ions have been made. One of the most obvious methods for detecting the presence of metastable[2] electronic states is to try to induce a reaction which is not energetically allowed with ground state reactants. This approach is conceptually very simple but in general will not quantitatively reveal the percentage of metastable present. Also, if the reaction to be monitored does not occur, one is not guaranteed that the excited state is absent because the reaction may have a small cross section for other reasons. Nevertheless, this method has been put to good use by Jones et al.[3] who unambiguously verified the presence of $Cl^+(^1S)$ in a Cl^+ beam by studying the energetic threshold of the reaction $Cl^+(CO,O)CCl^+$.

Another dynamical approach to elucidating state distributions is the inelastic scattering technique of Moore.[4] In this method one collides a beam of fast (1-5 keV) ions with a gas, and energy analyzes the beam as it emerges. Since most ions are not involved in collisions with the scattering gas, the energy distribution has a large peak at the initial ion energy, but often small satellite peaks are visible. These peaks result from either inelastic or superelastic collisions. Since the energy levels of the collision partners are known, it is a simple matter to assign the transitions, and see if any originate with metastable reactants.

[illegible] to determine quantitatively the composition of an [illegible] assuming a Boltzmann distribution within the electronic manifold of states and applying the principle of microscopic reversibility to relate certain inelastic cross sections. The former assumption, while perhaps applicable in Moore's duoplasmatron ion source, will not be good in general. Nevertheless, the results obtained in this study are in satisfactory agreement with those found using other methods. It should be mentioned that this technique has not seen widespread use.

A third approach to detecting excited ions in a beam, and the most popular, is the beam attenuation method of Turner, Rutherford, and Compton.[5] In this technique, a beam of mass selected ions is directed through a scattering cell containing a gas. The fraction of transmitted ions (I/I_0) is measured as a function of attenuating gas pressure and an analogue of Beer's Law is applied. If the primary ion beam contains a single electronic state, a semi-logarithmic plot of I/I_0 vs. attenuating gas pressure should yield a straight line. The slope of this line is proportional to the attenuation cross section. If two electronic states are present, and the states have different attenuation cross sections, the semi-logarithmic plot can be decomposed into the sum of two lines having different slopes. This situation is expressed mathematically by

$$I/I_0 = (1-f)\exp(-n\sigma_1 \ell) + f \exp(-n\sigma_2 \ell), \qquad (2)$$

where f is the fraction of type 2 ions in the beam, n is the attenuating gas number density, σ_j is the attenuation cross section for type j ions, and ℓ is the path length. The y-intercepts of these lines give the fraction of the corresponding electronic state in the beam.

Rather precise measurement of the scattering gas pressure and the transmitted beam intensity are required to obtain data of sufficient quality to resolve the subtle curvature which indicates multiple states. This is especially true if there is not a large difference in the attenuation cross sections of the two states present. Data are seldom good enough to justify more than a double exponential fit, but triple exponential fits, indicating three electronic states, have been made.[1]

A final technique for detecting the presence of excited species in an ion beam involves the measurement of chemiluminescence from beam-gas collisions. This method relies on the fact that the cross section for forming products in emitting states depends on the electronic states of the reactants. As early as 1970 it was suggested that more light was produced in collisions of excited states of Ar^+ and N_2^+ with C_2H_2 than collisions involving ground state ions. As will be discussed later, the primary emitters in such collisions are neutral and ionic fragments of C_2H_2. Ottinger and collaborators have extended the technique and clearly demonstrated that luminescent cross sections vary sharply with reactant electronic state.[1,7] An advantage of this method is that it is easy experimentally to add a

photomultiplier tube and count photons. No dispersion of the luminescence is necessary, although it may, of course, be done. A disadvantage is that quantitative results are difficult to obtain because the chemiluminescent cross sections of the individual electronic states are largely unknown.

Charge Transfer

The microscopic processes which lead to the removal of an ion in a beam attentuation experiment are charge transfer and large angle scattering. If the charge transfer reaction has an appreciable cross section, it should dominate. Similarly, charge transfer yielding products which readily fluoresce (reaction (1) is an example), is usually responsible for most of the light seen in total luminescence experiments. For these reasons, our interpretation of attenuation and luminescence experiments relies on our ability to predict state-to-state charge transfer cross sections; hence, a discussion concerning charge transfer is appropriate.

There is a wealth of information available on charge transfer cross sections measured at high energies, but much less work has been done at laboratory energies below 1 keV. In the high energy regime, charge transfer is for the most part "non-chemical" in nature. By this we mean, cross sections and product distributions are relatively independent of the initial projectile and generally resemble those obtained using high energy electrons. Vertical transitions dominate, which implies that the product distribution is governed by the

Franck-Condon factors between the ground state of the neutral and the states of the ion. Some information as to the nature of the reactant ion can be gleaned using the Massey or adiabatic criterion. The Massey criterion predicts that for atoms, the energy at which the charge transfer cross section attains a maximum is given by[8]

$$D = m \frac{a\Delta E}{0.57}^{2} \tag{3}$$

where m is the mass of the ion in amu, ΔE is the difference in ionization potentials in eV, and a is the interaction path length. It has been found empirically that a is best approximated by 7Å. Since ΔE will vary depending on the electronic state of the reactant ion, one can sometimes gain information as to which states are present by studying the charge transfer cross section as a function of projectile kinetic energy.

At lower projectile energies, charge transfer cross sections are noticeably dependent on the chemical nature of the reactants. Vertical transitions still dominate, but the importance of energy resonance becomes more pronounced. In fact, the best indicator as to whether a particular reaction will be favorable is the presence of a peak in the photoelectron spectrum of the neutral reactant at the recombination energy of the ion. This situation implies that a state which has favorable vibrational overlap with the neutral reactant is located such that near-resonant charge transfer can take place. It

has been observed that spin is generally conserved in these reactions. Hence, a collision between two singlets will not give a quartet product even if the reaction is otherwise favorable.

It is interesting to compare charge transfer reactions to other ion-molecule reactions. A typical ion-molecule reaction is well described by the Langevin polarization model while charge transfer is not. Thermal near-resonant charge exchange is usually a factor of 2 or 3 slower than the Langevin rate, and the cross section does not fall as $E^{-1/2}$ as predicted by the polarization model.[9] This is because charge transfer is a curve crossing phenomenon, and the actual electron transfer takes place at about the same distance regardless of the energy. The distance corresponds to the point where the $X^+ + Y$ potential energy curve crosses (or comes near) the $X + Y^+$ curve. Since the electron is exchanged at roughly a constant distance, the cross section for the process is not strongly dependent on the collision energy; this has been experimentally verified for most systems at moderate energies. An additional feature of charge transfer reactions is that the separation at which the curves cross may be quite large (several angstroms). Hence, the electron can be exchanged with negligible momentum transfer between the collision partners. Recent crossed beam experiments have verified this assertion for processes with large cross sections.[10,11]

As mentioned earlier, the total luminescence experiments used to detect metastable states also rely heavily on charge exchange reactions This is because charge transfer usually has a higher cross section than

other processes which can lead to luminescence. In fact, in very favorable cases such as

$$He_2^+ + N_2 \rightarrow N_2^+ (B^2\Sigma_u^+) + 2He, \tag{4}$$

the luminescence cross section is so large, $\sigma > 10\text{Å}^2$,[12,13] that the reaction has been used to produce lasing on several lines in the near uv;[14] the lines belong to the $N_2^+(B \rightarrow X)$ system. However, there are other processes in addition to simple charge exchange which can lead to chemiluminescence. They are excitation, e.g.

$$N^+ + NO \rightarrow N^+ + NO^*, \tag{5}$$

reaction, e.g.

$$N^+ + NO \rightarrow N_2^{+*} + O\ , \tag{6}$$

and dissociative charge transfer, e.g.

$$Ne^+ + CO \rightarrow Ne + C^{+*} + O. \tag{7}$$

As discussed by Brandt et al.,[15] these reactions generally have low cross sections and will be unimportant for collision partners with a favorable charge transfer pathway.

Experimental

To investigate the state distribution of our ion beams, the beam attenuation and total luminescence methods were used. The apparatus employed to perform the attenuations is quite similar to the one described in Chapter 2 except that it contains a scattering cell to introduce the neutral reactant and generally works at higher ion energies. It has been used previously to study the state distributions of O_2^+ and O^+ ion beams from various sources.[16,20] An ion collector which has an acceptance angle of ±45° is located inside the scattering cell and ion current is measured using a Keithley 417 high speed picoammeter. The entrance aperture of the scattering cell is a 2 x 2 mm square, and there is also a circular rear aperture of 2 mm diameter. The main chamber is pumped by two 6" liquid nitrogen trapped oil diffusion pumps which allow the cell pressure to exceed the background pressure by about three orders of magnitude. The attenuating gas is introduced to the cell through a Granville-Phillips variable leak valve and cell pressure is monitored indirectly by a capacitance manometer (MKS Baratron type 144). The pressure, relative to the main chamber pressure which is assumed to be zero, is measured directly at a location remote from the scattering cell. This location is connected to the cell with metal tubes whose conductance may be calculated using standard techniques.[17] The formula obtained for the cell pressure (p_{cell}) given the measured pressure (p) in microns is[18]:

$$p_{cell} = 0.289p + .0006303p^2. \qquad (11)$$

Since precise knowledge of the cell pressure is essential to the accurate interpretation of the results of beam attentuation experiments, the pressure is further corrected in a way which will be described later.

An attentuation experiment is performed in the following manner. A mass analyzed beam of ions at a known energy (typically 100 eV) is directed into the scattering cell and the total ion current reaching the back of the cell is monitored. After the beam has stabilized, data taking commences by establishing a baseline (I_0) and zero; the baseline corresponds to the unattenuated beam current and zero is obtained mechanically with the picoammeter. Then, by leaking gas into the cell and simultaneously measuring pressure and transmitted beam current, data points are taken. After every fourth point, the valve to the cell is closed and in a few seconds, when the residual gas has left, the unattenuated beam current is again measured; this helps account for small amounts of beam drift. Approximately 25 points, ranging from about 1 to 95% attenuation constitute a full experiment. It is also desirable to leak in an excess of attenuating gas so that a "minimum" beam current can be measured. More discussion of this minimum current, which is generally negative, is given later.

In practice the transmitted beam intensity and pressure are measured to three or four place accuracy using digital voltmeters which monitor the output of the picoammeter and manometer. It is also helpful to check for instability or abrupt intensity changes by plotting the output of the picoammeter on a strip-chart recorder.

Once data taking begins, an experiment can be completed in 10 to 15 minutes.

There are other points which should be mentioned that are important to the successful completion of an attentuation experiment. Beam stability is essential; generally short-term intensity fluctuations should be less than 0.1%, though slow, steady intensity drifts may be acceptable. The capacitance manometer should, of course be, accurately zeroed and tuned. It is also advisable to float the ion collector in the scattering cell at a modest positive voltage. This is done to prevent the colection of slow ions. As stated earlier, charge exchange often takes place with negligible momentum transfer and, hence, the product ions will be at near-thermal energy. Since in an attenuation experiment we desire that charge transfer events remove ions from the beam, the slow ions should be rejected by the ion collector. We do this by floating the collector at +8 V with a battery.

Because the important quantity in these experiments is the fraction of ions transmitted, a large beam flux is unnecessary; excellent results have been obtained with currents of less than 10^{-12}A.

For the total luminescence experiments reported in this thesis, the apparatus described in Chapter 2 was used with only minor modifications. The modifications consisted of adding a very rudimentary scattering cell, removing the catcher chamber, adding a window flange, and placing a photomultiplier tube against the window. The scattering cell used was a 1" length of 1" I.D. thin walled brass tube, with a mirror glued on one end and a glass window on the other. The inner glass surfaces were covered with a high-transparency steel mesh to

ensure that the collision center was at ground potential. Ions entered and exited the cell through .187" dia. circular apertures; the cell was aligned manually with the aid of a cathetometer. Ion current was monitored using a broad ion collector placed after the cell. The neutral reactant was admitted via a stainless steel tube hard-soldered onto the bottom of the cell; the flow rate was controlled by a Granville-Phillips variable leak valve. Light exiting the cell was gathered by a short focal length lens and collimated by a second lens. The RCA 8575 photomultiplier tube used to measure emission was located ~12" from the collision center; provisions were made so that wavelength filters could be added between the photomultiplier tube and scattering cell. The spectral range covered by the optical detection system was primarily determined by the response of the photocathode in the photomultiplier tube. This curve is peaked near 400 nm where it is nearly 100% efficient; it falls to 50% at 290 and 520 nm and 10% at 260 and 600 nm. The low wavelength limit of the detection system is actually determined by the transmission of the glass windows and lenses which pass little radiation below 330 nm.[19] The spectral range covered by the detection system is nearly ideal for our purposes as the emission spectra of many ions lie close to 400 nm.

Due to the inherent sensitivity of modern photomultipliers, total luminescence experiments are quite easy to perform. Signal levels were so high that it was unnecessary to cool the photomultiplier tube; in favorable reactive systems the luminescence could be seen with one's eye. The tube was typically operated at 2200 V, and the output pulses were fed to a Lecroy 333 amplifier and then to a Lecroy 321B

discriminator. The logic pulses output by the discriminator were counted by a Harshaw NS-30 scaler; if counting rates exceeded the capabilities of the system, the tube voltage was decreased. The background counting rate from the uncooled tube was about 3000 cps.

It should be noted that the luminescence intensities measured with this system do not represent or are even proportional to the actual cross section for the formation of the emitting state. This is because of the non-uniform wavelength sensitivity of the optical detection system and the inabililty to accurately measure the pressure of the gas in the scattering cell. Since the pressure could not be readily measured, data were taken at the pressure which was found empirically to give the most light. Figure 1 shows, for a typical system, how the light intensity varies as a function of the percentage of beam transmission. As beam transmission decreases, light intensity initially increases as more of the ions have a chance to collide with the neutral and produce emitting species. A point is reached, however, where the curve turns downward, presumably because the luminescence is produced prior to the center of the cell and is not efficiently collected. Fortunately, in the vicinity of the apex, the curve is rather flat which indicates that reproducibility should not be a severe problem as long as data are taken at roughly the same beam transmittances.

The effectiveness of the luminescence technique was checked by monitoring total emission produced in collisions between O^+ and CO, N_2O, and H_2S. O^+ formed in a microwave discharge through O_2 is expected to be almost exclusively in the ground ^4S state[20],

Fig. 1. Plot of the light intensity (in photons x 10^3/sec) produced by colliding a 7 x 10^{-9} A beam of 32 eV Ne^+ ions with C_2H_2 at various scattering cell pressures. The pressure was not measured directly but is given implicitly by the percentage of ions transmitted by the cell.

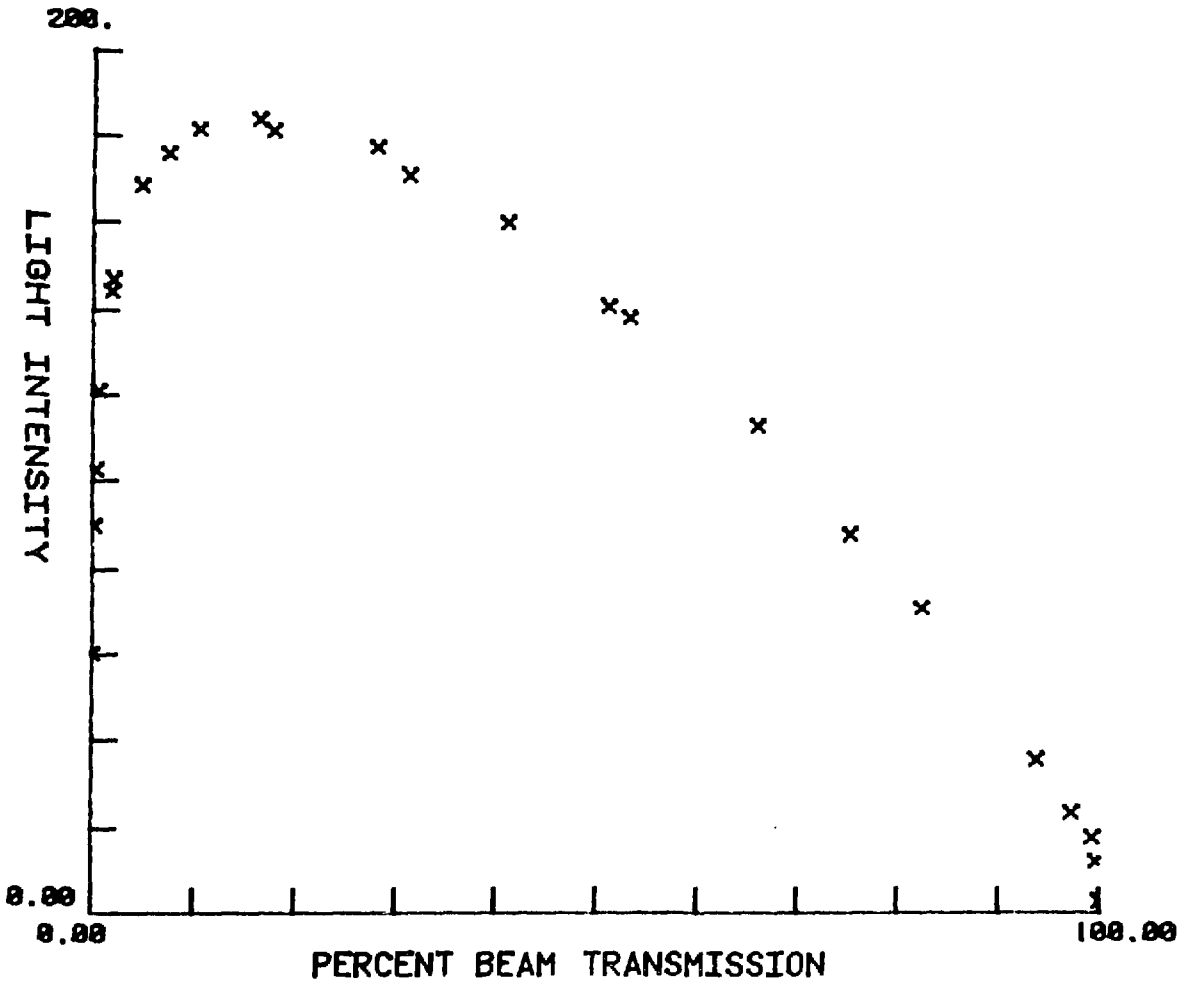

XBL 807-10761

Fig. 1

while electron impact will give significant amounts of the metastable ^2D and ^2P states.[5] One would expect that collisions of $O^+(^2D)$ with CO would produce large amounts of light because of the favorability of

$$O^+(^2D) + CO \rightarrow O(^3P) + CO^+(A^2\Pi_{v=2}) \quad \Delta E = -0.02 \text{ eV}, \tag{12}$$

and the fact that $CO^+(A \rightarrow X)$ emission is strong in the blue. A similar case exists with N_2O for which $O^+(^2D)$ has a near resonant charge transfer channel to low vibrational states of $N_2O^+(A)$. The subsequent $N_2O^+(A \rightarrow X)$ emission which is centered in the near uv[21] should be easily seen by our optical detection system. Charge transfer to the A states of CO^+ and N_2O^+ using $O^+(^4S)$ is much less likely as both proceses are 2.8 eV endothermic.

When H_2S is used as a collision partner, the situation is reversed because the energetics of the reactions

$$O^+(^4S) + H_2S \rightarrow O(^3P) + H_2S^+(A\ ^2A_1) \quad \Delta E = -0.35 \text{ eV} \tag{13}$$

$$O^+(^2D) + H_2S \rightarrow O(^3P) + H_2S^+(A\ ^2A_1) \quad \Delta E = -3.6 \text{ eV} \tag{14}$$

imply that the cross section for $H_2S^+(A)$ formation should be larger using $O^+(^4S)$ than $O^+(^2D)$. The product A state emits to $H_2S^+(X)$ giving visible light.[22]

In Fig. 2 we see the results of total luminescence experiments comcomparing electron impact and microwave discharge produced O^+ in CO, N_2O and H_2S. The precision of these data is not great as indicated by the somewhat random variation in emission intensity with collision energy. Nevertheless, the fact that significantly more light is seen in the collision of electron impact produced O^+ with CO and N_2O, and less in collisions with H_2S, is consistent with our expectation that this beam contains large amounts of $O^+(^2D)$. Hence the validity of the total luminescence approach is confirmed.

Control of State Distributions

Before making the final, irreversible leap into the experimental results, a short digression is in order. In previous sections it has been shown how to detect and/or measure excited species in an ion beam, but no discussion has been given as to how to influence the state distribution in the beam. It is of little consolation to the reaction dynamicist to know that his reactant beam contains 50% metastables if he is unable to decipher the different dynamics of the two (or more) states. He would be much better off to produce a beam which was exclusively one state, and hence, have no ambiguity in interpreting results. The modern physical chemist's approach to this problem would be to use a laser to pump ions into the state of interest or out of the state contaminating the results. Unfortunately, for most ions which have been studied this is impractical due to the lack of tunable laser systems in the uv. It is also impractical to excite a

Fig. 2. Plot of total luminescence in thousands of photons/sec/nA of beam current vs lab kinetic energy for O^+ produced by electron impact on CO_2(x) and microwave discharge (circles) through O_2 using CO, N_2O, and H_2S as collision partners.

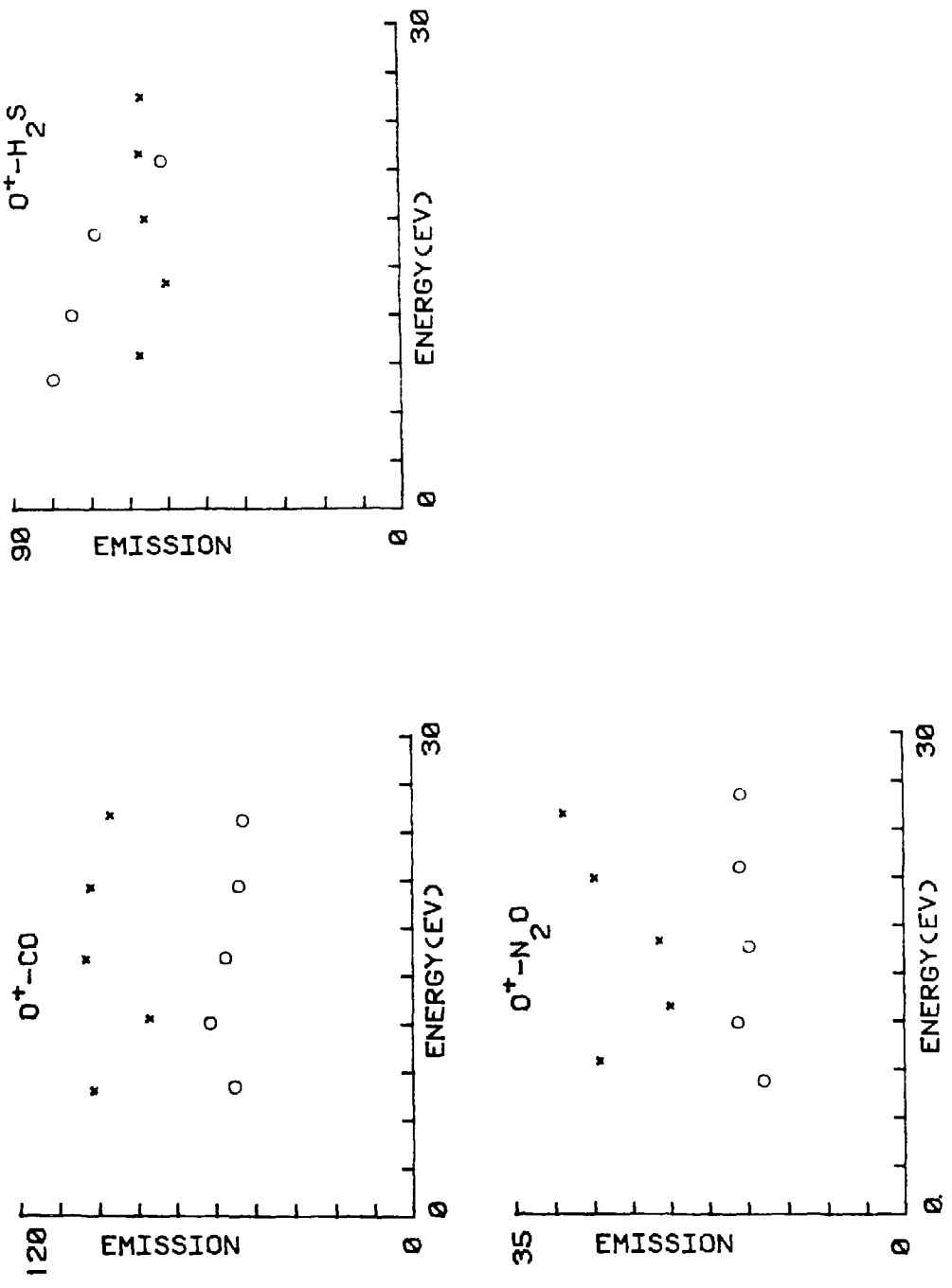

XBL 807-10772

Fig. 2

metastable level directly because of the low oscillator strength. A variation of this technique has been successfully used by Carrington and co-workers to obtain spectroscopic information about ions.[23] By Doppler-tuning a fast beam of CO^+ ions into resonance with a coaxial Ar^+ laser beam, absorption could be detected by monitoring changes in the charge transfer cross section of CO^+ with various collision gases. It should be noted though that the state pumped in this study is quite short-lived ($\tau(CO^+A\ ^2\Pi) \approx 2 \times 10^{-6}$s), and even if dynamical studies could be performed, their importance would be diminished by the scarcity of this species in nature.

Although there exists much interest in the dynamics of excited states,[24] we should first direct our attention to reactions involving the ground electronic state. The production of a beam of pure ground state ions is no easy matter, however. The original, and still widely-employed method for ion production involves electron bombardment of a source gas. High energy electrons (> 50 eV) are usually required if one is to obtain a suitably intense beam, and there is plenty of energy available to yield ions in excited states. One interesting approach to this problem is the storage ion source of Teloy and Gerlich.[25] Here ions are formed by electron impact and stored with the aid of an inhomogeneous rf field; they undergo many collisions prior to leaving the source. The many collisions allow for the relaxation of metastable electronic states.

Another approach used for the production of more purely ground state beams is to form the ions in gaseous discharges. Because discharges require moderate (~.01-10 torr) pressures to operate, high energy electrons become rapidly thermalized and any metastable species formed are subject to numerous collisions and may be quenched. Even so, some discharge ion sources such as the commercially available "duoplasmatron" and "Colutron" are quite hot and are known to produce non-negligible amounts of excited ions. It is somewhat curious that the DC discharge source described in Chapter 2 was patterned after the Colutron, but in the mode in which it is operated, produces predominately ground state ions. Probably the most successful approach to producing nearly pure ground state beams involves the use of a microwave discharge source. This source, which has been in use in our laboratory for over ten years, is also described in Chapter 2. The low electron temperature within the microwave discharge is not conducive toward the production of excited state ions; it is puzzling that other groups have not employed similar sources.

Other ideas for the production of ground state ions have been implemented by Koski's group. Beam attenuation experiments showed that the addition of a small amount of a paramagnetic gas such as NO to their electron impact source would significantly quench excited metastable states.[26,27] This, presumably, is due to the unpaired electron on NO which is easily exchanged upor collision, allowing rapid interconversion between states in different spin manifolds. This technique was not successful in quenching $B^+(^3P)$; so, a different approach was tried.

It was found that while electron bombardment of BF_3 produced a mixture of ^1S and ^3P states, BI_3 gave only the ground, ^1S state.[28] There is no doubt that a certain amount of luck is necessary in finding a system which upon ionization gives a single electronic state, but the work may be worth the effort.

N^+ State Distribution

Previous workers have put considerable effort into understanding the states of N^+ produced upon ionization, and we can profit from their discoveries. In 1963, McGowan and Kerwin[29] investigated the mass spectrum of $^{29}N_2$ as a function of electron energy. It was their intention to find out what fraction of $\frac{m}{e} = 14$ seen in the mass spectrum of $^{28}N_2$ actually was N_2^{++} rather than N^+. Although their results showed that the fraction had a strong dependence on electron energy and source pressure, it was found that N_2^{++} could amount to 10% of an $\frac{m}{e} = 14$ beam when the ions were produced by bombarding N_2 with 180 eV electrons.

Because of this demonstrated contamination in an N^+ beam, a number of subsequent workers have studied the state distribution under conditions which precluded the formation of N_2^{++}. This is fairly easily done as the appearance potential for N_2^{++} is 42.7 eV while $N^+(^3P)$ from N_2 requires only 24.3 eV. The first three excited states of N^+ are all metastable; the ^1D, ^1S, and ^5S states lie 1.90, 4.05, and 5.85 eV respectively above the ^3P state.[30] The radiative lifetimes as obtained from the estimated Einstein A coefficients are 300 seconds

for $N^+(^1D)$ and 0.9 seconds for $N^+(^1S)$.[31] Moore, using the inelastic scattering technique described earlier in this chapter, found that his duoplasmatron source produced 87.5% $N^+(^3P)$, 12% $N^+(^1D)$, and 0.5% $N^+(^1S)$.[4] No $N^+(^5S)$ was observed. Similarly, Rutherford and Vroom,[32] who studied N^+ produced by the impact of 24 to 40 eV electrons on N_2, concluded that a maximum of 15% excited state was formed. The threshold for the appearance of the new state was 26.2 eV which corresponds to the minimum energy for $N^+(^1D)$ formation. Above 26.2 eV electron energy, the fraction of metastable rapidly increased to ~15% at 30 eV but then stayed constant up to 40 eV. No obvious breaks were seen at the threshold for ^1S or ^5S formation. Moran and Wilcox[33] also concluded from their charge transfer experiments that the N^+ state distribution did not change about 30 eV, and in fact stays constant up to 60 eV. It should be mentioned though that the electron energy resolution in these experiments is probably not great enough to conclude with absolute certainty that there are no additional thresholds which might correspond to ^1S or ^5S production.

Kusunoki and Ottinger[34] studied the emission from collisions of N^+ with small hydrocarbons and included data on light intensity as a function of source voltage. They found that emission from $NH(A\ ^3\Pi)$ decreased by 20% as the voltage between cathode and anode in their Colutron source was increased from 40 to 85 V. It is unlikely that N_2^{++} is a significant contaminant under these conditions; so it was concluded that the $N^+(^1D,^1S)$ concentration noticeably increased

as the source voltage was raised. Previous work had shown that $N_2^+(B \rightarrow X)$ emission observed following N^+-N_2 collisions, was constant in the 20-40 V source voltage range indicating that a pure ground state beam is formed under these conditions. For this system though, emission did increase above 40 V and was attributed to a small amount of N_2^{++} in the beam.

Tichy et al.[31] have also reported on the metastable states of N^+ produced by electron impact. To prevent contamination from N_2^{++}, NO was the preferred source gas in their low pressure electron impact source. The beam of N^+ produced was injected into a flow tube and a technique called the "monitor ion method," which is similar to the beam attenuation approach, was used to detect metastables. Their measurements indicated that 30% of the ions were in metastable electronic states, but the population of individual states was not determined.

Perhaps of most interest are the results of Matic and collaborators. By performing attenuation experiments of 5 keV N^+ on Ne, it was seen that at low source pressures, up to 60% of the electron impact produced beam was in, what appeared to be, a single metastable state.[35] The fraction of this state in the beam increased steadily as the electron energy was raised to 80 eV; above this energy the fractional increase was small and was attributed to a larger production of N_2^{++}. In this publication, it was assumed that the metastable state formed was $N^+(^1D)$. A subsequent publication, however, concluded that the dominant metastable is the ^5S state.[36] This was determined by studying the charge transfer cross section of the ions as a function of kinetic energy and applying the Massey criterion.

Ine process:

$$N^+(^5S) + Ne \rightarrow N(^4S) + Ne^+ \qquad (15)$$

is endothermic by only 1.17 eV while spin-allowed charge transfer from the other N^+ states is at least 5 eV endothermic. Equation (3) predicts that the charge transfer cross section curve for $N^+(^5S)$ will look very different from those of the other states. Since the maximum in the experimental curve is in good agreement with the value predicted for $N^+(^5S)$, the argument is convincing. It should be noted that this experiment was not expected to be sensitive to ^1D or ^1S states in the beam.

The result that the impact of 80 eV electrons on N_2 can produce up to half $N^+(^5S)$ is quite remarkable when one considers that $N^+(^5S)$ had not been observed by other workers. Its possible presence was reported by our group, due to an inelastic feature in N^+-He collisions which was best assigned to $N^+(^5S \rightarrow {}^3D)$.[37]

We performed beam attentuation experiments on N^+ ions extracted from each of the three ion sources described in Chapter 2, using various attenuating gases. It was discovered rather early in the course of experiments that the calculated cell pressure given by equation (11) was inadequate. This was particularly true for systems where the attenuation cross section was small and high pressures were necessary; often "negative curvature" in the plots appeared. A double

exponential fit to data with negative curvature yields the unphysical result that one state is present in over 100% abundance; this was believed to be an experimental artifact. Therefore the pressure was further corrected in the following way. Beam attenuations of Ne^+ formed in a microwave discharge of 90% Ne-10% He were performed using each of the attenuating gases. Because of the mildness of the ionizing conditions and the fact that the first excited state of Ne^+ lies 26.9 eV above the ground state,[30] all of the Ne^+ ions should be in the lowest $^2P_{3/2,1/2}$ states. Assuming equal attenuation cross sections for the two fine structure states, a semi-logarithmic plot of I/I_o vs pressure must give a straight line. It was observed that for some attentuating gases there was negative curvature while for others there was slight positive curvature. A computer program, PFIX, was written which further adjusted the pressure measurement so that the semilog plots gave straight lines. This process consisted of finding coefficients a,b,c so that a final corrected pressure (p_{cor}) could be determined from the previously calculated pressure (p) using

$$p_{cor} = ap + bp^2 + cp^3. \tag{16}$$

To determine the coefficients, PFIX utilizes a standard least squares matrix algorithm[38] which has been slightly modified to account for the fact that the fit is constrained to go through the point $p_{cor} = 0$, $\log(I/I_o) = 0$.[39] Once the second and third order coefficients were determined for a particular attenuating gas, they were applied to

systems involving the same attenuating gas but different ions. Curvature in the subsequent plots should be real, and the data were fit to a double exponential using an iterative non-linear least squares program written by J. E. Kleckner.

It was observed that when the pressure correction coefficients were applied, results were most successful if the data the correction was being applied to covered a pressure range similar to that for which the coefficients were determined. This observation suggests that in addition to the expected gas specific nature of the pressure correction, presumably due to differences in viscosity, there is a contribution coming from the apparatus which probably reflects the inadequecies of equation (11) over all pressure ranges. Further support for this notion comes from the fact that coefficients obtained using a beam of Ar^+, also expected to be all ground state, were not always in good agreement with coefficients obtained using Ne^+. Therefore, judicious application of the coefficients was necessary in order to prevent the inducement of artifacts; usually the Ne^+ results were used, but occasionally only up to second order. For some gases, the Ar^+ determined coefficients were preferred while in others it was apparent that neither set did a suitable job, and other methods had to be applied.[40]

In Figs. 3-5 we see typical results for the attenuation of 100 eV beams of N^+ ions in CO. The fractional abundances and attentuation cross sections in $Å^2$ for the two states as determined by the computer program are given in the figures. The absolute cross sections are

Fig. 3. Semilog plot of the fraction of a 100 eV N^+ beam passed as a function of CO attenuating gas pressure. The N^+ was produced in a microwave discharge through N_2. The diamonds represent data points and the squares denote the difference between the data and the lower cross section (slow) exponential fit to the data. The upper line is the slow exponential. The CO pressure was corrected to second order in Figs. 3-5 using the coefficient -1.33×10^{-3} for the quadratic term.

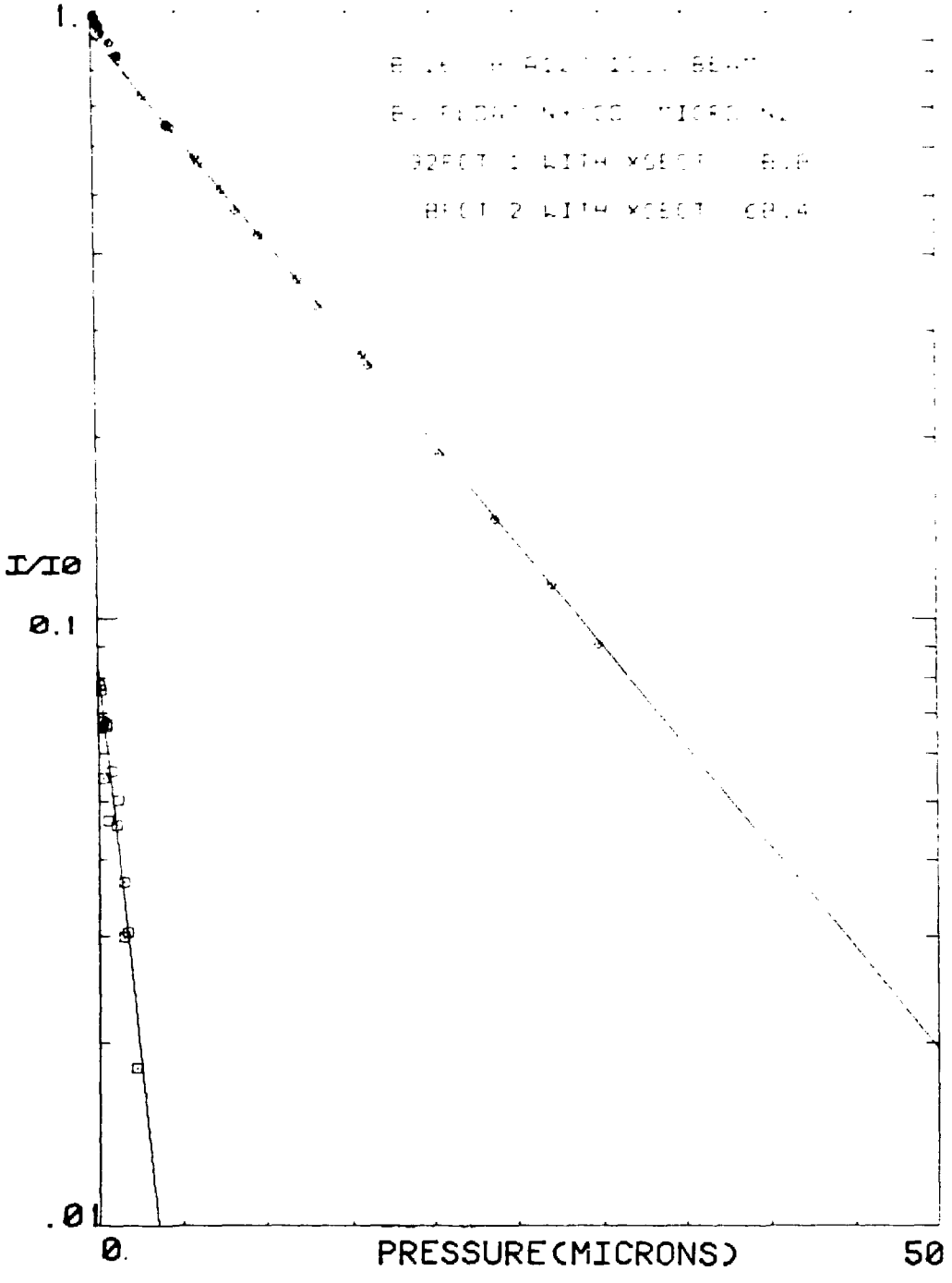

XBL 807-10760

Fig. 3

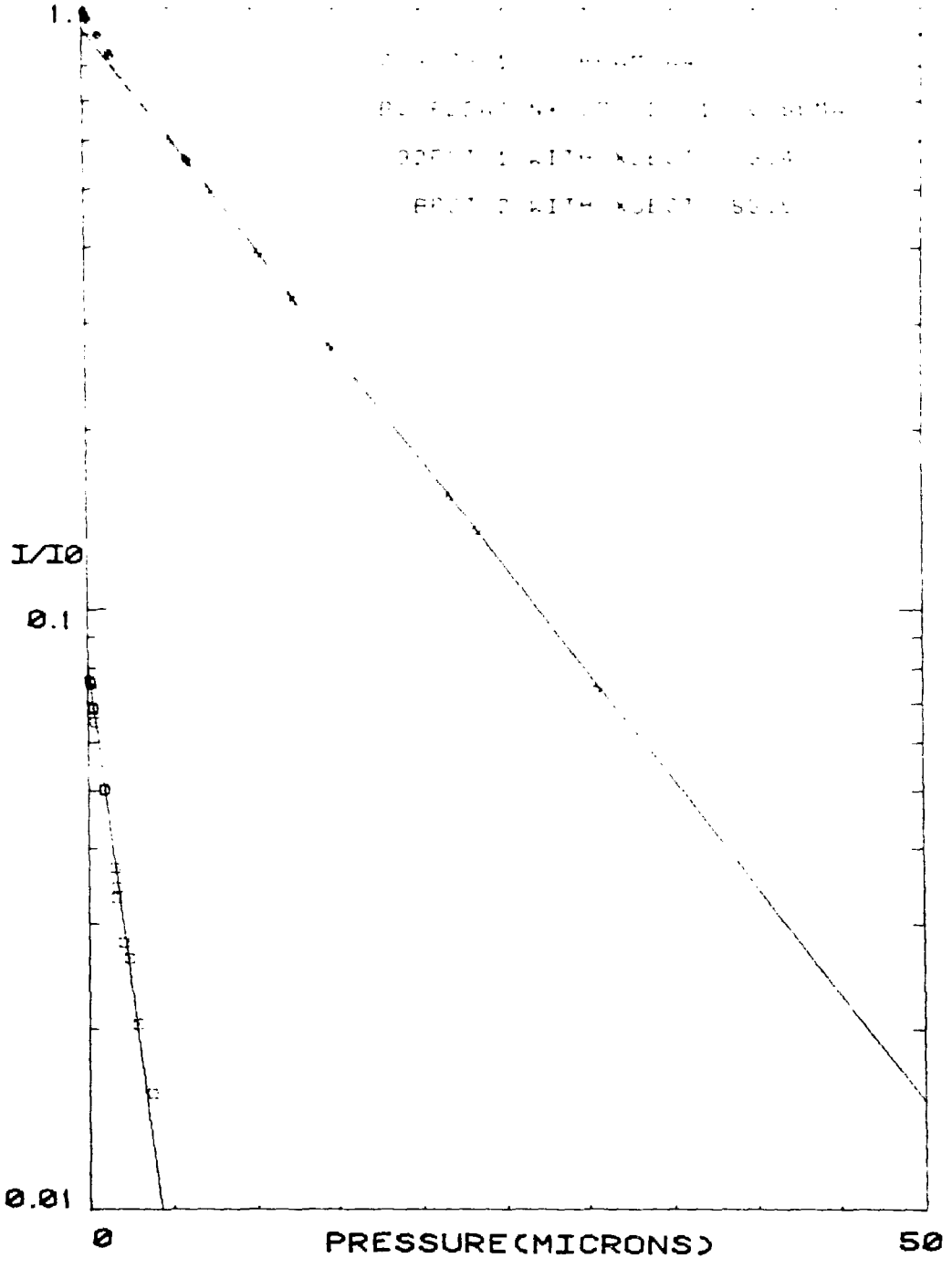

Fig. 4. Results of a beam attenuation experiment for 100 eV N^+ in CO with the N^+ extracted from the DC discharge source.

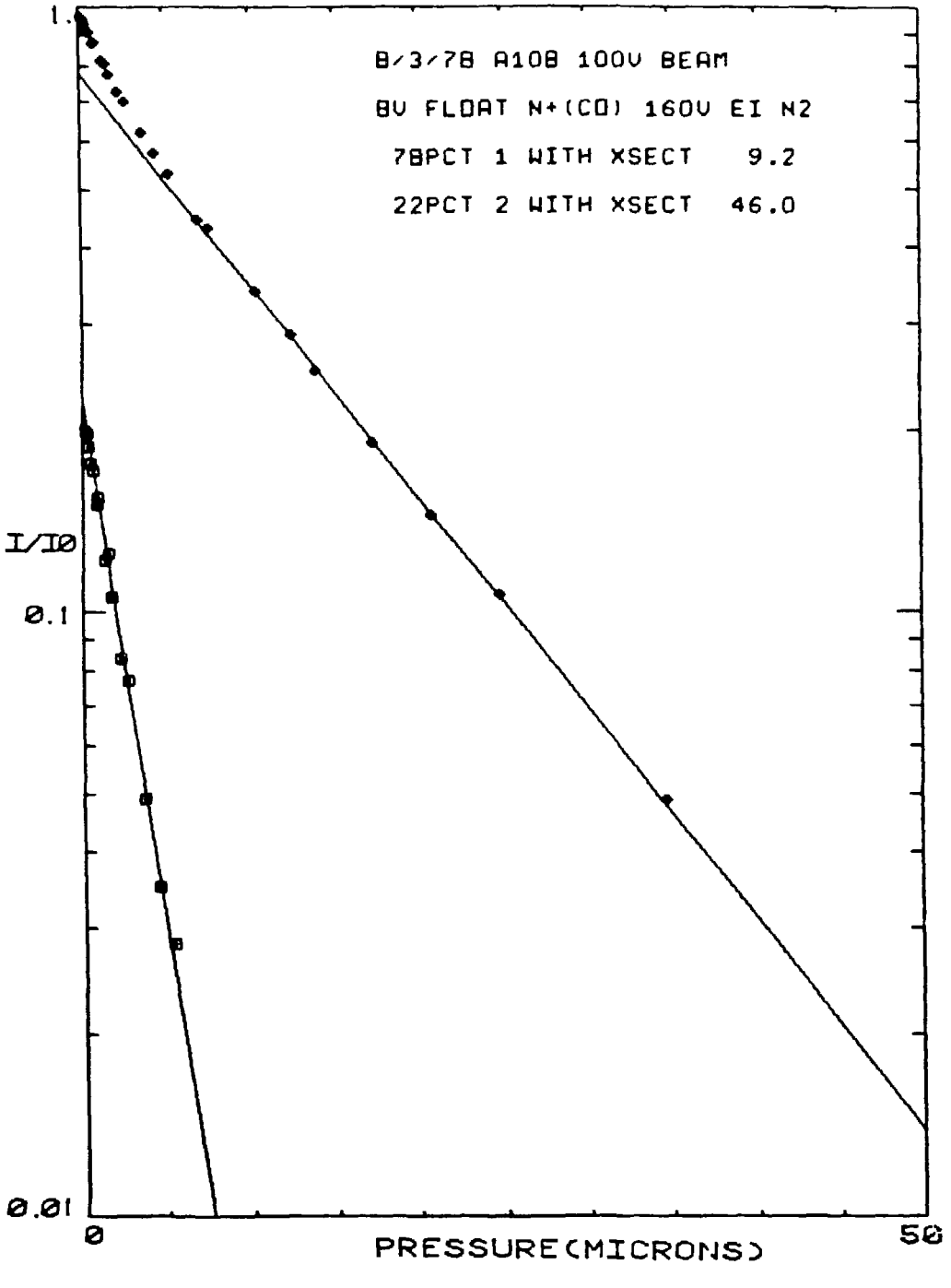

XBL 807-10758

Fig. 5. Results of a beam attenuation experiment for 100 eV N^+ in CO with the N^+ produced by the impact of 160 eV electrons on N_2.

determined using a value of 2.7 cm for the path length in the scattering cell; these numbers are considered accurate to about ±5 relatively and ± 20% absolutely for the species present in large abundance. We observed a fairly large variation in the cross section for the more sparcely populated state, and so these cross sections are probably only good to ±50%. The fractional abundances are believed accurate to ±3 percentage points. Comparing Figs. 3 and 4 we see good agreement as to the fraction of excited state present when the ions are produced in either of our discharge sources. The observed small variation in the cross sections is probably within experimental error. In Fig. 5, we see that when N^+ is produced by high energy electron impact, the expected result is obtained that more excited metastable ions are produced. Figs. 3 and 4 show that in a two state approximation ~8 of the ions emanating from our discharge sources are in metastable states. This implicitly assumes that the dominant ion present is the ground state, which is reasonable, at least for the discharge sources.

To help decide which metastable state(s) is (are) present in the beams from our discharge sources, we should consider the energy level diagram given in Fig. 6. This diagram is useful because it shows at a glance if charge transfer should be favorable. On the far left, line segments located at the proper transition energies for $N^+(^3P, ^1D, ^1S, ^5S) + e^- \rightarrow N(^4S, ^2D, ^2P)$ are given; short line segments indicate that the transition is spin-forbidden. On the right side, transition energies for forming the indicated ions from the neutral ground state are given. The length of these lines is proportional to the Franck-Condon overlap

Fig. 6. Transition energies for the various N^+ states to different states of N, and ionization energies for various attenuating gases. For the molecules, the length of the lines signify the magnitude of the vibrational overlap of that state of the ion with the v = 0 level of the ground electronic state of the neutral molecule. The three levels associated with each N^+ electronic state correspond to recombination to $N(^4S,^2D,^2P)$. Short lines associated with these levels denote transitions which are not favorable. This figure is similar to one given in Ref. 41 but has been extended using photoelectron spectra given in Ref. 42.

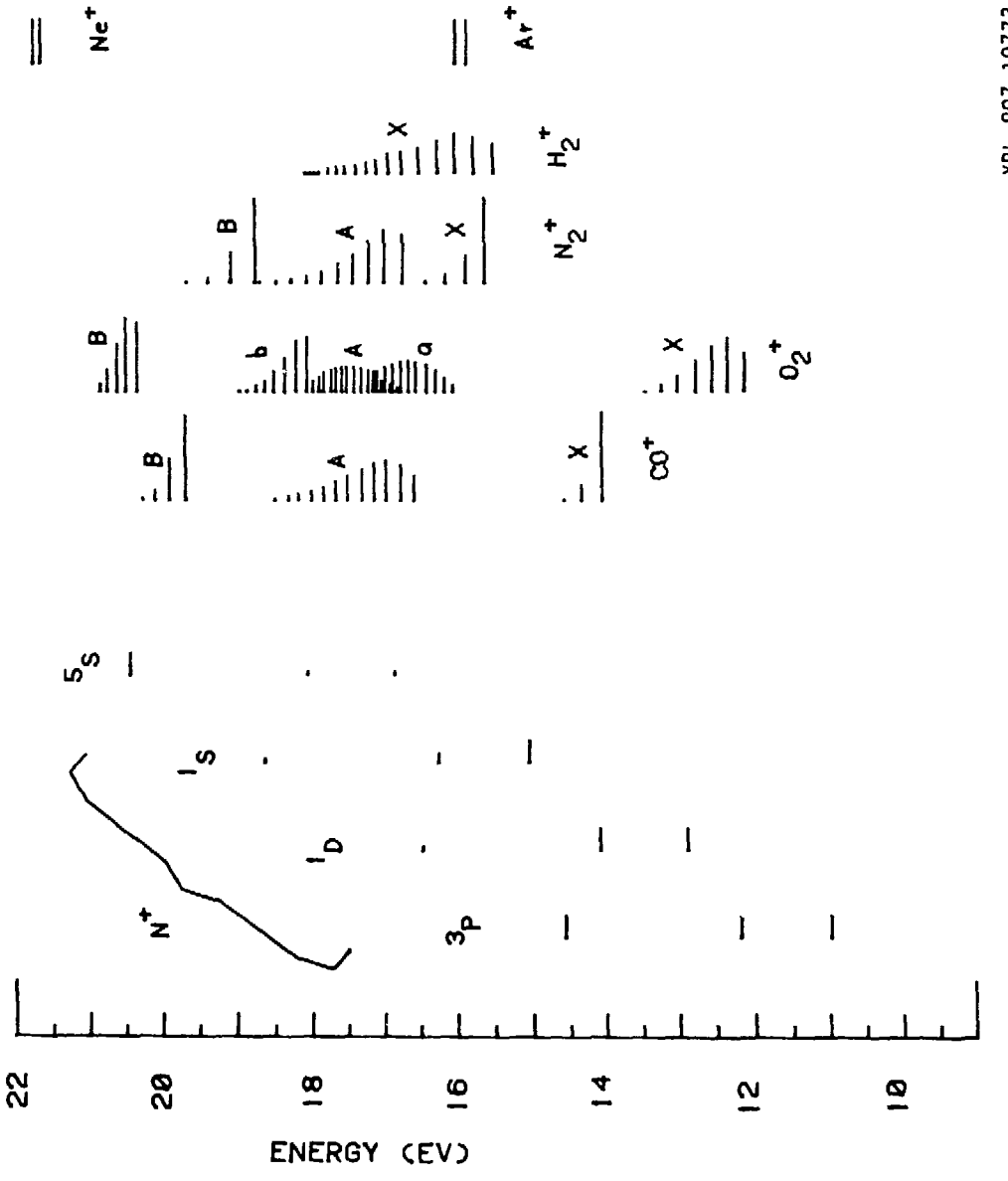

XBL 807-10773

Fig. 6

of that ionic state with lowest state of the neutral. As stated earlier, charge transfer processes which are resonant to ionic states with favorable vibrational overlap should have large cross sections. Such a process, as can be seen in Fig. 6, is

$$N^+(^1D) + CO \rightarrow N(^2D) + CO^+(X). \qquad (17)$$

This reaction is exothermic by only 0.05 eV to the v = 0 level of $CO^+(X)$ which has good overlap with CO (X, v = 0). Neither $N^+(^1S)$ or $N^+(^5S)$ has such a favorable charge transfer channel with CO and the reaction involving the ground state is also less likely since it is 0.53 eV off resonance. Therefore it is reasonable to attribute the fast exponential ($\sigma \approx 60$ Å^2) in Figs. 3 and 4 to the ^1D state and the slower one ($\sigma \approx 9$Å^2) to ^3P. Rutherford and Vroom[33] measured the charge transfer cross section for $N^+(^3P)$ and $N^+(^1D)$ with CO at 100 eV and obtained 4Å^2 and 40Å^2 respectively. Since a number of other products are possible in this reaction, and they might also be scattered to large enough angles that they would not be detected, agreement can be considered good. Further confirmation comes from Frobin et al.[43] who measured the charge transfer cross section of $N^+(^3P)$ at 20 eV to be 3.3Å^2 but found the total attenuation cross section to be 6.9Å^2.

The observation that the microwave discharge and DC discharge sources produce similar state distributions was further verified using other attentuating gases. However, it was noticed that the state distributions produced by the DC discharge source were somewhat variable. This was seen not only in attentuation experiments where values approaching 15% metastable were sometimes obtained, but also in reactive product distributions. These product distributions, which were discussed in Chapter 3, were not always reproducible using this source presumably because of fluctuations in the electronic state population. Although the cause of such variations was never unambiguously determined, it appeared that lower discharge currents favored metastable production. Also if the orifice in the anode of this source became enlarged, it seemed that more metastables were produced.

Interpreting the state distribution of the electron impact produced beam is complicated by the fact that a number of states are formed by this process. Further discussion of this point is given later.

Figs. 7-9 show the results of attenuations of N^+ produced in the microwave discharge source using Ar, O_2 and N_2 as attenuators. The percentage of metastable state obtained is in good agreement using all attenuating gases except for N_2. This would be expected only if the states present in the beam attenuated with equal cross sections in N_2. One might initially think that the charge transfer cross section for $N^+(^1D)$ to N_2 might be higher than for $N^+(^3P)$ because the former process is exothermic and the latter endothermic. However, the reaction

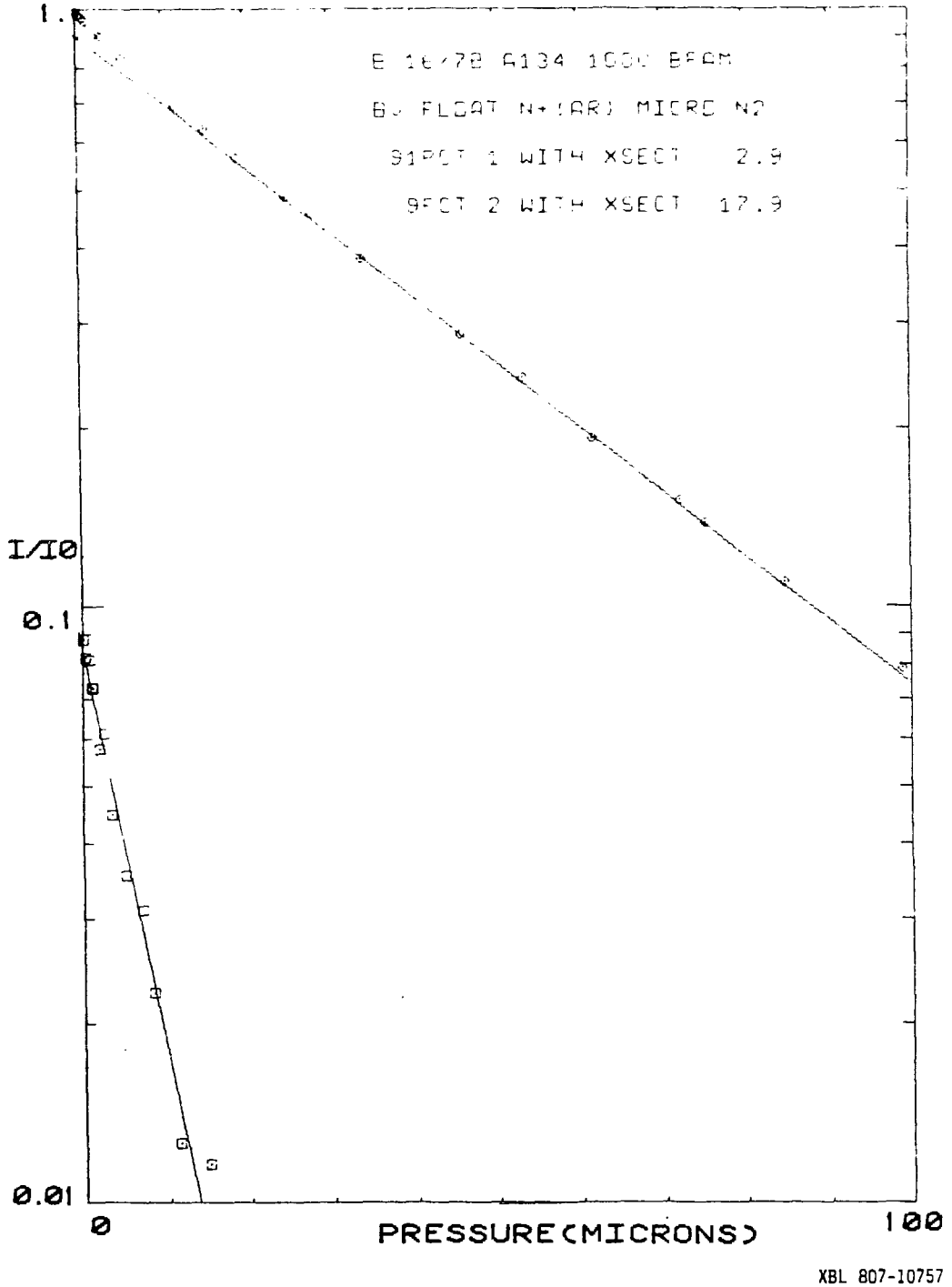

Fig. 7. Results of a beam attenuation experiment for 100 eV N^+ in Ar. N^+ in Figs. 7-9 was produced in a microwave discharge.

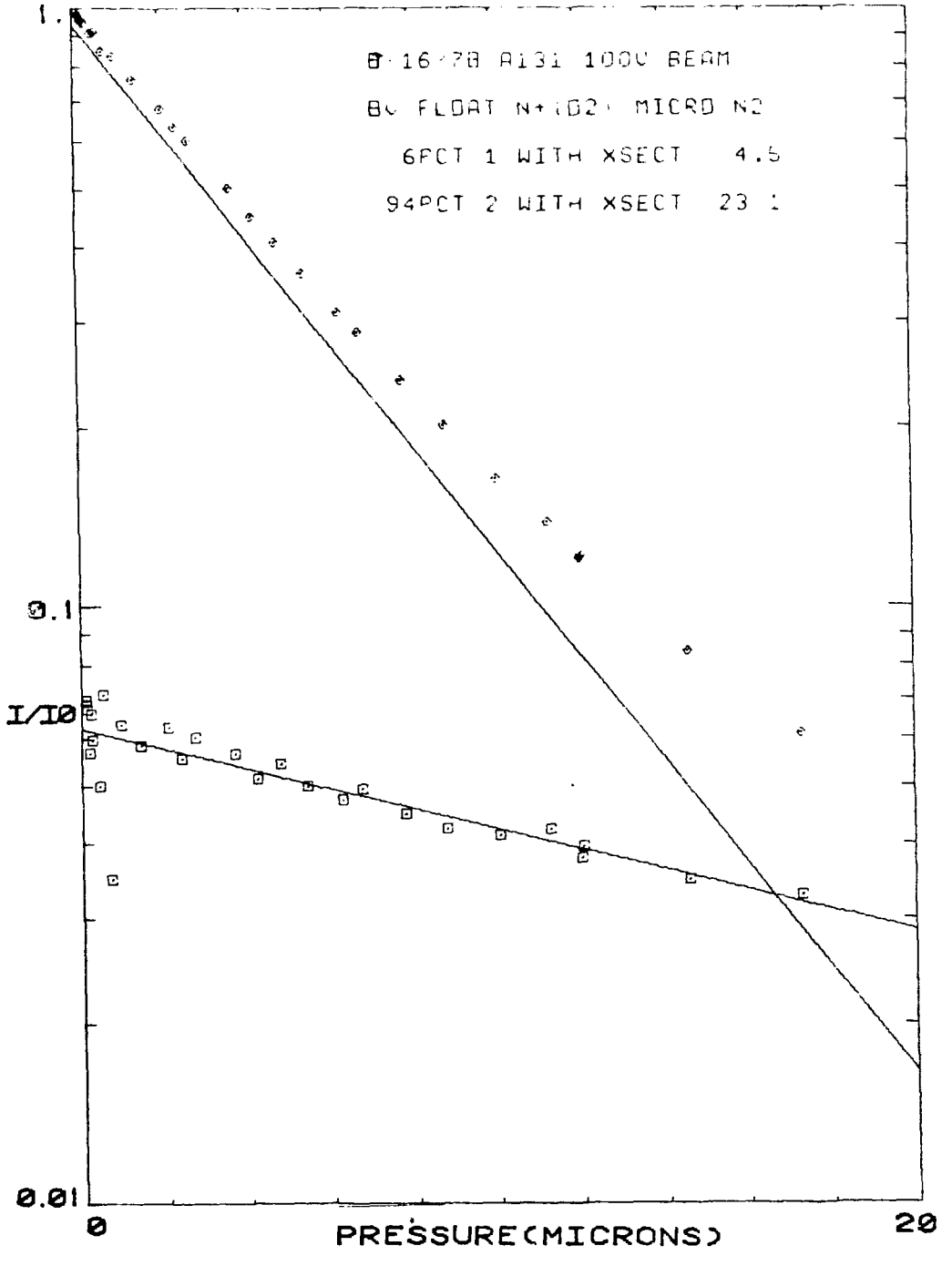

XBL 807-10756

Fig. 8. Results of a beam attenuation experiment for 100 eV N^+ O_2.

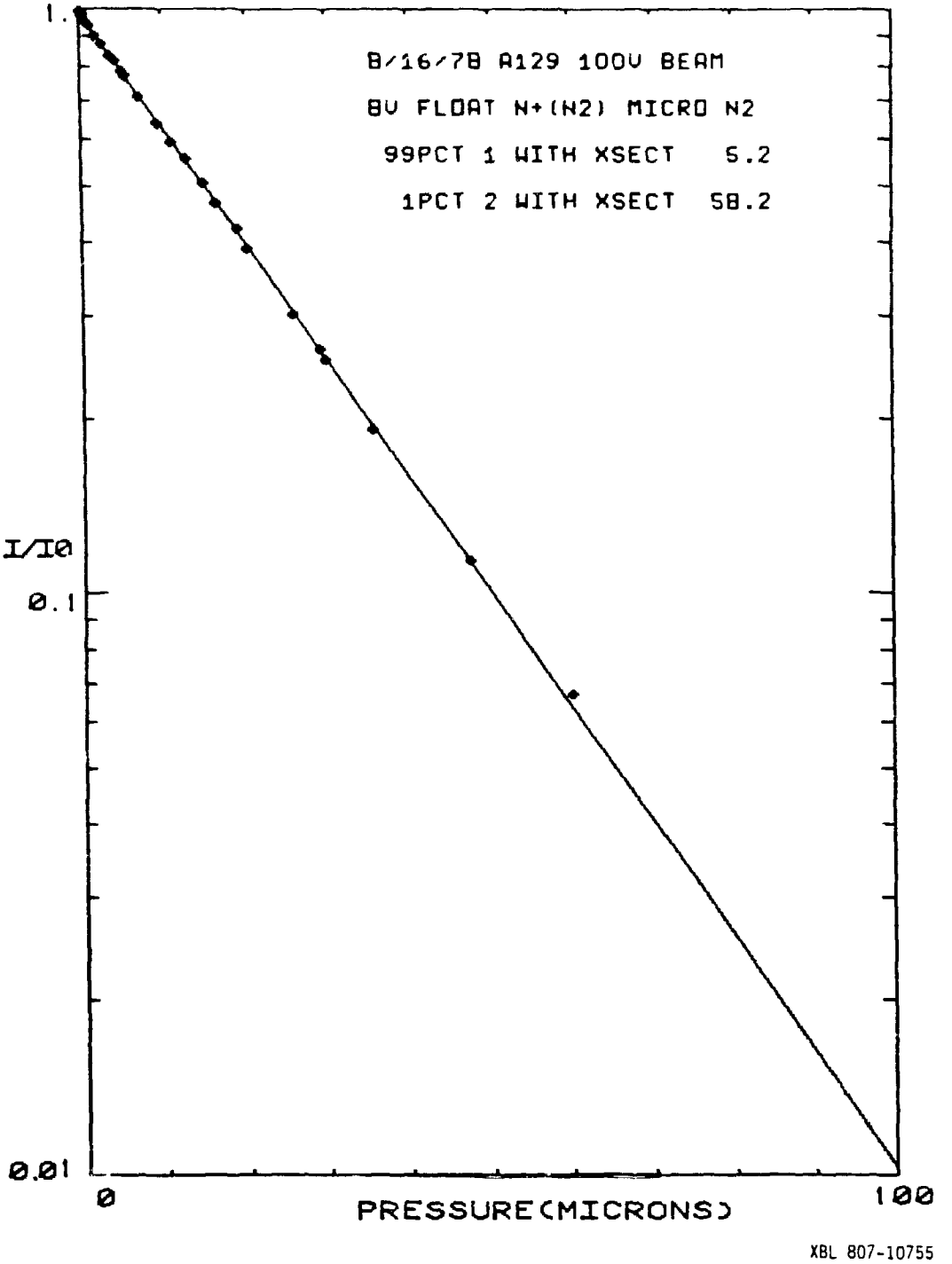

XBL 807-10755

Fig. 9. Results of a beam attenuation experiment for 100 eV N^+ in N_2. The N_2 pressure in Figs. 9 and 12 was corrected using the coefficients -3.27×10^{-3} and 4.4×10^{-5} for the second and third order terms respectively.

$$N^+(^1D) + N_2(^1\Sigma_g^+) \rightarrow N(^4S) + N_2^+(^2\Sigma_g^+) \quad \Delta E = -0.96, \qquad (18)$$

does not conserve spin and hence is unlikely. The most favorable spin allowed charge transfer reaction with $N^+(^1D)$ is to form $N(^2D)$; this yields an effective recombination energy for $N^+(^1D)$ of 14.06 eV. The recombination energy of $N^+(^3P)$ is 14.54 eV which makes N^+ a somewhat interesting case in that more energy is released in charge transfer with the ground state than with the excited state. Because of this fact there is no reason to expect either ^1D or ^3P to have large charge transfer cross sections in N_2, as both processes are at least 1 eV endothermic. Moran and Wilcox[34] found these states to have identical charge transfer cross sections with N_2 below 1 keV and at the lowest energy studied, 600 eV, the cross sections for both were 4.5Å^2. Hence the attenuation results using N_2 confirm our belief that the microwave discharge produced beam contains only $N^+(^3P)$ and $N^+(^1D)$. Attenuations performed using N^+ from the DC discharge source also gave nearly straight lines.

Figs. 7 and 8 are consistent with Fig. 3, and we may conclude that approximately 8% of the ions extracted from the microwave discharge source are in the ^1D state. In the case where Ar is used as the attenuator, the $N^+(^1D)$ has a higher attenuation cross section than $N^+(^3P)$ while for O_2, the opposite is true. The value given for the cross section of $N^+(^1D)$ in Ar is very approximate since other experiments yielded numbers ranging from 6-22Å^2. The cross section

measured for $N^+(^3P)$ attenuating in Ar, 2.9Å^2, probably reflects large angle scattering (which will be discussed later) rather than charge transfer. We conclude this from the fact that the charge transfer cross sections to Ar for $N^+(^3P)$ and $N^+(^1D)$ are 2 and 5Å^2, respectively, at 1 keV,[34] and the values are decreasing as a function of energy. It is not obvious why the ^1D state would have a higher cross section than ^3P because the processes

$$N^+(^3P) + Ar \rightarrow N(^4S) + Ar^+(^2P) \tag{19}$$

$$N^+(^1D) + Ar \rightarrow N(^2D) + Ar^+(^2P) \tag{20}$$

are endothermic by 1.14 and 1.62 eV respectively. It is possible that ^1D charge transfer to give $N(^4S)$, which is exothermic by 0.76 eV, contributes to the depletion of the ^1D state.

The fact that $N^+(^3P)$ has a large charge transfer cross section in O_2 could be easily predicted by glancing at Fig. 6. The reaction

$$N^+(^3P) + O_2(X^3\Sigma_g^-) \rightarrow N(^2P) + O_2^+(X^2\Pi_g) \quad \Delta E = -0.09 \text{ eV} \tag{21}$$

should be quite favorable, and, in fact, the cross section for (21) at 100 eV has been measured at 20.5 Å^2.[44] This is in good agreement with our total attenuation cross section of 23.1Å^2 at the same energy. Moran and Wilcox[34] measured the charge transfer cross section for 1 keV N^+ in O_2 and obtained 3Å^2 for the ^1D state and 23Å^2 for $N^+(^3P)$.

It should be noted that it is quite difficult to correctly fit data which contain a small percentage of a species with a low attenuation cross section, because the curvature introduced is rather subtle. Small variations in the data and pressure correcting coefficients caused large fluctuations in the cross section for the ^1D state and we were not able to obtain similar results for N^+ extracted from the DC discharge source. In fact the fit to the data in Fig. 8, which seems quite correct given other information we have on this system, was not possible until yet another correction was included. This is described in the following paragraphs.

A point which was mentioned in passing earlier is that when an excess of gas was added to the scattering cell, negative current could be measured by the picommeter. This apparently resulted from electrons or negative ions produced upon collision, and these charge carriers were attracted to the ion collector by the +8 V bias. The negative current we measured increased gradually as a function of pressure but then decreased, apparently because it was attenuated by the gas in or before the cell. For some ion-molecule combinations the negative current was quite large and amounted to greater than 10% conversion of the primary beam current. Such a system was N^+-O_2. The original way that negative current was taken into account was to treat the maximum negative point obtained as zero and measure I and I_o with respect to it. Clearly this is an approximation but not a serious one for most systems as it amounts to a change of a few percent or less. However, for systems like N^+-O_2, where the difference between the mechani-

cal zero, which corresponds to no current, and the maximum negative current, is significant, the approximation is not justified. A more accurate approach to the problem is to assume that the number of negative charge carriers produced is proportional to the pressure in the cell. This is likely to be a good assumption in the "low pressure" range where competition from processes which deplete the negative current is negligible. Since virtually all the data points are taken at pressures at least a factor of 5 lower than that at which the maximum negative current occurs, a low pressure regime assumption is probably valid.

The quantity we wish to measure, I/I_o, concerns the positive current transmitted and any negative current present is a contaminant. Hence, we need to subtract the effects of the negative current from our measurement of I at each point; because the negative current is dependent on pressure the adjustment amounts to making "zero" pressure dependent. This is done in practice using the equation

$$I_{adj} = I + N_{max}(p/p_{emp}) \tag{22}$$

where I_{adj} is the adjusted value of the transmitted beam current, I is the raw value measured with respect to mechanical zero, N_{max} is the maximum negative current measured, p is the pressure at which the data point is taken, and p_{emp} is an empirically determined pressure. Physically p_{emp} corresponds to the pressure at which the negative current produced is equal to N_{max}. Unfortunately, this could not be

directly measured because at the high pressure at which N_{max} is obtained, processes attenuating the negative signal are important. The best value for p_{emp} lies between the pressure at which the signal first becomes negative and the pressure at which N_{max} is measured; in practice we used the pressure at which the measured negative current was equal to half of N_{max}. This correction had virtually no effect on systems which produced little negative current, but was rather successful when applied to N^+-O_2 as demonstrated by Fig. 8.

Figs. 10-13 show Ar, O_2, N_2 and H_2 attenuations of N^+ produced by the impact of 160 eV electrons on N_2. Figs. 10, 12 and 13 are similar to Fig. 5 in that they indicate that 20-30% of the beam is in a metastable state which is attenuated with a much larger cross section than the ground state. Table 1 summarizes the average of results for N^+ attenuations with CO, Ar, O_2, N_2 and H_2. It is obvious if one considers the cross sections, that the two states present in the microwave discharge produced ions are not the same as the two states determined for the electron impact produced beam. It was well-established by the microwave data that $N^+(^3P)$ has an attenuation cross section of 23Å^2 in O_2, while neither of the states fit in the electron impact results have this cross section. There is also a noticeable discrepancy in the two cross sections for $N^+(^3P)$ in N_2. Similarly, it is clear that the metastable species produced by electron impact are attenuated by Ar much faster than $N^+(^1D)$ itself. The evidence leads us to the conclusion that the two state

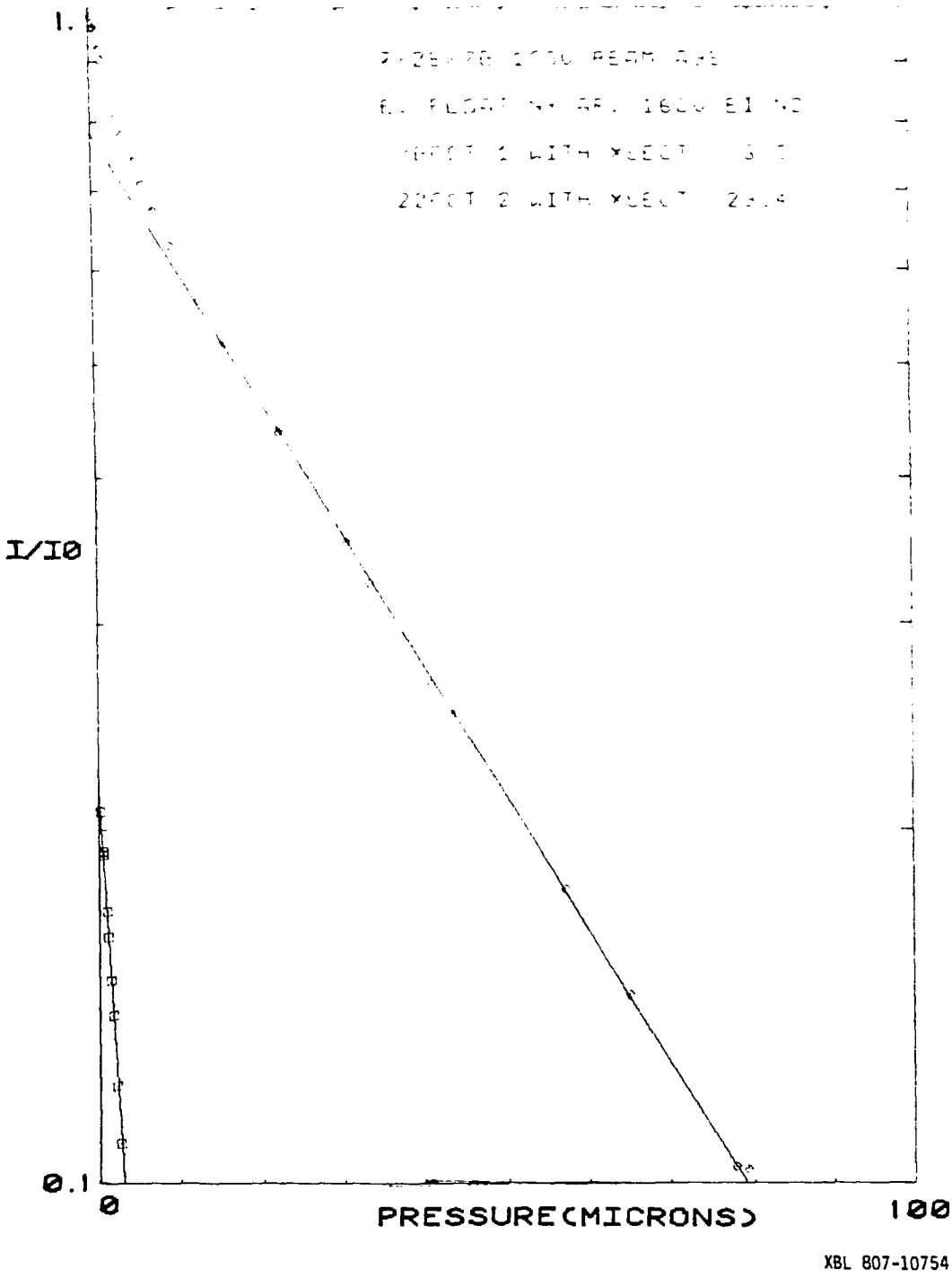

Fig. 10. Results of a beam attenuation experiment for 100 eV N^+ in Ar. N^+ was produced by electron impact on N_2 in Figs. 10-13.

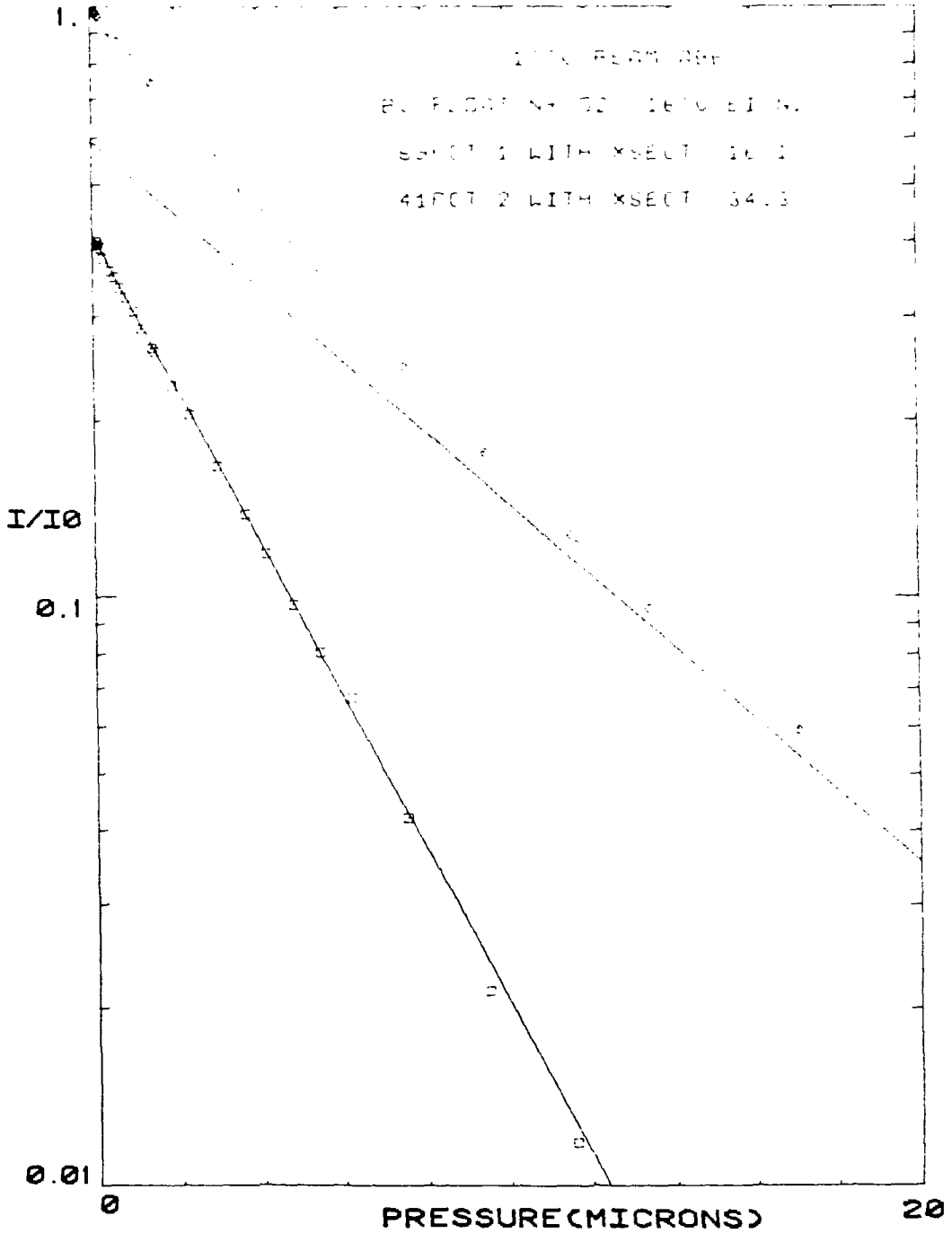

XBL 807-10753

Fig. 11. Results of a beam attenuation experiment for 100 eV N^+ in O_2.

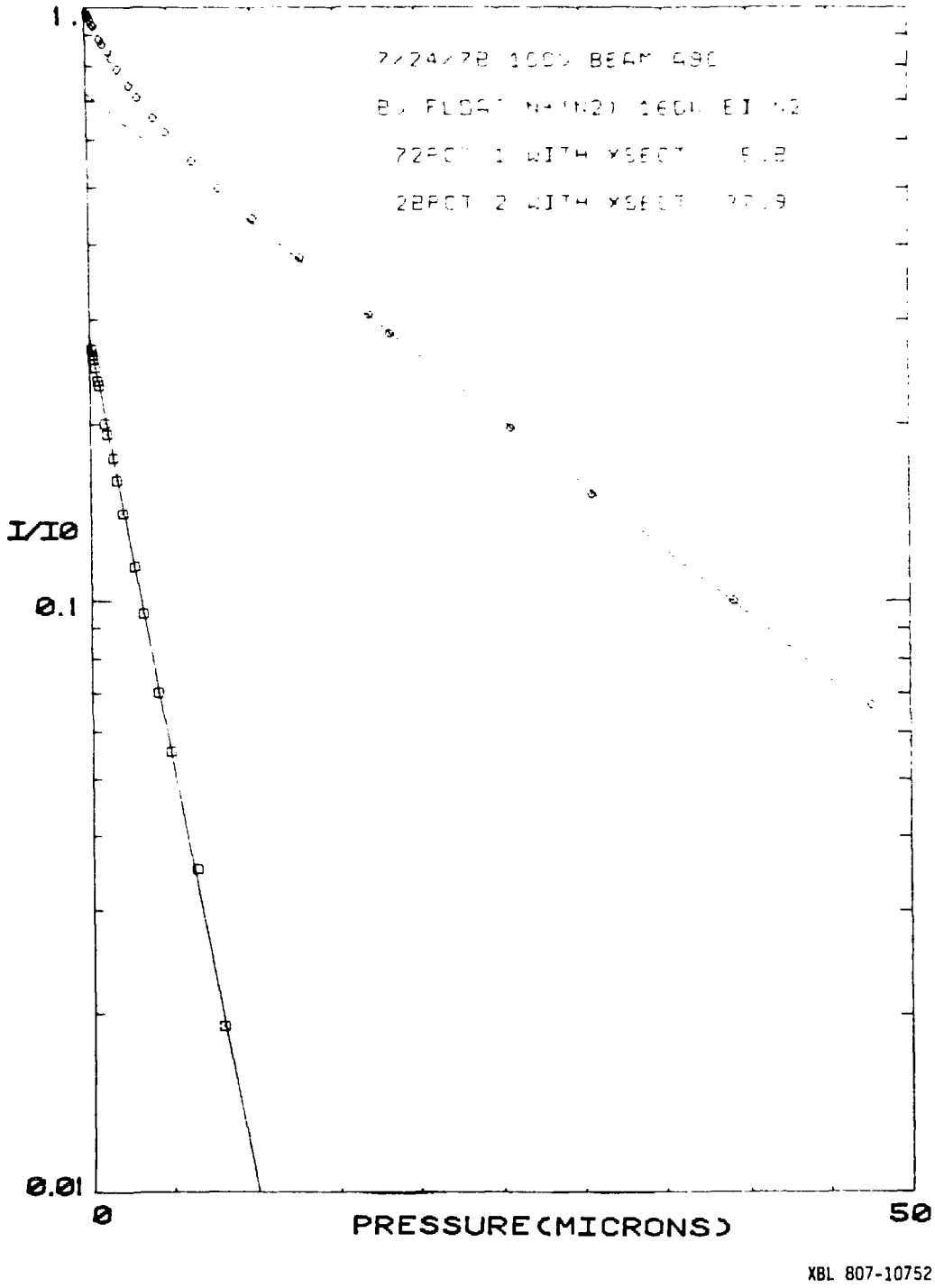

XBL 807-10752

Fig. 12. Results of a beam attenuation experiment for 100 eV N^+ N_2.

Fig. 13. Results of a beam attenuation experiment for 100 eV N^+ in H_2. The H_2 pressure was corrected using the coefficients -2.39×10^{-3} and 6.85×10^{-6} for the second and third order terms respectively. These coefficients were chosen because when applied to data obtained with microwave discharge produced N^+ attenuating in H_2, a single exponential was obtained.

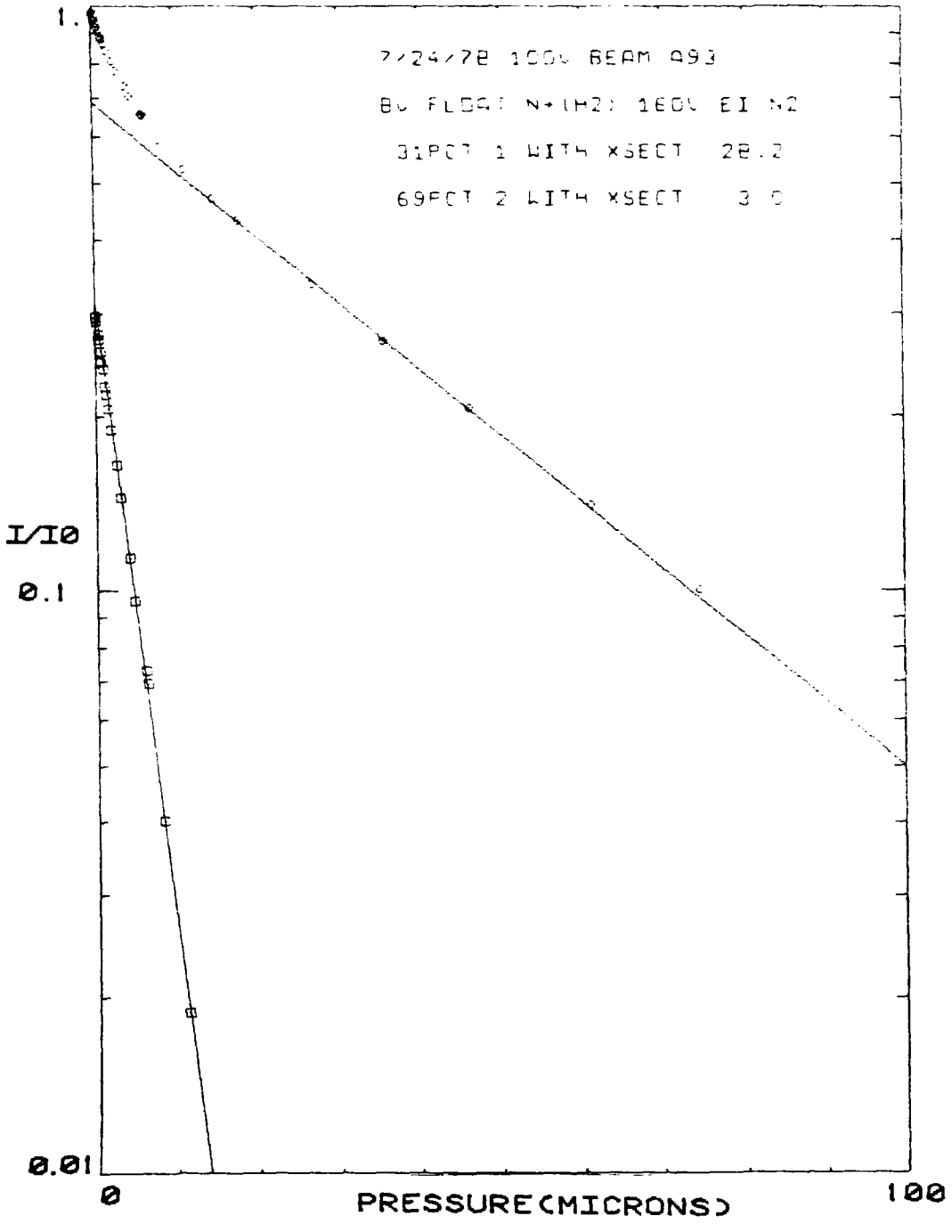

XBL 807-10751

Fig. 13

Table 1

	Microwave Discharge				Electron Impact			
	$N^*(^1D)$		$N^*(^3P)$		Species 1		Species 2	
Attenuating Gas	Fraction	Cross-Section	Fraction	Cross-Section	Fraction	Cross-Section	Fraction	Cross-Section
CO	0.08	35–65	0.92	9.0	0.23	40	0.77	9.2
Ar	0.09	6–22	0.91	2.9	0.25	36	0.75	3.1
O_2	0.06	1–8	0.94	2.3	0.40	14	0.60	3.0
N_2	0.01	——	0.99	5.2	0.25	38	0.75	5.8
H_2	(0)	——	(1.0)	2.7	0.30	28	0.70	3.0

Average apparent fractions and attenuation cross sections ($Å^2$) for species present in m/e = 14 beams produced by microwave discharge or electron impact on N_2.

approximation is not valid when applied to the electron impact produced ions. This is certainly reasonable in light of our earlier discussion which concluded that significant amounts of $N^+(^5S)$, N_2^{++}, $N^+(^1D)$ and $N^+(^3P)$ could be formed. Since virtually nothing is known about the charge transfer cross sections of N_2^{++} or the higher states of N^+ to the gases in question, our discussion as to the possible presence of these states will have to be qualitative.

The effect that N_2^{++} has on the attenuation results is not immediately clear. Since the second ionization potential of N_2 is 27.1 eV,[45] the transfer of a single electron to N_2^{++} will be far from resonant for ground state products. However, because there exist many excited vibronic states of N_2^+, a favorable reaction pathway might be present.[46] It has been experimentally determined at thermal energies that the single electron transfer rate to a doubly charged ion can be quite high when one of the collision partners is a molecule.[47-49] Also it would be expected that for resonant processes such as:

$$N_2^{++} + N_2 \rightarrow N_2 + N_2^{++} \quad , \tag{23}$$

the cross section would be large. Recent work with rare gases has shown that the cross section for symmetric double charge exchange is $\sim 25 Å^2$ at 20 eV lab.[50] Hence any N_2^{++} in the beam surely attenuates rapidly in N_2. It should also be realized that a double charge

transfer process effectively removes two charges from the beam. This means that a beam containing 10% N_2^{++}, attenuating via double charge transfer, will appear to contain ~20% metastable ions.

We can estimate the likelihood for single charge transfer involving N_2^{++} with the aid of Fig. 14. The vibrational overlaps indicated for $N_2^{++} \rightarrow N_2^{+}$ were determined theoretically by Moran and collaborators[46] including reasonable assumptions about the vibronic state distribution of N_2^{++} produced by electron impact. The transition energies for $N_2^{++} \rightarrow N_2^{+}$ actually extend up to 29 eV and the vibrational overlap is quite favorable in the 24–27 eV range.[46] These transitions are not indicated in Fig. 13, however, due to the lack of available levels for the attenuating gases in this energy range.

It is clear that there is favorable overlap with all the gases included in Fig. 13 except for Ar. Ar, however, may have a significant double charge transfer probability. The reaction

$$N_2^{++} + Ar(^1S) \rightarrow N_2(X^1\Sigma_g^+) + Ar^{++}(^3P) \qquad (24)$$

is approximately 0.7 eV endothermic for N_2^{++} in its ground $^3\Sigma_g^-$ state but virtually resonant for N_2^{++} in the metastable $^1\Sigma_g^+$ state. Thus it is reasonable to expect that any N_2^{++} present in the beam is attenuated with a fairly large cross section in all the gases listed in Fig. 14 and contributes to the fast exponential in our experiments.

Fig. 14. Comparison of the absolute value of the transition energies for $N_2^{++} \rightarrow N_2^{+}$ and $X \rightarrow X^{+}$ where X = CO, O_2, N_2, H_2, Ar, and Ne. The length of the lines indicate the vibrational overlap of the product state with the reactant state.

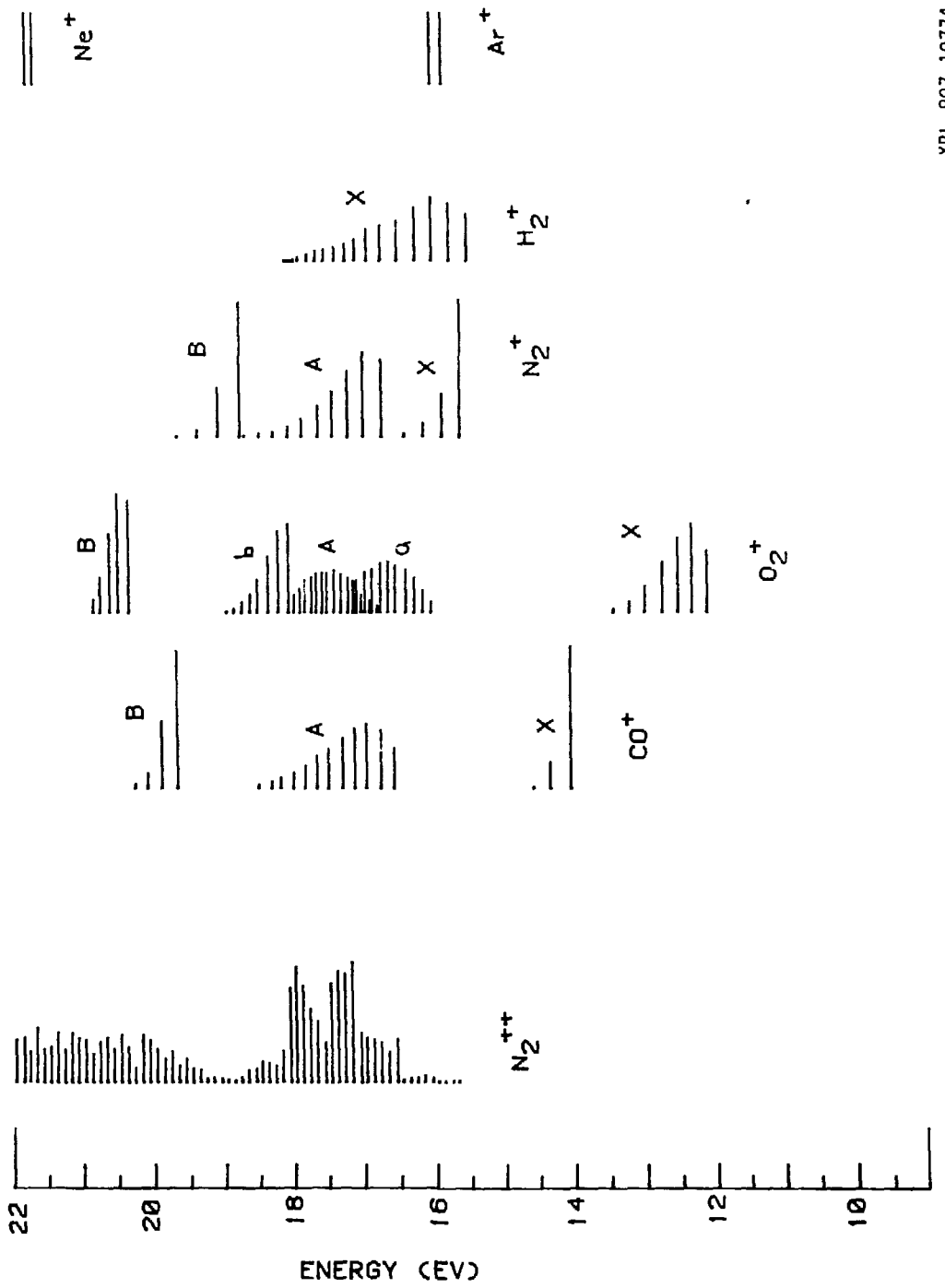

XBL 807-10774

Fig. 14

We can consider the favorability of electron transfer to $N^+(^5S)$ with the aid of Fig. 6. The only likely product formed is $N(^4S)$ and the energy released in this process is 20.39 eV. At this energy, vibrational overlap between ions and the neutral ground state of N_2 and CO is not outstanding. In fact, the reactions

$$N^+(^3P) + N_2(^1\Sigma_g^+) \rightarrow N(^4S) + N_2^+(X^2\Sigma_g^+) \qquad \Delta H = 1.04 \text{ eV} \qquad (25)$$

$$N^+(^5S) + N_2(^1\Sigma_g^+) \rightarrow N(^4S) + N_2^+(B\ ^2\Sigma_u^+) \qquad \Delta H = -1.65 \text{ eV} \qquad (26)$$

$$N^+(^5S) + N_2(^1\Sigma_g^+) \rightarrow N(^4S) + N_2^+(C\ ^2\Pi_g) \qquad \Delta H = 1.68 \text{ eV} \qquad (27)$$

might be expected to yield similar attenuation cross sections for these two states in N_2. In CO, the similar energetics of

$$N^+(^3P) + CO(^1\Sigma^+) \rightarrow N(^4S) + CO^+(X^2\Sigma^+) \qquad \Delta H = -0.53 \text{ eV} \qquad (28)$$

$$N^+(^5S) + CO(^1\Sigma^+) \rightarrow N(^4S) + CO^+(B^2\Sigma^+) \qquad \Delta H = -0.69 \text{ eV} \qquad (29)$$

might also indicate about equal cross sections. In Ar, there is no spin-conserving charge transfer reaction of $N^+(^5S)$ within 4 eV of resonance and hence its charge transfer cross section is probably less than that of $N^+(^3P)$. As previously mentioned though, the cross sections for the ^3P state is so small that what we actually measure in our experiments is a hard-sphere scattering cross section; this

would also be true for $N^+(^5S)$ in Ar and these values for $N^+(^3P)$ and $N^+(^5S)$ at 100 eV should be quite similar. Hence, in N_2, CO, and Ar, $N^+(^5S)$ which according to our earlier discussion could comprise about half of the electron impact produced beam, would probably contribute to the slow exponential and not be readily discernable.

One of the more likely attenuating gas for demonstrating the presence of $N^+(^5S)$ is O_2. While in the three gases previously discussed the attenuation cross section for $N^+(^3P)$ is small, it is quite substantial in O_2. Unfortunately, the charge transfer cross section for $N^+(^5S)$ in O_2 is also expected to be large due to the near resonance of

$$N^+(^5S) + O_2 \rightarrow N(^4S) + O_2^+(B^2\Sigma_g^-) \qquad \Delta E = -.05 \text{ eV}. \qquad (30)$$

It is apparent when comparing Figs. 8 and 11 that a double exponential fit is inadequate for describing the electron impact produced ions and that at least three states with noticeably different cross sections are likely to be present. This could be taken as evidence for $N^+(^5S)$ in the beam, but N_2^{++} might also produce the same effect.

The only obvious attenuating gas in which $N^+(^5S)$ is expected to have a much higher charge transfer cross section than $N^+(^3P)$ is Ne. This is because of the favorability of

$$N^+(^5S) + Ne \rightarrow N(^4S) + Ne \qquad \Delta E = 1.17 \text{ eV} \qquad (31)$$

relative to

$$N^+(^3P) + Ne \rightarrow N(^4S) + Ne^+ \qquad \Delta E = 7.0 \text{ eV}. \qquad (32)$$

Fig. 15 shows results for attenuations of N^+ in Ne using both the microwave and electron impact sources. The thing to notice here is that the slow exponential is about 30% steeper for the electron impact produced ions than for the discharge produced ions. This is actually about what one would expect if $N^+(^5S)$ was present in a significant amount. Reaction (31) is near enough to being resonant that a reasonable estimate for its cross section at 100 eV would be a few square angstroms. Charge transfer to Ne with $N^+(^3P, ^1D, ^1S)$ is far from resonant and these states would probably be attenuated due to hard-sphere scattering processes. This cross section can be taken as $\sim 2.5 Å^2$ using the microwave data. The shift to $3.4 Å^2$ for the slow exponential in the electron impact data is consistent with the addition of a significant amount of a new species, with a slightly higher cross section; this species is very likely to be $N^+(^5S)$. The fast exponential present in the electron impact results is probably attributable to N_2^{++}, which according to Fig. 14, should charge transfer to Ne fairly readily.

Fig. 15. Comparison of N^+-Ne attenuation results using 100 eV ions from the microwave (circles) and electron impact sources (diamonds). The second and third order pressure correction coefficients used, -2.5×10^{-3} and 9.7×10^{-6}, were chosen because when applied to the microwave results, a single exponential was obtained. The squares denote the computer fit to the fast exponential for the data taken using the electron impact source.

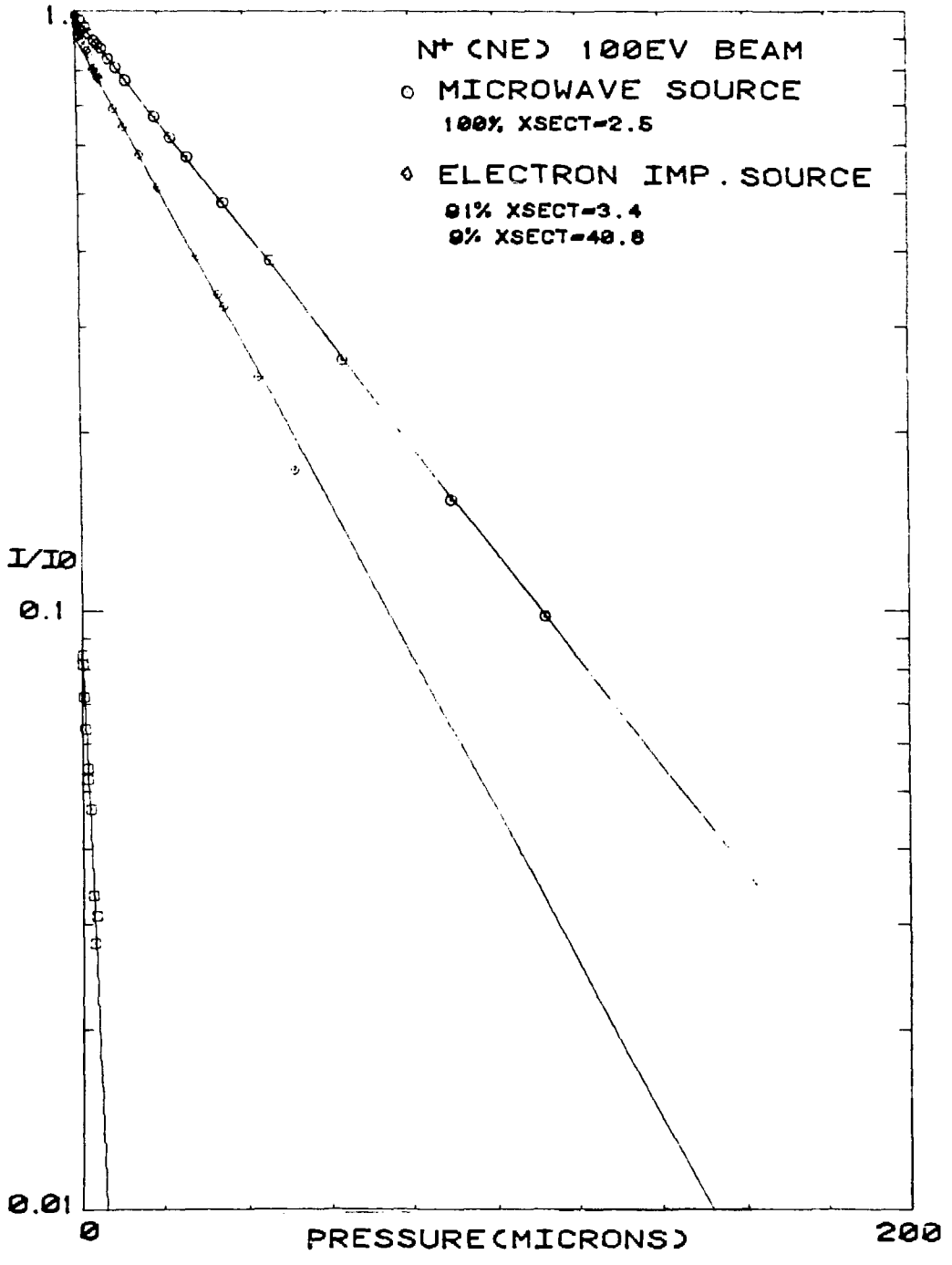

XBL 807-10750

Fig. 15

We have at this point given all our pertinent attenuation data and can now estimate the fractional abundances of the various states in the electron impact produced beam. McGowan and Kerwin[29] observed that 9% of the ions in an $\frac{m}{e} = 14$ beam were N_2^{++} under these source conditions, and none of our observations seriously dispute this. The Ne results, where the only process expected to contribute to the fast exponential is charge transfer from N_2^{++}, yields an estimate of 9%. In the other attenuating gases both single and double charge transfer should be reasonably favorable and so the interpretation of these data is difficult. Also, $N^+(^1D)$ is certainly expected to be present. As stated earlier up to 15% of the ions produced by 30 to 40 eV electron impact are in the ^1D state and it seems unlikely that this fraction would decrease noticeably as the electron energy is raised further. The fact that the ^1D attenuation cross section is large in CO implies that in Fig. 5 there are probably at least two contributors to the fast exponential: $N^+(^1D)$ and N_2^{++}. Table 1 indicates that the average apparent fraction of the metastable state measured using CO is 23%. It would be possible to interpret this as arising completely from double charge transfer, indicating ~11.5% N_2^{++}, but this would imply no $N^+(^1D)$ present. Since $N^+(^1D)$ is expected, it is more likely that N_2^{++} is attenuating via single charge transfer, and 23% represents the sum of the N_2^{++} and $N^+(^1D)$ concentration. This would imply a ^1D concentration of approximately 14%. The results obtained using Ar and N_2 as attenuators are best explained assuming that the double charge transfer probability is high.

We are now left with about 80% of the beam to divide between $N^+(^3P)$, $N^+(^1S)$, and $N^+(^5S)$. $N^+(^1S)$ has been reported only once previously,[4] and even then only in 0.5% concentration. This coupled with the fact that any statistical approach to the ionization products would be unfavorable for ^1S formation, leads us to the conclusion that it is probably present in negligible amounts. Between the two remaining states it seems likely that the 80% is distributed approximately equally between them. This is based mainly on the work of Cobic et al.[35,36] and the belief that our source operates under similar conditions to theirs'. These conditions (high electron energy, low pressure) efficiently produce both $N^+(^5S)$ and N_2^{++}, and since N_2^{++} has been shown to be present, it is reasonable to assume that $N^+(^5S)$ is as well.

It is somewhat amazing that $N^+(^5S)$ did not show itself prominently in the attenuation results but reasons were given rationalizing this behavior. The data with Ne in particular are helpful in confirming the notion that $N^+(^5S)$ is present in large amounts. Also the results of the scattering experiments described in Chapter 3 carry substantial weight. Without the presence of a significant fraction of $N^+(^5S)$ in the electron impact produced beam, those results become difficult to understand. The estimated fractions of the various states are compiled in Table 2.

Total luminescence experiments were also performed on N^+ beams. Unfortunately they are of little help in elucidating the state distributions. One reason for this is, as discussed earlier, the

Table 2

State	Microwave Discharge N_2	DC Discharge N_2	160 eV Electron Impact N_2
N_2^{++}	0	0	~0.10
$N^+(^5S)$	0	0	~0.40
$N^+(^1S)$	0	0	~0
$N^+(^1D)$	0.08	0.09	~0.10
$N^+(^3P)$	0.92	0.91	~0.40

Estimated fraction of various states in m/e = 14 beam from the indicated sources.

effective recombination energy of $N^+(^1D)$, is actually lower than the recombination energy of the ground state. This is in sharp contrast to O^+ which was quite successfully treated using the total luminescence method. Also the presence of N_2^{++} led to some serious problems in data interpretation.

Table 3 gives a compilation of the results we obtained. Note in particular that light is seen in collisions of Ar and Ne, with ions produced by electron impact on N_2. There are no known emitting states of Ar^+ or Ne^+ which are energetically accessible in collisions with $N^+(^3P, {}^1D, {}^1S, {}^5S)$ and the light is almost certainly attributable to processes such as

$$N_2^{++} + X \begin{cases} \nearrow N_2^+(B) + X^+ \rightarrow N_2^+(X) + h\nu & (33) \\ \searrow N_2^+(C) + X^+ \rightarrow N_2^+(B) + h\nu \rightarrow N_2^+(X) + h\nu. & (34) \end{cases}$$

The $N_2^+(B \rightarrow X)$ transition has a large oscillator strength and gives light in the near uv and the visible. Reactions (33) and (34) have been proposed previously to explain results obtained when $\frac{m}{e} = 14$ beams impinged on various gases.[34] It is interesting that no light is observed in collisions with He. This is probably because reaction (33), with X = He, is endothermic by 0.7 eV and T → E conversion is not favorable in this system. The fact that no light is produced in collisions of the ions from our discharge sources with Ar and Ne is consistent with our conclusion that no N_2^{++} is produced by these

Table 3

Gas	160 eV Electron Impact on N_2	160 eV Electron Impact on NO	DC Discharge N_2	Microwave Discharge N_2
CO	10	9.2	8.9	6.4
N_2	7.6	6.6	4.6	4.9
CO_2	6.9	4.6	2.6	2.6
N_2O	3.9	2.4	0.9	0.8
H_2O	4.9	1.0	0.4	0.4
H_2	3.2	1.0	0.5	0.2
CH_3CN	3.1	---	---	---
H_2S	---	---	---	2.3
Ar	2.7	0.3	0	0
Ne	2.1	---	---	---
He	0	---	---	---

Total light intensity produced by the collision of 24 eV beams of m/e = 14 ions with the listed gases. The values are normalized for beam current and placed relative to each other by defining as 10 the amount of emission produced by N^+-CO collisions. The uncertainty in these numbers is believed to be either ±15 percent or ±0.3, whichever is larger.

sources. A small amount of emission is seen with Ar when the N^+ is produced by electron impact on NO. N_2^{++} formation is precluded under these conditions, so this light, which is at the limit of our detection capabilities, must result from collisions involving high-lying metastable states of N^+. It is not clear what ransition is responsible for this emission, but the Ar^+ laser line at 4880Å has been observed by other workers in collisions involving Ar^+.[15] Since N_2^{++} is present when ions are formed by electron impact on N_2 there will almost always be a contamination from $N_2^+(B \rightarrow X)$ emission. The magnitude of the contamination is not easily estimated and so detailed interpretation of these results is virtually impossible.

For the most part there is good agreement as to the amount of light produced when the ions are extracted from our discharge sources. Only when CO is used is there a major discrepancy and it seems likely that one of these numbers is in error. This suspicion is based on the fact that the total luminescence experiments using the other gases, and the attenuation experiments, consistently indicated identical state distributions for these two beams.

Very little work has been done on the states of N^+ produced by electron impact on NO and our own interest in this problem is marginal since no scattering experiments were performed using these ions. It is apparent from Table 3 though that the state distribution is different from that of the discharge sources. Significantly more light was obtained with virtually all the collision partners and this indicates

the presence of higher energy states. Since it has been demonstrated that near resonant but spin-forbidden reactions such as

$$N^+(^1S) + N_2(^1\Sigma_g^+) \rightarrow N(^4S) + N_2^+(B\ ^2\Sigma_u^+) \quad \Delta E = 0.14\ eV \qquad (35)$$

are not favorable,[1] it is likely that the responsible state is $N^+(^5S)$. This conclusion is based on the fact that the ^5S state is the only one of the three lowest metastable states to have a recombination energy significantly higher than that of the ground state.

F^+ State Distribution

It appears that the attenuation and charge transfer properties of the various states of F^+ have been sorely neglected by those who work in that field. The only information we found on this subject, at energies below 10 keV, is the beam attenuation data of Lin et al.[27] They produced F^+ by electron impact on CF_4, and attenuated it in Ne. It was observed at electron energies of 50, 60, 80, and 100 eV, that 4 , 9 , 18 , and 45% respectively of the F^+ ions emerged in a metastable electronic state. By examining the appearance potential, it was ascertained that the metastable state formed was $F^+(^1D)$, which lies 2.59 eV above the ^3P ground state. Lin et al. also reported that electron impact on a 70%-30% CF_4-NO mixture at 20μ source pressure produced a pure ground state beam. In addition to the attenuation experiments, the charge transfer reaction $F^+(Ne,F)Ne^+$,

was examined. Their results show that using $F^+(^3P)$, this reaction has a threshold near 9 eV and the cross section attains a maximum value of $4Å^2$ near 30 eV. The cross section using $F^+(^1D)$ has a fairly sharp peak near $12Å^2$ at 15 eV, but falls rapidly with increasing energy and is actually less than that of $F^+(^3P)$ above 50 eV laboratory energy.

This is a somewhat unexpected result because the charge transfer reaction involving $F^+(^3P)$ is 4.14 eV endothermic while $F^+(^1D)$ is only 1.55 eV endothermic. The energetics are such that neither cross section should be very high, and one would anticipate that the reaction probability of the ^1D state is greater than that of ^3P throughout this energy range. Similar processes between monatomic reactants such as $Kr^+(Ar,Kr)Ar^+$, $Ar^+(Ne,Ar)Ne^+$, and $Ne^+(He,Ne)He^+$ which are 1.7, 5.9, and 3.0 eV endothermic respectively, all have cross sections of less than $0.1Å^2$ in this energy range.[51] It is true though that the number of low-lying potential energy curves for $(F + Ne)^+$ will be much larger than for the rare gas-rare gas ion systems, and since charge transfer depends on curve crossings, the higher values reported for F^+-Ne might be justified.

In addition to the ^1D metastable state there is a low-lying ^1S state at 4.17 eV and two very high states (^5S and ^5P) at 21.9 and 25.1 eV. The recombination energies for $F^+(^3P,^1D,^1S)$ going to $F(^2P)$ are 17.42, 20.01, and 22.59 eV respectively.

The high value (17.42 eV) for the ionization potential of F is the source of some experimental difficulties. For instance it was only after much travail that we were able to obtain F^+ from either of our discharge sources. Presumably this is related to the high ionization potential and the fact that the average electron energy may be too low to effect ionization. The problem was compounded even further because fluorine containing gases such as CF_4 and NF_3 seem to inhibit the formation and continuation of the discharge. In spite of these obstacles, the production of F^+ beams via discharge was considered essential to the understanding of the state distribution of electron impact produced ions.

Both beam attenuation and total luminescence experiments were performed in our attempt to characterize the electronic state distribution of the F^+ beams used in the experiments described in Chapter 4. Since these ions were generally created by the impact of 160 eV electrons on CF_4, our state distribution should be similar to that of Lin et al.[27] As stated previously, they observed that 45% of the F^+ produced by 100 eV electron bombardment of CF_4 was in the ^1D state. Our ion source operates at a lower pressure than theirs, and this combined with our higher electron energy might imply that we produce even a larger fraction of metastables. Such a conclusion seems unrealistic though, for a number of reasons. One reason is that the degeneracy of the ^1D state (5) is less than that of the ^3P state (9) and hence a purely statistical approach would favor ^3P production. Of course, there is no guarantee that a statistical

approach is valid, but similarly there is no a priori reason to expect dynamical effects to favor ^1D formation. Also any approach which gives approximately 50% ^3P and 50% ^1D, completely neglects the other metastable states, which seems unreasonable.

Fig. 16 shows an energy level diagram which will aid us in estimating the charge transfer cross section of F^+ in its three lowest states to various collision partners. It appears that for most of the molecules listed, the possibility of resonant charge transfer with $F^+(^3P)$ is quite good.

Attenuations were performed on 100 eV beams of F^+ using all the gases present in Fig. 16 as collision partners. However, the results are not quantitatively conclusive for several reasons. Unlike N^+, which was discussed in the previous section, we were unable to produce an F^+ beam which was known to be predominantly ground state, and we were unable to get good quantiative agreement using several attenuating gases. The fact that $F^+(^3P)$ has a near-resonant charge transfer channel available to it with virtually all these molecules implies that its attenuation cross section will be large; $F^+(^1D)$ might also have a large cross section and since a substantial difference in cross sections is essential for high resolution in attenuation experiments, our resolution might not be terribly good.

Fig. 17 shows the results of two consecutive experiments where F^+ was attenuated in N_2. In the first run, F^+ was produced by 160 eV electron bombardment of CF_4 and in the second an electron

Fig. 16. Energy level diagram showing the recombination energies of F^+ (^3P,^1D,^1S) and the ionization potential to the various states of the indicated species. The length of the lines denotes the magnitude of the vibrational overlap of that state of the ion with the v = 0 level of the ground electronic state of the neutral. For CF_4 a continuum is presented which reflects the appearance of its photoelectron spectrum.[42]

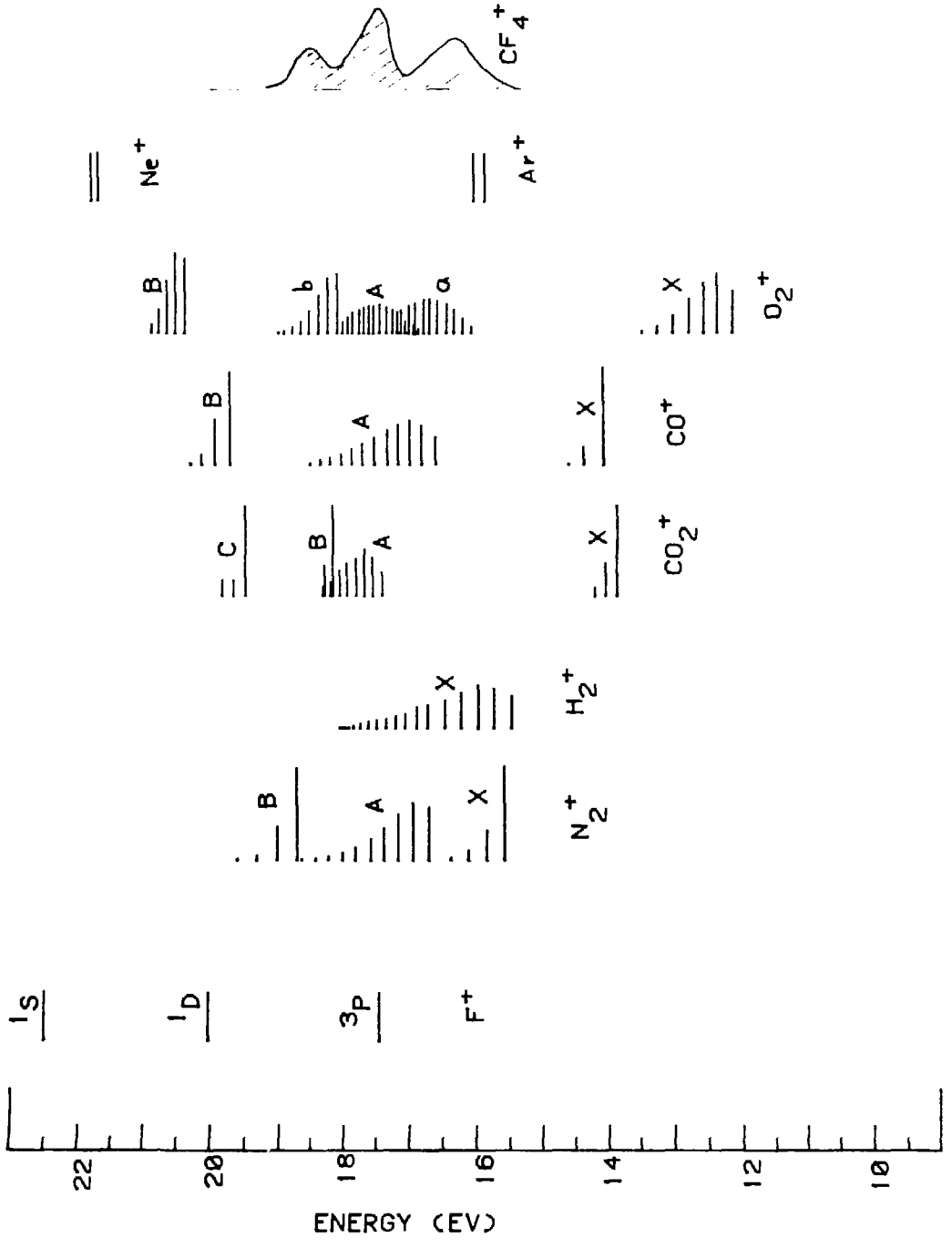

XBL 807-10775

Fig. 16

Fig. 17. Comparison of 100 eV F^+-N_2 attenuation results using ions produced by 160 eV (diamonds) and 60 eV (closed circles) electron impact on CF_4. The line drawn is the computer fit double exponential to the results obtained using 160 eV electrons.

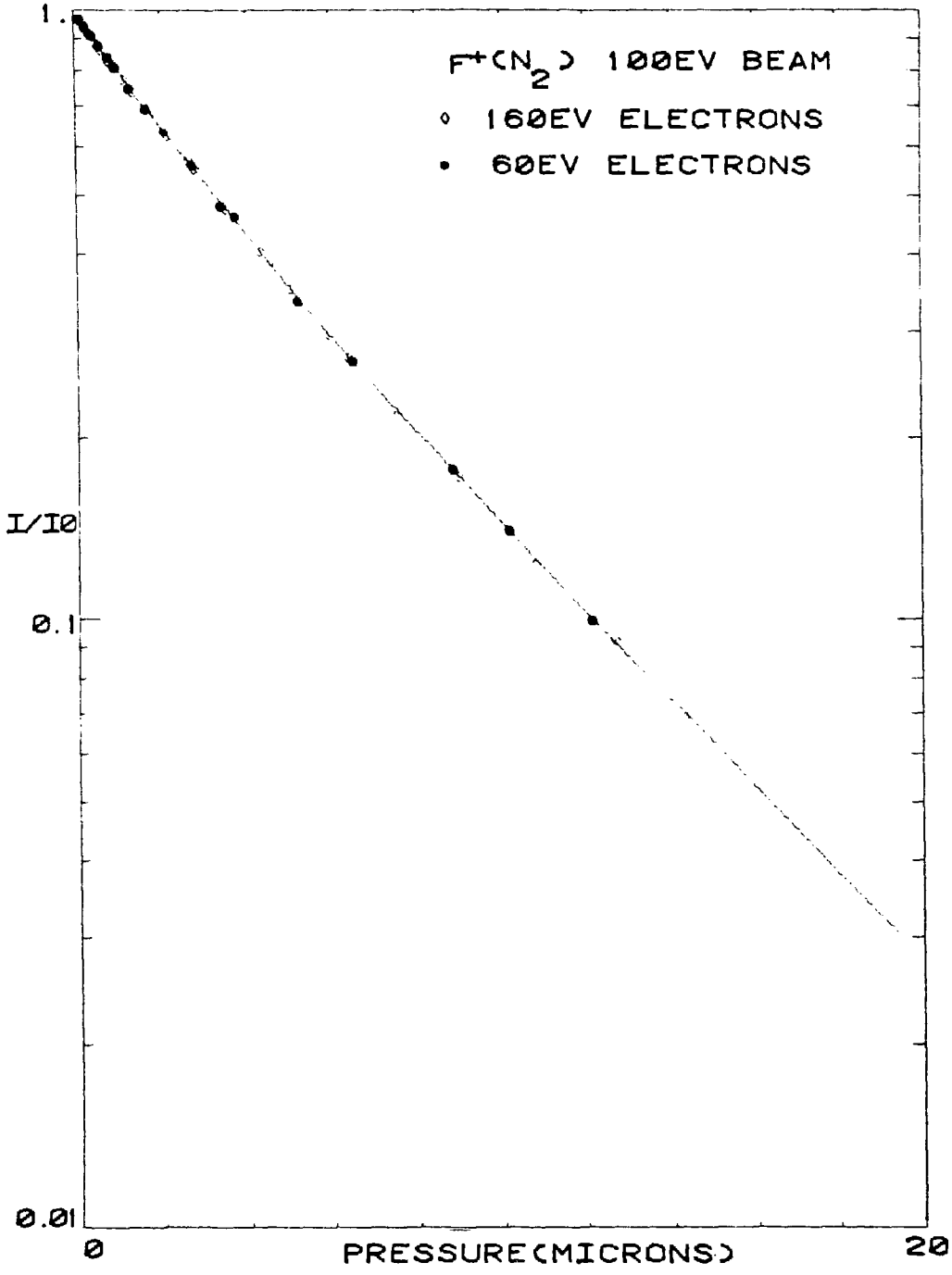

XBL 807-10749

Fig. 17

energy of 60 eV was used. As can be plainly seen, there is excellent agreement between these two sets of data indicating that either the state distributions are identical or that the states attenuate with similar cross sections in N_2. The former possibility is contrary to the results of Ref. 27 and the latter is inconsistent with an interpretation of Fig. 16 which would predict a larger cross section for $F^+(^3P)$ than either of the higher states. The observed cross section is indeed quite large, averaging to 25Å^2, but there is some subtle curvature present in both plots. This may be indicative of multiple states. The application of various pressure corrections (obtained using Ne^+ and Ar^+) was unable to remove the curvature. Results using F^+ formed by 160 eV electron impact on NF_3 were also superimposable with the data in Fig. 17.

The most logical interpretation at this point is that the attenuation cross sections of the various states present, are equal in N_2. This interpretation is clouded somewhat by our observation that F^+ produced by 160 eV electron impact on a 3:2 CF_4: NO mixture at an elevated pressure in our source yielded a plot that is slightly less steep. Also a weak F^+ beam extracted from a 6:1 Kr: C_2F_6 mixture in our DC discharge source gave, in N_2, an attenuation plot which was even less steep. As demonstrated with N^+, we would expect such a beam to have a higher fraction of ground state ions and therefore these results indicate that the attenuation cross section of $F^+(^3P)$ in N_2 is less than that of the metastable; this is contrary to our prediction. It should also be noted that the DC

discharge results retained substantial curvature and that the double exponential fit was not in good agreement with the fit to the electron impact data. By this we mean that the cross sections obtained did not match. If a double exponential fit is appropriate, then the cross sections obtained pertaining to these states will be found by the computer program. Different sets of data should yield the same cross section with only the abundances of the two states changing. Since this was not the case in the F^+-N_2 system no quantitative answer can be given and in fact the two state approach has to be questioned.

CF_4 seems to be a good candidate for distinguishing the states of F^+. There is very favorable vibrational overlap between CF_4^+ and CF_4 at the recombination energy of $F^+(^3P)$, which would imply a large charge transfer cross section. The higher states of F^+ are again expected to have a smaller cross section. It should be mentioned that CF_4^+ is not a stable ion and decomposes shortly after formation; this is partially responsible for the continuous nature of the energy levels plotted in Fig. 16.

Attenuations in CF_4, performed on ions produced by high energy electron impact on CF_4 and NF_3 (not shown), were super-imposable, indicating a similar state distribution. The average cross section, 44Å^2, was indeed very high but once again subtle curvature was present. A single experiment performed using a weak beam of F^+ created by 50 eV electron bombardment of CF_4 gave a plot which was significantly less steep than the others. This result may have been caused by some experimental error, however, since once again the shift

is in the wrong direction. Certainly if any change is made by lowering the electron energy it should be toward the production of more ground state ions. This in turn should give a steeper attenuation plot which is the opposite of what we observe. Results obtained using F^+ extracted from a 6:1 Kr: C_2F_6 mixture in the DC discharge source were only slightly less steep (~ 6%) than the high energy electron impact data.

The only attenuator used for F^+ which provided a high degree of curvature in the plots, is H_2. This is demonstrated in Figs. 18 and 19. In Fig. 18, F^+ was produced by high energy electron impact on CF_4 and the results obtained are superimposable with data produced using NF_3 as a source gas. The data was fit quite well by a double exponential indicating that a species with a large (10.9Å^2) attenuation cross section constitutes 73% of the beam, and 27% is a species with a smaller attenuation cross section.

Fig. 16 shows that $F^+(^3P)$ has a near-resonant charge transfer path to produce H_2^+ in a high vibrational state. Although the vibrational overlap between this state of H_2^+ and H_2 is not outstanding, one would still expect that charge transfer involving $F^+(^3P)$ would be more favorable than with the other states. Hence the results of Fig. 18 can be interpreted as implying 73% $F^+(^3P)$ and 27% metastables. Unfortunately Fig. 19, which uses F^+ produced in a DC discharge, does not substantiate these conclusions. Although there is fairly good agreement between the cross sections given in Figs. 18 and 19, the abundances shift in the opposite direction of

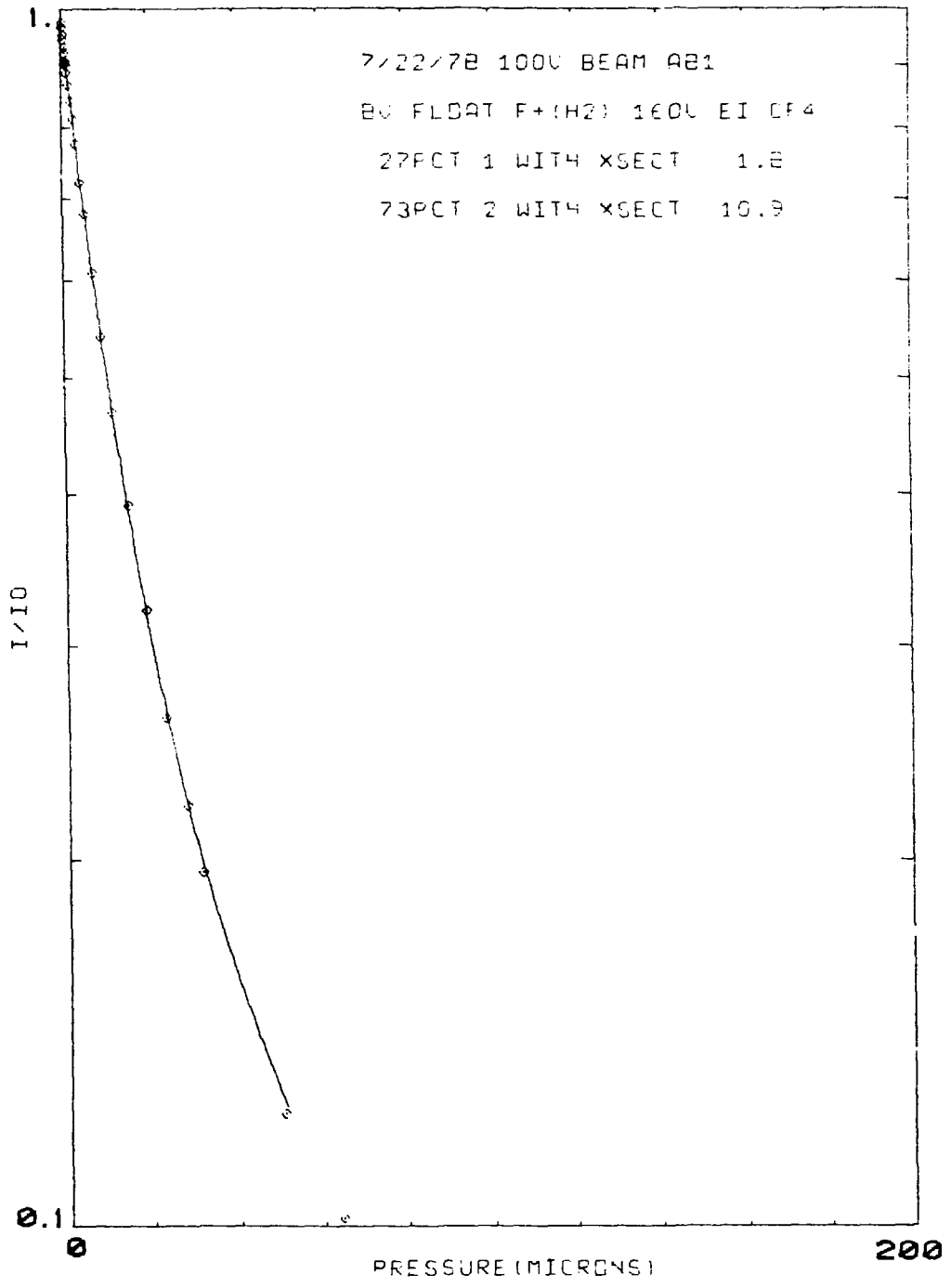

XBL 807-10748

Fig. 18. Attenuation of 100 eV F^+, produced by the impact of 160 eV electrons on CF_4, in H_2. The pressure correction coefficients used in Figs. 18 and 19 are the same as in Fig. 13. The line represents the double exponential fit.

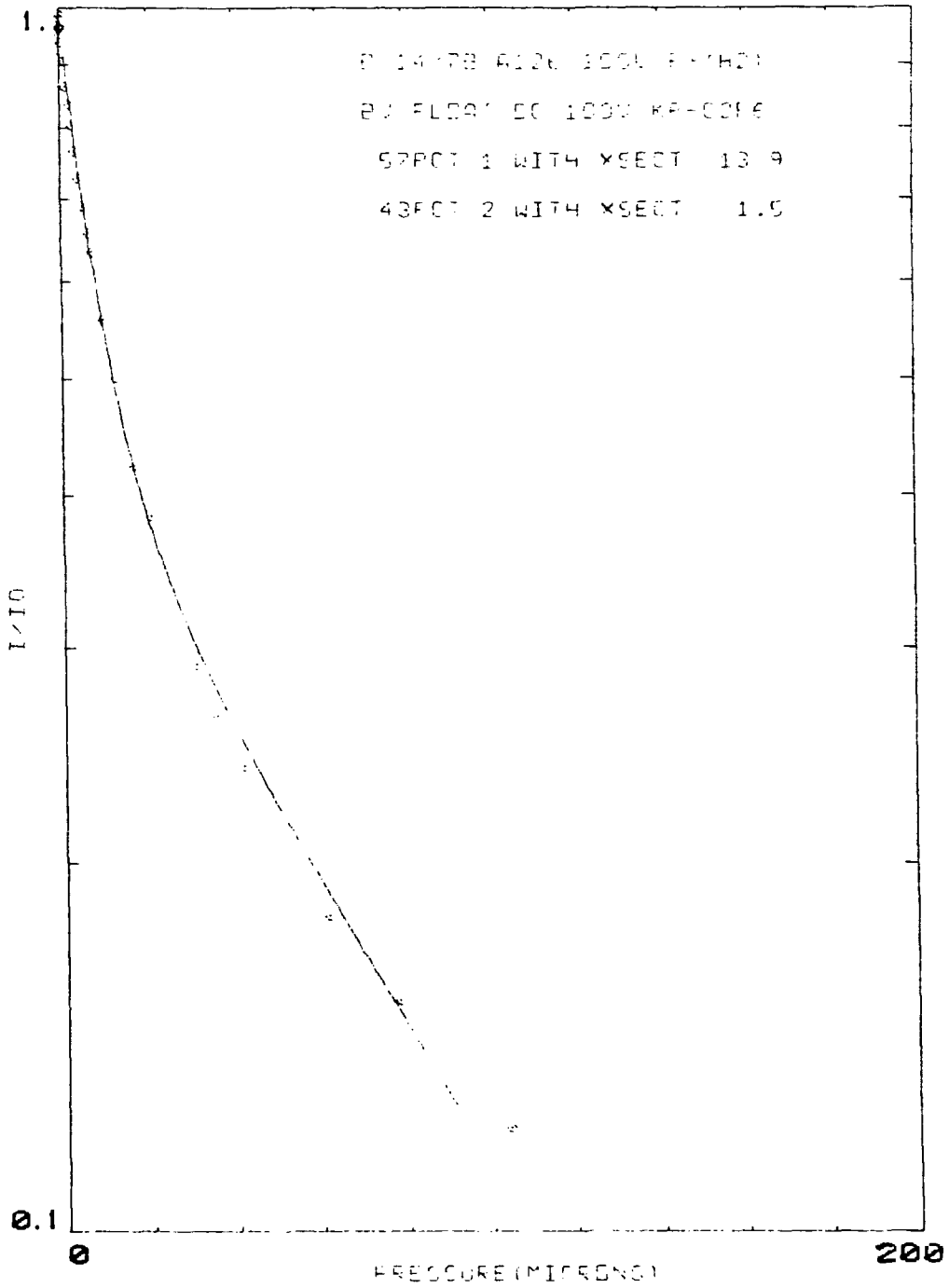

XBL 807-10747

Fig. 19. Attenuation of 100 eV F^+, produced by a 6:1 $Kr:C_2F_6$ mixture in a DC discharge, in H_2. The line represents the double exponential fit.

what we expect. This implies that either the metastable has a higher attenuation cross section in H_2 than the ground state and that the metastable dominates the electron impact produced beam, or that the DC discharge source produces a higher fraction of metastable ions than the electron impact source. Neither of these possibilities is likely. Some evidence for the notion that the attenuation cross section of $F^+(^1D)$ and $F^+(^1S)$ should be low comes from our observation that Ne^+, with a recombination energy in the same vicinity, has a very low attenuation cross section ($< 0.5\text{Å}^2$) in H_2.

It should be noted in Fig. 19 that the double exponential fit is not very good. This could be the result of a third electronic state in the beam, or perhaps, the result of experimental error. It is not very likely that an additional state would be present which does not appear in the electron impact produced beam. Therefore, one must question the data. Indeed, all of the data obtained using F^+ produced in the DC discharge source are difficult to rationalize. Using N_2, CF_4, and H_2 as attenuators these results were consistently less steep than when electron impact produced ions were used, and the opposite trend had been expected. If we also take into account the fact that the DC discharge produced beam was very weak and that all of the DC discharge data were taken in one day, the possibility of systematic error seems increased. It will probably be necessary for state specific chage transfer cross sections to be measured before these attenuation results can be adequately interpreted.

Attenuations of F^+ in a number of other gases were performed in an attempt to find distinct curvature which would aid in assigning the state distribution. Unfortunately, all of these experiments resulted in plots which were nearly straight. Nevertheless, attenuation cross sections were measured, and since these values are related to the unknown charge transfer cross sections, we have compiled them in Table 4.

We also performed a series of total luminescence experiments which we hoped would shed some light[52] on the F^+ state distribution subject made murky by the attentuation results. Fig. 20 shows results obtained for various ions colliding with C_2H_2. It is apparent that He^+ produces much more light than F^+, which in turn is considerably brighter than Ar^+. The interesting point, however, is that microwave discharge and electron impact produced F^+, have identical chemiluminescent cross sections.

We were successful in obtaining weak F^+ beams from the microwave discharge source after some difficulty, and such a beam, even from a pure CF_4 discharge, is expected to contain almost all $F^+(^3P)$. The addition of NO as a paramagnetic quencher should guarantee an entirely ground state beam. Since the electron impact produced beam has similar light producing characteristics, either it is also a pure ground state beam, or the states present have similar chemiluminescent cross sections.

Table 4

Gas	Attenuation Cross Section ($Å^2$)
Ne	2.2 ± 0.4
Kr	7.5 ± 1.5
Ar	5.5 ± 1
O_2	24 ± 4
CO	31 ± 4
H_2O	18 ± 2
N_2O	26 ± 4
CO_2	33 ± 4
N_2	25 ± 2
CF_4	44 ± 4
H_2	9 ± 2

Average attenuation cross section for a 100 eV beam of F^+ ions produced by 160 eV electron impact on CF_4, in various gases. The quoted error limits are estimated for relative comparison of the data; the absolute accuracy of the cross sections is estimated at ±20 percent.

Fig. 20. Plot of total luminescence in thousands of photons/sec/nA of beam current vs lab kinetic energy for He^+, F^+, and Ar^+ impinging on C_2H_2. He^+ and Ar^+ were produced by electron impact. The open squares and diamonds depict two different runs in which F^+ was produced by 160 eV electron impact on CF_4 and the closed squares are for F^+ produced in a 2:1 CF_4:NO mixture in a microwave discharge.

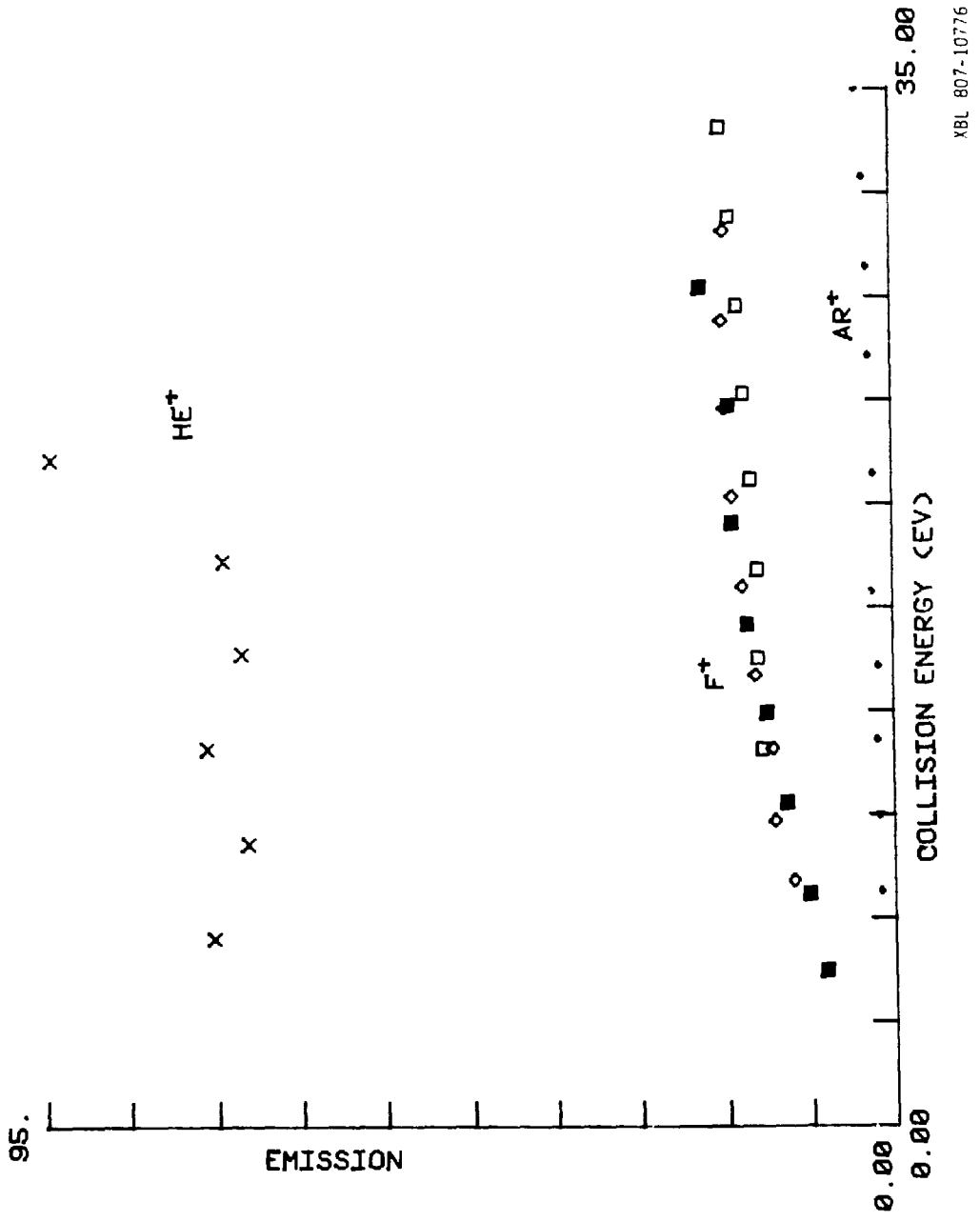
95.
EMISSION
0.00
0.00
35.00
COLLISION ENERGY (EV)
HE+
F+
AR+
XBL 807-10776

Fig. 20

Luminescence in near-thermal reactions between He^+ and C_2H_2 has been extensively studied in the 185-500 nm range by Marx and collaborators.[53] They found the emission spectrum was dominated by the CH(A → X) transition with weaker contributions from CH(B → X) and CH^+(A → X) transitions. The appearance potential for all of these emitting states is ~23.5 eV which is less than the recombination energy of He^+ but greater than the recombination energies of Ar^+ and the three lowest states of F^+. However, there do exist some emitting states of $C_2H_2^+$ and C_2H^+ accessible below 20 eV, and they may be responsible for some of the light seen in Fig. 20. This is almost certainly true for Ar^+ which should have a laboratory kinetic energy threshold of 19 eV for the production of CH(A) but clearly gives light at lower energies. The kinetic energy thresholds for CH(A) production are 11.2 and 6.3 eV for $F^+(^3P)$ and $F^+(^1D)$ respectively; however, the curve in Fig. 20, while showing definite threshold behavior, is not helpful in pinpointing an exact threshold.

Fig. 21 shows the results of total luminescence experiments for F^+-CO_2 collisions. Again the striking fact is the similarity in total light intensity regardless of how the ions were formed. The small discrepancy at higher kinetic energies is within experimental error; other measurements showed the electron impact produced ions to give a few percent more light than the discharge produced ions. The largest source of experimental error comes from normalizing for beam

Fig. 21. Plot of total luminescence in thousands of photons/sec/nA of F^+ vs lab kinetic energy using CO_2 as a collision partner. The squares denote data taken with ions produced by 160 eV electron impact on CF_4, and the diamonds are for microwave discharge produced F^+.

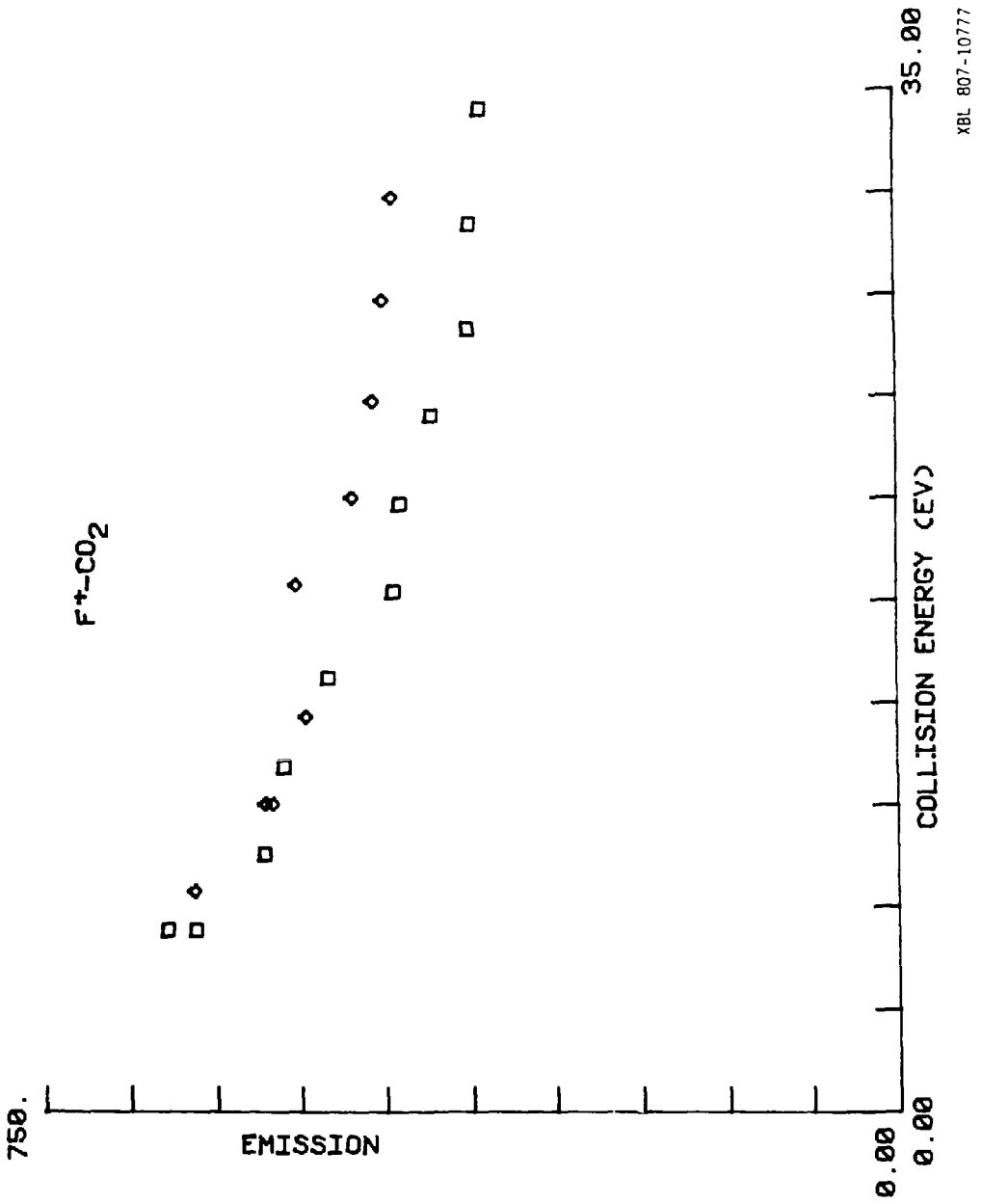
750.
EMISSION
0.00
0.00
COLLISION ENERGY (EV)
35.00
F^+-CO_2
XBL 807-10777

Fig. 21

current (the discharge produced beam was weaker), and normalizing for slight changes in photon counting efficiency; this was done using N^+-CO as a standard. The points in Fig. 21 are considered accurate to ± 10%.

Fig. 16 shows that $F^+(^3P)$ can charge transfer very efficiently to CO_2^+ ($A\ ^2\Pi_u$). The $CO_2^+(A \rightarrow X)$ transition has a large oscillator strength and produces light in the 290–490 nm range;[21] therefore we would expect this reaction to be very bright. It is indeed bright, the brightest one that we studied, and the emission is easily visible with the naked eye. The shape of the curve in Fig. 21 is consistent with that of a resonant process in that the cross section decreases with increasing kinetic energy.

This system should be an excellent one for qualitatively demonstrating the presence of metastable ions. The ^1D and ^1S states of F^+ would be expected to produce $CO_2^+(A)$ with a much lower probability than does $F^+(^3P)$. The cross section for the formation of $CO_2^+(B\ ^2\Sigma_u^+)$ or $CO_2^+(C^2\Sigma_g^+)$ with the metastable states might be fairly large, but $CO_2^+(B \rightarrow X)$ and $CO_2^+(C \rightarrow A)$[54] emission occur at wavelengths outside of our detection range. Thus the luminescence cross section for the excited states of F^+ should be considerably less than that of $F^+(^3P)$. The similarity of the results in Fig. 21 coupled with the expected high cross section of $F^+(^3P)$ suggests both beams are nearly pure ground state.

The brightness of the F^+-CO_2 reaction indicates that this might be an excellent candidate for a charge transfer pumped laser operating in the uv.

Fig. 22 shows the results of a total luminescence experiment for F^+ colliding with N_2. Once again there is excellent agreement between the electron impact and microwave results. The several volt discrepancy in the threshold area is probably within experimental error. This is because the beam energy spread was about 2 eV, and the actual beam energy was only measured twice per experiment, and estimated from power supply settings in between.

As can be seen in Fig. 16, charge transfer from $F^+(^3P)$ probably favors $N_2^+(A)$ formation, but the subsequent $N_2^+(A \rightarrow X)$ emission is too red for our detection system. Thus the expected emitting state in F^+-N_2 collisions is $N_2^+(B)$. The laboratory kinetic energy threshold for $N_2^+(B)$ formation is 2.4 eV and the curves given in Fig. 22 could be construed as consistent with such a value. Hence Fig. 22 not only supports the notion that electron impact and microwave discharge produced beams have similar state distributions but also that the single state present is $F^+(^3P)$.

The results of a number of additional total luminescence experiments performed with 25 eV ions are presented in Table 5. Intensities measured using Ne^+ and Ar^+ are included for comparison purposes. Fig. 16 would predict that less light is produced with N_2, CO_2, and CO using these ions, and indeed that is observed.

Fig. 22. Plot of total luminescence in thousands of photons/sec/nA of F^+ vs lab kinetic energy using N_2 as a collision partner. The squares denote data taken with ions produced by 160 eV electron impact on CF_4, and the diamonds are for microwave discharge produced F^+.

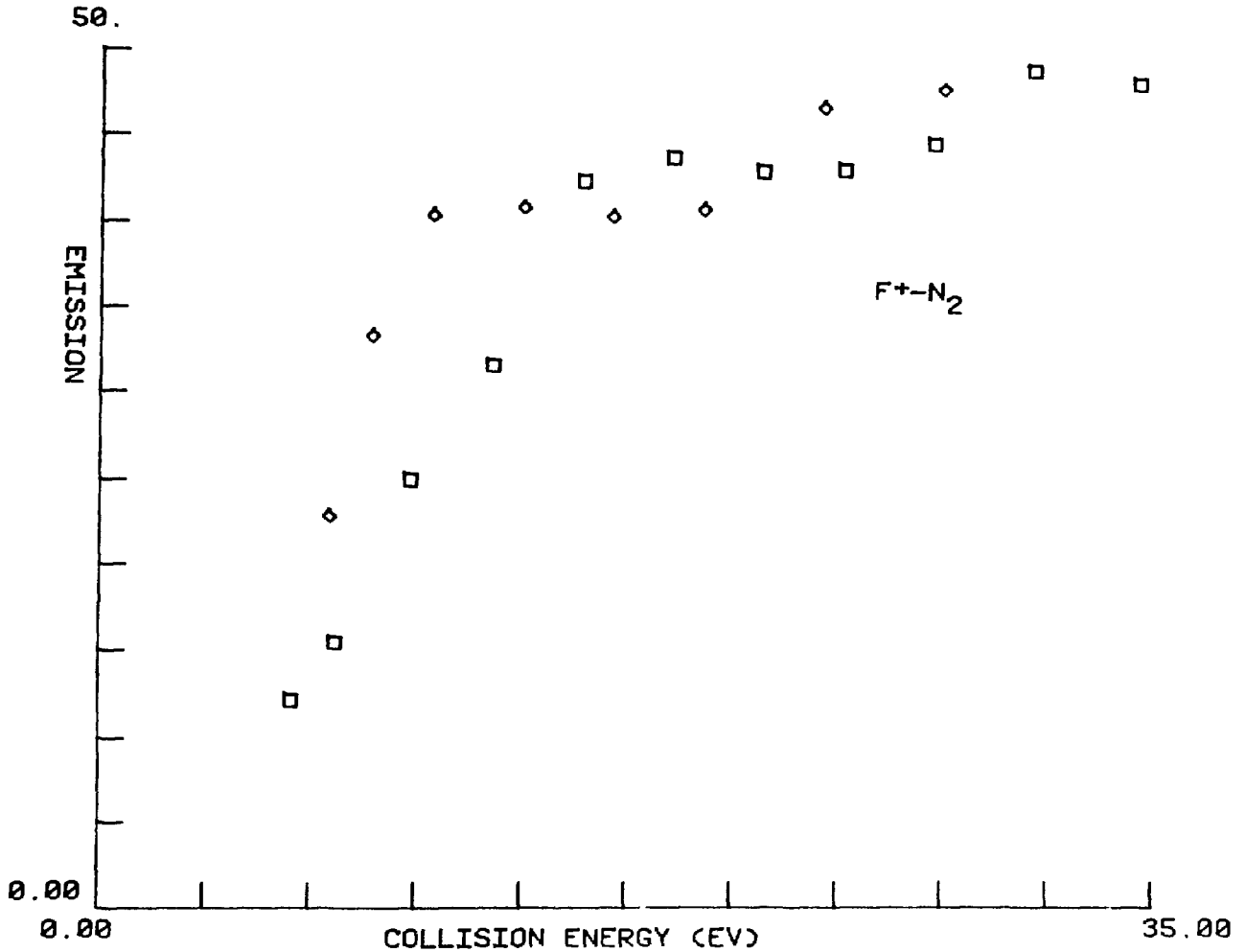

XBL 807-10778

Fig. 22

Table 5

Gas	F^+ 160 Electron Impact On CF_4	NF_3	SF_6	μ Wave Discharge CF_4:NO 2:1	Ne^+ 160 eV Elec. Impact	Ar^+ 160 ev Elec. Impact
N_2	9.4	9.6	8.6	10.7	6.0	0.9
CO_2	96	98	98	92	9.7	0.2
CO	63	64	65	64	1.2	5.2
C_2H_2	4.1	4.9	3.8	-	-	-

Total luminescence intensity measured for the indicated ions colliding with the indicated collision partners at 25 eV. The values are normalized so that they are comparable to those in Table 3.

The agreement between the first four columns in Table 5 is striking. Regardless of how the F^+ is produced, the ions have similar chemiluminescent cross sections in all gases used. It is inconceivable that the different electronic states of F^+ have identical chemiluminescent cross sections in all these gases, so we are led to the conclusion that within experimental error, the beams have similar state distributions. As discussed previously, we have reason to believe that only ground state ions are present.

Before we could be happy with this conclusion we need to go back and consider the attenuation experiments. In these experiments we observed that occasionally plots of varying slopes could be obtained depending on the method in which F^+ was produced. For the set of experiments performed using the DC discharge source we were able to rationalize this behavior as perhaps being due to some systematic error. If we then neglect the results obtained with this source there exists only one set of data which still causes problems. This was an experiment in which F^+, formed by the impact of 50 eV electrons on CF_4, was attenuated in CF_4. The experiment yielded an attenuation cross section equal to roughly 2/3 the cross-section measured immediately prior using F^+ produced by 160 eV electrons. This can be taken as strong evidence against the conclusions drawn from the total luminescence results. However, since the measured attenuation cross section decreases, rather than increases, as we would expect for a beam containing a higher fraction of $F^+(^3P)$, this result is also

suspect. We have no other a priori reason to doubt this result; however, the F^+ beam used was very weak (~0.2 pA), and this might have caused some problems.

Basically our decision depends on which we believe more: a few attenuation experiments performed with weak beams, or our ability to predict attenuation cross sections. In particular let us consider the attenuation cross sections of the various states of F^+ in CF_4. As discussed previously, $F^+(^3P)$ has a favorable near-resonant charge transfer pathway and hence should have a large attenuation cross section. $F^+(^1D)$ and (^1S) do not have a similar favorable path and should attenuate more slowly. We can check our logic by considering Ne^+ which lies in between the metastable F^+ states with a recombination energy of 21.56 eV. Attenuations of Ne^+ (and Ar^+) were performed in various gases to determine pressure correction coefficients but simultaneously the total attenuation cross section was determined; these numbers are given in Table 6. The attenuation cross section for Ne^+ in CF_4, $14.8 Å^2$[55], is considerably less than that measured for F^+, $44 Å^2$. Also, Ar^+, which, as can be seen in Fig. 16, has good overlap with CF_4^+, has a high attenuation cross section. Numerous other examples demonstrating the validity of our cross section predicting approach can be found by considering Tables 4 and 6 along with Fig. 16, but will be omitted to avoid redundancy. Hence, our conclusion is that we can qualitatively estimate attenuation cross sections, and since some of the attenuation data are suspect, the total luminescence results better reflect the truth.

Table 6

Gas	Attenuation Cross Section ($\AA^2$) Ne^+	Ar^+
CF_4	14.8	39
H_2	0.4	19
H_2	7.7	15
O_2	8.0	9.0
CO	9.3	10
Ar	5.1	42
Ne	-	1.5
CO_2	-	9.4
Kr	-	7.3

Measured attentuation cross sections for 100 eV Ne^+ and Ar^+, produced in a microwave discharge, in various attenuating gases. The values are considered accurate to ±5 percent (or ±0.5, whichever is greater) relatively, and ± 20 percent absolutely.

Apparently then, F^+ ions, whether produced by high energy electron impact on CF_4, NF_3, or SF_6, or in a microwave discharge, are almost exclusively in their ground state. This conclusion is contrary to the results of Lin et al.[27], the conventional wisdom that numerous states result from high energy electron impact, and some of our attenuation results, but is the most logical conclusion given the information available.

CO_2^+ State Distribution

We performed both beam attenuation and total luminescence experiments in an attempt to elucidate the state distribution of the CO_2^+ ions used in our scattering experiments. The two methods utilized to prepare these ions were high energy electron impact and microwave discharge. Our results are of some added interest because it has been speculated that different states of CO_2^+ are populated by these two methods. In thermal energy studies of the reaction $CO_2^+(H_2,H)HCO_2^+$, it was noticed that ions which were allowed to equilibrate in a microwave discharge reacted faster than ions produced at low pressures by electron impact.[56,57] A further study[58] established that this behavior was due to the fact that CO_2^+ ions in higher vibrational levels had a smaller reactive rate constant with H_2 than vibrationally cold ions. One would infer from these results that electron impact produces CO_2^+ in high vibrational states. This is a somewhat unexpected result in that the Franck-Condon factors between $CO_2(X)$ and $CO_2^+(X\ ^2\Pi_g)$, as can be seen in Fig. 16, indicate a better

than 80% overlap between the ground vibrational states. However, high energy electron impact will create CO_2^+ in a number of different electronic states and the Franck-Condon factors to some of these states might favor high vibrational levels. As these excited electronic states radiatively decay to $CO_2^+(X)$, the vibrational excitation might be preserved. If we consider only the lowest states of CO_2^+ (shown in Fig. 16), we see that production of $CO_2^+(A\ ^2\Pi_u)$ will tend to skew the vibrational distribution to higher energies, although production of the $B\ ^2\Sigma_u^+$ and $C\ ^2\Sigma_g^+$ states favors low vibrational levels. Apparently the fraction of $CO_2^+(X)$ which results from cascading transitions going through $CO_2^+(A)$ is large enough to significantly affect the vibrational distribution.

At the present time there are no known metastable electronic states of CO_2^+. A $^4\Pi_u$ state has been calculated[59] to lie ~7.3 eV above the X state, but has never been observed experimentally. It is intersting to speculate as to why this state has not been seen. One possibility is that it is subject to predissociation and hence has a short lifetime. Another reason could involve the fact that it is a quartet and hence is not easily transformed to singlet CO_2. Normally a state lying 7.3 eV above the ground state could be found rather easily by performing beam attenuation and/or total luminescence experiments. However, in this case, that might not be true because the actual recombination energy of $CO_2^+(^4\Pi_u)$ may be less than that of the X state (13.77 eV).

The low recombination energy is attributable to spin conservation which inhibits the reaction

$$CO_2^+(^4\Sigma_u) + X \rightarrow CO_2 \text{ (singlet)} + X^+ \quad , \tag{36}$$

and the fact that triplet states of CO_2 (if they exist) lie quite high in energy.

The results of total luminescence experiments performed with CO_2^+ produced both by electron impact and microwave discharge are given in Table 7. The most obvious points made by this table are that CO_2^+ produces very little light with these collision partners and that equal amounts of light are produced regardless of how the ions are formed. The latter point can be put forth only weakly because the light levels measured are approximately equal to the uncertainty in the measurement. Nonetheless, these results can be taken as consistent with the presence of 100% $CO_2^+(X)$. This statement can be made because spin forbidden reactions such as (36), though unfavorable, have been observed,[15] and given the sensitivity of the total luminescence method we should be able to see the results of such a reaction. Since the total amount of light produced is miniscule, and there is good agreement between the electron impact and microwave results, it seems likely that only ground state ions are present. It appears that the larger vibrational excitation reputed to be present in the electron impact produced ions does not manifest itself in the total luminescence data.

Table 7

Gas	CO^+ Produced by: 160 eV Electron Impact	Microwave Discharge
CO	0.3	0.4
N_2	<0.1	<0.1
H_2	0	---

Total luminescence intensity measured for 25 eV CO_2^+ colliding with the indicated gases. The intensities are normalized so that they are comparable to the results given in Tables 3 and 5.

Attenuation experiments were performed on CO_2^+ beams extracted from both sources using CO_2 as an attenuator. The results were quite similar in appearance except that the ions produced by electron impact attenuated with a slightly higher cross section (36Å^2) than the microwave discharge produced ions (33Å^2); the experiments were performed at a laboratory collision energy of 60 eV. There was a slight, but approximately equal amount of curvature, in each set of data. It is not clear whether both the curvature and the small differences in cross section are within experimental error limits, but it is reasonable that such behavior could be caused by the presence of different vibrational states of $CO_2^+(X)$. This is due to the fact that the charge transfer cross section can be dependent on the initial vibrational state. The reaction

$$CO_2^+(v = n) + CO_2(v = 0) \rightarrow CO_2(v = 0) + CO_2^+(v = n) \qquad (37)$$

is always resonant, but the cross section will vary according to the vibrational overlap of CO_2^+ $(v = n)$ and CO_2 $(v = 0)$. Fig. 16 shows that the overlap is most favorable for $n = 0$, and hence the reaction probability should decrease for higher values of n. Our results indicate that the attenuation cross section is slightly larger with the electron impact produced ions which is the opposite of what one would predict if a larger fraction of these ions were in high vibrational levels. Therefore the difference in total cross sections measured with the two sources is probably due to experimental error.

In conclusion, it is indicated by our results tha virtually all of the CO_2^+ ions produced by each of our sources are in the ground electronic state. We have some evidence that the vibrational temperature of CO_2^+ produced by electron impact is not significantly higher than that of CO_2^+ formed in a microwave discharge. This latter temperature is expected to be low because of the Franck-Condon factors between the ground states of CO_2^+ and CO_2 and due to thermalizing collisions in the discharge. We cannot positively conclude that the former temperature is low because our data are limited and there is much evidence from other labs that this temperature is high.

Hard Sphere Contribution to Attenuation Results

As mentioned earlier, the two major contributors to ion attenuation are charge transfer and large angle scattering. When the measured attenuation cross section is small, large angle scattering is probably dominant. A theoretical estimate of this contribution can be obtained in the following manner. By considering a velocity vector diagram such as Fig. 23, assuming elastic scattering, and appplying simple geometry, we obtain:

$$\tan \Theta = \frac{m_n \sin\theta}{m_n \cos\theta + m_i} \quad , \tag{38}$$

where Θ and θ are the laboratory and center-of-mass scattering angles, m_n is the mass of the neutral, assumed initially at rest, and m_i is

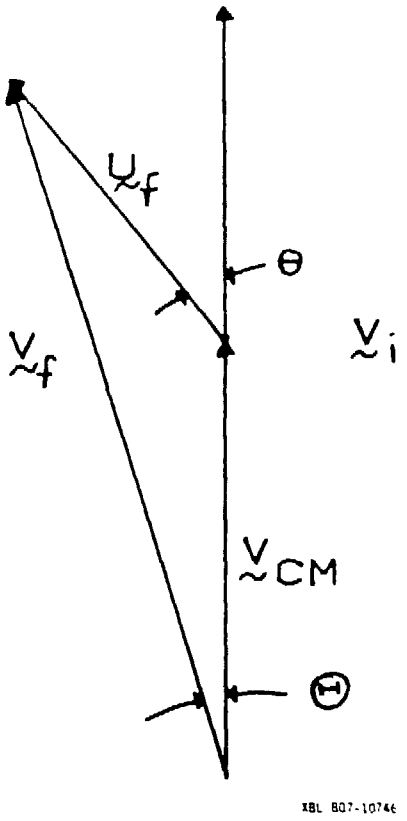

Fig. 23. Velocity vector diagram where v_i and v_f represent the initial and final laboratory velocity vectors of the projectile ion, v_{cm} the center-of-mass velocity vector, u_f the final center-of-mass velocity vector of the ion, and θ and Θ the center-of-mass and laboratory scattering angles.

the mass of the projectile ion. Since the acceptance of our ion collector is ± 45°, if $\theta > 45°$, the ion has been "attenuated."

Now if we assume that the collision partners can be treated as billiard balls (not unreasonable at 100 eV laboratory collision energy), then we can estimate a hard sphere attenuation cross section. The center-of-mass scattering angle obtained from a hard sphere approach is:[60]

$$\theta = \pi - 2 \sin^{-1} \frac{b}{d} \qquad \text{for } b \leq d$$

$$= 0 \qquad \text{for } b > d, \tag{39}$$

where b is the impact parameter and d the hard sphere diameter. Equation (38) implicitly defines a minimum θ for removal of an ion from the beam and this in turn leads to a maximum value for the impact parameter (b_{max}). All closer approaches lead to large angle scattering out of the detector acceptance angle and hence the cross section is given by πb_{max}^2. We obtain hard sphere diameters for atoms from Pauling's estimates[61] and for molecules from the potentials given by Amdur and Jordan.[62] These estimates range from 0.7Å for Ne to 1.8Å for CF_4. The hard sphere diameters of the ions were taken to be equal to $\frac{2}{3}$ the diameter of the neutral species. A sampling of the hard sphere cross sections estimated using these values are listed in Table 8. If these numbers are compared to the attenuation cross sections given previously, we find that for

Table 6

Gas	Hard Sphere Attenuation Cross Section (A^2)		
	N^+	Ne^+ and F^+	Ar^+
N_2	4.7	4.2	0
CO	4.7	4.2	0
Ar	4.3	4.0	-
H_2	0	0	0
O_2	4.8	4.4	0
He	2.4	-	0
CF_4	-	12.0	13.0

systems with a negligible charge transfer channel, the agreement is quite satisfactory, especially in light of the crude hard sphere diameter estimates. For instance charge exchange between Ne^+ and Ar has a cross sectin of ~0.2$Å^2$ at 100 eV,[51] and, as discussed previously, Ne^+ with CF_4 should also be slow. The measured attenuation cross section (Table 6) of 5.1 and 14.8$Å^2$ respectively are in reasonable agreement with the hard sphere estimates of 4.0 and 12.0$Å^2$ respectively. For N^+ with Ar the agreement is less satisfactory, 2.9$Å^2$ to 4.7$Å^2$, but the overall approach seems quite satisfactory.

Summary

The state distributions of N^+, F^+, and CO_2^+ ions emerging from our various ion sources was studied using both the beam attenuation and total luminescence techniques. N^+ formed in our discharge sources was shown to be 92% $N^+(^3P)$ and 8% $N^+(^1D)$. The impact of 160 eV electrons on N_2 gives a complicated mixture of states; we have estimated the composition of an $\frac{m}{e} = 14$ beam to be 40% $N^+(^3P)$, 40% $N^+(^5S)$, 10% $N^+(^1D)$, and 10% N_2^{++}.

The state distributions of F^+ formed by the impact of 160 eV electrons on CF_4 and NF_3 was not unambiguously determined. Total luminescence experiments indicated that the source gases yielded identical distributions, and, that the distribution was the same as produced by a CF_4-NO mixture in a microwave discharge. The latter

source should give only ground state ions. Beam attenuation experiments also showed identical state distributions using CF_4 and N_2 in the electron impact source, but it was not clear that only ground state ions were present.

No difference was detected in the state distributions of CO_2^+ ions formed by electron impact and microwave discharge. Total luminescence experiments indicated that only the ground electronic state was produced. The beam attenuation data did not support the widely-believed notion that electron impact produced CO_2^+ is vibrationally hot; however, the present work was not extensive enough to refute this notion.

REFERENCES

1. Ch. Ottinger and J. Simonis, Chem. Phys. 28, 97 (1978).
2. Only long-lived electronic states are expected to be involved because the transit time between source and collision center is $\sim 10^{-4}$ seconds. This period is greater than the radiative lifetime of "non-metastable" excited states.
3. C. A. Jones, I. Sauers, J. J. Kaufman, and W. S. Koski, J. Chem. Phys. 67, 3599 (1977).
4. J. H. Moore, Jr., Phys. Rev. A 8, 2359 (1973).
5. B. R. Turner, J. A. Rutherford, and D. M. J. Compton, J. Chem. Phys. 48, 1602 (1968).
6. C. Liu and H. P. Broida, Phys. Rev. A 2, 1824 (1970).
7. I. Kusunoki, Ch. Ottinger, and J. Simonis, Chem. Phys. Lett. 41, 601 (1976).
8. J. B. Hasted, Physics of Atomic Collisions (Buttersworths, London) 1964, p. 421.
9. J. Durup, in Interactions Between Ions and Molecules, Ed. P. Ausloos (Plenum Press, NY) 1975, pp. 619-633.
10. Z. Herman, V. Pacak, A. J. Yencha, and J. Futrell, Chem. Phys. Lett. 37, 329 (1976).
11. P. M. Hierl, V. Pacak, and Z. Herman, J. Chem. Phys. 67, 2678 (1977).
12. J. J. Leventhal, J. D. Earl, and H. H. Harris, Phys. Rev. Lett. 35, 719 (1975).

13. G. H. Bearman, J. D. Earl, R. J. Pieper, H. H. Harris, and J. J. Leventhal, Phys. Rev. A 13, 1734 (1976).

14. C. B. Collins, A. J. Cunningham, and M. Stockton, Appl. Phys. Lett. 25, 344 (1974).

15. D. Brandt, Ch. Ottinger, and J. Simonis, Ber. Bunsenges Phys. Chem. 77, 648 (1973).

16. M. H. Chiang, E. A. Gislason, B. H. Mahan, C. W. Tsao, and A. S. Werner, J. Phys. Chem. 75, 1426 (1971).

17. S. Dushman, Scientific Foundations of Vacuum Technique, 2nd Ed., J. M. Lafferty, Editor (John Wiley and Sons, NY) 1962.

18. J. E. Kleckner, unpublished results.

19. Handbook of Chemistry and Physics, 55th edition, Ed. R. C. Weast, (CRC Press, Cleveland) 1974.

20. K. T. Gillen, B. H. Mahan, and J. S. Winn, J. Chem. Phys. 58, 5373 (1973).

21. G. Herzberg, Electronic Spectra and Electronic Structure of Polyatomic Molecules (Van Nostrand, Princeton, NJ) 1966.

22. R. N. Dixon, G. Duxbury, M. Horani, and J. Rostas, Mol. Phys. 22, 977 (1971).

23. A. Carrington, D. R. J. Milverton, and P. J. Sarre, Mol. Phys. 35, 1505 (1978).

24. W. S. Koski, in Interactions Between Ions and Molecules, Ed. P. Ausloos (Plenum Press, NY) 1975, pp. 215–229.

25. E. Teloy and D. Gerlich, Chem. Phys. 4, 417 (1974).

26. R. J. Cotter and W. S. Koski, J. Chem. Phys. 59, 784 (1973).

27. K. C. Lin, R. J. Cotter and W. S. Koski, J. Chem. Phys. 61, 905 (1974).

28. Ibid. 60, 3412 (1974).

29. W. McGowan and L. Kerwin, Proc. Phys. Soc. 82, 357 (1963).

30. C. E. Moore, NSRDS-NBS 35, Volume 1, 1971.

31. M. Tichy, A. B. Rakshit, D. G. Lister, N. D. Twiddy, N. G. Adams, and D. Smith, Int. J. Mass Spectrom. Ion Phys. 29, 231 (1979).

32. J. A. Rutherford and D. A. Vroom, J. Chem. Phys. 62, 1460 (1975); Erratum 65, 1603 (1976).

33. T. F. Moran and J. B. Wilcox, J. Chem. Phys. 70, 1467 (1979).

34. I. Kusunoki and Ch. Ottinger, J. Chem. Phys. 70, 699 (1979).

35. B. Cobic, R. Petrovic, M. Vujovic and M. Matic, in Proc. 8th Int. Summer School and Symposium on the Physics of Ionized Gases, Dubrovnik, Ed. B. Navinsek (Ljubljana J. Stefan Institute, University of Ljubljana) 1976, pp. 97-100.

36. M. Vujovic, M. Matic, B. Cobic, and P. Hvelplund, J. Phys. B10, 3699 (1977).

37. E. A. Gislason, B. H. Mahan, C. W. Tsao, and A. S. Werner, J. Chem. Phys. 54, 3897 (1971).

38. W. Mendenhall and R. L. Schaeffer, Mathemaical Statistics and Applications (Duxbury Press, North Sciatuate, MA) 1973, p. 386.

39. The method given in Ref. 38 determines coefficients for $y = a + a_1x + a_2x^2 + a_3x^3 + \ldots$ The constraint is included by deleting the first column of the $\underline{X}$ matrix which forces $a = 0$.

40. The other methods will be discussed later; they involve fitting data obtained using ions from the microwave discharge source to a straight line, then applying these coefficients to electron impact produced ions. This approach seemed justifiable for the $N^+(H_2)$ and $N^+(Ne)$ systems and gave reasonable results.

41. A. F. Hedrick, T. F. Moran, K. J. McCann, and M. R. Flannery, J. Chem. Phys. 66, 24 (1977).

42. D. W. Turner, C. Baker, A. D. Baker, and C. R. Brundle, Molecular Photoelectron Spectroscopy, (Wiley-Interscience, London) 1970.

43. W. Frobin, Ch. Schlier, K. Strein, and E. Teloy, J. Chem. Phys. 67, 5505 (1977).

44. R. F. Stebbings, B. R. Turner, and J. A. Rutherford, J. Geophys. Res. 71, 771 (1966).

45. K. P. Huber and G. Herzberg, Constants of Diatomic Molecules (Van Nostrand Rheinhod, NY) 1979.

46. T. F. Moran, M. Cobb, and R. F. Borkman, Chem. Phys. Lett. 70, 166 (1980).

47. K. G. Spears, F. C. Fehsenfeld, M. McFarland, and E. E. Ferguson, J. Chem. Phys. 56, 2562 (1972).

48. W. Lindinger, E. Alge, H. Stori, M. Pahl, and R. N. Varney, J. Chem. Phys. 67, 3495 (1977).

49. J. Glosik, A. B. Rakshit, N. D. Twiddy, N. G. Adams, and D. Smith, J. Phys. B 11, 3365 (1978).

50. K. Ukuno, T. Koizumi and Y. Kaneko, Phys. Rev. Lett. 40, 1708 (1978).

51. W. B. Maier, J. Chem. Phys. 69, 3077 (1978).

52. Pun only partially intended.

53. M. Gerard, T. R. Govers, and R. Marx, Chem. Phys. 30, 75 (1978).

54. C → A emission probably is weak to non-existent because the C state completely predissociates. See J. H. D. Eland and J. Berkowitz, J. Chem. Phys. 67, 2728 (1977).

55. It will be shown later that this value corresponds fairly closely to the expected hard sphere scattering cross section.

56. K. R. Ryan, J. Chem. Phys. 61, 1559 (1974).

57. T. McAllister and P. Pitman, Int. J. Mass Spectrom. Ion Phys. 19, 423 (1976).

58. D. L. Albritton, in Interactions Between Ions and Molecules, Ed. P. Ausloos (Plenum Press, NY) 1979, pp. 119-142.

59. W. B. England, B. J. Rosenberg, P. J. Fortune, and A. C. Wahl, J. Chem. Phys. 65, 684 (1976).

60. M. S. Child, Molecular Collision Theory, (Academic Press, London) 1974.

61. W. L. Masterton and E. J. Slowinski, Chemical Principles, (W. B. Sauders Co. Philadelphia) 1973, p. 660.

62. I. Amdur and J. E. Jordan, in Advances in Chemical Physics, Vol. 10, Ed. J. Ross (Interscience, NY) 1966, pp. 29-74.